Dynamic Inertia Monitoring and Optimisation for Modern Grid Flexibility

Peter Makolo

A thesis submitted to
Auckland University of Technology – (AUT)
in fulfilment of the requirements for the degree of
Doctor of Philosophy
(PhD)

2022

School of Engineering, Computer and Mathematical Sciences

Abstract

Towards a low carbon energy future, the interest in Renewable Energy Sources (RES) as sources of electrical energy in the grid has increased significantly. As most RES are converter based, the electric power system is currently undergoing a drastic transition from synchronous generators (SG) dominated to converter-based generation units dominated. As a result, the network is losing its precious SG inertia used for instant frequency response after a contingency in the network. Low SG inertia in the network leads to rapid and significant frequency fluctuations becoming considerable challenges to address. As a result of low SG inertia in the network, the introduction of control strategies of some RES to provide the so-called synthetic inertia (SyI) are becoming popular. However, due to the stochastic nature and physical characteristics of RES, the provided SyI may be a time-varying and tradeable quantity in the contemporary network. Therefore, it is crucial to understand the values of network inertia in the time ahead to avoid rapid and significant frequency fluctuations in the network due to low and time-varying inertia. Prior knowledge of the system inertia values is essential to help operators plan and apply appropriate measures and suitable control schemes to mitigate stability issues.

Therefore, this study aims to monitor and optimise inertia values in modern networks with high penetration of RES. The monitoring part of the research is further subdivided into three subparts presented in separate independent Chapters. The three subparts are offline inertia estimation, online inertia estimation, and long-range inertia forecasting. The inertia optimisation part is discussed in a separate Chapter as well.

In addition to Chapter 1 which gives a general introduction to this thesis, Chapter 2 provides a comprehensive literature review on inertia's role for grid flexibility under the high penetration of variable renewables. Chapter 2 reviews the challenges and solutions related to the role of inertia in maintaining frequency stability in the network. Further, a comprehensive literature survey on the need for inertia estimation, monitoring, forecasting, and optimisation is presented in Chapter 2. This part of the study reveals the research gaps that need attention in modern networks. The subsequent Chapters further cover the identified gaps by developing techniques to fill up the research gaps.

The proposed methods start with the offline inertia estimation method presented in Chapter 3. This part of the study develops a data-driven method to estimate the time-changing inertia in the network based on the frequency gradient of an estimated model of the network. This approach uses phasor measurement units (PMUs)-measured network data to estimate a network's dynamic model. Next, a system identification approach is applied to estimate the power system model, from which the estimated inertia can be extracted. The benefits of the proposed method include, i) reduction of a high order model to a low order model to avoid computation burden, ii) extraction of the inertia from the low order model using the gradient mapping on RoCoF of the

system response, and iii) estimation of the inertia constant of the network using normal operating conditions.

Then, Chapter 4 proposes an online method to estimate the inertia in the network based on the recursive least-squares approach. The proposed method uses network measurements with a non-recursive system identification approach to estimate the network's hypothesis model. Then, the recursive method is used together with time changing measurements to recursively estimate model parameters and extract online estimates of the inertia in the network. During estimation, the technique does not need to store previous data after each sample step; therefore, significantly reducing the computation burden. More importantly, the method incorporates the use of available electromechanical oscillation modes in the system, which are linked with system parameters to determine the estimates of the network's inertia.

After establishing the offline and online inertia estimation methods, Chapter 5 gives the long-range forecasting of inertia in modern and future power networks. Due to quick inertial responses, there is practically a short time for control actions in real-time that is difficult to be addressed by online approaches. Therefore, system operators need to understand the inertia values in advance to plan, control, and operate the network securely. Unlike short-range forecasting methods, long-range forecasting of inertia values in the network can identify when the network is likely to be potentially at risk in a reasonable time ahead. Thus, this Chapter proposes an improved ARIMA model ($\boldsymbol{i}$-ARIMA) approach to long-range forecast inertia values in a modern network. The $\boldsymbol{i}$-ARIMA uses strong periodic and seasonality patterns of historical time series data to long-range forecast future inertia values.

Finally, the participation of SyI in the market of RES-rich networks to provide instant frequency support when required proposes an increase in the operation cost of modern networks. Consequently, depreciation of operation costs by optimising the required SyI in the network is inevitable. The provided optimal values of SyI should also ensure stability resilience of the network is retained. Therefore, Chapter 6 proposes a flexible SyI optimisation method to address these issues. The algorithm developed in the proposed technique minimizes the operation cost of the network by giving flexible SyI at a given SG inertia and different sizes of contingency events.

Contents

List of Acronyms

ACF	Autocorrelation function
ARIMA	Autoregressive integrated moving average
BESS	Battery energy storage system
COI	Centre of inertia
DG	Distributed generation
ES	Energy storage
Exp	Experiment
GW	Gigawatts
Hz	Hertz
Hz/s	Hertz per second
HVDC	High voltage direct current
IEEE	Institute of Electrical and Electronics Engineers
KE	Kinetic Energy
LCF	Linear combination factor
MAE	Mean absolute error
MAPE	Mean absolute percentage error
MW	Megawatts
NZ	New Zealand
NSG	Non-synchronous generator
PACF	Partial autocorrelation function
PCC	Point of common coupling
PLL	Phase-locked loop
PMU	Phasor measurement units
PSO	Power system operators
PV	Photovoltaic
RESs	Renewable energy sources
RoCoF	Rate of change of frequency
SG	Synchronous generator
SyI	Synthetic inertia
SMAE	Symmetric mean absolute error
SVD	Singular value decomposition
TSO	Transmission system operator
UK	United Kingdom
VSG	Virtual synchronous generator
WECC	Western electricity coordination council
WT	Wind turbine

List of Figures

List of Tables

Attestation of Authorship

I hereby declare that this submission is my work and that, to the best of my knowledge and belief, it contains no material previously published or written by another person (except where explicitly defined in the acknowledgements), nor material which to a substantial extent has been submitted for the award of any other degree or diploma of a university or other institution of higher learning.

Chapters 2 – 6 of this doctoral thesis comprise separate peer-reviewed published articles, a manuscript under revision and a manuscript to be submitted. Chapters 2 – 4 are comprised of published papers, while Chapter 5 is a manuscript to be submitted to a journal, and Chapter 6 is a manuscript under review. All co-authors have approved the inclusion of the joint work in this doctoral thesis.

July 2022

_____	_____
Signature	Date

Co-Authored Articles and Contributions

Chapter Title	Author	Contribution (%)
Chapter 2: The role of inertia for grid flexibility under high penetration of variable renewables-A review of challenges and solutions	P. Makolo R. Zamora T.T. Lie	85 10 5
Chapter 3: Data-driven inertia estimation based on frequency gradient for power systems with high penetration of renewable energy sources	P. Makolo I. Oladeji R. Zamora T.T. Lie	82 5 8 5
Chapter 4: Online inertia estimation for power systems with high penetration of RES using recursive parameters estimation	P. Makolo R. Zamora T.T. Lie	85 10 5
Chapter 5: Long-range forecasting and tracking of inertia values in modern power systems	P. Makolo R. Zamora T.T. Lie	85 10 5
Chapter 6: Flexible synthetic inertia optimisation in modern power systems	P. Makolo R. Zamora T.T. Lie	85 10 5

We, the undersigned, hereby agree to the participation percentages and contribution to the Chapters identified in the table above.

……..…….

Dr Ramon Zamora
(Primary Supervisor)

……..…….

Prof Tek-Tjing Lie
(Secondary Supervisor)

……..…….

Mr Ifedayo Oladeji
(Collaborator)

Publications During the PhD Programme

Articles in peer-reviewed journals

P. Makolo, R. Zamora, and T.-T. Lie, "The role of inertia for grid flexibility under high penetration of variable renewables-A review of challenges and solutions," Renewable and Sustainable Energy Reviews, vol. 147, p. 111223, 2021. ISSN 1364-0321, doi.org/10.1016/j.rser.2021.111223. **(Published).**

P. Makolo, I. Oladeji, R. Zamora, and T.-T. Lie, "Data-driven inertia estimation based on frequency gradient for power systems with high penetration of renewable energy sources," Electric Power Systems Research, vol. 195, p. 107171, 2021. ISSN 0378-7796, doi.org/10.1016/j.epsr.2021.107171. **(Published).**

P. Makolo, R. Zamora, and T. Lie, "Online inertia estimation for power systems with high penetration of RES using recursive parameters estimation," IET Renewable Power Generation, 2021. doi.org/10.1049/rpg2.12181. **(Published).**

P. Makolo, R. Zamora, and T.-T. Lie, " Long-range forecasting and tracking of inertia values in modern power systems", Sustainable Energy, Grids and Networks. **(To be Submitted).**

P. Makolo, R. Zamora, and T.-T. Lie, "Flexible synthetic inertia optimisation in modern power systems," International Journal of Electrical Power and Energy Systems, IJEPES-D-22-01790. **(Under review).**

Conference contributions

P. Makolo, J. J. Justo, F. Mwasilu, and R. Zamora, "Fault Ride Through Technique for DFIG-based Wind Turbines Under Grid Three-phase Faults," in 2018 Australasian Universities Power Engineering Conference (AUPEC), 2018: IEEE, pp. 1-5. **(Published).**

P. F. Gutman, **P. Makolo**, and R. Zamora, "Modelling and Analysis of Load Frequency Control in Small Power Systems: a Case Study of New Zealand Network," in 2020 Australasian Universities Power Engineering Conference (AUPEC), Hobart, Australia, 2020: IEEE, pp. 1-6. **(Published).**

P. Makolo, R. Zamora, and T.-T. Lie, "Heuristic Inertia Estimation Technique for Power Networks with High Penetration of RES," in 2020 2nd International Conference on Smart Power & Internet Energy Systems (SPIES), 2020: IEEE, pp. 356-361. **(Published).**

P. Makolo, I. Oladeji, R. Zamora, and T.-T. Lie, "Short-range Inertia Prediction for Power Networks with Penetration of RES," in TENCON2021 Conference, Auckland, New Zealand, 2021: IEEE, pp. 1-6. **(Published).**

Acknowledgements

This doctoral thesis provides the synopses of the research pursuits undertaken during my time as a research student at Auckland University of Technology (AUT), Auckland, New Zealand. Many people have participated in one way or another to help and support the achievement of this work.

First and foremost, I glorify the Almighty God, the giver of life, for providing me with health, strength, knowledge and wisdom to positively deal with all the ups and downs during this journey. Finally, the PhD milestone is achieved.

Then, I would like to express my heartfelt gratitude to my primary supervisor, Dr Ramon Zamora for accepting my research proposal and allowing me to pursue my PhD program at AUT. He has been an exemplary advisor who has strengthened my research footsteps from day one I joined AUT. He didn't not only encourage me publishing but also participating fully by taking his precious time to review several manuscripts and provide useful comments and suggestions that fine-tuned the manuscripts. I would also extend my thanks to my secondary supervisor Prof Tek-Tjing Lie for helping me direct my research topic to the current research area and for his support, guidance, and training. I boldly say, the mentorship of these two academicians has made an excellent researcher out of me.

Moreover, special thanks go to Prof Francisco Gonzalez-Longatt and Prof Farhad Shahnia who accepted to be the examiners for this thesis. I appreciate the time they spent reading this thesis and providing very constructive comments that improved the quality of this thesis. I benefited a lot from the insightful and fruitful discussion we had during the oral examination. I am so humbled to getting the opportunity to discuss low rotational inertia in modern and future networks with these two experts.

I would also like to address my sincere appreciation to Mr. Ifedayo Oladeji for the fruitful collaboration in two journal articles and one conference paper. Apart from collaboration in papers, he has contributed to this work for his productive discussions during research and regular friendly meetings. In line with Ifedayo, I would also thank our research group members under Dr Ramon Zamora for their constructive discussions, questions, comments, and suggestions. Special appreciations to Dr Nicholas Mukisa, Xin Lin, Asaad Mohammad, Uvini Perera and all master students who happened to participate in our research group.

Special thanks go to the Ministry of Foreign Affairs and Trade (MFAT), New Zealand, for the financial support provided in the New Zealand Scholarship. I would like to mention MFAT representatives at the AUT scholarship office: Sacha Pointon, Margaret Leniston, Petrina Hibben, George Kimani, Sandelyn Lu, Prerna Taneja, and Rebecca Van Dam.

This research would not have been possible had it not been for the support from AUT and the School of Engineering, Computer, and Mathematical Sciences team. The conducive research environment and the general support were crucial for accomplishing this research work.

I am also indebted to my family. I am deeply grateful to my lovely wife Lilian Mutalemwa and our gorgeous children, Perlian, Bless and Christian. At the end of this journey, you all understand and value the hustles of PhD life. You deserve a certificate a certificate for your contribution to the achievement of this milestone. Thank you for your consistent love, support and prayers, which were the primary source of energy and happiness. To my dear Mama, Mwalimu Laurencia Peter, thank you for the sacrifices you made for me to get educated. My dear sister Maria Makolo, grandpa Mzee Peter Makolo and grandma Suzana Bunga, your prayers kept me moving in the PhD journey. May God bless you abundantly.

I am also grateful to all my friends who have been a source of happiness and extended their brotherly hands whenever I needed them during the challenging research times. Blessings to Dr Francis Mwasilu, Dr Herman Wandabwa, Dr Sweya Lukuba, Peter Katalyeba and family, Segunda Leswila and family, Steven Mbalazi and family, Isaya Mpangaji and family and the entire Tanzania diaspora in New Zealand.

Chapter 1 Introduction

1.1 Background and motivation

There are numerous factors that have intensified the interest in low carbon energy sources for power generation. These factors include growth of global energy demand and consumption, an international call for a low carbon economy, depletion of fossil fuel and geopolitics of oil economy [1-3]. In response to these drivers, the shares of renewable energy sources (RES) such as solar photovoltaic (PV) and wind energy rapidly increase in the power network. The fast-growing shares of RES are likely to replace some of the traditional synchronous generators (SGs) in the network. However, due to the stochastic nature of these RES and the reality that converters connect them to the grid, their interaction with the grid is considerably unique compared to the conventional SGs.

The replaced SGs have significant inertia and damping constants crucial for frequency stability. The replacing generating units, such as solar PV and wind turbines (WT), do not have inertia, or their inertia is decoupled from the rest of the network by the converters connecting them to the grid. Nevertheless, it is a fact that system inertia is a crucial property that responds immediately after power contingencies to slow down the rate of change of frequency (RoCoF) in the network. Therefore, phasing out of traditional SGs technically reduces the conventional inertia in the modern grid [4]. Networks with reduced traditional SG inertia experience significant operational and stability challenges [5]. Low classic SG inertia problem has resulted in several wide-area outages such as South Australia (SA) – 2016, Great Britain – 2019, Tenerife Island – 2019, etc., as explained in [6-8].

Low inertia, which is currently a fundamental challenge facing transmission system operators (TSOs) in the modern grid, needs to get appropriate solutions to save the network from frequency instabilities and increase stability resilience under various contingency events. As a result, different control strategies of non-synchronous RES have been introduced to the modern grid to address the underlying operational and stability challenges caused by low SG inertia [8, 9]. The control topologies primarily provide the so-called synthetic inertia (SyI) to improve the network's resilience in low SG inertia.

The time changing inertia values in the network is another new challenge facing the modern network. Due to the contribution of SyIs that depend on control of intermittent RES, the total network inertia constant, which was relatively independent of time, is expected to become a time-changing quantity. In this way, if the system inertia constant (H) can significantly change with time, then the RoCoF values after a power imbalance will also be highly changing and unpredictable with time [10, 11]. The time changing inertia values in networks is a new challenge facing the modern grid. For this reason, there is a growing need for estimating, and hence,

monitoring time-changing values of the power system inertia constant for stability control reasons [10, 11]. Tracking the dynamic values of the power system inertia can provide valuable information to power system operators (PSO) on how much and how fast the frequency will respond and deviate after a disturbance. This information is crucial as it will provide an alert, and hence, appropriate measures can be taken in advance to mitigate the effects of fast frequency response. A prior assessment of frequency response will help implement more robust control schemes for system stability [12, 13].

Pertain to understanding the behaviour of network inertia, the body of literature establishes several offline and online inertia estimation techniques. The techniques develop algorithms to identify inertia values in the power system. For instance, offline methods such as in [14-16] determine the historical inertia values when events happen in power systems for analysis purposes. Therefore, offline inertia estimation techniques cannot be used for protection and remedial measures in real-time. For this reason, online inertia estimation techniques such as in [6, 17, 18] come in place for establishing algorithms that can monitor the inertia values in the power system and, therefore, can be used for analysis in real-time.

Nevertheless, as inertia is becoming a time-dependent parameter in the power system, offline and online inertia estimation techniques are limited in grid protection purposes. Also, it should be noted that due to fast transient responses, the online inertia techniques may also be prone to instabilities in power systems in case of contingencies happening at low inertia, which is not predicted in the time ahead [19]. Therefore, prior understanding of network inertia well in the time ahead is also vital to the long-range forecast of the behaviour of the power system. The reduction of total rotating inertias, which results in fast transients, needs to be forecasted in networks to plan and maintain a minimum level of inertia in the network for secure operation [20].

The participation of SyI in the market of RES-rich networks to provide instant frequency support when required proposes an increase in the overall marginal operation cost of contemporary networks[21-23]. As SyI is a short term-quantity that functions in line with the available conventional synchronous generator inertia, it needs to be operated depending on the size of the contingency event and the pre-known values of existing traditional SG inertia in the network [24]. The amount of SyI to be procured depends on how much online conventional system inertia is on hand. The lower the traditional inertia of the system, the higher the SyI to be procured [24, 25].

Apart from SyI becoming a critical quantity for providing frequency stability and raising its value in the modern network, it also plays a major role for ancillary service [26]. For these reasons, SyI is an inevitable quantity for current network operation. However, considering the operation cost of the modern network, which is appreciated because of the

procurement of SyI, there is a need for methods to give optimal values of SyI for frequency control at different conditions. The provision of SyI to control frequency during contingency events in low inertia networks needs to be at values that can achieve as minimum operating cost as possible [27, 28].

1.2 Research gaps

Although several techniques propose inertia estimation algorithms in power systems, the impact of high penetration of RESs on the time-changing total inertia in the modern network is not thoroughly covered in published papers leading to a first research gap addressed in this study as highlighted in the bullet below.

- Most of existing methods are computationally complex with high computational burdens.

Considering the inadequacies discovered through the extensive review, there is a need for an enhanced and improved inertia estimation technique. The new techniques should be less computationally complex, consider the impacts of phase steps and account for time variations on the network inertia.

For the safety and reliable operation of modern and future power systems with low and time-changing values of inertia, online estimation and tracking of inertia and assessment of frequency response in power system are essential. By successfully assessing frequency response in the network online, appropriate measures such as control schemes can be planned [11]. This leads to a second identified research gap in this study as bulleted bellow.

- There are no well-established methods to give quick and continuous information of the inertia value in the network that will help power system operators (PSO) to plan and act either before the contingency or very rapidly after the contingency with appropriate measures.

Therefore, there is a need to develop a new online inertia estimation and monitoring technique. The developed technique should consider time-varying inertia, should not suffer from phase step issues and should have minimum computation burden.

Nevertheless, due to fast transient response in low inertia networks, the conventional inertia estimation techniques may be susceptible to instabilities in power systems in case of contingencies [19]. For these circumstances, a third research gap is revealed as bulleted below.

- There are no well-established techniques to provide prior knowledge of network inertia in order to forecast the behaviour of the modern network well in time ahead. The variation of total inertias, which results in fast transients, needs to be forecasted in modern networks.

Lastly, due to increasing marginal operational cost of contemporary networks, a fourth research gap is bulleted below.

- There is no proposed method that gives optimal values of SyI for frequency control at different contingency events in low inertia networks to minimize the operational cost.

1.3 Research objectives

Based on the challenges facing the modern network due to reduced total inertia, this research work is based on the following research questions:

- How can time changing inertia be monitored in real time using network data?
- How can optimal value of synthetic inertia co-existing with a specific value of conventional synchronous generator inertia in the grid be obtained that will ensure fast but low-cost frequency stability control?

To address the research questions in relation to the challenges facing modern networks due to phasing-out of traditional SGs and being replaced by non-synchronous generators (NSG) RES, the objectives of this PhD thesis are derived. Collectively, the objectives of this PhD thesis are to monitor the dynamic inertia behaviour in modern networks and optimise the new digital/synthetic inertia to minimize the operation cost of modern networks under contingency events. Specifically, these two objectives are further split into four specific objectives as bulleted below:

- To develop an offline inertia estimation method to compliment the gaps existing in the current offline inertia estimation methods. The developed method helps to analyse the behaviour of the low SG inertia network post contingency events.
- To develop an online inertia estimation technique with improved attributes compared to existing online inertia estimation approaches. The technique monitors the dynamic inertia behaviour in modern networks with high shares of RES and SyI.
- To develop long range inertia forecasting method to estimate the dynamic values of inertia in modern networks for longer time ahead than the current inertia forecasting techniques. The developed method will help TSO to pre-understand the estimate of the future inertia values to help in planning to maintain the frequency stability in case of any event.
- To optimise the dynamic value of SyI in modern networks to minimize the operation cost during power imbalances.

1.4 Contributions

The work presented in this PhD thesis is divided in the form of manuscripts, where each manuscript has unique contributions to the body of knowledge. Addressing the challenges identified in research gaps, this thesis makes the following significant contributions to the body of knowledge:

- An advanced offline inertia estimation technique with improved attributes using a coordinated frequency gradient mapping approach on RoCoF is developed.
- A high-tech online inertia estimation method using recursive parameters estimation and not storing previous data after each sample step is proposed. The method covers most gaps identified from other techniques.
- A state-of-art long-range inertia forecasting approach using the improved ARIMA algorithm is developed. The developed method uses the periodic patterns and seasonality of historical time series data to forecast dynamic inertia values for longer time ahead than most of existing forecasting methods.
- A dynamic SyI optimisation approach is proposed. The proposed method is intended to minimize the high operation costs caused by procurement of SyI for frequency control in modern networks.

1.5 Thesis outline

This PhD thesis follows the Auckland University of Technology (AUT) institution's doctoral thesis Format Two, also referred to as the "Manuscript Format". The thesis comprises seven Chapters. Apart from Chapters 1 and 7, which present the overall thesis introduction and conclusion, respectively, Chapters 2 – 6 are manuscripts published or submitted to the journals for publication. Therefore, there could be some repetition encountered within this thesis from one chapter to another. An introductory preamble is included for each of Chapters 2 – 6 to link the chapters and give the thesis a good flow. The rest of each chapter is identical to the journal article published or submitted with minor revisions as suggested by the examiners.

Chapter 1 presents the overall thesis introduction. It highlights the background and motivation for carrying out this study. It further points out the research gaps and the objectives of this research. Finally, it summarizes the contributions of this research. Chapters 2 covers literature survey on the role of inertia for grid flexibility under the high penetration of non-synchronous RES to modern power systems. It further provides comprehensive information on the challenges and solutions related to fast frequency responses and stability in contemporary networks. Then, it highlights the need for carrying out inertia monitoring, forecasting, and optimisation in modern networks.

To address the challenges highlighted in Chapter 2, different methods developed are presented from Chapter 3 to Chapter 6. To start with, an offline inertia estimation technique is presented in Chapter 3. In this chapter, a data-driven method to estimate the time-changing inertia in the network based on the frequency gradient of an estimated model of the network is developed. Advantages of this method include estimation of the inertia constant of the network using normal operating conditions and reduced computation burden.

Next, Chapter 4 covers the online inertia estimation in power systems. In this technique, a recursive approach is used together with time changing measurements to recursively estimate model parameters and extract online estimates of the inertia in the network. One of the advantages of this technique is that it does not need to store previous data after each sample step; therefore, it significantly reduces the computation burden.

Moreover, inertia forecast is covered in Chapter 5. In this Chapter, an improved ARIMA model ($\boldsymbol{i}$-ARIMA) approach to long-range forecast inertia values in a modern network is presented. The proposed technique uses strong periodic and seasonality patterns of historical time series data to long-range forecast future inertia values. One of the advantages of the proposed technique is that it can identify when the network is likely to be potentially at risk in a reasonable time ahead and therefore proper actions can be taken to mitigate the effects of fast frequency responses in modern and future low inertia networks.

Furthermore, Chapter 6 presents the final technique proposed in this study. This chapter presents inertia optimisation method to minimize the overall marginal operation cost in modern and future networks. The proposed technique developed an algorithm that gives flexible SyI at a given SG inertia and different sizes of contingency events. Finally, Chapter 7 describes this thesis's overall discussion and conclusion and gives future work related to the low inertia in modern and future networks. Fig. 1.1 shows the thesis structure and the Chapter titles. For each of Chapters 2 – 6, a selected manuscript is presented in Fig. 1.1.

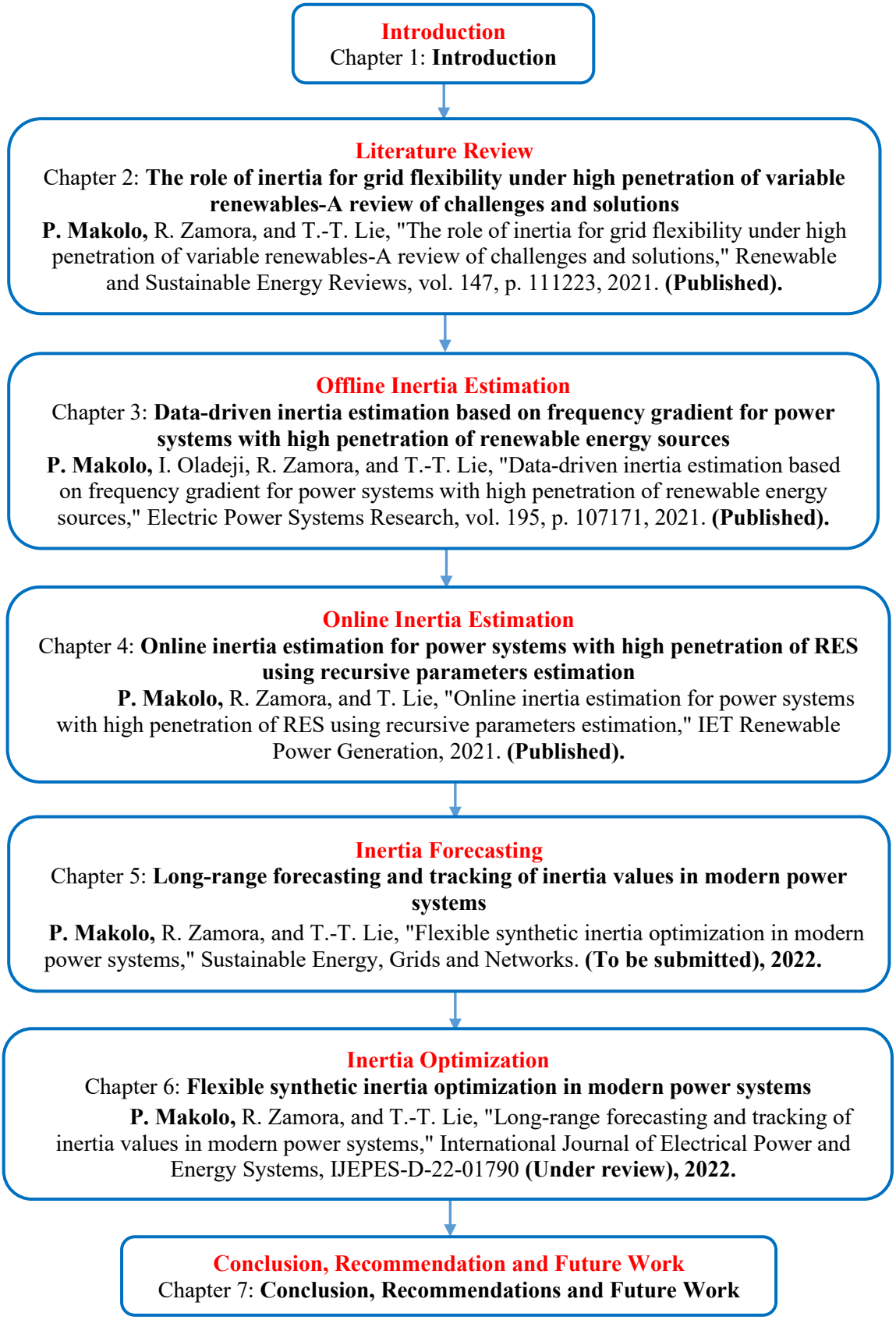

Fig. 1.1 Thesis structure

Chapter 2 Publication 1: Literature Review

Preamble

Chapter 2 unfolds in detail the motivation behind this study. It presents a comprehensive literature survey on the role of inertia for grid flexibility under the high penetration of non-synchronous RES to modern power systems. As total inertia in modern networks is becoming a time-changing quantity, inertia estimation techniques have been gaining popularity as solutions to stability challenges faced by power systems. This survey research discusses the following aspects related to time-changing inertia in networks. Initially, it examines synthetic inertia provision and the need for inertia estimation in the networks. Then, it addresses the importance of prior knowledge of the system inertia, which can further help operators apply suitable control strategies to mitigate stability challenges.

Generally, this Chapter opens up the discussion and studies conducted and presented in subsequent Chapters. Moreover, the survey research emphasizes the significance of co-existence, coordination and optimisation of conventional SG inertia and synthetic inertia as crucial features of a reliable and flexible grid in a low inertia environment. Finally, it highlights technical challenges and critical issues, and further research needs to address these challenges. The Chapter discusses the need to develop offline and online inertia estimation techniques. Furthermore, it justifies inertia forecasting and optimisation requirements in modern power systems.

The role of inertia for grid flexibility under high penetration of variable renewables - A review of challenges and solutions

Peter Makolo*, Ramon Zamora and Tek-Tjing Lie

Department of Electrical and Electronic Engineering, Auckland University of Technology, Auckland 1010, New Zealand

Abstract: Several studies show that grid-integrated renewable energy sources (RESs) have the potential to replace conventional synchronous generators in the network. This means the grid will experience low conventional inertia that is currently provided by synchronous generators. Low, unpredictable and time-changing inertia in the power system, as a result of high penetration of non-synchronous RESs, can cause rapid frequency oscillations. The rapid and unpredictable frequency oscillations are the major source of stability challenges in the power system. Therefore, this research presents a comprehensive literature survey on the role of inertia for grid flexibility under the high penetration of non-synchronous RESs to the power system. As inertia is becoming a time-changing quantity, inertia estimation techniques have been gaining popularity as solutions to stability challenges faced by the power system. Related to time-changing inertia, the following are discussed in this survey research. First, synthetic inertia provision in the network and the need for inertia estimation are intensively discussed. Second, the importance of prior knowledge of the system inertia, which will help operators to apply suitable control strategies to mitigate stability challenges, is also addressed. Third, the significance of co-existence, coordination and optimisation of both conventional synchronous generator's inertia and synthetic inertia, as a key feature towards reliable and flexible grid in low inertia environment, are also emphasized. Finally, technical challenges, key issues, and further research needs are highlighted.

2.1 Introduction

Several factors have intensified the interest in finding low carbon energy sources for power generation. These factors include the growth of global energy demand and consumption, a global call for a low carbon economy, depletion of fossil fuel and geopolitics of the oil economy [2, 3, 29]. On this note, the vastly available RESs are a promising solution to the global energy demand crisis. As a result, their shares in the energy mix for power generation keep increasing [3, 30-32]. According to the global energy review by the International Energy Agency (IEA), the global share of RESs into the power system was almost 13% by 2019 [33]. The global share of RESs into the power system is expected to further rise to 45% by 2040 according to the renewables global status report [34]. Therefore, hybrid generation systems comprising conventional electric power generation sources and stochastic RESs are inevitable in the power system [35, 36]. In this way, the rapidly growing stochastic RESs, which have been intensively researched, are likely to replace some of the traditional synchronous generators.

Most of these RESs such as solar PV, wind and fuel cells are linked to the power system using power electronic devices and, hence, decoupled from the rest of the power system [37]. Except for wind power generation that has a small amount of inertia, the rest of the RESs including the linking power electronic devices do not provide a mechanical inertial response to the power system dynamics unlike the traditional power plants with synchronous generators [38-41]. For this reason, they are generally termed inertia-less RESs. As the penetration of these inertia-less RESs in the power system increases, the conventional generation units, which have huge rotating mass with large kinetic energy referred to as inertia, are being substituted. The substituted mechanical inertia is exclusively responsible for instant response to dynamics in the power system before controllers and operators take action [42, 43]. The remaining mechanical inertia in the system after replacement with high penetration of RESs may be inadequate to immediately and effectively respond to frequency oscillations when exposed to disturbances. The reduced inertia will, therefore, lead to a high rate of change of frequency (RoCoF) and large frequency deviations (peak and nadir) after a disturbance [44-46]. Similarly, since most of the RESs are intermittent as they are weather dependent, changes in weather conditions will impact RESs and, therefore, affect the number of committed synchronous generators into the network over time. This tendency, consequently, leads to challenges in the planning, operation and control of the power system networks [35, 47-49]. Subsequently, the stability and flexibility of the grid are at risk as the converter-based RESs keep increasing in the network. This replacement of conventional synchronous generators is, however, changing the conventional property of the traditional power system. Consequently, the traditional stability of the power systems is put at risk.

Despite the challenges brought about by RESs, many countries worldwide have intensively invested in alternative energy sources such as solar power, wind power, fuel cells, micro-turbines, combined heat and power (CHP), biogas, etc. This move is geared by the global

agenda towards clean energy. Some countries, such as Denmark, Ireland and Germany have a high penetration of RESs, comprising more than 20% in their grids [50]. In this perspective, PV and wind power generation are the fastest-growing power sources worldwide at the moment. Globally, PV power generation grows at an annual average rate of 15%, while wind power generation grows at an annual average rate of 10%. As it stands, the global installation for the new power generation technologies topped 620 GW for PV [51] and 651 GW for wind [52] by the end of 2019. This trajectory informs that there will be a continuous decrease of mechanical inertia from conventional synchronous generators in the power system as they get replaced by the non-synchronous RESs.

Owing to this continuous decrease of mechanical inertia systems in the grid, as exhaustively studied in [47, 53-55], potential solutions have been proposed to address the related challenges. The solutions include running multiple synchronous generators lightly loaded while much of the power generation coming from RESs [56]. Although this approach is a very effective method of providing adequate inertia during power imbalances, it is limited by the cost due to a substantial requirement of dedicated rotating reserves. On the other hand, another technique proposed is to use energy storage devices such as batteries, super-capacitors and flywheels operating together with proper control strategies to flexibly compensate for frequency deviations [57-59]. This approach has been of interest as the controlled ES systems respond quickly to frequency events in power systems. Control of both ES systems and other RESs, which are linked to the grid for frequency support, are collectively referred to as virtual or synthetic inertia [60-64].

It is worth pointing out that virtual or synthetic inertia has become a point of interest and focus for modern and future grid stability and flexibility. The decrease of inertial machines such as synchronous generators and the increase of the stochastic renewable energy sources in the power system needs more research to ensure the stability and flexibility of the modern and future power grid [35, 47]. The introduction of synthetic inertia into the power system causes the overall power system inertia to be a time-varying quantity. Therefore, the likeliness of inertia becoming a time-varying quantity in the network triggers more attention to the power system stability and reliability. As a result, for the safe and reliable operation of modern and future power systems with low and time-varying values of inertia, estimation and monitoring of inertia as well as an assessment of frequency response in power systems are essential. Prior knowledge of the value of inertia in the system will help in planning for frequency response in the system. By successfully assessing frequency response in the network, appropriate flexibility measures of the system can be planned. Generally, preceding information of the inertia values in the network will help power system operators (PSO) to plan and act either before the contingency or immediately after the contingency with appropriate measures.

In the context of frequency control as related to the increase of converter-based generation units, the “modern grid” is the grid with hybrid generation units (conventional synchronous

generators and converter-based generation units). Though there are converter-based generation units integrated into the modern grid, the frequency is still dictated by synchronous generators. These converter-based generation units are termed “grid-following” [65]. On the other hand, the “future grid” will also comprise hybrid generation units with the exception that the network will solely be dominated by converter-based generation units. The frequency control will be dictated by converter-based generation units and digital/synthetic/virtual inertia. Therefore, the term “grid-forming converter” is often used [65].

The rest of the paper is structured as follows: the role of inertia in power system dynamics related to frequency stability and flexibility is reviewed and discussed in Section 2. On the other hand, the synthetic inertia approach, as dynamic frequency support for stability control in the network, is intensively analysed and discussed in Section 3. Furthermore, Section 4 comprehensively reviews and assesses different inertia estimation techniques in power systems. Moreover, a comprehensive discussion on synthetic inertia, its significance, related challenges and solution in the modern grid, as well as future trends and the possible way forward in this research direction, are presented in Section 5. At last, the conclusion of this comprehensive literature survey is drawn in Section 6.

2.2 The role of inertia in power system’s frequency stability and flexibility

2.2.1 Inertia versus RoCoF: an overview

The fundamental power balance between the generated and consumed powers at all-time in the network is vital in maintaining the network frequency at its desired nominal value. Any power imbalance in the system such as disconnection of one or more generating units will lead to rotor swings of the remaining generators in the network. Due to this swing, kinetic energy stored in the rotating mass of the remaining generators in the network will instantly react to the change. This phenomenon is profoundly known as an inertial response [56, 66, 67]. In other words, inertia can be described as the stored rotating energy that responds instantly to grid disturbances by resisting changes to the grid frequency. Inertia plays a substantial role and influences the eigenvalues and vectors, which determine the stability of the grid after the occurrence of contingencies [68, 69]. During this inertial response time, only kinetic energy from rotating mass is conventionally responsible for frequency damping before activation of primary frequency control by the governor, which takes place several seconds after the contingency [70]. For a clear understanding of frequency stability, it is worth recapping on highlights of primary and secondary frequency controls.

Primary frequency control

Primary frequency control is also called governor control. In the primary frequency control, the speed of the generating units is regulated to gain the balance between generation and load. The governor control, which is externally implemented from the synchronous generator, is designed in such a way that it changes the prime mover power to control output power from the generator. By changing the generator's output power, the frequency of the grid is controlled. For instance, when the frequency drops due to load increase or generation decrease, speed governors of generating units are regulated to increase the remaining turbine mechanical power output in direct response to the frequency variations. Since the primary frequency control is a local control action to the generating unit, it does not restore the frequency to the pre-disturbance nominal value [56, 70].

Secondary frequency control

Since the primary frequency control is a local control action to the generating unit, another control action is needed to restore the frequency to the nominal value. The secondary frequency control restores the frequency to a pre-disturbance nominal (i.e., reference) value. It operates from a central system that provides a wide area control action to several generators to regulate the active power production for system frequency restoration to desired values. Specifically, secondary frequency control operates by changing the base generation of the generators in the system. In some cases, if the system frequency after imbalance is less than the nominal value, then some reserved generation units need to be started or the load needs to be decreased to maintain the generation and load balance in the network. On the contrary, if the system frequency is larger than the nominal value, then some generation units need to be stopped or the load needs to be increased to maintain the generation and load balance in the network.

It is a matter of fact that before the primary and secondary frequency controls are activated, the inertia of the network determines how fast or slow the frequency will change after the disturbance. To make this clear, the following well-known swing equation (1) is presented [56].

$$2H\frac{d\omega_r}{dt} = T_m - T_e \tag{2.1}$$

The swing equation (2.1) can be transformed using Laplace transform from a function of time variable (t-domain) to a function of a complex variable (s-domain) to obtain (2.2) in which s denotes the Laplace transform operator.

$$\frac{\omega_r}{T_m - T_e} = \frac{1}{2Hs} \tag{2.2}$$

The mathematical model of the swing equation presented in (2.2) is further represented in the block diagram in Fig. 2.1 where ω_r is the rotor angular speed of the generator, T_m is the mechanical torque, T_e is the electrical torque and H is the inertia constant of the system in (s). The block diagram model in Fig. 2.2 is obtained by including the frequency-dependent loads with load

damping constant of D in (Nms) and also considering small deviations in mechanical power (ΔP_m) and electrical power (ΔP_e) in (W), and further replacing the small deviations in mechanical torque (ΔT_m) and electrical torque (ΔT_e) in (Nm) at steady state as explained in [56].

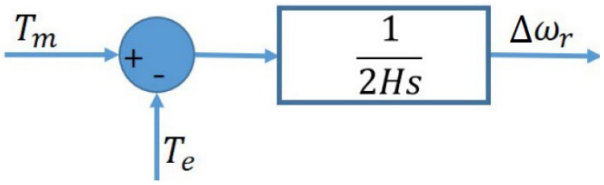

Fig. 2.1 Block diagram of the swing equation

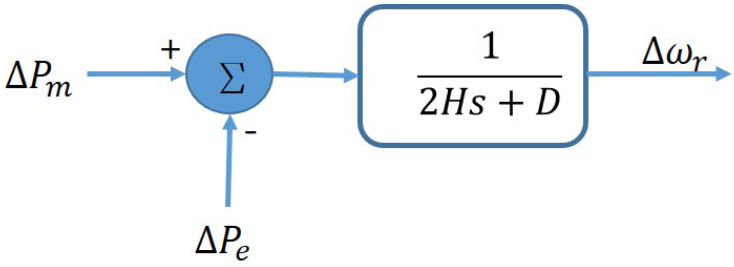

Fig. 2.2 Block diagram of the swing equation with damping constant

The target of (2.2) is to observe the system frequency (f) at the electrical output of the generator. Then, by using the number of the generator's field poles (np) and the relationship of the rotor speed ω_r in (rad/s) and rotor frequency f_r in (Hz), which is $\omega_r = 2\pi f_r$, the system frequency (f) in (Hz) is calculated as $f = np \times f_r/2$. To observe the system frequency response due to power mismatch and the impacts of inertia to the rate of change of frequency, the swing equation implemented in Fig. 2.2 is simulated using different values of network inertia constant *(H)* obtained from different literature works [71, 72]. The simulation results to demonstrate the impacts of different values of inertia constant to frequency response are presented in Fig. 2.3.

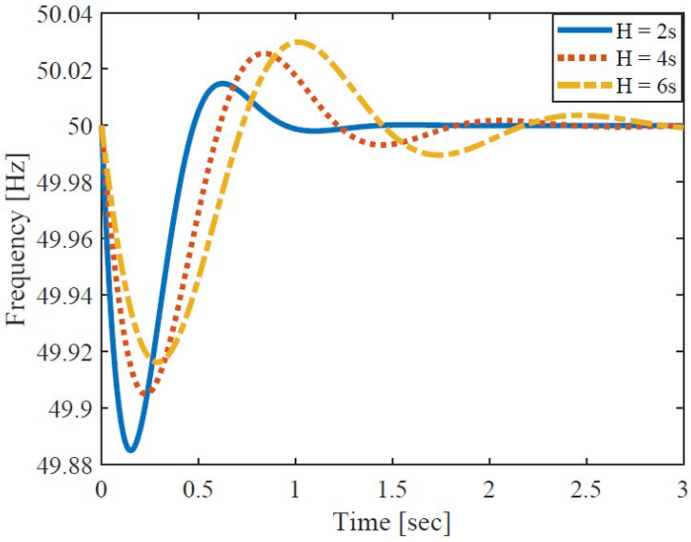

Fig. 2.3 Impact of inertia constant (H) to rate of change of frequency (RoCoF)

From Fig. 2.3, it can be well noted that different values of inertia constant *(H)* affect the rate of change of frequency (RoCoF) in the network. Increasing the value of system inertia *(H)* lowers the RoCoF when there is a disturbance in the network. This behaviour is essential as it allows ample time for governor control to be initiated before system frequency reaches unsafe high values. Subsequently, general observation from Fig. 2.3 is that the increase in system inertia decreases the rate of change of frequency in the network. In this way, the stability of the power system is guaranteed by high values of inertia in the network. Generally, to reduce the impacts of dynamics specifically frequency deviations in the power system, high inertia values in power systems are highly recommended [73]. Nevertheless, ever-increasing RESs penetration into the grid, which displaces the conventional synchronous generator, reduces the mechanical inertia in the system. This prevailing trend leads to the importance of further extensive research on RoCoF, frequency peak and nadir [9, 74].

At this juncture, it is worth highlighting that the size of synchronous generator inertia in the system determines how fast or slow the frequency will change after disturbance. This means high values of synchronous generators inertia prevent the fast change of the system frequency after disturbance and vice versa [75]. This fact highlights the importance of allowing a sufficient amount of system inertia to fast track and reduce RoCoF and ensuring the stability of the network before the activation of primary frequency control.

2.3 Frequency stability challenges in low-inertia systems

As explained from the previous sub-section, a synchronous generator (SG) has the required inertia and damping capability, which instantly respond to frequency oscillations during power imbalance in the conventional grid [76]. This happens before the primary and secondary frequency controllers regulate the power balance in the system. However, a large scale integration

of RESs has led to a significant decrease of this conventional rotational inertia in the system, and therefore, increase RoCoF values in the power system [71]. For the low values of mechanical inertia in the system, any disturbance occurring in the system can result in very fast and large frequency variations. This fast frequency response is a risk for the secure operation of the power system. This is a significant challenge to the power system as a result of the high penetration of RESs.

From a power system stability perspective, it is known that for secure and reliable operation of the power system, the system frequency should be maintained within acceptable limits even after contingencies [42]. To achieve this, the power balance in the system should be constantly observed and maintained. Nevertheless, the uncertainty of power output from stochastic and low-inertia RESs may significantly disturb the power balance in the system and lead to unpredictable frequency oscillations [5, 77]. The unpredictable frequency oscillations may be fast and large enough to result in the triggering of protection systems before primary frequency controllers are activated. This situation may lead to cascading failures and possible blackouts [5].

As far as control is concerned, the primary frequency control scheme is activated few seconds after the inertia response to regulate the speed of the synchronous generators in the network. As the primary frequency control is not instant, the high RoCoF in the low inertia power system is generally a serious challenge to be addressed [78]. For instance, in 2010, Ireland was among the first countries to observe that high RoCoF values were serious problems in the power system. Therefore, penetration of non-synchronous RESs was to be kept under 50% in order not to exceed the RoCoF of 0.5 Hz/s [79]. Owing to the high penetration of RESs in their networks, other countries and regions have reviewed and updated their grid codes. For instance, the continuous operational frequency is between 49-51 Hz for Germany, Great Britain, Norway and Denmark. For the lower frequency range of 47.5-49 Hz and the higher frequency range of 51-51.5 Hz, an operation is allowed for a specific time according to respective TSO. Outside these lower and upper ranges, protective relays must disconnect within a minute [80]. To allow fast RoCoF, the maximum RoCoF for these networks is allowed to 2.5 Hz/s [81].

To reflect further on the severity of the fast RoCoF problem, there have been other real cases reported around the world. The reported cases are caused by low system inertia as a result of the recent high penetration of RESs. A South Australia (SA) blackout on 28 September 2016 as reported in [82] is a good example. It is reported that, after disconnection of the SA system from the rest of the National Electricity Market (NEM), there was very low inertia in the remaining islanded SA system, which resulted in a very high RoCoF. The frequency dropped below 47 Hz very fast that triggered generator protection systems to operate and resulted in cascading failures before primary frequency controls had a chance to respond. The situation ended up in a blackout [79]. As a result of this event, low levels of inertia in large systems like the Australian system have been known to be a threat to the safe operation of the network. Yet, the

highest penetration of solar photovoltaics in the southern part of Australia's network, which is 58%, needs more attention to mitigating stability challenges in the country.

Furthermore, in 2011, the New Zealand network under the operation of Transpower noticed the frequency nadir of 47.5 Hz and RoCoF of 0.73 Hz/s on the North Island system following a significant disturbance. Based on this experience, the engineering planning team had to take precautions for establishing the plans for the future integration of more wind and solar power into the network. Studies show that with the penetration of 1300 MW of inertia-less variable RESs into the network, the RoCoF would increase to 2.1 Hz/s, which is unsafe RoCoF compared to 1.2 Hz/s for the network operation [83].

To illustrate more on the effects of high penetration of RESs to the RoCoF in the network, a network model simulation with different levels of RESs penetration as obtained from refs. [14, 84] was studied. Fig. 2.4 shows how RoCoF is significantly affected by the high penetration of RESs. From Fig. 2.4, it is shown that the frequency response for the network with 0% penetration of RESs is quite different from the frequency response with 40% penetration of RESs. The frequency response with 40% penetration of RESs exhibits much faster RoCoF with the higher value of frequency nadir than the response without any penetration (i.e., 0% penetration of variable RESs).

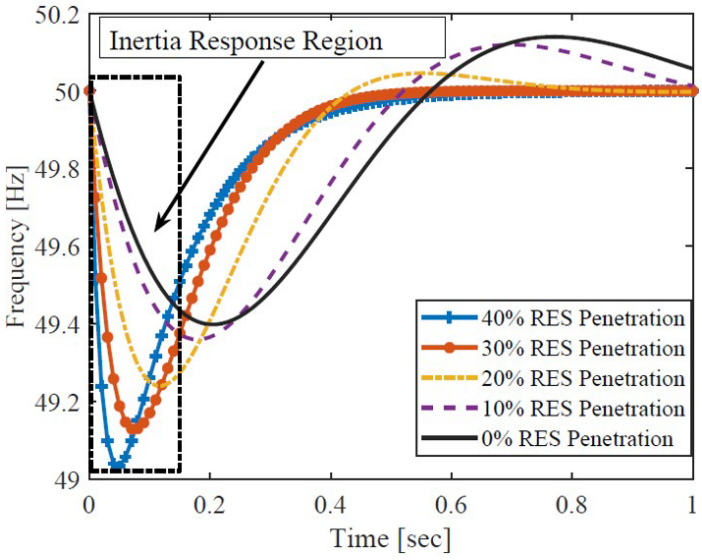

Fig. 2.4 Impacts of penetration of RESs to the system frequency response

If more attention is put on the inertia response region of Fig. 2.4, it is obvious that the frequency response with 0% penetration of RESs is slowly reaching the nadir point, giving ample time for the primary frequency control to take action to stabilise the network. This is contrary to when the levels of RESs penetration are increased. As the levels of RESs penetration are increased, the frequency response reaches the nadir value very fast. The fast reaching nadir value does not give enough time for the primary frequency control to act and protect the

network. Therefore, the fast reaching nadir value might lead to serious stability problems in the network.

2.4 Towards 100% renewable grid

Despite the challenges related to the high penetration of RESs, several studies such as [85-90] have anticipated that a reliable 100% renewable energy powered grid can be achieved in the near time to come. However, it should be clear that the concept of 100% does not essentially mean 100% converter or non-synchronous dominated grid. It should be noted that mainly converter-based renewable energy generation technologies such as WTs, PV solar and battery are the ones referred to as non-synchronous generation units. The rest of the renewable power generation units that comprise hydropower, geothermal, biogas, biomass, and solar thermal use the conventional synchronous generator. As the introduction of synthetic inertia in power system stability control is getting more attention, and hence, increases the level of its application into the grid, this trend indicates that there is a possibility of achieving 100% renewable grid soon as depicted in [91, 92]. Several countries have demonstrated this to be possible and feasible. The countries include Iceland with 100%, Norway (97%), Uruguay (97%), Costa Rica (93%), New Zealand (82%), Brazil (76%) and Canada (62%) to mention a few [92, 93]. According to the Government of Iceland, the 100% renewable energy power generation for the Iceland network comprises 73% hydropower and 23% geothermal power [94]. The two types of power generation units in Iceland are high inertia plants, therefore, the Iceland grid does not experience the problem of low inertia. Although the wind power sector grows in Norway, hydropower dominates the energy mix by comprising 91.8% of total RESs in the country [95]. Therefore, with the high share of the hydropower generation in the energy mix with relatively high inertia, the problems with low inertia do not apply in the Norwegian grid. High shares of hydropower also apply to Costa Rica, Brazil and Canada. On the other hand, an interesting example of a country with a high RE share without solely hydropower dominance is Uruguay. Around 38% of the electricity in Uruguay is supplied by wind, making it the second-largest in the world in terms of the percentage of this energy. Among countries with a close-to-100% renewable grid, Uruguay appears to be the least hydro-dependent one [34]. Continental wise, the level of penetration of RESs is projected to increase year after year. For instance, the European Union (EU) anticipated that by 2050, 62% of its installed capacity will be from RESs [96]. The same trends can be observed in America, Asia, and Africa.

Although there is a promising trajectory towards this transformation of the power grid, yet the challenges associated with this transformation cannot be underestimated [97, 98]. Measures related to grid planning, operation and control need to be taken to make the move smooth and viable [12]. Besides, the stochastic nature of wind and solar PV power generation, optimisation, and coordination of synthetic inertia when co-existing with conventional inertia should be

addressed. Wind and solar powers as the main promising sources of renewable power are variable and uncertain as determined by local weather conditions. [99, 100].

Moreover, PV energy sources generate dc power while wind power generators give ac power outputs at low and variable frequency, which is not consistent with system frequency [101]. Therefore, most of these new generation technologies are integrated into the grid through power electronic equipment such as converters and inverters. As the number of these distributed renewable generation units are increasing in the power system, the grid is likely to be dominated by the converter-based generation units soon [57, 102]. The fact that RES sources do not participate in frequency regulation operations due to lack of adequate reserves, their increasing share to the grid is challenging. Therefore, it is crucial to mimic the conventional synchronous generator inertial response behaviour in the power electronic-based converters as a solution to low inertia in the power system [103, 104]. The use of electronic converters as a means of mimicking inertial response is commonly referred to as synthetic inertia.

2.5 Synthetic inertia approaches for frequency control in grid

2.5.1 Virtual inertia topologies in the power system

Synchronous generators have been driving the traditional power systems in a unidirectional power flow for a long time. The introduction of distributed generation units and RESs, as a result of intensive prioritization of clean energy sources, paved the way for a transformation of the network towards a new concept of a grid layout with flexible power flow [64]. As described in the previous sections, the evolution of the traditional power systems towards modern and flexible networks has a price to pay for. The challenges related to this evolution need solutions to make the move smooth. One of the challenges is the high inertia of SGs, which resists sudden frequency change during power imbalances in the network, is being replaced. Despite the challenges related to the transformation, many studies have been carried out on the control of converters to integrate RESs into the grid [105, 106].

However, more penetration of RESs, which most of them do not contribute to inertia response in the network, replaces some of the SGs in the network. Consequently, this leads to a decrease of overall system mechanical inertia and, hence, an evolution from high inertia systems to low inertia systems as pictured in Fig. 2.5. The significant decrease in overall system mechanical inertia causes frequency stability issues as discussed in [107]. With the reduced inertia in the network, power imbalances will result in large frequency deviations that are associated with large RoCoF that may lead to loss of stability of the network.

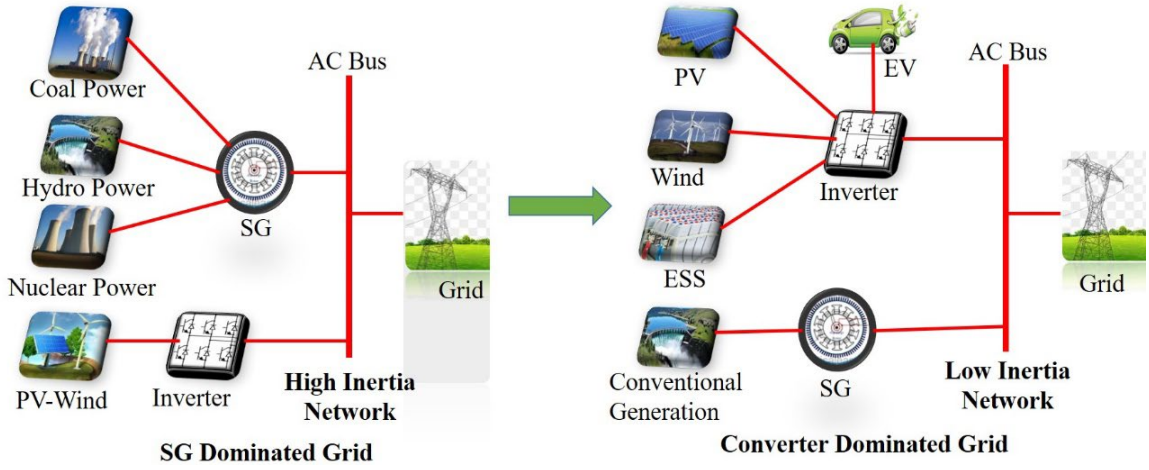

Fig. 2.5 Grid transformation from high to low mechanical inertia network

To respond to stability issues related to inertia challenges caused by the high penetration of RESs in the grid, the new concept of synthetic inertia is introduced into the power system [39, 59, 102, 106, 108-123]. Synthetic inertia is an artificially made frequency support service by controlling converters connecting RESs to the grid. The term synthetic inertia is described by ENTSO-E as "the facility provided by a power park module or HVDC system to replace the effect of the inertia of a synchronous power generating module to a prescribed level of performance" [10]. Likewise, in the clarifying article by Robert Eriksson et al, synthetic inertia is defined as "the controlled response from a generating unit to mimic the exchange of rotational energy from a synchronous machine with the power system" [60]. Other literature works have used other names to refer to synthetic inertia. Common names are such as virtual, emulated, hidden and digital inertia [124-127].

Back in 2007, Beck and Hesse introduced a VIrtual Synchronous MAchine (VISMA) topology [61]. The VISMA topology was designed to introduce synthetic or virtual inertia to the network. The reason for introducing the topology was to make possible integration of more non-synchronous renewable generation units such as PV, wind and fuel cell systems to the grid. After the inventions of Beck and Hesse topology, many other topologies and approaches established by different studies followed [111, 121, 128, 129]. Among the many topologies was the Virtual Synchronous Generator (VSG) [103]. VSG refers to an inverter control to mimic a synchronous generator in the provision of synthetic inertia in the network [62, 63, 130, 131]. The main target of the VSG topologies is to emulate the behaviour of real synchronous machines in frequency control of the power network [132]. Mainly, the topologies are supported with algorithms that control inverters coupled to distributed generation units to provide an inertial response to grid frequency discrepancies [67]. The control strategies for VSG are designed to mimic both steady-state and transient characteristics of SGs. The VSG virtually comprise important attributes of a synchronous generator during the inertial response. For instance, the ES system for VSG imitates

the flywheel of SG as it can absorb and provide power in case of imbalances. There are different control approaches, which are designed to implement VSG. Some of the approaches try to implement all the attributes of SG making the algorithms complicated [133-135]. However, some approaches consider only essential attributes of SG to be implemented in VSG and achieve the intended control goals. For instance, the iterative method of swing equation is considered in [110], droop control is implemented in [136] and power-sharing is made possible by VSG control in [137]. For an in-depth comparison of VSG and SG, interested readers are recommended to read [138].

Despite the similarities existing between VSG and SG, there are also some differences existing between them as:

- VSG controls do not give instantaneous inertial response as SGs do. VSGs provide an inertial response after a dead band limit [67, 139].
- VSG frequency response services depend solely on the capacity of the ES system associated with them and other control characteristics to emulate inertial response. In this way, they depend on the tuning of these parameters to respond to frequency events properly [67, 139].

Also, the VSG topologies experience some challenges for their application in the modern network as:

- VSG controls mainly rely on a phase-locked loop (PLL) to detect the grid voltage, phase angle and frequency. This is one of the main drawbacks in achieving a complete converter dominated grid as the presence of SG is still crucial to provide reference values [105].
- Another drawback of this invention is lacking power reserve for RESs used in VSG to ride-through under large oscillations [140]. Although this problem has been addressed in [116, 121] by using ES systems, the limited capacities of ES systems are still challenging.

Table 2.1 categorises different topologies of synthetic/virtual inertia proposed by different researchers. For each category, the table summarises generalized advantages and disadvantages for each approach. Besides, related references for further reading are also provided for each topology.

Table 2.1

Categories of synthetic/virtual inertia technologies in power systems

Synthetic inertia category	Pros	Cons	Topologies included in the category	Ref.
Synchronous generator emulation	Use inverter together with ES systems to mimic an SG behaviour	Instability problems led by the use of PLL	Synchronverters	[103, 129, 141]
	Imitate traditional behaviours of an SG in the operation of the power system with high penetration of the converter based RESs	Difficult to implement complex differential equations		
	Able to self-synchronize in the grid	Prone to numerical instabilities	VISMA	[61-63]
			Kawasaki Heavy Industries (KHI)	[9, 41]
Swing equation	Control the inverter of a DG unit together with ES systems to support inertial response	Prone to numerical instabilities	Ise Lab topology	[9, 41, 110]
	Use the swing equation of the SG within the control algorithm to develop a virtual inertia	Difficulty in obtaining accurate control parameters	Synchronous Power Controller (SPC)	[142]
Frequency-power response	Emulate the inertial response characteristics of an SG during power system dynamics	Not applicable for island mode	VSG	[143]
	Use DGs as dispatchable sources	Inaccurate frequency derivative data from PLL	VSYNC lab topology	[15, 48
	Implement control strategies with short-term energy buffers	Instability due to sensitivity in noise		
Other topologies	Use conventional active power droop controls to implement inertial response for converter-based power systems by imitating the behaviours of the Synchronous/Induction generators	Respond slowly to transients	Droop-based topology	[104, 120, 144]
			Virtual oscillator control (VOC)	[145]
			Inducverters	[9, 146, 147]

2.5.2 Application of synthetic inertia for frequency stability in power systems

Several approaches have been proposed to imitate the inertial behaviour of SG involving a combination of RESs, ES systems, power electronic converter and control algorithms as

described in the previous sub-section. The simplified concept of how VSG is analogous to the conventional synchronous generator in the grid is presented in Fig. 2.6. To make it clearer from the figure, distributed generation (DG) is analogous to the prime mover in the conventional power system, while the inverter altogether with the controls (not shown in the figure) represent the VSG. The VSG can imitate the properties of a synchronous generator by utilizing the ES systems for feeding or absorbing power to or from the grid during power imbalances, respectively [138].

Using proper control algorithms to the inverter together with ES systems as proposed in [54, 57, 102, 109, 114, 136, 148, 149], distributed generation units can mimic the performance of synchronous generators such as damping, power droop and inertia. Fig. 2.7 shows a simplified general basic operating principle of the synthetic inertia provision by a VSG. From the figure, the algorithm to control the inverter in the provision of virtual inertia depends solely on the information from the grid. The phase-locked loop (PLL) is used to collect the grid information such as frequency response that is used to decide how much virtual inertia should be supplied to respond to the frequency change. Fig. 2.8 describes how virtual inertia provision is generally achieved in the network. The virtual inertia algorithm shown in Fig. 2.8 controls the ES systems to provide frequency support in terms of virtual inertia into the network for any power imbalance. K_{VI} represents the control gain of virtual inertia in (s) while K_P is the constant that emulates damping in the power network in (MW/Hz). Besides, T_{VI} stands for the time constant in (s) for the dynamic model of the ES system. The control algorithm of the VSG model can be realized by using the swing equation, which is used to describe the relation of inertia, damping and rotor angular velocity of SG [122, 150, 151].

It is worth stressing that from the control principle of SG; it is noted that active power is regulated by controlling the power angle between the SG internal voltage and the voltage at the point of common coupling (PCC) of the grid. A similar control approach can be imitated for VSG to mimic the electromechanical dynamics of the SG to regulate the active and reactive power of the inverter.

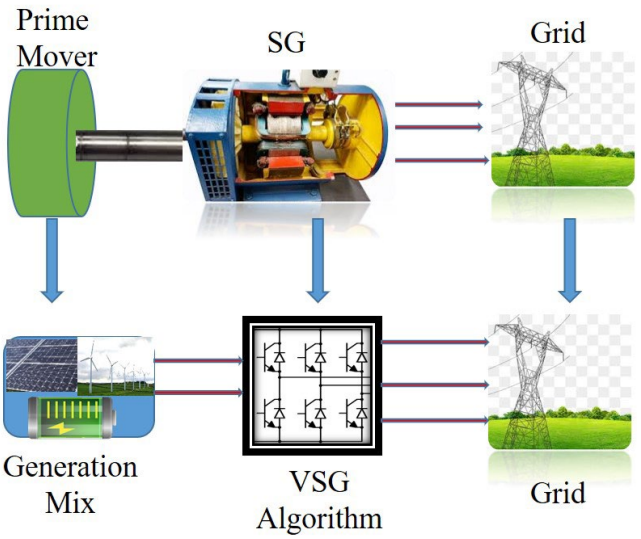

Fig. 2.6 Analogy of VSG with conventional SG

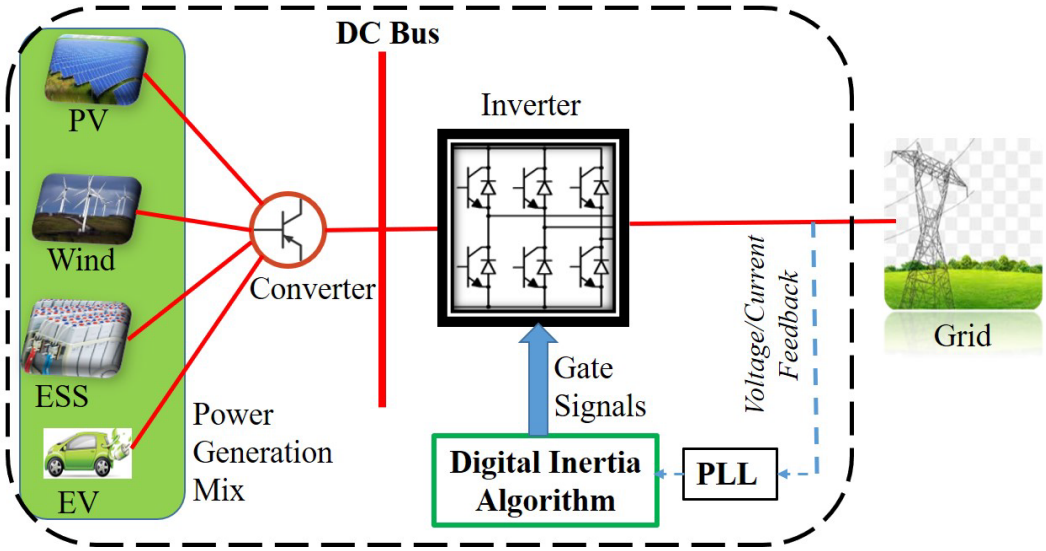

Fig. 2.7 General inverter-based virtual inertia emulation in grid

It is also known that the dynamics of an SG are governed by the swing equation as it ensures that stability is adhered to if accelerating power is zero [107]. Using a virtual inertia algorithm, the swing equation can be executed mathematically to implement the behaviour of an SG in the inverter. As mentioned in the previous sub-section, power converter with ES systems can be controlled to provide synthetic inertia in the grid as generally demonstrated in Fig. 2.7. The point of focus from Fig. 2.7 is the use of grid information to generate an algorithm for providing virtual power for frequency response. The derivative control of grid frequency is mainly used to provide a virtual inertia component to the grid in case of more penetration of RESs. In case of any power imbalance that leads to frequency deviation, the VSG control will deliver the desired virtual inertial power ΔP_{VSG} as shown in (2.3) [115]

$$\Delta P_{VSG} = K_{VI}\frac{d\Delta\omega}{dt} + K_P\Delta\omega \tag{2.3}$$

where $\Delta\omega = \omega - \omega_o$ and ω_o is the nominal frequency of the grid in (rad/s). Using the control gain of virtual inertia K_{VI} in (s), the product K_{VI} and derivative of frequency deviation $\frac{d\Delta\omega}{dt}$ in (rad/s^2) as $K_{VI}\frac{d\Delta\omega}{dt}$ is the power to be injected or absorbed depending on the position of frequency deviation from the nominal value. K_P is the constant that emulates damping in the power network.

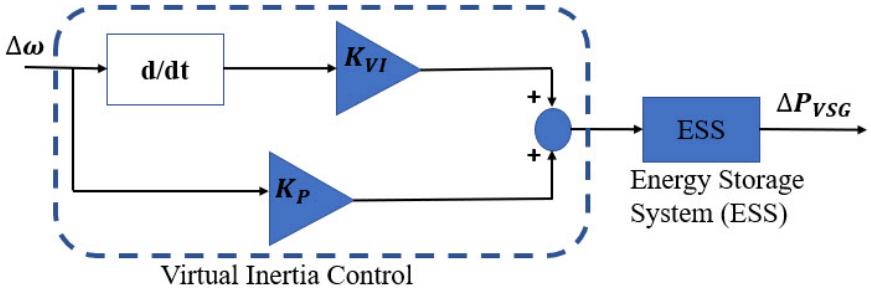

Fig. 2.8 Virtual Inertia provision and control in grid

To mitigate the problems related to increasing levels of RESs connected to power systems and, hence, replacing conventional generators, synthetic inertia has shown much potential to reduce the problems [152, 153]. One of the important benefits of synthetic inertia in the power system is to encourage more penetration of RESs. When VSG exists in the network with conventional synchronous machine inertia, this means the equivalent inertia in the network will comprise two components. The two components are conventional inertia (H_S) and synthetic/virtual inertia (H_{VI}). Therefore, the conventional equation to compute for equivalent inertia in the system can be further modified to include the synthetic inertia (H_{VI}) as presented in (2.4) [71].

$$H_{eq} = \frac{\underbrace{\sum_{i=1}^{N} H_i \times S_{B,i}}_{H_S} + \underbrace{\sum_{j=1}^{V} H_{VI,j} \times S_{B,j}}_{H_{VI}}}{S_B} \tag{2.4}$$

where, H_i and $S_{B,i}$ are the inertia constant in (s) and rated power in (MVA) of the i^{th} synchronous generator, N is the total number of SGs connected to the network and S_B is the base power in (MVA) of the system. $H_{VI,j}$ and $S_{B,j}$ are virtual inertia in (s) constant and rated power in (MVA) of the j^{th} virtual synchronous machine, V is the number of the virtual synchronous machine connected to the network.

2.5.3 Case study of virtual inertia application for frequency stability in the power system

To describe the application of virtual inertia on frequency stability in the power system, a complete model set-up representing the network with penetration of RESs is given in Fig. 2.9. The network comprises both conventional synchronous generator inertia and synthetic inertia. To incorporate the penetration of RESs, active powers from combined solar and wind power plants are increased by equivalently 20%. This penetration of RESs replaces equally active power generation from the conventional generator. Therefore, inertia associated with this replaced conventional generation is also reduced from the network. Finally, the virtual inertia provision is activated with different levels of K_{VI} constant in the network to evaluate the improvement of frequency response as a result of increased penetration of RESs.

Fig. 2.10 demonstrates network frequency responses with different case scenarios. To start with, the frequency response is simulated with the only conventional synchronous generator in place. Then, a low inertia scenario is activated with a 20% penetration level of RESs and the SG inertia is reduced equivalent to the RESs active power added into the network. Finally, VSG is implemented with different levels of K_{VI} to study its impacts on frequency response in networks with penetration of RESs.

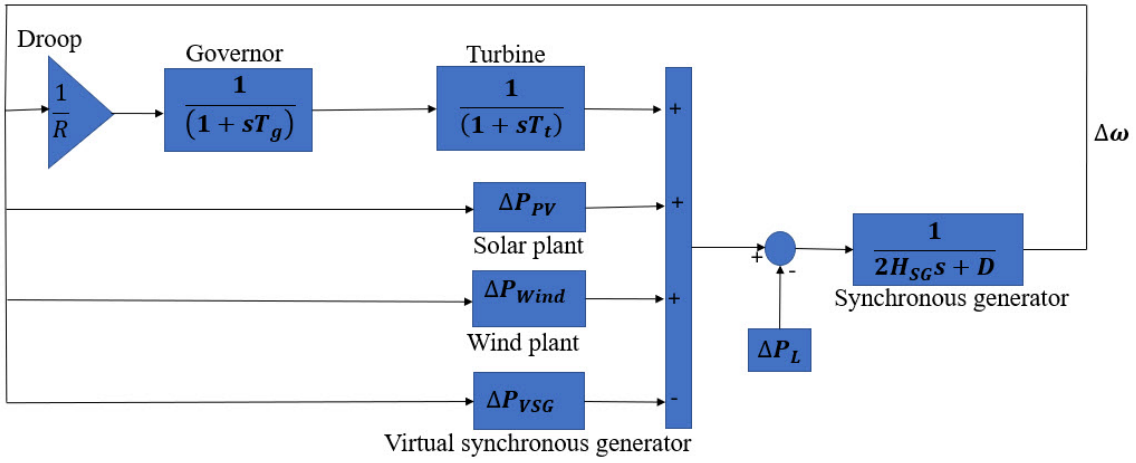

Fig. 2.9 Power system model to show the impact of VSG on the frequency response of a network with penetration of RESs

From the simulations represented in Fig. 2.10, different scenarios are presented. The responses show how inertia affects frequency response in the network. To be more precise, it can be noted how the penetration of RESs affects both RoCoF and the peak value of the frequency after disturbance. Finally, the introduction of VSGs, with different K_{VI} constants, displays the improvement in RoCoF, the frequency peaks and settling time as the figure signifies.

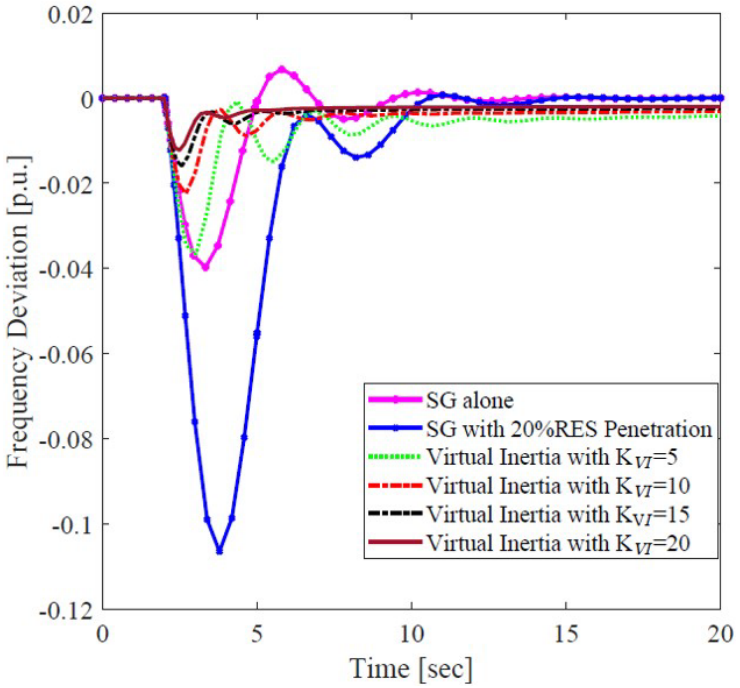

Fig. 2.10 Frequency responses with different scenarios of inertia in the power system

2.5.4 Significance of synthetic inertia in frequency stability control

So far, synthetic inertia has proven practical potential to stabilize frequency response in low inertia networks. The inertial response it provides by rapidly injecting/absorbing power to mitigate fast RoCoF events and out-of-limits frequency deviations is crucial as seen in Fig. 2.10. The value of synthetic inertia is noticed during the response period of the system after imbalance. This inertial response period is very essential in frequency stability as it is described as the "buying" or "waiting" time before primary frequency control comes into action. Making this time adequately long is very important for the secure operation of the network. Delaying synthetic inertia provision beyond frequency nadir or peak may result in severe stability issues. Therefore, synthetic inertia controls should be designed in such a way that they provide their services before frequency peaks or nadirs to avoid frequency stability issues in the network.

To explicate the concept of when synthetic inertia has to take action in the stability and flexibility control of the power system after a contingency, the time scale of the frequency response and frequency control for the conventional network are provided in Fig. 2.11 (a) and (b), respectively. From Fig 2.11 (b), the position at what time scale the synthetic inertia is supposed to come into play during frequency contingency is presented. The frequency response presented with a red solid line in Fig 2.11 (a) represents a response at a low synchronous inertia while the dotted line represents a response with additional synthetic inertia. Synthetic inertias are faster than primary frequency control but slower than the conventional SG inertia, which reacts instantly after power imbalances. Therefore, if coordination algorithms of SG inertia with synthetic inertia in the modern grid are

developed, they will ensure the secure operation of the power system even with high penetration of non-synchronous RESs.

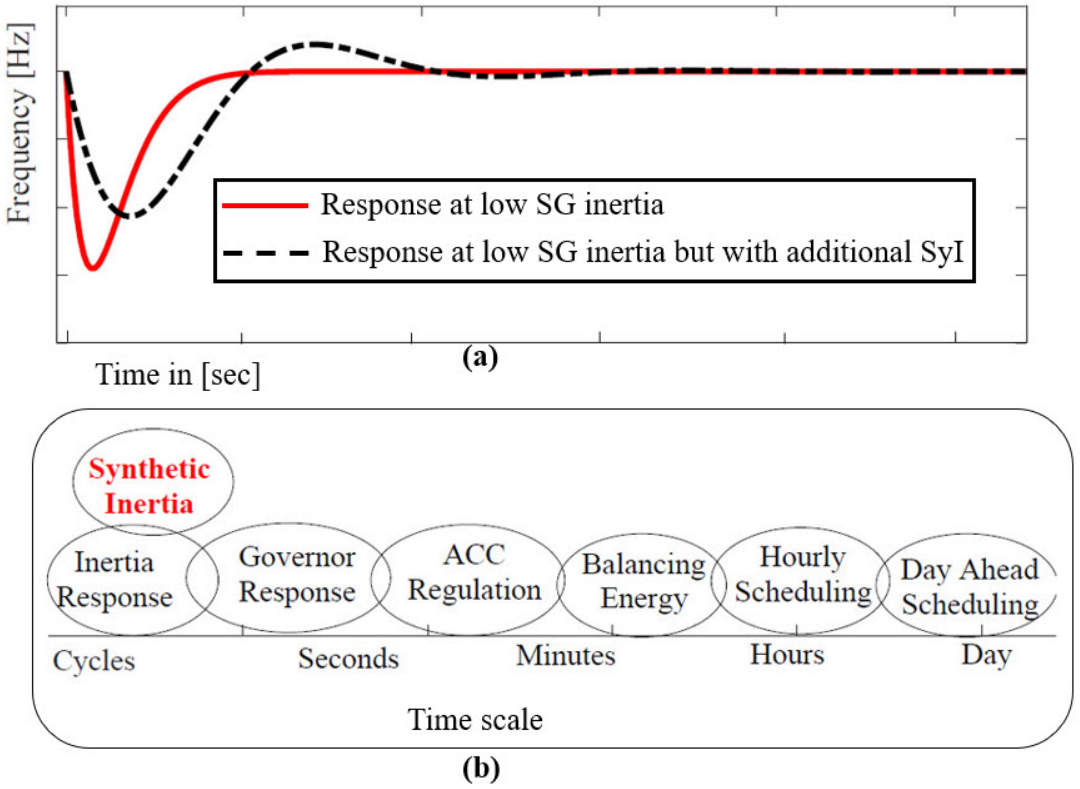

Fig. 2.11 (a) Frequency responses at a low synchronous inertia with and without additional synthetic inertia and (b) Time scale showing the synthetic inertia during frequency contingency

To link with the response time of synthetic inertia, Table 2.2 compares different ES systems with new power generation technologies, which are used with control techniques to provide inertia, can fast respond to frequency variations in the grid. Understanding the different response times of these different technologies is crucial to achieving quality synthetic inertia provision designs in the power system. This discussion shows that synthetic inertia is essential in maintaining frequency stability in reduced mechanical inertia networks. Since primary controls can take up to seconds to be activated, synthetic inertias show that they can be activated before the primary frequency control.

Table 2.2

Different inertial source technologies with their response times [154, 155]

Technology	Activation Time
Lithium Batteries, Flow Batteries, Super-Capacitor	10-20 ms
Lead-Acid Batteries	40 ms
Wind Turbine with Virtual Inertia Response	40 ms
Solar PV and ES systems	100-200 ms
Flywheels	≤ 4 ms

2.5.5 Synthetic inertia versus fast frequency response debate

To smoothly go through this part, it is good to recap on the inertia concept in the network. As described before, inertia is responsible for reacting instantly to system frequency changes as a result of any disturbance in the power balance in the network [60]. On the other hand, RESs that are connected to the grid via converters do not contribute to instant inertial response as SGs do. In that regard, RESs do not contribute to mechanical inertia in the system. Consequently, they do not instantly or naturally release or absorb energy as a result of frequency change. However, they depend on controllers, which control ES systems to release or absorb energy during frequency variation to mimic the performance of SGs [60]. Thus, from conventional frequency theories, mechanical inertia from SGs can directly determine the initial RoCoF, while synthetic inertia cannot. However, initial RoCoF in the network is used to determine how much synthetic inertia is needed to support the frequency during contingencies.

A debate, therefore, arises on how synthetic or virtual inertia is perceived in the network. There have been different opinions of the term depending on the context. Many studies do not make a clear distinction between virtual inertia and fast frequency response. After becoming aware of this misunderstanding, a research study [60] introduced a distinction between these terms to avoid their misuse. The term synthetic inertial response must, therefore, correspond to the controlled response from a generating unit to mimic the exchange of rotational energy from a synchronous machine with the power system. Any other form of fast controlled response can, then, be termed as fast frequency response. To elucidate more, synthetic inertial response is a subset of fast frequency response, which contains different responses based on frequency and RoCoF.

Finally, the explanations of synthetic inertia and fast frequency response from the European Network of Transmission System Operators for Electricity (ENTSO-E) and [60, 156] clearly defined these two terms as follows: “Synthetic inertia is the controlled contribution of electrical torque from a unit that is proportional to the RoCoF at the terminals of the unit; while

fast frequency response is the controlled contribution of electrical torque from a unit, which responds quickly to frequency changes to counteract the effect of a reduced inertial response."

2.6 Inertia estimation techniques in power system

It is well known that the inertia constant for the conventional power system, in general, is a constant and steady quantity. Based on the prior knowledge of the constant inertia value in the conventional network that is defined by (2.4), the frequency response of the network can be anticipated and assessed before a disturbance occurs in the network. However, inertia in modern and future networks with high penetration of RESs will not only become low but also time-varying as clarified in the preceding sections. For this reason, it can be said that inertia in the modern grid is becoming a dynamic quantity. Therefore, dynamic inertia can be defined as a time-varying of the total inertia value in the power system caused by the extensive use of stochastic synthetic inertia to support frequency response in low mechanical inertia systems. The stability problems related to low and dynamic inertia in the network have been discussed in the previous sections. To account for stability problems related to low values and dynamic inertia, increased awareness regarding this quantity has been given priority in the network [157]. Prior estimation and monitoring of this quantity are essential for planning purposes and therefore for the secure operation of the power system. Since inertia affects the network frequency response just after the contingency, its prior understanding and management in the system are critical.

To attain this goal of understanding the value of inertia in the network, several studies such as [11, 14, 84, 114, 158, 159] have been conducted to establish algorithms to estimate the value of inertia constant in the network. Different methods of inertia estimation in the literature can be classified into three main categories, namely: offline, online, and predictive estimations. Different approaches are used interchangeably in these categories to estimate the inertia constant in the network. Of these three categories, most of the studies have been conducted on offline and online categories [11, 14, 84, 158-162]. Very little has been done on predictive inertia estimation [19, 163-165].

The inertia estimation has been made possible by significant advancements in measurement systems, which have been of potential in the power network for tracking real-time measurements of the entire network. As a result of this advancement in measurement technology, phasor measurement units (PMUs) have been widely installed to record operating conditions in power networks. The recorded information is very crucial for inertia estimation purposes in the network.

2.6.1 Offline inertia estimation approaches

Most of the offline estimation techniques are post-mortem approaches. This means the offline inertia estimation techniques are used to study and evaluate the values of inertia constant

in the network after occurrences of contingencies. They can tell how much inertia was available during significant disturbance incidents [159]. Most offline approaches use historical data that is recorded using the PMU. Information such as active power and frequency behaviour post power imbalance events are used to estimate the inertia in the network. Some of the proposed techniques that use post-event disturbances can be found in [15, 166]. Of the offline studies, some studies [14, 15, 84, 158, 159] use records of major disturbances to establish the estimation algorithm, while other approaches [11, 162] use normal operating conditions of the network to establish estimates of inertia values in the network.

However, there are challenges associated with the offline inertia estimation process in the network. These challenges are results of poor frequency measurements, which are coupled with oscillatory components and noises mainly during transients [84]. Polluted frequency measurements lead to inaccurate calculation of RoCoF and, hence, poor inertia estimation. To address the problem, Refs. [14, 167] introduced some techniques to eliminate measurement noise and oscillations that distort the RoCoF calculations. On the other hand, locating the exact time of disturbance in the network has been another challenge to look at. When disturbance time is not exactly located in the network, the alignment of RoCoF and the corresponding disturbance (ΔP) will be inaccurate. This further leads to inaccurate inertia estimation in the network. This drawback motivated research work in [84] to be conducted on moving average filter and the research work in [167] to be focused on detrended fluctuation analysis to locate the time of disturbance in the network towards inertia estimation.

Nevertheless, most of the techniques introduced in this field do not precisely consider the effects of the penetration of RESs in the estimation process. As pointed out in the previous sections, modern and future networks will be highly penetrated with inertia-less power generation units. The effects of the stochastic nature of these non-synchronous generation units have to be taken into consideration when estimating the inertia constant of the network. The problem associated with penetration of stochastic RESs is the complexity introduced in the network that is not taken care of by the conventional equations to handle the dynamics of the modern network.

2.6.2 Online inertia estimation approaches

The need for real-time inertia estimation in the network has been gaining popularity for almost a decade now. The motive behind this move to online inertia estimation is the move to time-varying inertia values in the network due to the high penetration of RESs and fast frequency response devices in the network. Due to this need, several online inertia estimation methods have been proposed in published works. The proposed methods have different techniques and algorithms in achieving real-time inertia estimation in the modern and future power system.

Most of the proposed methods use PMUs to record real-time measurements from the network. The recorded measurements are used for the online estimation of the inertia constant in different perspectives. Examples of the methods that use PMUs as sources of network measurements are such as [17, 168-171]. Some of the approaches used for inertia estimation are such as dynamic regressor extension and mixing on time series data [172]. Other methods with time series modal approaches are proposed in [11, 170]. In Ref. [171], a robust Kalman filter is used with the derivative of the linear discrete-time state-space form to online estimate the inertia of a network. Other methods such as that are proposed in Ref. [173] use autoregressive data centred models, which can describe the dynamic evolution of the power system inertia. Furthermore, a method using a sliding discrete Fourier transform (SDFT) technique to online estimate the inertia of the network is proposed in [174]. On the other hand, Ref. [175] used the approach of electromechanical oscillation modal extraction from synchronized ambient data to online estimate the inertia of the power system.

Like offline inertia estimation approaches, online approaches also face some challenges in the estimation process. First, measurement errors in PMU due to noise are the main source of large estimation errors. Although filtering techniques are employed in some methods, the accuracy is not satisfactory in some of the methods [11]. Second, most methods consider only inertia from synchronous generators in their analysis. Therefore, there is an underestimation of the total inertia of the network as the demand-side inertia contribution is not considered in most research works [20]. Third, some proposed methods are irrelevant for online applications as they take a long time to give inertia estimation from the time the imbalances are detected in the network. The time taken for modal analysis, execution, inertia extraction and finally sending the inertia value to operators is very long making them irrelevant for network protection. Normally, the protection decision needs to be made very quickly after the occurrence of the contingency in the network. Fourth, the huge network model and a large amount of time series data involved in most of the proposed methods lead to significantly large computational burdens. Updating the huge network models at high sampling rates and respectively updating a large amount of time series data make the methods very slow [18, 176].

2.6.3 Inertia prediction approaches

There is also an increasing need to forecast the values of inertia constant in the network. The instantaneous reaction of inertia after power imbalance in the network gives no time for frequency control schemes to safeguard the stability of the network [20]. Unanticipated low network inertia conditions and inadequate frequency response reserves could pose a serious risk to the reliability and security of the grid. Therefore, the anticipation of network inertia is becoming important in modern and future power systems. Prediction of time ahead network inertia is

essential for PSO to plan for alternative sources of inertia in the network in anticipation of reduced inertia. Forecasting inertia values in the network will determine when the network will be at risk, and appropriate measures can be taken well in advance. As synthetic and other fast frequency response reserves are likely to be tradeable quantities in the future network, contractual arrangements to procure these services can be planned as inertia values can be forecasted in the network [9, 20]. However, there is not much research done on this area. Ref. [19] shows the need for the prediction of network inertia by proposing a prototype tool to forecast system inertia and to assess the sufficiency of frequency response reserves. Using the ERCOT network, inertia was forecasted, and fast frequency reserves could be planned well in advance. The need to predict system inertia as one of the major attributes to assess the operational impact of non-synchronous machines on a power grid is justified in this literature. Besides, Ref. [164] proposes a short-term kinetic energy forecast using a decomposable time series model approach. Using the Nordic network, they could predict the kinetic energy of the network one hour ahead of time with a forecasting error of 5%. Also, a two-stage stochastic generation and primary frequency response scheduling model is proposed in [165] to predict the network inertia for primary frequency response adequacy under uncertain wind generation. Using the ARIMA model in scenario generation and reduction of wind power uncertainty, this research could forecast the inertia of the system one day ahead. However, this one-day ahead inertia prediction would need further research to justify. Furthermore, an artificial neural network approach to forecast the network inertia with high penetration of wind farms is recently proposed in [177]. As noted above, to ensure that the stability and flexibility of the modern and future grids are maintained, there is a need to research more on inertia prediction in the power system. The prediction of inertia values would be essential for predictive controllers in the power system.

2.6.4 General observations of system identification as used in inertia estimation techniques

Complicated interconnected power networks involving various stochastic components are very difficult to model and analyse using conventional mathematical models. Due to such complexities, modern grids become very difficult to be represented using conventional mathematical equations to fully model all stochastic elements in the network. Even the mathematical equations, which have been developed to represent these complicated stochastic networks, are also complex. Hence, they cannot be easily used to represent the time-varying behaviours in networks. Besides, complex equations are difficult to use in real applications such as control system design. Traditionally, mathematical modelling of power networks involves formulating mathematical models of every single significant component individually in the network. The mathematical models using the single component modelling method result in large and complex overall models that are very difficult to analyse [101, 178].

Given the complexity of the modern and future power systems due to the high penetration of RESs, system identification is the alternative approach to analyse the modern network [179-181]. System identification can be easily achieved using online recorded data of the network. Therefore, it can be said that an alternative way to represent complex modern networks is the data-centred system identification approach [182-184]. This approach has been useful to the power system industry in several ways. Initially, it can validate the complex system models by being able to modify the parameters of those models so that they best fit the actual measured performance of the network [185]. Moreover, the approach can also be used to benchmark system behaviour [180]. Real-time performance of the data-centred system identification approach can further provide system operators with valuable knowledge about the stability situation of the system [184]. In addition to its advantages, the system identification approach can be used even if the inside structure of the system is not known. The measured input and output data in the system identification approach provide useful information about the system behaviour [180, 181, 184]. Thus, mathematical models can be generated to explain the dynamics of the system of interest from observed input-output data.

To summarize the data-centred system identification and inertia estimation approach, Fig. 2.12 is presented. Inertia estimation based on the data-centred system identification approach solves the challenge of inertia estimation solely depending on recorded data for large disturbances only.

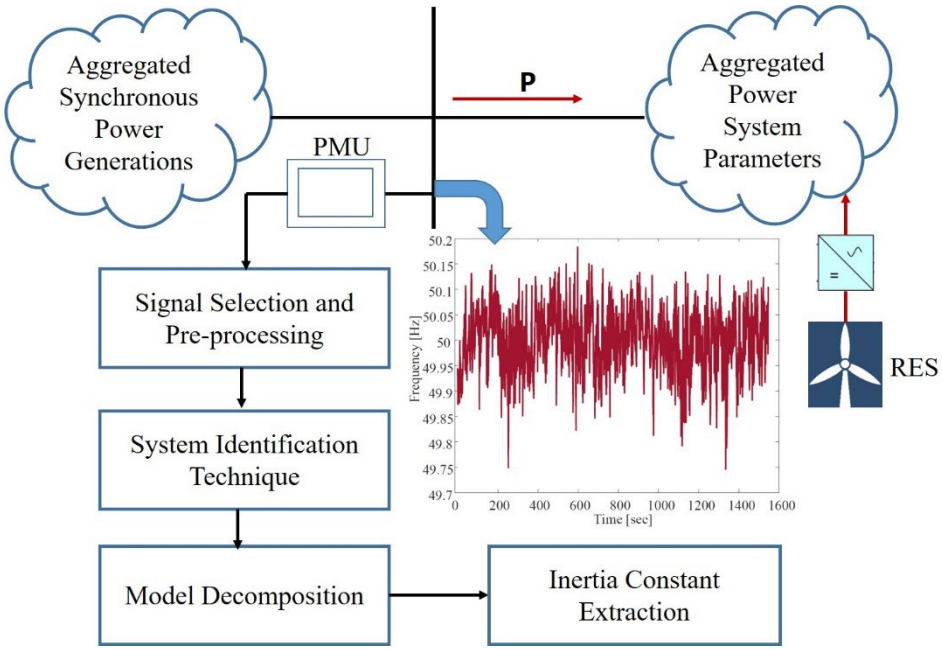

Fig. 2.12 Data-centred system identification and inertia estimation approach

PMUs that are presented in Fig. 2.12 can record a substantial volume of data in real-time. The recorded data contains adequate electromagnetic response information that is required for transient analysis [186]. The data recorded contain an input signal that is used as an exciting signal

just enough to cause a response to the system. For this reason, normal ambient data of the network can be used for the continuous inertia estimation process. To be specific for the case of inertia estimation in the power system, the signals of interest are the active power and frequency changes as input and output signals, respectively. The two signals are sampled and then used for system model identification [187]. Some techniques such as linear regression and least-squares estimate are then used to decide the validity of the estimated model and optimise the parameters associated with the estimated model of the system. The identified system models are usually high order models, which are complex to analyse and compute. Therefore, some decomposition techniques such as singular value decomposition (SVD) are further used to not only simplify the analysis but also reduce the computation burden associated with the models [188]. From the decomposed model, inertia can be extracted and communicated to PSO for planning and control purposes.

Due to some improvements in addressing the challenges associated with the inertia estimation process, some studies have been put in place to estimate the inertia constants of some countries and regions as presented in Table 2.3. For instance, Ref. [14] used reliable data from PMU to estimate the inertia constant of the Great Britain network. In [84], frequency measurements from 10 disturbance based events were used to estimate the inertia constant of the Japanese power system. Furthermore, frequency measurements from a centre of inertia (COI) point in the network were used in [158] to estimate the inertia constant of the Western Electricity Coordination Council (WECC) system. Last but not least, the Nordic region network was researched for inertia estimation in [161] where a comparison of the following two approaches was done. The COI frequency for the whole network approach was compared by dividing the network into 12 areas, and the COI frequency for each area was used to estimate the inertia of the whole network. It was noted that the estimation using COI of the divided areas gave a more accurate estimation compared with one COI for the whole network.

Table 2.3

Inertia estimation techniques used to estimate the inertia of different networks

Network	Inertia estimation approach	References	Year
Great Britain	An offline approach using PMUs to record events from different locations of the network	[14, 189]	2014, 2016
Japan	An offline approach using ten transient events	[84]	1997
Nordic	An online approach using real-time measurements power plants in the Nordic network	[161]	2015
Western Electricity Coordination Council (WECC)	An offline approach using several year historical data of frequency, load and outage events to determine the network inertia.	[158]	2004

Table 2.4 summarises different inertia estimation techniques in power systems. It extracts important features of each technique from different sources and analyses pros and cons.

Table 2.4

Inertia estimation techniques classifications [20]

Estimation category	Description/ application	Pros	Cons	Refs.
Offline	Inertia estimation techniques depending on large disturbances historical data of the network	• Can estimate inertia available at a specific disturbance • Can simultaneously estimate system inertia and determine the size of disturbance • Can use frequency and voltage responses to estimate system inertia • Can estimate inertia of multiarea interconnected networks	• The size of the disturbance to be known • Time of events to be known • Post-mortem approaches • Errors in RoCoF calculation due to noise affect accuracy • No continuous estimation •	[7, 11, 12, 14-16, 159, 186, 190, 191]
Online	Inertia estimation techniques that use real-time measurements of the network as inputs for estimations	• Can estimate real-time network inertia • Can use PMU measurements to estimate inertia • Give continuous inertia of the network • Can use normal operating conditions of the network	• Inaccuracy due to measurement errors • Slow and not reliable for online estimation due to long execution time • Impractical for online estimations due to large computational time because of large network models	[162, 168-170, 172, 175, 192]
Forecast	Inertia estimation techniques that predict the future system inertia to predict the frequency response of the network ahead of time	• Can plan stability control schemes well in advance • Determine when the network will be at risk • Plan procurement of synthetic inertia and fast frequency response reserves • Can increase situational awareness for more RESs integration in the network	• Challenges to include inertia contribution from the demand side in the forecast • Limited to short-time forecast • Prediction accuracy affected by stochastic weather change and noise in the measurements	[19, 163-165, 177, 193]

2.7 Discussion and future trends

2.7.1 Overall summary of inertia behaviour in modern and future power system

Fig. 2.13 summarizes the whole discussion of this literature survey. From traditional power systems theories, it is understood that inertia constants from synchronous generators in the system are generally constant. There is no substantial variation in inertia present in the system over time. As a result, this known conventional inertia constant can provide an adequate initial inertial response when imbalances happen in the system. In that way, conventional inertia provides enough time for primary controls to act on the contingency [15, 42].

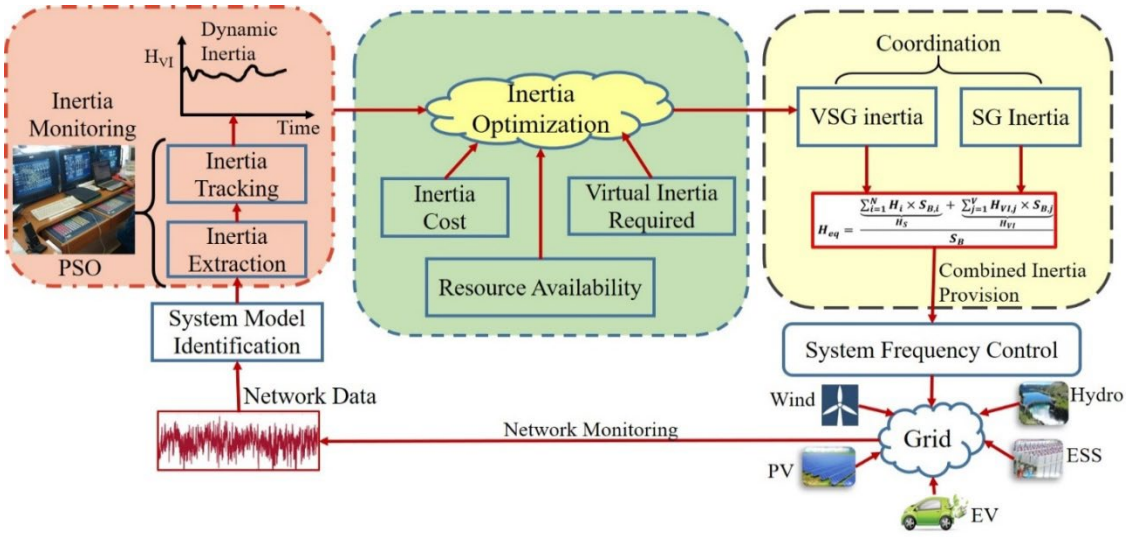

Fig. 2.13 Concept of inertia monitoring, coordination, and optimisation in modern and future power systems

As stochastic RESs keep on replacing more synchronous machines from the power system, some concerns need to be addressed. Many synchronous machines with their related inertia will be replaced when weather conditions favour provisions of RESs. Nevertheless, power supply by stochastic RESs to the grid depends primarily on resources availability such as irradiance, wind speed and state of charge (SOC). Consequently, integrated stochastic RESs make power balancing in the grid more difficult. As a result of problematic power balancing, costs for power balancing are getting higher as more RESs are integrated into the grid. The UK, for instance, spends £1 billion a year balancing the grid, and it was projected to double by 2021 [194]. Unfortunately, all these power balancing related costs are reflected in the customers' energy bills [195, 196].

This trend is, therefore, raising the concern of continuous power imbalances in the system [142, 197]. In fact, in addition to power imbalance problems, the stochastic nature of RESs is

resulting in frequency control being unpredictable, hence, exposing power system stability at risk. The unpredictability of system frequency is due to the total system inertia becoming a time-variable quantity. Therefore, time-changing inertia in modern networks is becoming difficult to monitor and control, unlike in the traditional system [15, 76]. The generation mix dispatched at any point in time primarily affects the total inertia present in the system.

In connection to challenges brought by high penetration of stochastic RESs, many power system operators (PSO) are concerned about how to deal with low and time-changing inertia issues in the future grid. This concern intends to establish adequate levels of inertia at any point in time to guarantee system stability by alerting PSO and give valued support for adaptive frequency control schemes [15, 198]. To this point, it is essential to model system inertia as a time-dependent variable that needs to be integrated with PSO and control for fast and guaranteed frequency control [42].

2.7.2 Inertia monitoring in modern and future power systems

As discussed in the preceding sections, RoCoF after a disturbance in the network is informative when discussing the impact of effective inertia on the stability of the power system. Before governor control is initiated, the frequency response due to power imbalance in the network is largely influenced by the system effective inertia (H). High inertia systems have low RoCoF $\left(\frac{\Delta f}{\Delta t}\right)$, which is very important for stability control in the power system [42]. High inertia values ensure governor controls are initiated before frequency reaches critical values. In contrast, low inertia systems have high RoCoF, which is risky for maintaining stability in power networks and can lead to cascading failures in the network. Since inertia is becoming a time-varying quantity due to penetration of stochastic RESs, estimation and monitoring of time-varying inertia values in the network are crucial as described in Fig. 2.13. Prior knowledge of the time-varying inertia values in the network will be very useful in assessing the frequency response before contingencies happen in the network. This will further help to ensure planning, operation, stability control of the network as well as optimisation of inertia values in the system. The prior estimation of inertia values at any given time would become a key input to adaptive control and security applications in the network.

2.7.3 Coordination of SG and VSG inertia in power networks

It has been observed that VSG are very supportive in frequency response in the networks with low inertia. The fast-virtual active power injection/absorption in the system by VSG to recover a system frequency following a disturbance is very crucial in the network. However, the fact that VSG inertia solely depends on the capacity of the ES systems behind them limits their applications. Consequently, conventional SG should be held in place to work together with VSG during disturbances. To avoid maloperation between SG and VSG inertias in the network, they

need to be coordinated to operate smartly as seen in Fig. 2.13. Besides, the coordination between SG and VSG inertias leads to the economical utilization of these two quantities for frequency support in the power system. If individual values of either SG inertia or VSG inertia are not adequate to damp the fast frequency response, then, they can be used simultaneously and in a coordinated way when disturbances occur. All this effort is to ensure that the operation of the network is not only reliable and secure but also economical.

If a scientific approach of coordination of SG and VSG is laid in place, it will encourage more penetration of VSG in the network for frequency control purposes. Interconnection techniques and specifications between SG and VSG should be developed to address inertial response, power control and frequency regulation. Additional research is required to standardize basic needs in these interconnection techniques and specifications. In this regard, areas to be looked at are regulation policies, size and operation technology of VSG, reserve margins and synthetic inertia to be considered as a tradeable commodity to mention a few research aspects.

2.7.4 Optimisation of VSG in networks

Accurately predicting the network inertia values in advance is a fundamental aspect in planning for frequency response. This aspect introduces another concern of optimal values of synthetic inertia from inertia emulating resources as highlighted in Fig. 2.13. Achieving optimal inertia values would assist to accurately control stability issues for weather-related power imbalances in the network. Although there have been several proposed control algorithms to make RESs and ES systems participate in inertial response in the grid [112, 141, 199], none of them has been able to accurately propose an optimal value of synthetic inertia provision during imbalances. There is a need for developing a systematic approach to determine optimal virtual inertia values in responding to frequency events in power systems. These optimal values of virtual inertia will co-exist with well-established conventional mechanical inertia in the grid for frequency stability control.

Furthermore, VSG has been introduced to emulate the inertial behaviour of a conventional synchronous generator. To achieve inertial emulation, inverter-based distributed energy resources (DERs) used as VSG need some kind of temporary energy storage systems similar to that of the rotating mass of the rotor of a synchronous generator. Due to limitation in temporary and dynamic energy storage systems, VSG provides constant values of inertia and damping constants during grid dynamics to decrease frequency deviation and the RoCoF [39-41]. However, the use of more flexible and optimal values of virtual inertia constants for frequency response in modern and future power systems would be more advantageous [114]. Therefore, VSG with control techniques that would provide dynamic and optimal values of inertia and damping constants would address this challenge in frequency control. Incorporating wind and PV

data would also be useful in this research direction to attain accurate inertia constant estimation for proper power system operation and planning [200, 201].

2.7.5 Future Trends

As the move towards more renewable energy resources integration to the grid is limited by reduced mechanical inertia, more penetration of stochastic RESs can lead to stability issues in the grid. With this challenge, there should be a limit of stochastic RESs capacity to be integrated into the grid. However, the introduction of synthetic inertia has been a potential move towards replacing mechanical SG inertia and, therefore, increasing the penetration of stochastic RESs to the grid. If further studies and improvements are performed in the virtual inertia research area, they would promise attainment of a more renewable and flexible grid in the near time to come.

To make the move attainable, there is a need to focus on different challenges, which are still unsolved in this research direction. It is noted that most of the stochastic RESs are interfaced to the grid via power electronic converters. The fast control algorithms on converters allow stochastic RESs with ES systems to respond to system dynamics faster than primary frequency control of conventional power plants. Since power electronic converters depend on the speed of the controllers, there is a serious concern that they may not be effective instantly after the contingency. In other words, power imbalances in the system cannot be naturally addressed by a power electronic converter, which is subject to delays. Consequently, the natural synchronous generators instant inertial response is still of most importance. Therefore, there is a need to carry out more research in this area to make synthetic inertia respond as fast as possible.

Another area to focus on is the limitation of reserve power delivery from RESs to provide primary frequency control. This has been a serious limitation for stochastic RESs, especially when they are operated at their maximum power points. If more research is done in making the RESs participate in primary frequency control by ensuring sufficient reserve margin, it would be a significant contribution towards more penetration of RESs in the power system. Adequate reserve margin can help power system ride-through during power contingencies. On the contrary, the currently existing insecurity due to incapability of reserve power delivery by RESs is a major limiting factor for more penetration of RESs. Enough reserve power delivery by RESs would ensure RESs participation in the primary frequency control. Therefore, this aspect needs to be addressed in future research works.

Moreover, existing stability theories, which were established several decades back such as the swing equation, do not hold when incorporating both SG and VSG response to frequency change. The conventional equations do not reflect the new stochastic generation units and new dynamic loads, which are recently penetrating the network. This issue also needs a dedicated platform to develop new theories, which will consider all stochastic behaviours of the modern and

future grid with the presence of both SG and VSG. If this platform is well achieved, it will ensure flexibility and reliability of the grid with more penetration of RESs.

Also, the inertia that is primarily provided by the conventional synchronous generators is apparently treated as a free resource. As the power network is now transitioning to converter based, there is a need for conventional inertia and synthetic inertia to be treated as tradeable commodities. A proper market framework for these resources is an effective approach to ensure their availability for power system stability control and power quality management. This is also an open area for more research to be done.

Finally, weather forecasting studies related to power imbalances, as a key factor in system stability studies, is another research area to work on. As more power generation units in the network are weather dependent therefore stochastic, there is a need to focus on the weather forecast and integrate this data to PSO to plan for power balances in the network. Predicting power imbalances due to weather forecast in the network is useful for the controller design to ensure stability control of the network is maintained.

2.8 Conclusion

This paper has presented an intensive review of the role of inertia for ensured stability and flexibility of the modern and future grid. The challenges related to low inertia in the network have been reviewed. Various proposed solutions to address these challenges have been discussed. Further possible research areas to address the challenges in future networks have been proposed. In short, to fully enjoy the benefits and opportunities of the new power generation technologies, the conventional grid must transition to a dynamic interactive real-time infrastructure that is more flexible and efficient to accommodate stochastic generation units. The benefits of a flexible grid, which include management of power balance, enhanced network reliability and optimised asset utilization, are guaranteed with proper control of the parameters of the network such as frequency. As conventional synchronous generators are getting replaced in the grid transformation, synthetic inertia is a centre of discussion for this grid transformation. Therefore, proper estimation, monitoring, coordination, optimisation, and management of synthetic inertia related to conventional mechanical inertia may guarantee the achievement of a flexible modern renewable grid soon. To achieve this massive transformation, research areas with challenges suggested in future trends need to be researched more to get useful solutions for implementation. These altogether can ensure the attainment of a complete renewable grid, which is environmentally friendly.

Chapter 3 Publication 2: Offline Inertia Estimation

Preamble

One of the challenges explained in Chapter 2 is inertia analysis in networks with high shares of RES. The time-changing inertia can cause rapid frequency fluctuations leading to significant challenges in the power system. Prior knowledge of the system inertia will help operators apply appropriate measures and more suitable control schemes to mitigate stability issues. Therefore, to address this issue, Chapter 3 presents a method to offline estimate network's inertia. The proposed method is a data-driven that estimates the time-varying inertia in the network based on the frequency gradient of the estimated model of the network. The approach uses phasor measurement units (PMUs) to measure network data and then estimate the network's dynamic model. Based on the system identification approach, the model estimate of the power system is identified, and then the estimated inertia is extracted. While the proposed method can easily analyse the network dynamics, it is also developed using the decomposition technique that reduces the computation burden.

Data-driven inertia estimation based on frequency gradient for power networks with high penetration of RES

Peter Makolo*, Ifedayo Oladeji, Ramon Zamora and Tek-Tjing Lie

Department of Electrical and Electronic Engineering, Auckland University of Technology, Auckland 1010, New Zealand

Abstract: The time-changing inertia can cause rapid frequency fluctuations, which are major challenges in power system. Prior knowledge of the system inertia will help operators to apply appropriate measures and more suitable control schemes to mitigate stability issues. This paper, therefore, proposes a data-driven method to estimate the time-varying inertia in the network based on frequency gradient of the estimated model of the network. In this approach, phasor measurement units (PMUs) are used for measurement of network data, which is then used to estimate the dynamic model representing the network. Based on system identification approach, the model estimate of the power system is identified and then the estimated inertia is extracted. The benefits of the proposed method include reduction of high order model to low order model to avoid computation burden, coordinated inertia extraction from the low order model using gradient mapping on RoCoF of the system response and, more importantly, estimation of inertia constant of the network using normal operating conditions contrasted to other approaches using large disturbances to estimate the inertia in networks. The effectiveness of the technique has been tested using numerical simulations of IEEE 39-bus network modelled in DIgSILENT™ PowerFactory® tool and real data from the actual New Zealand power system.

3.1 Introduction

3.1.1 Motivation

Synchronous generators have been an integral part of power systems for several decades. They have been used conventionally to generate active power, to regulate frequency and voltage, and to provide inertia in power systems [42]. The power system's inertia potentially determines the ability of the network to maintain stability when subjected to power imbalances. More specifically, power system inertia is vital in compensating for variations and disturbances up to 5 seconds after the contingency [42, 162]. Although the inertia is important only in the first instants after the occurrence of power imbalance, its impact is very crucial in the network as it determines the stability of the network.

In recent years, there have been numerous factors that have intensified the interest in finding low carbon energy sources for power generation. On this note, vastly available renewable energy sources (RESs) are a promising solution to the global energy demand crisis. In this way, RESs are increasing their shares to the grid. Gradually, the electric power generation sector is under transition to be comprised of both conventional synchronous generators and stochastic electric power generations such as solar PV and WTs. These RESs will make significant contribution to the power system [32, 73, 202]. Thus, the rapidly growing stochastic RESs are likely to replace some of the traditional synchronous generators in the future power networks. For instance, the value of inertia constant for Great Britain grid was estimated to be 9s in 2008 and it was projected to drop to as far as 3s by 2020 due to high non-synchronous RESs penetration [203]. Furthermore, Australia has anticipated to retire coal generation and replace them with full RESs by 2030 [204].

3.1.2 Literature review

The constant replacement of synchronous generators by RESs is changing the conventional property of the traditional power system [205]. It is also worth to note that weather conditions impact most of RESs that are integrated into the network, and therefore, affecting the number of synchronous generators to be committed in the network over time. Consequently, inertia that is supplied by synchronous generators in the network will likely be a time-varying quantity. Therefore, if the system inertia constant (H) becomes highly variable with time, then, the rate of change of frequency (RoCoF) after a disturbance will also become highly variable and unpredictable with time [186].

To this point, conventional approaches that are mainly used to calculate the inertia constant of the network comprised of mainly synchronous generators may fail to provide accurate values of equivalent inertia constant of the network with significant penetration of non-synchronous RESs. Failure to identify the actual values of power system inertia constant at a

particular time may lead to challenges on the planning, operation, and control of the power system. Recent challenges related to failure of identifying and anticipating the actual inertia values in the network are blackouts in the UK's grid and Spanish Island of Tenerife [206]. More challenges on high penetration of non-synchronous RESs in the modern power system have been discussed in [35, 47-49].

Regarding these trending challenges of increasing RESs in the power system, there is a rising need for estimating and hence monitoring time-varying values of power system inertia constant for stability control purposes [10, 11]. Tracking the dynamic values of power system inertia will provide valuable information to power system operators (PSO) on how much and how fast frequency will respond and deviate after a disturbance. This information is important as it will provide alert, and hence, appropriate measures can be taken in advance to mitigate the effects of unpredicted/blind frequency response. Prior assessment of frequency response will help in implementing more compact control schemes for system stability [12, 13].

The inertia estimation can be conducted either online or offline. For offline inertia estimation, network data that is stored for a certain period of time is processed at once for estimation. The one-time processing of data for offline estimation is contrary to online estimation where the system model is updated each time data is available. Therefore, for the sake of analysing the behaviour of the system in advance, offline inertia estimation approach can be used.

Although inertia estimation has been carried out in the network from a long time ago, the techniques used previously may not, however, work for modern, complex, low, and time-varying inertia networks. Some of the techniques used previously include the famous power system inertia constant estimation using probing test [182, 207] and transient test [208], which all of them estimate the inertia constant of the networks mainly consisting of synchronous generators. As the modern grid is becoming more complex due to more integration of inertia-less RESs, hence, leading to low and time-varying inertia constant, these techniques may no longer be applicable in estimating the inertia constant of the power system. Even though other methods have been developed in recent years such as in [209], most of them are grounded on post-mortem analysis after large frequency events.

In [175], inertia estimation is tackled by using an electromechanical oscillation model; while in [191], measurement based on a variable order model inertia estimation technique in AC microgrid is proposed. Unfortunately, the variable order model requires big data of measurements making the whole process slow in real application. Similarly, Ref. [210] uses energy storage and system identification approach to estimate the inertia of system. However, the method could not be verified as it only uses a genset model, which is not realistic when considering a complex modern power system with several heterogenous components. In addition, the method proposed in [170] suffers from computational problem as it uses large and complex network model. Though

Ref. [7] suggests an approach to reduce computation burden, it overestimates network model and, therefore, missing out important dynamics of the network. On the other hand, the method in [211] has a drawback of interruption during changing and updating the equivalent system model when considering addition or elimination of a generator or load in the system. Updating the model for every event makes the method insignificant for extension to online inertia estimation. A problem of reduced accuracy due to phase step issues as explained in [212] makes the inertia estimation technique proposed in [213] impossible for extension to online inertia estimation approach. Although Ref. [168] develops an online inertia estimation technique using phasor measurement units (PMUs) together with finding the dynamic modes by employing the swing equation, it does not consider the effect of time-varying inertia due to high penetration of renewable energy sources in modern networks. Therefore, there is a need to develop a new inertia estimation technique, which considers time-varying inertia, does not suffer from phase step issues and has low computation burden.

3.1.3 Novelty of this paper

This paper, therefore, proposes a data-driven inertia constant estimation based on frequency gradient technique. The technique uses phasor measurement units (PMUs) to record power system's normal operating conditions. The novelties of the proposed method are:

a) Using time-domain data with small disturbances in estimating the dynamic model of the power system. This is contrary to conventional approaches, which need to have large disturbance events such as load rejection and line switching in inertia estimation.

b) Applying a decomposition technique to reduce unnecessary high orders of the model estimate from system identification approach, which makes it not only easy to analyse the RoCoF but also reduces computation burden.

c) Employing coordinated frequency gradient mapping on the RoCoF of the system's frequency response makes it easy to estimate and extract inertia from the estimated network model.

The remaining parts of this paper are structured as follows: The importance of inertia in power system dynamics in relation to frequency stability is discussed in Section 2. Section 3 presents the data-driven based on frequency gradient technique for estimating inertia values in the network. Testing the applicability of the technique and analysing the results on IEEE 39 – bus network numerical simulations is discussed in Section 4. Validation of the proposed technique on the real network data is presented in Section 5. Finally, Section 6 concludes the discussion and briefly highlights the future work.

3.2 Inertia in power system frequency stability

The power system inertia potentially determines the ability of the network to maintain or lose stability when subjected to power imbalances [42, 43]. It specifically resists frequency changes due to power imbalances in the network [162, 214]. Generally, the conventional swing equation for a single generator system describes the dynamics of power and frequency during a short time power imbalance as seen in (3.1) [215].

$$\Delta\omega = \frac{1}{2Hs + D}(\Delta P_m - \Delta P_e) \tag{3.1}$$

where $\Delta\omega$ is the deviation in the rotor speed, ΔP_e represents the active electrical power deviation, ΔP_m denotes the mechanical power deviation, H is the inertia constant, D is the damping coefficient and s denotes the Laplace transform operator. When the mechanical input power of the generator is not changed, ΔP_m becomes zero and the frequency deviation will be affected by the active electrical power deviation only. Then, (3.1) can be restructured as (3.2) [162].

$$\frac{\Delta\omega}{\Delta P_e} \approx -\frac{1}{2Hs + D} = G(s) \tag{3.2}$$

where $G(s)$ is the transfer function from ΔP_e to $\Delta\omega$. When (3.2) is normalized with respect to the unit values, the rotor speed deviation can be represented by the rotor frequency deviation for low frequency values as shown in (3.3).

$$\Delta f \approx \Delta\omega \tag{3.3}$$

where Δf represents the frequency deviation of the generator. In this case, the transfer function $G(s)$ in (3.2) can now be written as (3.4).

$$G(s) = \frac{\Delta f}{\Delta P_e} = -\frac{1}{2Hs + D} \tag{3.4}$$

Generally, D has no impact on the RoCoF as it only determines the damping of oscillations after disturbance [11, 56, 215]. To this point, when phasor measurement units (PMUs) are used for measurement of the network's input active power variations (ΔP_e) and frequency response variations (Δf), a data-driven system estimation approach can be used to obtain the estimate of the transfer function of the network and, hence, to estimate the parameters of the network, such as inertia constant.

Traditionally, for a multi synchronous generators network, the equivalent inertia constant of the entire network is calculated using the conventional equation as provided in (3.5).

$$H_{eq} = \frac{\sum_{i=1}^{N} H_i \times S_{B,i}}{S_B} \tag{3.5}$$

where H_{eq} is the equivalent inertia constant of the entire network, S_B is the base power of the system, H_i and $S_{B,i}$ are the inertia constant and rated power of the i^{th} synchronous generator, respectively, and N is the total number of synchronous generators connected to the network.

Furthermore, for a multi-generators network, it is possible to aggregate the network and assume the network to behave as a single generator [11]. This is done by aggregating all the generators to have a single value of active power as well as centre of inertia (COI) frequency. When a network is aggregated, its (COI) is used. The COI frequency of the entire network is calculated by (3.6) [158].

$$f_{COI} = \frac{\sum_{i=1}^{N} H_i \times f_i}{\sum_{i=1}^{N} H_i} \tag{3.6}$$

where, f_{COI} is centre of inertia frequency of the network, H_i and f_i are the inertia constant and frequency of the i^{th} synchronous generator, respectively, and N is the total number of synchronous generators connected to the network. This approach is used in this research when considering a multi-generators network, which is discussed in subsequent Sections.

It is also established that when all rotating masses of the network are aggregated into a single mass, it can be shown that, following an active power disturbance (ΔP), the frequency deviation from nominal frequency is given by (3.7) [186].

$$\Delta f(t) = \left(1 - e^{-\frac{D}{M}t}\right)\frac{\Delta P}{D} \tag{3.7}$$

where t is the time in seconds from the start of the disturbance, Δf is the frequency deviation in p.u. of nominal frequency (f_0), $M = 2H$, (M is the system aggregated inertia coefficient), D is the damping of the system and ΔP is the active power disturbance in the network (i.e., loss or increase of load or generation). Differentiating (3.7) and evaluating for H at $t = 0$ for small time interval (Δt) gives (3.8).

$$H = \frac{\Delta P}{2\frac{\Delta f}{\Delta t}} \tag{3.8}$$

Equation (3.8) is informative when discussing the impact of effective inertia on power system stability. Before governor control is initiated, the frequency response due to power imbalance in the network is largely influenced by the system effective inertia (H). High inertia systems have low RoCoF $\left(\frac{\Delta f}{\Delta t}\right)$, which is extremely useful for stability control in power system [42]. High inertia values in power system ensure that governor controls are initiated before frequency reaches critical values. On the contrary, low inertia systems have high RoCoF, which is risky for maintaining stability in power networks [42, 43]. High RoCoF in a low inertia system causes the frequency to quickly reach unsafe values and trigger the protection system before governor control is initiated [214, 216]. Since inertia will be time-varying due to high penetration of stochastic renewable energy sources, estimation and hence monitoring of time-varying inertia

values in the network is crucial. Inertia estimation will provide essential information to power system operators for planning, operation, stability control of the network as well as optimisation of inertia values in the system. The estimated inertia values at any given time would become a key input to adaptive control and security applications in the network.

As can be seen from this Section 2, it is possible to use power variations and frequency responses data of the power system to estimate the system model. From the estimated model, equivalent inertia of the network with specific penetration of RESs and possibility of presence of synthetic inertia can be extracted. For offline inertia estimation, time-invariant transfer function system identification approach of the network can be employed [7, 11, 162, 170, 186].

3.3 Synthetic inertia approach for frequency control in grid

This Section describes the proposed inertia estimation technique using model estimation of the power system. In this proposed technique, power system data is obtained from the network using PMUs, which are commonly installed in modern power systems. The recorded data is used to estimate the transfer function model of the network as described in the next subsection 3.1.

3.3.1 System's model estimation

It is assumed that a sequence of PMUs measurements represented as input vector $(u_0, u_1, u_2, \ldots . u_m)$ and output vectors $(y_0, y_1, y_2, \ldots . y_m)$ are obtained from a power system. Furthermore, the measurements are assumed to be uniformly sampled with the sampling frequency f_s and, therefore, sampling period $T_s=1/f_s$. The value of time t at a discrete time index k is given by $t_k=kT_s$. These data vectors can be used to find the estimated model to represent the system and the system parameters. The obtained system parameters determine how the model gives a good fit to the measurement data used. This whole procedure of using network's data to estimate a model that represents the system is called system identification.

During system identification and estimation process, there may be some noises from the PMU measurements. Noise may corrupt PMU measurement data and lead to a poor performance of a proposed method. In signal flow analysis, noise term can be represented in the measurement signal covariance $v(t)$ by a straightforward but completely valid approach to postulate its model. The measurement signal covariance containing noise is modelled by $v(t) = H(z, \theta)e(t)$ with $e(t)$ being the white noise with variance λ while $H(z, \theta)$ is the ratio of the output to input signal sequence in z-domain with θ parameters of the system model [179]. By resampling the signals and observing the signal data spectrum, the frequency range where noise is detected in the data can be identified. Based on the identified frequency range where noise is detected from the data, a smoothing filter (moving median) is designed to remove the noise.

To get started with system identification procedure, a linear parametric system in terms of a transfer function $G(s)$ in (3.9) is supposed to be the hypothesis of a general transfer function needed to estimate its parameters.

$$G(s) = \frac{b_{n-1}s^{n-1} + b_{n-2}s^{n-2} + \cdots + b_0}{a_n s^n + a_{n-1}s^{n-1} + \cdots + a_0} \tag{3.9}$$

where b_k (for *k = 0* to *n-1*) and a_m (for *m = 0* to *n*) represent the parameters of the system in the numerator and the denominator, respectively. $n-1$ and n represent the highest orders of the operator "*s*" in the numerator and the denominator, respectively. As previously mentioned, measurements of input and output data sets can be used to estimate the parameters of the hypothesis transfer function $G(s)$.

It is worth mentioning that the data collected from the system are discrete data sets. Therefore, to use the discrete data samples for model identification, the *s* domain transfer function (3.9) needs to be transformed to *z* domain as given in (3.10).

$$G(z) = \frac{b_1 z + b_2 z^2 + \cdots + b_m z^m}{1 + a_1 z + \cdots + a_{n-1} z^{n-1} + a_n z^n} \tag{3.10}$$

whereby $a_1 \ldots a_n$, $b_1 \ldots b_m$ are system parameters, n and m are real numbers, while z is a backward shift operator. To be able to incorporate different data samples into the equation to estimate the parameters of the hypothesis transfer function, (3.10) needs to be in a difference equation form. Thus, the associated difference equation of (3.10) is given by (3.11) [179].

$$y(k) + a_1 y(k-1) + \cdots + a_n y(k-n) = b_1 u(k-1) + \cdots + b_m u(k-m) \tag{3.11}$$

From (3.11), *y(k)* is the output discrete data sample at time index *t=k*, while *u(k-1)* is the input discrete data sample at time index *t=(k-1)*. Equation (3.11) can be rearranged to obtain (3.12).

$$y(k) = -a_1 y(k-1) - \cdots - a_n y(k-n) + b_1 u(k-1) + \cdots + b_m u(k-m) \tag{3.12}$$

In a more compact way, (3.12) can further be simplified to (3.13).

$$y(k) = [-y(k-1) \ldots -y(k-n)\ u(k-1) \ldots u(k-m)] \begin{bmatrix} a_1 \\ \cdot \\ \cdot \\ \cdot \\ a_n \\ b_1 \\ \vdots \\ b_m \end{bmatrix} \tag{3.13}$$

From (3.10), the order *m* for the numerator and *n* for the denominator of the transfer function $G(z)$ determine how many parameters to be identified. These quantities are proportionally related. The higher the value of transfer function order, the higher the number of parameters to be estimated, as seen from (3.13). Therefore, the rows of a vector obtained from the vector difference equation are determined by the number of data points used in the experiment. If

N data points are available for the experiment and only *l* data points are used, i.e., (*l* < *N* and *l* > *n*), then, general matrices (3.14) - (3.16) are defined to represent the vector equations of measurements data and system parameters, respectively.

$$\boldsymbol{Y_l} = \begin{bmatrix} y(n) \\ \vdots \\ y(l-1) \end{bmatrix} \tag{3.14}$$

$$\boldsymbol{X_l} = \begin{bmatrix} -y(n-1) & \cdots & -y(0) & u(n-1) & \cdots & u(0) \\ \vdots & \ddots & \vdots & \vdots & \ddots & \vdots \\ -y(l-2) & \cdots & -y(l-n-1 & u(l-2) & \cdots & u(l-n-1 \end{bmatrix} \tag{3.15}$$

$$\boldsymbol{\Theta} = \begin{bmatrix} a_1 \\ \vdots \\ a_n \\ b_{n-m} \\ \vdots \\ b_n \end{bmatrix} \tag{3.16}$$

Combining (3.14), (3.15) and (3.16) as a means of representing (3.13) with vectors of several data points (*l*) will result in (3.17). Equation (3.17) is a general representation equation, which connects several input and output discrete data sets of the system with system parameters to be estimated.

$$\boldsymbol{Y_l} = \boldsymbol{X_l}\,\boldsymbol{\Theta} \tag{3.17}$$

When all *N* data sets available from the experiment are used in (3.17), i.e. $l = N$, it yields (3.18), which is similar to (3.17) but with more data sets used. Using as many data sets as possible is highly recommended since it makes (3.18) to be an overdetermined equation and therefore unknown system parameters can be easily identified [179].

$$\boldsymbol{Y_N} = \boldsymbol{X_N}\,\boldsymbol{\Theta} \tag{3.18}$$

$\boldsymbol{Y_N}$ and $\boldsymbol{X_N}$ are known vectors of experimental data sets for system identification and $\boldsymbol{\Theta}$ is a vector of unknown model parameters to be estimated. Then, this linear algebra problem can be solved to obtain the estimate of system parameters. Furthermore, the obtained system parameters are optimised by using the cost function and the least square estimation technique, which is given as in (3.19).

$$\boldsymbol{\Theta}^* = \boldsymbol{X_N^{\dagger}Y_N} = \left(\boldsymbol{X_N^T X_N}\right)^{-1}\boldsymbol{X_N^T Y_N} \tag{3.19}$$

where $\boldsymbol{\Theta}^*$ is optimised system parameters, and $\boldsymbol{X_N^{\dagger}}$ is a pseudoinverse matrix, which is given as $\left(\boldsymbol{X_N^T X_N}\right)^{-1}\boldsymbol{X_N^T}$. In this way, estimated and optimised parameters of the system model can be obtained. Therefore, the procedure provided here can be used to estimate a model of any system based on data sets of input and observed output of the system.

3.3.2 Estimated model order reduction

Generally, large dataset-driven system identification approaches result in a large and complex model with very high degree of freedom of the network. These high orders models are

not only complex to analyse but also cause high computational burden [217]. In addition, high order models are related with noise contents in their frequency response leading to erroneous in inertia estimation [168]. That is why an application of model reduction techniques is important. However, some approaches extremely reduced the model order that leads to loss of information, hence, errors in inertia estimation process. For example, Ref. [162] proposed to estimate the transfer function model of the network by the first order model to finally estimate the inertia. The optimal model order that gives best fit result for power system ranges between 4 – 20 [218]. The reduced model should be estimated in such a way that it captures essential dynamics of the system. For this reason, the obtained model is decomposed to low optimal order that captures necessary dynamics of the network. The technique used in this approach to obtain optimal order reduction is singular value decomposition (SVD). The singular value decomposition is applied on the oblique projection vector, which is given in (3.20) [183].

$$\boldsymbol{O_i} = \triangleq \boldsymbol{Y_N} \,/\, \boldsymbol{W_p} \tag{3.20}$$

whereby $\boldsymbol{W_p} = \begin{bmatrix} X_N \\ Y_N \end{bmatrix}$

Therefore, SVD is given as (3.21).

$$\boldsymbol{W_1 O_i W_2} = \boldsymbol{U \Sigma V^T} \tag{3.21}$$

where $\boldsymbol{W_1}$ and $\boldsymbol{W_2}$ are the identity weighting matrices, $\boldsymbol{U}$ and $\boldsymbol{V}$ are orthogonal matrices, while $\boldsymbol{\Sigma}$ is a diagonal matrix with real entries. Furthermore, SVD can be written as matrix multiplications by (3.22). Then, when significant singular values are detected in matrix $\boldsymbol{\Sigma}$ as σ_1, the reduced order of a system is selected and presented as σ_1 [183].

$$\boldsymbol{U \Sigma V^T} = [U_1 \;\; U_2]. \begin{bmatrix} \sigma_1 & 0 \\ 0 & \sigma_2 \end{bmatrix}. \begin{bmatrix} V_1^T \\ V_2^T \end{bmatrix} \tag{3.22}$$

where U_1 and U_2 are the components of $\boldsymbol{U}$, while V_1 and V_2 are the components of $\boldsymbol{V}$, σ_1 and σ_2 are the generated singular values of the system model after decomposition process.

The reduced and optimal order obtained in (3.22) as σ_1 is used to represent the reduced optimal transfer function $G'(s)$ as in (3.23).

$$G'(s) = \frac{b_{n-1}s^{\sigma_1 - 1} + b_{n-2}s^{\sigma_1 - 2} + \cdots + b_0}{a_n s^{\sigma_1} + a_{n-1}s^{\sigma_1 - 1} + \cdots + a_0} \tag{3.23}$$

3.3.3 Inertia extraction

It should be noted that in multi-input multi-output system models, it is possible to determine the inertia of the whole system using the COI frequency of the network. The COI frequency is obtained by finding the average area frequencies weighted by inertia of each area [158], as given in (3.6). In this way, when a disturbance is applied to the identified reduced model $G'(s)$, a frequency response whose RoCoF depends on the equivalent inertia value of the network will be obtained. For this purpose, an active power disturbance is applied to the estimated reduced

model and the corresponding response is the network frequency at the COI bus. It should also be noted that the identified and reduced transfer function model $G'(s)$ representation of the network is valid if the model cross-validation works perfectly.

Therefore, if estimated reduced model transfer function of the system $G'(s)$ is subjected to a unit step signal, namely, *ΔPi = u(t)*, where u*(t)* is the unit step function, then Δf can be expressed as (3.24).

$$\Delta f(t) = \frac{1}{D}\left(1 - e^{-\frac{D}{2H}t}\right) \tag{3.24}$$

The gradient of the function in (3.24) at $t = 0$ is given by (3.25).

$$\left.\frac{d\Delta f}{dt}\right|_{t=0} = \frac{1}{2H} \tag{3.25}$$

The given gradient in (3.25) can be used to determine the inertia constant of the network if the RoCoF (the initial gradient of the frequency response of the network) can be recorded just after the disturbance. It is also proved from [158] that using a curve fitting technique is effective in mitigating the impact of measured transients following a contingency. Otherwise, the calculated RoCoF may be substantially higher than the true value. It is also known that recording RoCoF is challenging as it is related to some noise content in the signal [168].

Therefore, to smoothen and filter $\frac{d\Delta f}{dt}$ towards inertia estimation process, a modified window method as proposed in [159] is incorporated at this stage. Since the estimated network model is subjected to a unit step function from zero steady state, only one window is used in this approach as the frequency response is tracked just after disturbance at $t = 0$. The window used to track the frequency at non-zero steady state in [159] is ignored as the average steady state for this case is normally zero. Interested readers can refer [159] for further reading. In this case, the average gradient of the frequency is given by (3.26).

$$Gradient_1 = \frac{1}{A}\sum_{t=0}^{t_e}\frac{d\Delta f(t)}{dt} \tag{3.26}$$

where each window has *A* data points. Therefore, each window has a width of (A-1)Δt, where Δt is the time interval between two adjacent data points, t is the time at the start of the window while t_e is the time at the end of the window. In this way, average RoCoF is obtained as $Gradient_1$. Therefore, inertia can be estimated as (3.27).

$$H = \frac{1}{2 \times Gradient_1} \tag{3.27}$$

where $Gradient_1$ is obtained at $\left.\frac{d\Delta f}{dt}\right|_{t=0}$. Equation (3.27) suggests that inertia constant (*H*) of a network can be calculated by the initial gradient of the unit step response of the estimated model.

The following steps summarize the procedure for inertia estimation using the proposed technique:

Step 1: An exciting input signal is applied to the system. This input signal should be small active power variations just enough to cause frequency responses (output signal) of the system but not interfere with normal operating conditions. It should be within normal operating conditions of the system.

Step 2: The applied input signals with the output signals are sampled using acceptable sampling time to obtain data samples.

Step 3: Collect sequence of input vector $(u_0, u_1, u_2, \ldots . u_m)$ and output vector $(y_0, y_1, y_2, \ldots . u_m)$ or $u_k \in \mathbb{R}^{l\times 1}$ (vector of input data) and$y_k \in \mathbb{R}^{l\times 1}$ (vector of output data), for time index *k,* where $k = 0,1,2,\ldots N$.

Step 4: Use the data samples with a linear model hypothesis to estimate the system parameters. Select the model that best fits the data sets of the system using the system identification procedure.

Step 5: Use cost function and least squares estimate with the estimated model in step 4 to optimise the parameters of the system.

Step 6: Decompose the high order estimated model using singular value decomposition SVD method to reduce the order of the identified system model.

Step 7: Subject the reduced order transfer function model to a unit step function *ΔPi = u(t).* Apply the modified window method to obtain the gradient of the frequency response.

Step 8: Extract the estimate of the system's inertia constant by using (3.27).

Fig. 3.1 summarizes the proposed method. The figure shows that the aggregated network with penetration of RESs can be used to estimate the inertia constant of the network. In practice, the total active power (P) and the centre of inertia (COI) frequency (f) can be measured by the PMUs installed at each generator connection bus. Therefore, in this approach, the aggregated information from all PMUs are used to identify the dynamic model of the system using *P* as the input and *f* as the output.

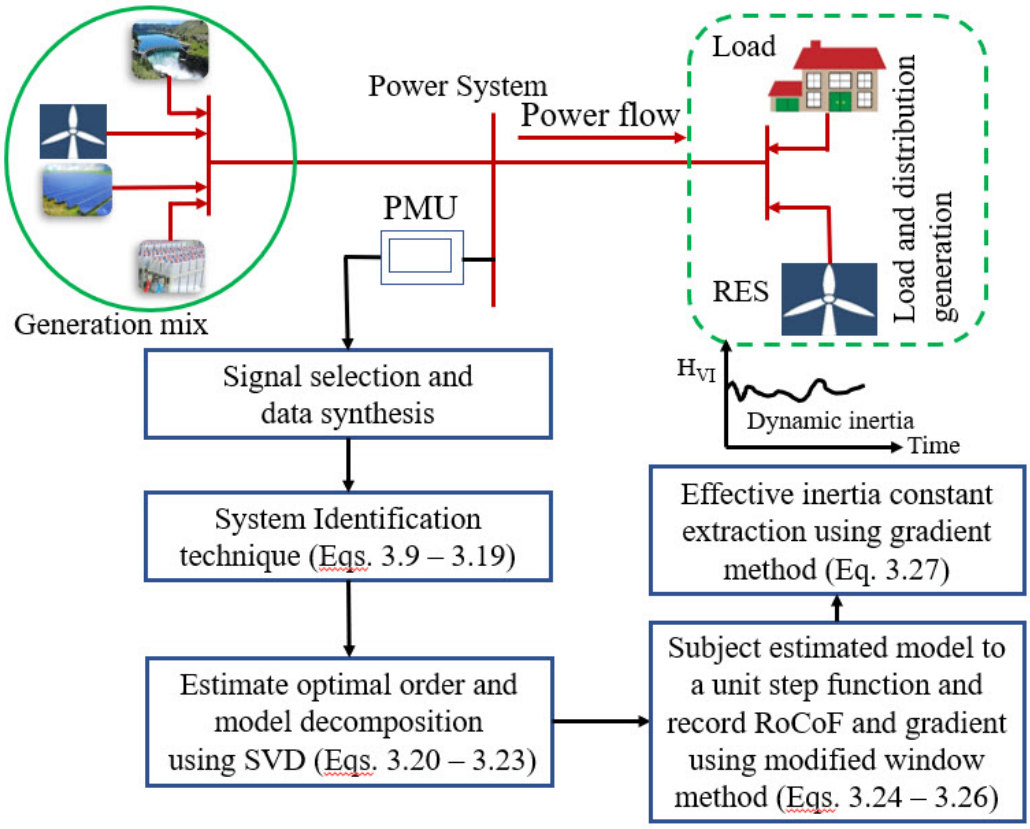

Fig. 3.1 Flow diagram for data-driven inertia estimation process

3.4 Simulation case study: IEEE 39 bus network

The method presented in this paper is tested using modified IEEE 39–bus network modelled using DIgSILENT™ PowerFactory® 2019 tool. The network comprises of 39 buses, 10 generators, 12 transformers, 34 lines and 19 loads. The single line diagram of the test network is presented in Fig. 3.2.

The test network is used to generate data sets for the inertia constant estimation process. The moving median smoothing filter with a default sampling frequency of 100 Hz is applied to filter any noise detected in the generated data. Known actual theoretical values of inertia constant *(H)* are set in synchronous generators of the network and the technique is used to estimate the value of equivalent inertia constant in the network. To capture transients of the network, root mean square/electro-magnetic transient is set in PowerFactory® as the simulation type. The network is aggregated to behave like a single generator network and all the PMUs measurements from all load buses are aggregated to have a single value of active power as well as frequency as measured from the COI. Equation (3.6) is used to locate the relatively good COI frequency. Good values of COI frequencies seem to be located in the middle of the network indicated by the red

dotted rectangle in Fig. 3.2. To be specific, the selected best bus to represent the COI frequency using (3.6) is bus 14.

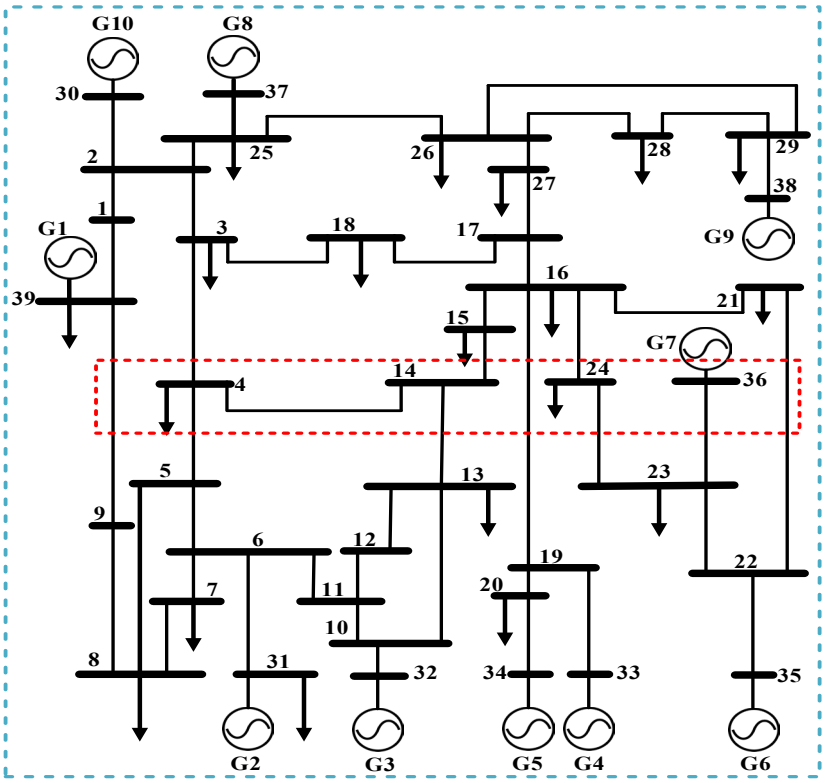

Fig. 3.2 Single line diagram representing the IEEE 39-bus network

To illustrate and validate the COI frequency of the test network, the simulation results in Fig. 3.3 are presented to demonstrate the step response of the network model. All frequencies at buses where generators are connected are recorded to compare with COI frequency at bus 14. From Fig. 3.3, it can be noted that frequency at bus 14 is a central (average) frequency of all generator's frequencies. This proves bus 14 to be the best representation of COI frequency of the network.

To further introduce the normal operating dynamics into the networks, random perturbations in terms of active power changes are introduced at different loads at different times. Frequency responses are observed from the performed simulations. Time sampled data sets that represent the dynamic frequency behaviours of the network are recorded at COI bus as shown in Fig. 3.4.

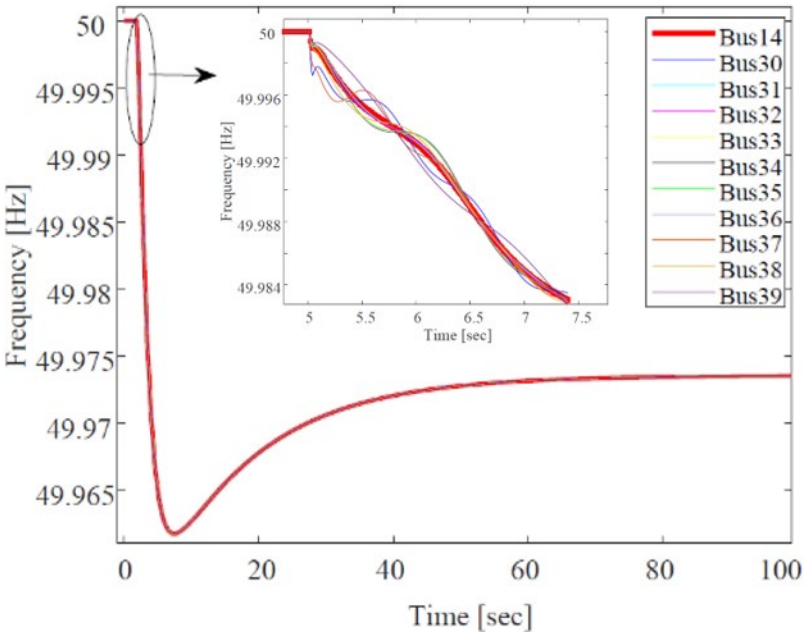

Fig. 3.3 Step response of the network model showing the COI frequency

Using the generated data sets, the algorithm for the proposed technique explained in Section 3 and summarized in Fig. 3.1 is used for inertia estimation process. It is important to monitor the system for an adequately long time with enough active power load events to capture important dynamics of the system. It should be remembered that inertial responses are observed in the first few seconds (up to 5 sec) after the disturbance. Adequate long simulation time with plenty of load events are important to capture reasonable inertial responses of the network.

From the estimation process, several models can be generated to represent the data. Different models that are generated between the input (i.e., active power load variations) and measured output (i.e., frequency responses) are tested for data fit by comparing the estimated models with actual network model response. The estimated models seem to have different data fits of the network they represent. The best and robust estimated model is the one with the highest percentage of the data fit among all other estimated models generated for a wide range of measured output and the chosen estimation data set. The best estimated model is used for further inertia estimation process.

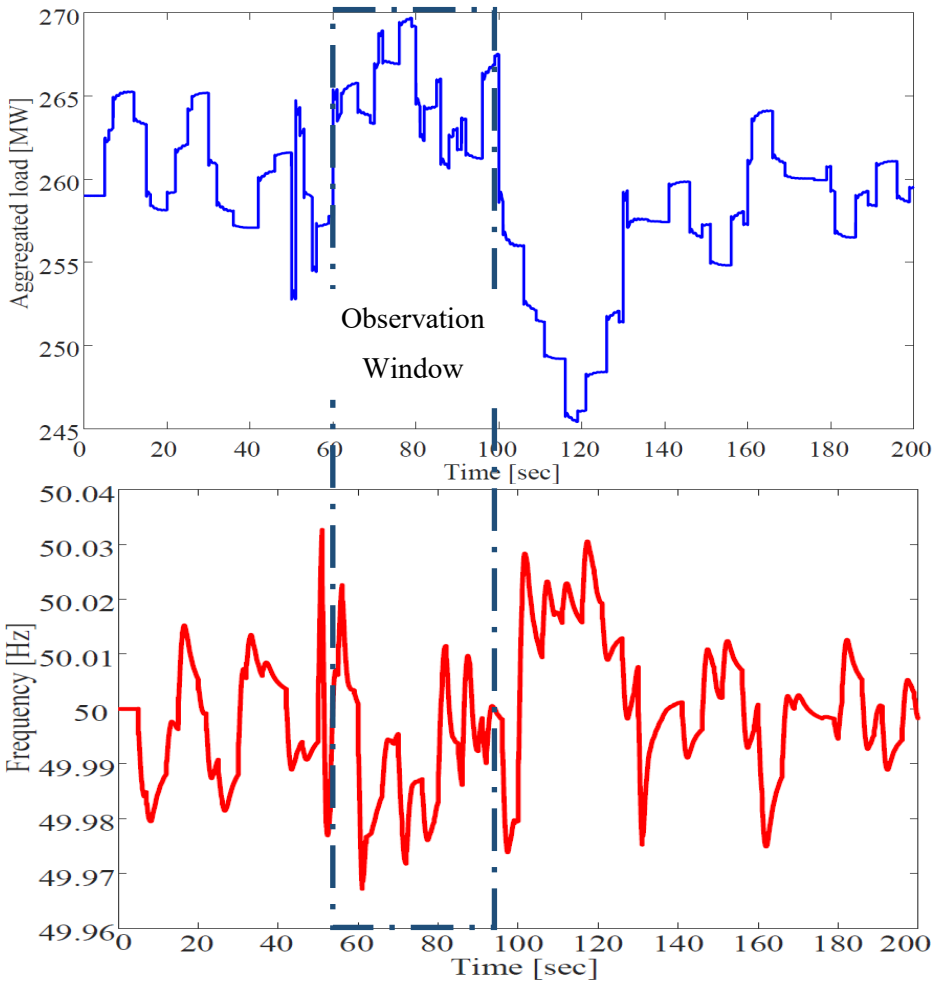

Fig. 3.4 Simulation results showing aggregated load variation and COI frequency response of the 39-bus network

The reliability of the chosen model is validated by comparing with responses of the actual model. The model cross-validation is achieved by comparing the responses of the actual system (Y_i) and the estimated model ($\hat{Y}_i$). To quantify this comparison, the fitting ratio (FR) relationship is given by (3.28) [162].

$$FR = \left(1 - \frac{\|Y_i - \hat{Y}_i\|}{\|Y_i - \bar{Y}_i\|}\right) \times 100\% \tag{3.28}$$

where $\bar{Y}_i$ is the mean of the actual system responses. If the FR index is closer to 100%, it indicates that the response of the estimated model under validation matches the actual system better [179].

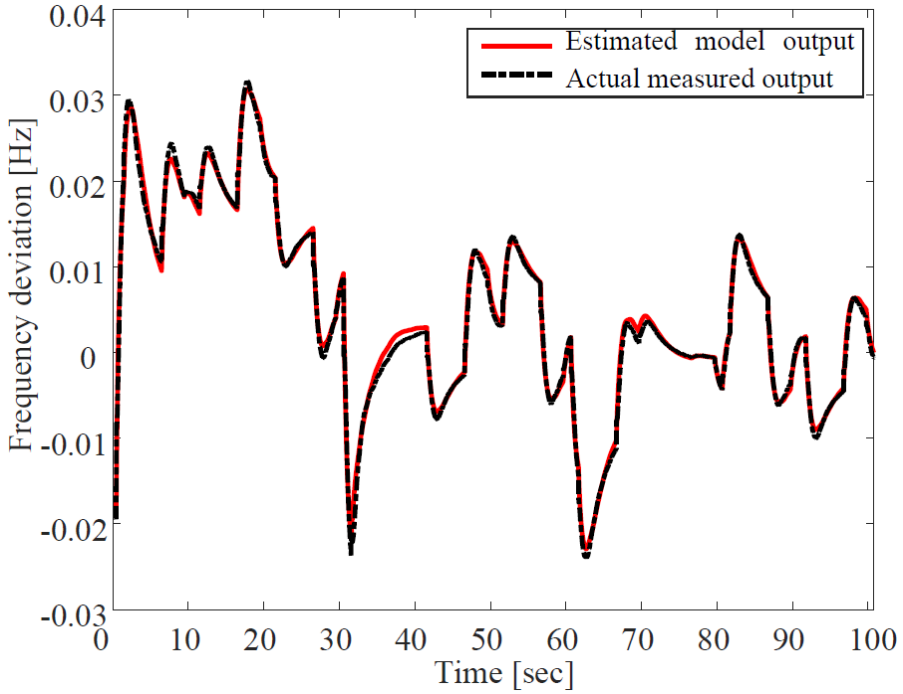

Fig. 3.5 Simulations results to validate the estimated model with data FR of 95%

The inertia constant is then extracted as described in the algorithm *step 8* of the proposed technique. The estimated inertia constant is extracted from the estimated and reduced order models. The extraction is achieved by initially subjecting the estimated and reduced order models to a unit step function. The unit step response is captured, and the average RoCoF is established using the observation window technique. Then, the gradient on the unit step response is mapped at the tangent of the initial RoCoF of the unit step response as shown in Fig. 3.6.

To avoid the uncertainty due to using a single data estimation, the estimation for each value of effective inertia is carried out five times by dividing the simulations into five portions of 40 s each as shown in Fig. 3.4 (observation window). In each portion, data of the network is extracted and used in the inertia estimation algorithm described in Section 3 to calculate the average inertia. Therefore, for each simulation, five different estimations by using five different data are obtained, and the average inertia estimation is calculated as presented in Fig. 3.7. Table 3.1 illustrates the inertia values for each generator in the network and the corresponding calculated equivalent inertia constant of the entire network. Equation (3.5) is used here to obtain the equivalent inertia value of the entire network. Additionally, more values of actual effective inertia of the network are tested to validate the approach. Table 3.2 shows the comparison of various true network inertia with estimated values of inertia.

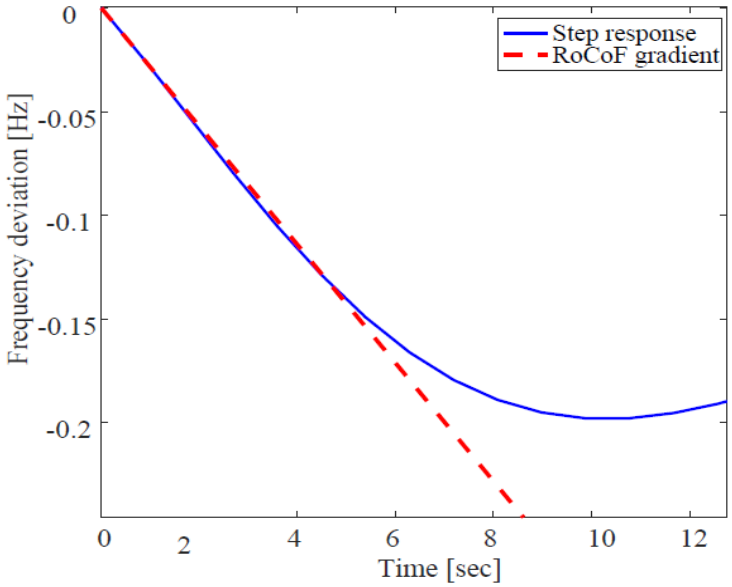

Fig. 3.6 Gradient line mapped on a unit step response curve of the estimated transfer function representing the network for inertia extraction

Table 3.1

The actual inertia constant of each generator and the equivalent inertia constant value of the entire network

Bus, *i*	Generator	$S_{B,i}$ *(MVA)*	H_i (S)	$S_{B,i}$xH_i
39	G1	10,000	5	50,000
31	G2	700	4.329	3,030.3
32	G3	800	4.475	3,580
33	G4	800	3.575	2,860
34	G5	300	4.333	1,299.9
35	G6	800	4.35	3,480
36	G7	700	3.771	2,639.7
37	G8	700	3.471	2,429.7
38	G9	1,000	3.45	3,450
30	G10	1,000	4.2	4,200
			Total	76,969.6
			S_B	10,000
			H_{eq}	7.6969

Table 3.2

Comparison of the actual and estimated inertia constant values

Exp	Actual value, H (s)	Estimated inertia constant values, $\bar{H}$ (s)		
		Mean	St. Dev.	% Error
1	3.87	4.21	0.51	8.79
2	4.65	4.32	0.54	7.10
3	5.56	5.33	0.59	4.14
4	7.69	7.19	0.50	6.50
5	8.12	8.66	0.53	6.65
6	9.21	9.79	0.47	6.30
7	10.02	10.59	0.31	5.69

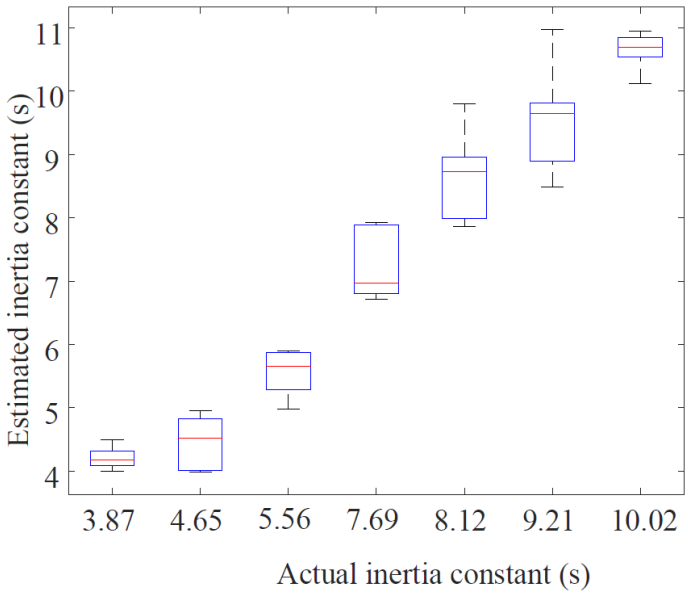

Fig. 3.7 Inertia estimation for different values of system's inertia

Moreover, wind power plants are represented by the percentages in Table 3.3 to reflect the penetration of non-synchronous renewable energies. Likewise, the effective actual inertia constants are calculated, and the inertia estimation algorithm is implemented again to estimate the effective inertia with RESs penetration. Equation (3.5) is again used to obtain the equivalent inertia value of the entire network after each step of RESs penetration. Four different RESs penetrations with related actual effective inertia constant of the simulation network case are tested to validate the approach. Table 3.3 demonstrates the comparison of different theoretical equivalent inertia constant values with estimated inertia constant values.

Table 3.3

Comparison of the actual and estimated inertia constant values for various percentages of RES penetration

% RES penetration	Actual value, H (s)	Estimated inertia constant values, $\overline{H}$ (s)		
		Mean	St. Dev.	% Error
0%	7.69	7.25	0.36	5.72
10%	6.98	6.55	0.39	6.16
15%	6.05	6.44	0.33	6.45
20%	5.16	5.52	0.23	6.98

To clarify more, Fig. 3.7 and Fig. 3.8 denote the results of the estimation for each effective value of theoretical inertia constant set in the simulation case study. As stated previously, for each effective inertia values, a full 200 s simulation is divided into five 40 s observation windows to get five different data of estimation to minimize estimation errors. For this case, each boxplot in Fig. 3.7 and Fig. 3.8 represents the mean value of the estimated inertia, which lies in the interquartile range of the estimations from different windows.

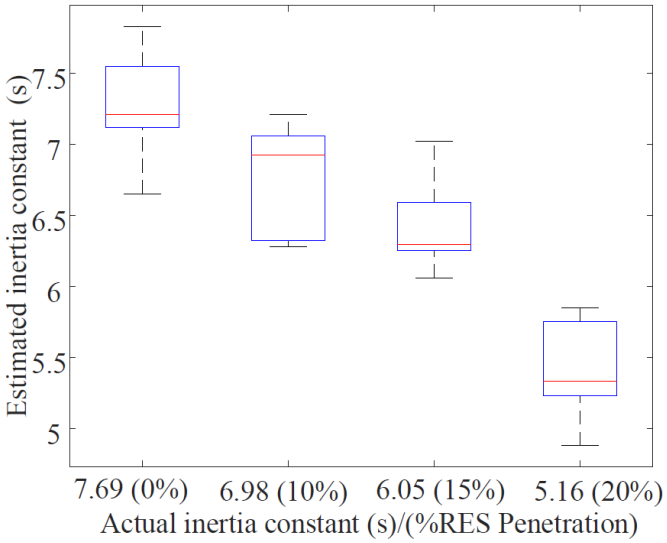

Fig. 3.8 Inertia estimation for various percentages of RESs penetration

The comparisons of the actual and estimated inertia constant values are presented in Fig. 3.9. So far, the technique can estimate the inertia constant of the test simulation case without penetration of RESs with errors ranging from 4.14% to 8.79% as stipulated in Table 3.2.

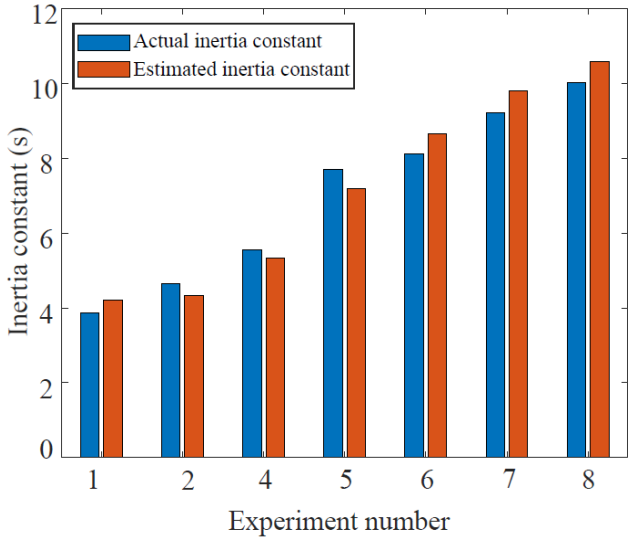

Fig. 3.9 Comparison of the actual and estimated inertia constant values for the case study without RESs penetration

Likewise, for the study case where some of the synchronous generators in 39-bus network are replaced by wind power generations, the technique is applied to observe the effect of penetration of RESs. The same procedure is followed in this study case as that is followed in the simulation network without penetration of RESs. The estimation results are presented in Table 3.3. As a result, the technique can estimate the inertia constant of the test simulation case with penetration of RESs with errors ranging from 5.72% to 6.98% as stipulated in Table 3.3.

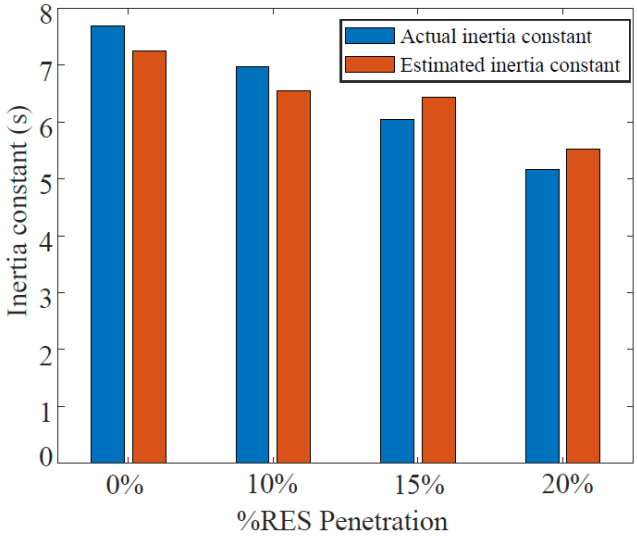

Fig. 3.10 Comparison of the actual and estimated inertia constant values for various percentages of RESs penetration

Since the errors between the actual and estimated values of inertia for the studied networks for both cases range in small values, that is 4.14% to 8.79%, this indicates that the

method is robust in estimating the values of inertia in the networks using operating conditions. The dynamics introduced in the network are the ones that make frequency responses to be within safe limits of ±0.1% of the nominal value, which are referred to as normal operating conditions. Therefore, apart from major fault cases like generator tripping, the method can use ambient operating condition of the network to estimate inertia of the network. However, since the method uses estimated model to capture the dynamics of the network, even big disturbance data can be used to estimate the model and therefore estimate the inertia of the network.

To test the validity of using a COI bus in the estimation process, non-COI buses are used as comparison. The estimations from all non-COI buses have bigger errors compared to the estimation taken from the COI bus. Geographically located at the furthest remote vicinity from the centre of the network, bus 10 is selected as a worst case. The estimations based on the measurements taken from this bus will be explained in the next paragraph.

First, the model estimated using the measurements from bus 10 is cross validated using (3.28). It is found that the FR of the estimated model is estimated to be 67%, which is the lowest among all buses. Furthermore, the estimated mean values of inertias in the network have biggest errors among all estimations as seen in Table 3.4. Comparisons between the actual equivalent inertias in the network and the estimated inertia constant are present in Fig. 3.11. The comparisons of the errors between estimations based on the COI bus measurement and the non-COI bus measurement are depicted in Fig. 3.12. These results suggest that the performance of the proposed method is affected by selection of the bus from where measurements are taken. Selecting a different bus from a COI bus results in higher estimation errors compared to the estimations based on a COI bus. Therefore, for more effective performance of the proposed method, it is highly recommended to use a COI bus for measurements of signals to be used for the inertia estimation process. Careful selection of a COI bus is required when using this method to achieve high accuracy of inertia estimation in power systems.

Table 3.4

Comparison of the actual and estimated inertia constant values at a non-COI bus

Exp	Actual value, H (s)	Estimated inertia constant values, $\overline{H}$ (s)		
		Mean	St. Dev.	% Error
1	3.87	4.65	0.61	20.16
2	4.65	3.23	0.58	30.54
3	5.56	7.15	0.69	28.60
4	7.69	10.28	0.76	33.68
5	8.12	5.33	0.63	34.36
6	9.21	6.97	0.57	24.32
7	10.02	14.35	0.71	43.21

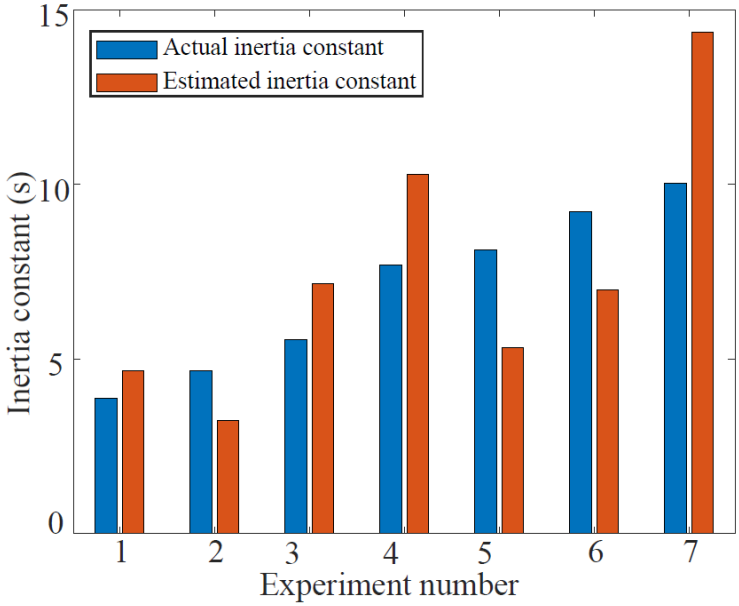

Fig. 3.11 Comparison of the actual and estimated inertia constant values for the data taken from a non-COI bus

The performance of the proposed method is also tested using noise corrupted data measured at COI. Unfiltered simulation data containing white noise is used with the proposed algorithm. From the power spectrum of the data, noise interference is detected between frequency bands 44 Hz – 46 Hz. The corrupted data is used for inertia estimation. The result is shown in Fig. 3.12, which compares estimation errors for different conditions. Compared to filtered data, the estimation errors for noise-corrupted data have bigger errors ranging between 9.3% to 11.79%. These bigger errors inform that the performance of the proposed method is also affected by noise. Therefore, filtering the data is important for effectiveness of the method to obtain good estimations.

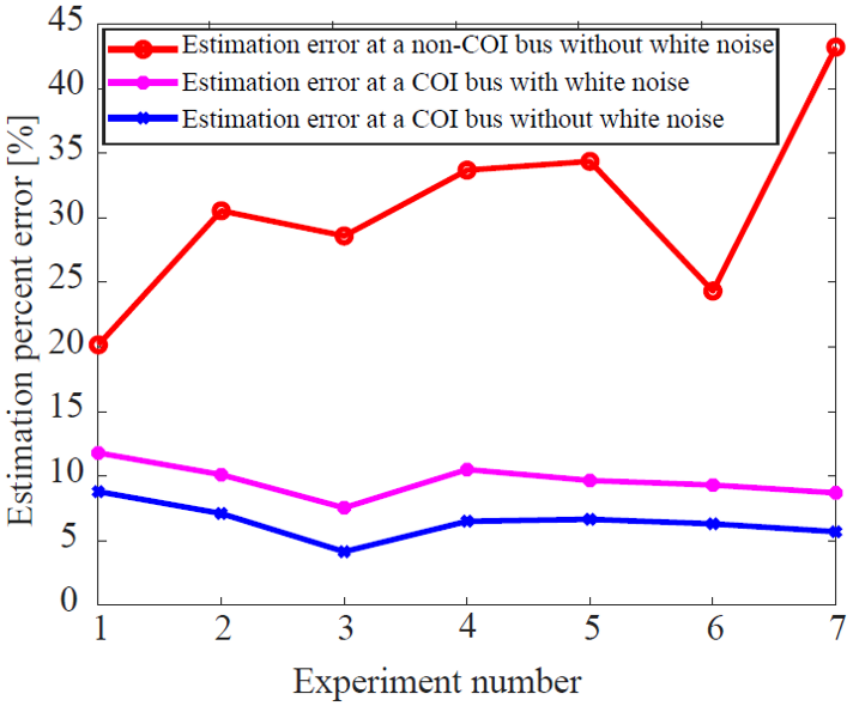

Fig. 3.12 Comparison of inertia estimation errors for different cases

3.5 Validating using real measurements data

To test its applicability, the proposed technique is used to estimate the equivalent inertia of an actual power system with a nominal frequency of 50 Hz. The tested network is the New Zealand grid, which is comprised of North Island and South Island systems that are interconnected with a HVDC line. The generation part of the New Zealand network consists of hydro generators with inertia ranging from 2 to 4 s, Combined Cycle Gas Turbines with inertia range of 5 to 6 s, geothermal stations with inertia range of 3 to 6 s and wind generation. The wind power generation does not supply any inertia in the network. Therefore, high penetration of wind power generation into power system will significantly affect the value of network inertia. However, New Zealand network currently does not have significant penetration of wind generation, which is only less than 5% of the entire installed capacity. The effective inertia value of the whole network, depending on the number and types of generators connected to the network, can be calculated by using (3.5).

To obtain the necessary data for inertia estimation, the network was tracked to record active load power variations and related frequency response on June 20, 2020 from 11:02:05 to 11:27:00. The frequency and active power load profile were recorded at the centre of inertia of the network. The COI frequency is presented in Fig. 3.13. The inertia values for each New Zealand power station are cited from the green grid report [219]. The actual equivalent inertia value for the generators that were online during data recording is calculated using (3.5) to be 8.02s. This value is obtained with wind power penetration of 1.9%, which is insignificant contribution to

make a note of the effect of inertia variation in the overall network. Furthermore, the effective inertia constant value is calculated using the system base value of 3000 MVA and frequency base of 50 Hz. Table 3.5 presents the average generation and capacity as well as equivalent inertia constant for each type of generation online during data recording time.

The algorithm provided in this approach is executed to identify the estimated model of the network and then estimate the value of network inertia using the data obtained. During the data recording, there is not any major fault such as load rejection, generator tripping, etc. Hence, the used data is within normal operating condition as used for simulation approach to estimate the system inertia constant.

Table 3.5

New Zealand power generation with related inertia constant

Generation	Average generation (MW)	Capacity (MVA)	Average Inertia constant H (s)
	North Island (NI)		
Wind	240	564	0
Hydro	720	1838	3.4
Geothermal	882	1064	3.1
Coal	184	500	1.5
Gas	797	1150	3.8
Co-Generation	160	277	1.2
NI Total	2799		
	South Island (SI)		
Wind	45	94	0
Hydro	2410	3670	3.5
SI Total	2455		
NZ Total	5254		8.02

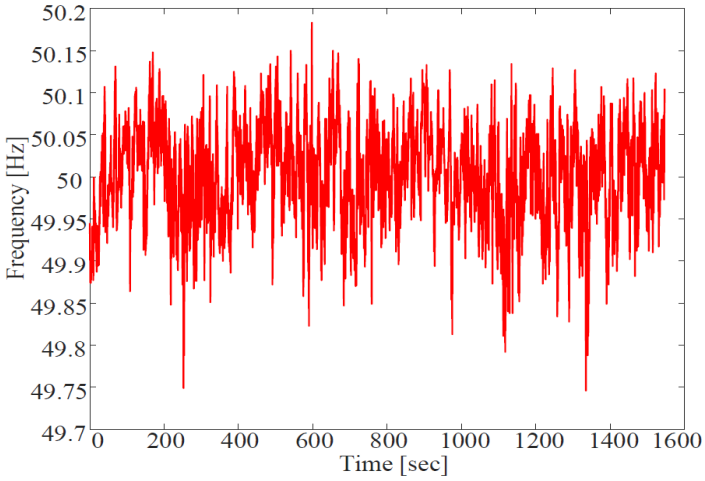

Fig. 3.13 Frequency response as recorded at the COI of the New Zealand network

The data is resampled at a sampling rate of 100 Hz. The spectrum of the data obtained from PMU is analysed to detect if there is any interference (noise) in the data. It is observed that there is interference (noise) between frequency bands 46 Hz-48 Hz. This noise is minimal and could be ignored. However, to be sure of the noise-free data, a smoothing filter (moving median) is applied to remove the noise from the data. The data is then prepared by sampling the active power variation and the frequency response as *u(t)* and *y(t),* respectively. Then, the estimated model to represent the network is identified using the proposed algorithm *steps 1* to *4* covering equations (3.9) to (3.19). To evaluate the effectiveness of the estimated model, fitting curves are generated and (3.28) is applied to find the FR, which is calculated to be 83%. This FR is identified to be the best fitting for the data used from the network. The fitting is satisfactory for system identification of the network according to [179]. Fig. 3.14 represents the fitting curve of the actual and estimated models of the network.

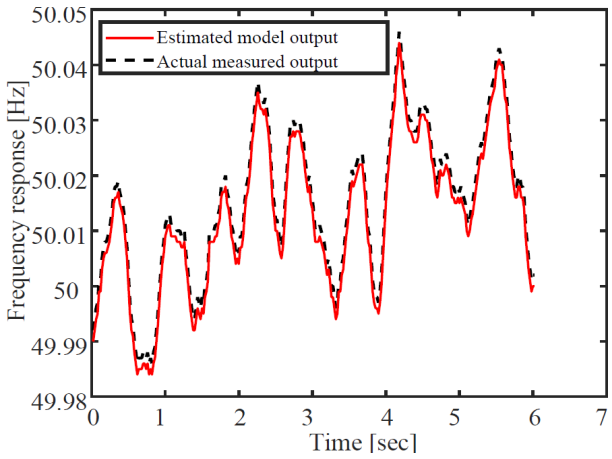

Fig. 3.14 Simulations of the estimated and actual model outputs to validate estimated model of the New Zealand network with data FR of 83%

The optimal transfer function order is 5, which is identified using the SVD as described in the proposed technique. The optimal order transfer function is then subjected to a unit step function and finally gradient method is applied to estimate the inertia value of the network as proposed in *step 7* of the proposed algorithm. From (3.28), the inertia constant ($\bar{H}$) estimation is obtained to be 7.1 s. Compared with the actual inertia constant H in Table 3.5, the percentage error between the actual and estimated inertia constant values is 11.47%. Since the estimated and actual inertia constant values are very close to each other with percentage error of less than 15%, which is acceptable for experimental results, this confirms and validates the effectiveness of the proposed method.

The presented method assumes that all parameters are primarily stored and are then processed in one batch (one pass processing). This implies that the parameter estimates are only accessible after the completion of measurements and estimation process. On top of that, model and parameters estimation and processing time for this proposed method on 25 minutes real network measurement data is around 258 seconds using a regular office computer (Intel(R) Core (TM) i7-9700 CPU @ 3GHz, 32GB RAM). For these reasons, the proposed method is limited to offline inertia estimation of the network.

3.6 Conclusion and future work

This paper presents a data-driven inertia estimation based on frequency gradient technique for various levels of inertia constant in power systems. The various levels of inertia constant presented imitate the time-varying inertia constant in the network due to different percentages of RESs penetration in the network. The proposed method introduces a decomposition technique to reduce unnecessary high orders of the model estimate. Model reduction does not only make it easy to analyse the RoCoF but also reduces computation burden. Moreover, the ability to use normal operating dynamic data of the system for inertia constant estimation is added advantage. Finally, the coordinated frequency gradient mapping on RoCoF is employed to make the process of extracting inertia from the estimated network model easy. The proposed technique gives consistent estimates of the observed ranges of inertia with errors in the ranges of 4.14% to 8.79% for simulation network and 11.47% for actual network. Therefore, this paper proposes that operating data of the network can be used to offline estimate time-varying inertia of the network.

Future work of this research is to extend the method to online inertia estimation/monitoring incorporating RESs penetration and weather forecast in the network. The speed of communicating the inertia estimated to power system operators (PSO) and duration of decision making for stability control purposes will be considered. This approach of inertia monitoring will help reducing frequency instability problems due to low and unpredictable inertia.

Chapter 4 Publication 3: Online Inertia Estimation

Preamble

As Chapter 2 highlights the need for online inertia estimation, Chapter 4 addresses the need by presenting the online inertia estimate method in modern power systems. Online inertia estimation techniques can quickly quantify the risks of power systems instabilities and quickly prompt actions to be taken to keep the network's resilience. Contrary to offline inertia estimation, which is used as a post-mortem after contingency events in networks, online inertia estimation techniques are real-time approaches to analysing the network as contingencies happen in networks. Therefore, the method developed in this Chapter is for monitoring the time-varying inertia values in modern networks. The proposed method uses the recursive process and time changing measurements to recursively estimate model parameters and extract online inertia estimates of the network. During the estimation, the technique does not need to store previous data after each sample step; therefore, significantly reducing the computation burden. More importantly, the technique incorporates available electromechanical oscillation modes linked with system parameters to determine the network inertia estimates.

Online inertia estimation for power systems with high penetration of RES using recursive parameters estimation

Peter Makolo*, Ramon Zamora, and Tek-Tjing Lie

Department of Electrical and Electronic Engineering, Auckland University of Technology – AUT, 55 Wellesley, Auckland, New Zealand

Abstract: Low and time-changing inertia values due to the high percentage of renewable energy sources (RESs) can cause stability problems in power systems due to rapid frequency instabilities. Inertia monitoring will assist operators to apply suitable actions and more proper control methods to alleviate stability issues. Therefore, this paper proposes an online method to estimate the total inertia of a network using a recursive least-squares approach. The proposed method uses network measurements with a non-recursive system identification approach to initially estimate the network hypothesis model. Then, the recursive method is used together with time changing measurements to recursively estimate model parameters and extract online inertia estimates of the network. During the estimation, the method does not need to store previous data after each sample step; therefore, the computation burden is significantly reduced. More importantly, the technique incorporates the use of available electromechanical oscillation modes in the system, which are linked with system parameters, to determine the network inertia estimates. The applicability of the proposed method has been validated by numerical simulations of the IEEE 39-bus network and the aggregated New Zealand network with its actual inertia data.

4.1 Introduction

4.1.1 Background and motivation

Inertia has a great impact on system dynamics. Inertia takes part in deciding the ability of the network to retain stability when exposed to power imbalances. Conventionally, inertia in power systems has been provided mainly by synchronous generators [42]. However, due to the increasing renewable energy sources (RESs) penetration level to power networks, some synchronous generators are replaced by converter-based RESs. Consequently, the inertia constant in power system has reduced. For instance, a Ref. [71] presents the inertia decrease for different countries between the year 1996 and 2016. The study shows a decrease of inertia value in Denmark by 60%. On the other hand, Ref. [203] estimated the inertia value of the UK network to be 9 s by 2008 and anticipated to be 3 s, around 67% decrease, by 2020. These are remarkable decreases of inertia in power systems. Therefore, the study of the power system's inertia is becoming vital.

While inertia is only essential in the first instants after the events of power imbalance, its influence is critical in the network as it suppresses frequency deviations under sudden power imbalances. When the inertia of the network decreases, the standard indicator is the rate of change of frequency (RoCoF), which increases. If the RoCoF increases beyond a critical value of a specific network, RoCoF protective relays will operate to isolate a generating unit from the network. Isolating a generating unit from the network may result in cascading failures and possibly blackout. To address the problem of the increased RoCoF because of the high penetration of RESs, some countries such as Denmark, Germany and UK have updated their critical RoCoF relay settings from 0.5 Hz/s to 2.5 Hz/s to accommodate high RoCoF in their networks [220]. Therefore, the challenges related to reduced inertia in power systems, especially during contingencies, should be given research attention [42, 162].

It is traditionally known that for a network with multi-synchronous generators, its system equivalent inertia constant can be obtained by using (4.1) [170].

$$H_{Total} \times S_{Total} = \sum_{i=1}^{N} H_i \times S_i \tag{4.1}$$

where H_{Total} and S_{Total} are the total inertia constant and the capacity of the entire system, respectively; H_i and S_i are the inertia constant and the capacity of the ith synchronous generator, respectively; N is the number of generators in the network [14, 162]. It is apparent that, for the conventional power system, the system inertia could be calculated by using (4.1). However, (4.1) may be unsuccessful at giving an accurate estimate of the actual network inertia in the presence of a high percentage of RESs. The RESs generation units have non-synchronous inertias called synthetic inertias. The existence of synthetic inertia in the power system can further complicate

the use of (4.1) in inertia calculation. Failure to estimate the network reduced inertia might result in difficulties in both network operation and control schemes planning [7, 49]. An Australian blackout in 2018 as well as UK's and the Island of Tenerife's blackouts in 2019 are good examples of the latest challenges related to a failure of estimating the values of network inertia [206]. Other problems related to the high percentage of RESs in power systems are presented in [24, 221, 222].

Some research works such as in [39, 119] have addressed the problem of low inertia in power systems by introducing synthetic inertia as a control strategy to replace reduced conventional synchronous generator's inertia. As most synthetic inertias are dependent on stochastic RESs, the future system inertia expected to be a time-varying quantity in power systems. The high probability of inertia becoming a time-varying quantity due to a high percentage of RESs in the network prompts more consideration of power system stability and reliability. As a result, for the safety and reliability of modern and future power systems with low and time-varying values of inertia, online estimation and monitoring of inertia values as well as evaluation of frequency response in power systems are necessary. Prior awareness of inertia values in power systems will help in planning for frequency response in power systems. Besides, the deployment of proper frequency containment services depending on the level of inertia at a given time in power systems can be planned in advance. Consequently, online inertia estimation techniques need to operate in real-time to quickly quantify the risks of power systems blackouts.

4.1.2 Literature review

A power system with a significant percentage of converter-based RESs has low inertia that may be inadequate to immediately and effectively respond to system dynamics when the network is exposed to power imbalances. The low inertia system is prone to the high RoCoF during contingencies and, hence, large frequency deviations. The high RoCoF may lead to frequency instabilities and consequently blackouts. Similarly, since most of RESs integrated into modern power systems are weather dependent, the number of committed synchronous generators over time will be affected by weather conditions. This tendency, consequently, leads to challenges in the planning, operation and control of networks [35, 47-49]. Subsequently, maintaining the stability of the grid is problematic as the penetration levels of the converter-based RESs keep increasing in the network.

The decrease in the percentage of inertial machines, which is a result of the increase in the percentage of stochastic RESs in the power system needs more research. The research is dedicated to ensuring that the stability and flexibility of the modern and future power grid are maintained [35, 47]. For the safe and reliable operation of modern and future power systems with low and time-changing values of inertia, online estimation and tracking of inertia in power systems are essential. Besides, real-time assessment of the frequency response in power systems is also important. By successfully assessing the frequency response in real-time, appropriate

measures such as control schemes can be planned [11]. Generally, quick and continuous information of the inertia value in the network will help power system operators (PSOs) to plan and act either before the contingency or very rapidly after the contingency with appropriate measures.

Even though inertia estimation methods have been implemented in the traditional network, the methods may not be suitable for modern and complex networks. The methods used traditionally include the well-established equation expressed by (4.1), probing test [182, 207] and transient test [208]; all these techniques estimate the inertia constants of the networks predominantly driven by synchronous generators. As synthetic inertia is becoming a reality in power systems, hence making the total inertia a time-varying quantity, traditional methods would not work in estimating variable inertia in modern power systems. To address inertia estimation in modern networks, new methods have been proposed recently [11, 159, 162, 214, 223]. However, the majority of them are still dependent on (4.1) and based on historical data analysis as well as large data sets after frequency events.

Furthermore, the system inertia estimation in [224] is conducted by using an equivalent system model. Unfortunately, the model requires a large amount of recorded data, which slows down the entire process. Therefore, this approach is not suitable for online inertia estimation. Similarly, Ref. [214] uses historical data and the Bayesian approach in the methods to estimate the aggregated inertia of the network. But, the approach is prone to computational problems owing to using a large and complex computational model that stores large historic data during computation. Therefore, it is unsuitable for online inertia estimation. Besides, Ref. [211] presents a method that has a drawback of downtime revising and updating the entire system model when considering the addition or exclusion of a generator or load in the system. Due to this drawback, the method irrelevant for online inertia estimation. A downside of decreased precision due to phase step issues as clarified in [212] makes the methodology for inertia estimation in [225] lack credibility for online inertia estimation.

Ref. [168] proposes an online inertia estimation technique, which overlooks the variable inertia due to the high percentage of RESs in modern networks. Furthermore, the method proposed in [226] is also built on the Bayesian approach, which is associated with high computation burden as analysed in [18]. The computation burden associated with the Bayesian approach makes the method impractical for online inertia tracking in power systems. Alternatively, Ref. [18] proposes two inertia estimation techniques for estimating synchronous and non-synchronous generators' inertias. The techniques are mainly developed based on the approach in [227] and [217]. However, the techniques are limited to individual devices only.

The challenges revealed in the analysed literature above lead to the development of a compact online inertia estimation and monitoring technique. The developed technique should

consider time-varying inertia for the entire network, should not suffer from phase step issues and should have minimum computation burden.

4.1.3 Novelty and organisation

To overcome the above-mentioned vulnerabilities and to provide an accurate and reliable online inertia estimation and tracking, this paper proposes a recursive parameter estimation and online inertia tracking in power systems. The proposed technique has the following merits:

- Reduces computation burden significantly as it does not need to store previous data after each sample step during estimation.
- Does not suffer from phase step issues and reduces the size of the estimated network model during computation.
- Provides only updates of the model parameter estimates after each sample step and not the whole model of the entire network.
- Incorporates the use of available electromechanical oscillation modes in the extraction of the network inertia estimates.

This paper covers the gaps that exist in most proposed estimation methods such as having high computation burdens, considering only electrical model information and leaving behind electromechanical oscillations, which limit most of the inertia estimation methods to only post-event analysis. The remaining parts of this paper are structured as follows. Theoretical background is presented in section 2. In this section, the role of inertia in frequency stability is discussed. Furthermore, dynamic modes and eigenstructures in relation to inertia extraction in power systems are introduced. Section 3 describes the proposed online inertia estimation method based on the recursive least-squares approach. Moreover, the application of the proposed technique on the case study network is presented and examined in section 4. The application and validation of the proposed technique on the real network data is examined in section 5. Lastly, section 6 presents the conclusion and briefly underlines the future work.

4.2 Theoretical background

4.2.1 Inertia in power system dynamics

Inertia has a critical role in maintaining the stability of the network after power imbalances [42, 43]. Inertia determines how fast or slow the frequency can change after power imbalances in the network [162, 214, 228]. To describe the behaviour of frequency response in networks, the traditional swing equation is very important. When the traditional swing equation is simplified and normalised with respect to the unit values as depicted in [7], the transfer function (TF) of the system expressed in (4.2) can be obtained.

$$G(s) = \frac{\Delta f}{\Delta P_e} = -\frac{1}{2Hs + D} \tag{4.2}$$

where $G(s)$ is the TF from ΔP_e to Δf, ΔP_e is the active electrical power deviation, Δf is the frequency deviation of the rotor of the generator, H is the inertia constant, D is the damping coefficient and s is the Laplace transform operator. As the PMUs are employed to measure the network's parameters, a system estimation technique can be employed to estimate the TF of the network. Then, network parameters such as inertia can be estimated.

For a network with several synchronous generators, the total inertia constant of the entire network can be obtained by employing (4.1). Also, a network with several synchronous generators can be combined and assumed as a single generator network [11]. To achieve the combined network, all generators' output active powers are aggregated to give a single value of active power. The frequencies of different buses can be averaged at a selected bus to have the so-called centre of inertia (COI) frequency. Traditionally, the COI frequency of the aggregated network is given by (4.3) [158].

$$f_{COI} = \frac{\sum_{i=1}^{N} H_i \times f_i}{\sum_{i=1}^{N} H_i} \tag{4.3}$$

where, f_{COI} is centre of inertia frequency of the network, H_i and f_i is inertia constant and frequency of the i^{th} synchronous generator, respectively, and N is the total number of synchronous generators in the network.

For traditional networks whose parameters of the installed generators are known in advance, the approach in (4.3) can be implemented when considering a multi-generators network. However, due to the nature of the modern grid with significant RESs penetration and synthetic inertia inclusion, the inertia of some components in the network may not be known in advance. The advanced wide-area measurement systems (WAMS) that are equipped in modern networks can provide measurements of different units in the network, which can facilitate real-time tracking of each component added in the network [172]. The information of each component can be obtained and immediately incorporated into the network. Therefore, the sum of active power deviations and the frequency responses, which are tracked in real-time, are used as inputs for the proposed adaptive algorithm to calculate COI frequency in actual networks. The algorithm in this proposed method is designed in such a way it adaptively adjusts to incorporate reduced inertia in the network.

4.2.2 Dynamic modes and eigenstructure analysis

An interesting interpretation of system dynamic behaviour can be achieved by examining the eigenvalues of a dynamic matrix $\boldsymbol{A}$ of the state-space model of a power system [229]. As matrix $\boldsymbol{A}$ describes the dynamics of the system as characterised by its eigenvalue, the system's

inertia constant can be extracted from this matrix. To do this, the dynamic modes of the system are found and then the eigenvalues of matrix $\boldsymbol{A}$, which are poles of the system, are calculated [175, 186]. The general form of a dynamic system can be expressed as in (4.4).

$$\dot{x} = \boldsymbol{A}x \tag{4.4}$$

where x represents the vector of the state variable and $\boldsymbol{A}$ is the state matrix. If it is assumed that matrix $\boldsymbol{A}$ is diagonalisable with eigenvalue decomposition, then the estimated state variable can be given as in (4.5).

$$\tilde{\boldsymbol{x}} = \boldsymbol{\Phi\Lambda\tilde{\Gamma}_m} \tag{4.5}$$

where $\boldsymbol{\Phi}$ is a set of functions obtained from the system data, which physically represents the oscillation of the system, $\boldsymbol{\tilde{\Gamma}_m}$ represents the estimated row vectors containing the temporary coefficient evaluated at each observation, and $\boldsymbol{\Lambda} = diag[\lambda_1 \ \ \lambda_2 \ \ \ldots \ \ \lambda_m] \in \mathbb{R}^{m\times m}$ is a diagonal matrix consisting of empirical Ritz eigenvalues λ_j of the dynamic matrix $\boldsymbol{A}$ [230]. Therefore, the estimated state variable $\tilde{\boldsymbol{x}}$ can then be expanded in a linear combination of modal components as in (4.6).

$$\tilde{\boldsymbol{x}} \approx \sum_{\boldsymbol{j=1}}^{\boldsymbol{m}} \boldsymbol{\phi_j}\, \lambda_j \tilde{\boldsymbol{a}}_{\boldsymbol{j}}(t) \tag{4.6}$$

where $\tilde{\boldsymbol{a}}_{\boldsymbol{j}}$ is a set of temporal amplitudes, $\boldsymbol{\phi_j}$ is a set of dynamic modes, and λ_j is the associated eigenvalues of the dynamic matrix $\boldsymbol{A}$ of the system model. In this way, the eigenvalues and eigenvectors of the state matrices can then be found.

Since there is a cross-coupling between the state variables and the dynamic matrix, it is reasonable to assume that, for n^{th} order system, the homogeneous response of each of n state variables $\boldsymbol{x}_i(t)$ is a weighted sum of n exponential components given by a derivative of a state variable in (4.7) [231].

$$\dot{\boldsymbol{x}}_i(t) = \sum_{j=1}^{n} \lambda_j m_{ij} e^{\lambda_j t} \tag{4.7}$$

If a set of m_{ij} and λ_j can be found that satisfy (4.7), the assumed exponential form is a solution to the homogeneous state equation. In this case, λ_j is the j^{th} eigenvalue and m_j is the corresponding eigenvector of a given square dynamic matrix. Since system dynamics correlate with eigenvalue and eigenvector, any change in dynamic parameters can indirectly change the eigenvalue and eigenvector through the state variable. By determining the modes of the system and analysing the eigenvalues of the dynamic matrix A, network parameters such as inertia can be determined.

4.3 The proposed online inertia estimation technique

The proposed online inertia estimation method is summarised in the algorithm flow diagram presented in Fig. 4.1. It should be noted that PMUs are used to measure power system data. The recorded data is passed through a non-causal Butterworth low-pass filter with 0.5 Hz cut-off frequency to attenuate the higher frequency components that may impair the inertia estimation. The filtered recorded data is then used to estimate the time-variant TF model of the discrete-time process as the hypothesis model of the system. From the hypothesis model identified, the recursive least-squares method is applied to recursively estimate the parameters of the model. A model reduction is then performed, followed by a transformation to the state-space model. From the state space representation, the dynamic matrix $\boldsymbol{A}$ can be obtained from which the eigenvalues and eigenvectors can be attained to extract the inertia estimate of the system.

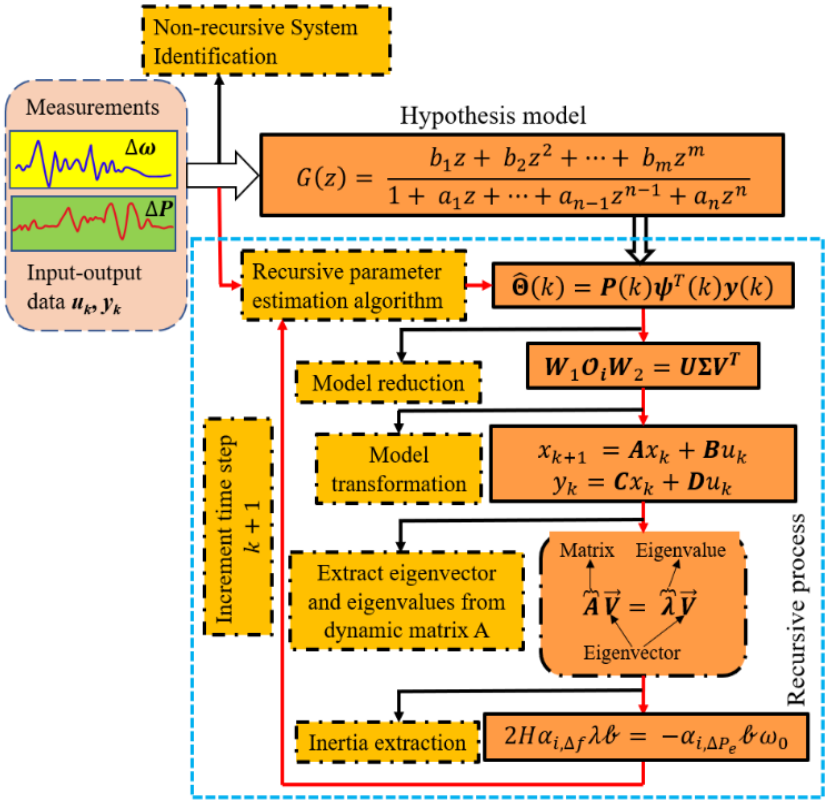

Fig. 4.1 Summarised diagram of the proposed method

4.3.1 Identification of the hypothesis model

The PMU network measurements are categorised as input vectors $(u_0, u_1, u_2, \ldots . u_m)$ and output vectors $(y_0, y_1, y_2, \ldots . y_m)$. The PMU measurements are evenly sampled with the sampling period Ts=1/fs, where fs is the sampling frequency. Considering a time t at a discrete-time index k, which corresponds to the maximum number of data points, tk is given by tk=kTs. The obtained data vectors are used to attain the estimated hypothesis model of the network.

For the identification procedure, a non-recursive least squares approach is employed to obtain a system hypothesis model. The hypothesis model is represented as a time-variant parametric system in the form of $G(s)$ in (4.8).

$$G(s) = \frac{b_{n-1}s^{n-1} + b_{n-2}s^{n-2} + \cdots + b_0}{a_n s^n + a_{n-1}s^{n-1} + \cdots + a_0} \tag{4.8}$$

where b_k (for k = 0 to n-1) and a_m (for m = 0 to n) define model parameters in the numerator and the denominator, respectively. $n-1$ and n are the highest orders of the operator "s" in the numerator and the denominator, respectively.

To use discrete data sets for model identification, the s domain TF (4.8) must be transformed to z domain as given in (4.9).

$$G(z) = \frac{b_1 z + b_2 z^2 + \cdots + b_m z^m}{1 + a_1 z + \cdots + a_{n-1} z^{n-1} + a_n z^n} = \frac{B(z)}{A(z)} \tag{4.9}$$

where $a_1 \ldots . a_n$, $b_1 \ldots . b_m$ are system parameters, n and m are real numbers, while z is a forward shift operator. For a decreasing time index (k-1), different data samples can be incorporated into (4.9) to estimate the parameters a_i and b_i of the hypothesis TF. However, (4.9) must be in the difference equation form as given by (4.10) [179].

$$\begin{aligned} y(k) + a_1 y(k-1) + \cdots + a_n y(k-n) \\ = b_1 u(k-1) + \cdots + b_m u(k-m) \end{aligned} \tag{4.10}$$

where y(k) and u(k-1) are the output and input discrete data samples at time indexes t = k and t=(k-1), respectively. Equation (4.10) can, therefore, be reordered to get (4.11).

$$\begin{aligned} y(k) = [-y(k-1) \ldots - y(k-n) \; u(k-1) \\ \ldots u(k-m)] \begin{bmatrix} a_1 \\ . \\ . \\ . \\ a_n \\ b_1 \\ \vdots \\ b_m \end{bmatrix} \end{aligned} \tag{4.11}$$

From (4.9), m and n determine the number of model parameters for the numerator and the denominator, respectively. For N data points available in the experiment but only l data points to be used, i.e., (l < N and l > n), then, general matrices (4.12), (4.13) and (4.14) are defined for the vector equations representation of measurements data and system parameters, respectively.

$$\boldsymbol{Y_l} = \begin{bmatrix} y(n) \\ \vdots \\ y(l-1) \end{bmatrix} \tag{4.12}$$

$$\boldsymbol{X_l} = \begin{bmatrix} -y(n-1) & \cdots & -y(0) \\ \vdots & \ddots & \vdots \\ -y(l-2) & \cdots & -y(l-n-1 \end{bmatrix}$$

$$\begin{matrix} u(n-1) & \cdots & u(0) \\ \vdots & \ddots & \vdots \\ u(l-2) & \cdots & u(l-n-1] \end{matrix} \tag{4.13}$$

$$\boldsymbol{\Theta} = \begin{bmatrix} a_1 \\ \vdots \\ a_n \\ b_{n-m} \\ \vdots \\ b_n \end{bmatrix} \tag{4.14}$$

Combining (4.12), (4.13) and (4.14) to represent (4.11) with vectors of several data points (l), (4.15) is obtained. Equation (4.15) connects several discrete data sets of the network to estimate $\boldsymbol{\Theta}$ system parameters.

$$\boldsymbol{Y_l} = \boldsymbol{X_l}\,\boldsymbol{\Theta} \tag{4.15}$$

It is also possible for N data sets to be used in (4.15). For this case, when $l = N$, (4.16) is obtained. Equation (4.16) is comparable to (4.15) with an exception that all data sets are used in (4.16). When more data sets are used, it makes (4.16) to be overdetermined, and therefore, the system parameters identification is simplified [179].

$$\boldsymbol{Y_N} = \boldsymbol{X_N}\,\boldsymbol{\Theta} \tag{4.16}$$

4.3.2 Recursive model parameter estimation

Before the recursive least square approach is applied, the non-recursive least square method is used to obtain the hypothesis model of the network. It should be noted that the non-recursive method is used with offline measurements of the network to estimate the network's model and its order dimension. Then, the recursive least square approach is employed for online inertia estimation. For online inertia estimation in this proposed approach, only parameters of the model should be recursively estimated and updated concurrently with the measurement process. After each sample step or a certain number of sample steps, the parameter estimates should be available. The recursive approach is appropriate in online estimation as it reduces the computation burden and provides an update of the parameter estimates after each sample step. The previous data do not need to be stored.

However, the recursive least squares approach is derived based on the non-recursive least-squares method. The parameter estimate $\widehat{\boldsymbol{\Theta}}(k)$ for the non-recursive method of least squares for the sample step k is given as (4.17) [232].

$$\widehat{\boldsymbol{\Theta}}(k) = \boldsymbol{P}(k)\boldsymbol{\psi}^T(k)\boldsymbol{y}(k) \tag{4.17}$$

where

$$\boldsymbol{P}(k) = \left(\boldsymbol{\psi}^T(k)\boldsymbol{\psi}(k)\right)^{-1} \tag{4.18}$$

$$\boldsymbol{y}(k) = \begin{pmatrix} y(1) \\ y(2) \\ \vdots \\ y(k) \end{pmatrix} \tag{4.19}$$

$$\boldsymbol{\psi}(k) = \begin{pmatrix} \boldsymbol{\psi}^T(1) \\ \boldsymbol{\psi}^T(2) \\ \vdots \\ \boldsymbol{\psi}^T(k) \end{pmatrix} \tag{4.20}$$

where $\boldsymbol{\psi}$ represents the data matrix of time sampled input and output measurement of the system as in (4.21).

$$\begin{aligned} \boldsymbol{\psi}^T = \ & (-y(k-1) - y(k-2) \ldots \\ & -y(k-m)|u(k-d-1) \ldots u(k-d-m)) \end{aligned} \tag{4.21}$$

Likewise, the parameter estimates $\widehat{\boldsymbol{\Theta}}(k+1)$ for the sample step $k+1$ can be given as in (4.22).

$$\widehat{\boldsymbol{\Theta}}(k+1) = \boldsymbol{P}(k+1)\boldsymbol{\psi}^T(k+1)\boldsymbol{y}(k+1) \tag{4.22}$$

When (4.22) is split up and evaluated for $\boldsymbol{\psi}(k)\boldsymbol{y}(k) = \boldsymbol{P}^{-1}(k)\widehat{\boldsymbol{\Theta}}(k)$ as in (4.17), then (4.23) is obtained.

$$\begin{aligned} \widehat{\boldsymbol{\Theta}}(k+1) = \ & \widehat{\boldsymbol{\Theta}}(k) + (\boldsymbol{P}(k+1)\boldsymbol{P}^{-1}(k) - \boldsymbol{I})\widehat{\boldsymbol{\Theta}}(k) \\ & + \boldsymbol{P}(k+1)\boldsymbol{\psi}(k+1)\boldsymbol{y}(k+1) \end{aligned} \tag{4.23}$$

Based on (4.18), (4.24) can be achieved.

$$\boldsymbol{P}^{-1}(k) = \boldsymbol{P}^{-1}(k+1) - \boldsymbol{\psi}(k+1)\boldsymbol{\psi}^T(k+1) \tag{4.24}$$

Combining (4.23) and (4.24) yields (4.25) and (4.26).

$$\widehat{\boldsymbol{\theta}}(k+1) = \widehat{\boldsymbol{\theta}}(k) + \boldsymbol{P}(k+1)\boldsymbol{\psi}(k+1) \tag{4.25}$$

$$\left(y(k=1) = \boldsymbol{\psi}^T(k+1)\widehat{\boldsymbol{\theta}}(k)\right) \tag{4.26}$$

where $\widehat{\boldsymbol{\theta}}(k+1)$ is the new parameter estimate, $\widehat{\boldsymbol{\theta}}(k)$ is the old parameter estimate and $\boldsymbol{P}(k+1)\boldsymbol{\psi}(k+1)$ is the correction vector. From (4.26), $y(k=1)$is the new measurement and $\boldsymbol{\psi}^T(k+1)\widehat{\boldsymbol{\theta}}(k)$ is the predicted measurements based on the last parameter estimate.

From (4.25) and (4.26), a recursive formulation of the estimation problem can be realised. To calculate $\boldsymbol{P}^{-1}(k+1)$ recursively as per (4.24), it needs one matrix inversion per update step. However, to prevent computation burden by inversion of a matrix each time step, (4.24) can be re-written as (4.27).

$$\begin{aligned} \boldsymbol{P}(k+1) = \ & \boldsymbol{P}(k) - \boldsymbol{P}(k)\boldsymbol{\psi}(k+1) \\ & (\boldsymbol{\psi}^T(k+1)\boldsymbol{P}(k)\boldsymbol{\psi}(k+1) + 1)^{-1}\, \boldsymbol{\psi}^T(k+1)\boldsymbol{P}(k) \end{aligned} \tag{4.27}$$

Since the term $(\boldsymbol{\psi}^T(k+1)\boldsymbol{P}(k)\boldsymbol{\psi}(k+1)+1)$ is a scalar quantity only, there is no need to invert a full matrix any longer. If (4.27) is multiplied by $\boldsymbol{\psi}(k+1)$, then (4.28) is obtained.

$$\boldsymbol{P}(k+1)\boldsymbol{\psi}(k+1) = \frac{1}{(\boldsymbol{\psi}^T(k+1)\boldsymbol{P}(k)\boldsymbol{\psi}(k+1)+1)}\boldsymbol{P}(k)\boldsymbol{\psi}(k+1) \tag{4.28}$$

When (4.28) is combined with (4.25), they return a recursive method of least squares as (4.29).

$$\widehat{\boldsymbol{\Theta}}(k+1) = \widehat{\boldsymbol{\Theta}}(k) + \boldsymbol{\gamma}(k)\left(\boldsymbol{y}(k+1) - \boldsymbol{\psi}^T(k+1)\widehat{\boldsymbol{\Theta}}(k)\right) \tag{4.29}$$

where $\boldsymbol{\gamma}(k)$ is the correction vector given by (4.30).

$$\boldsymbol{\gamma}(k) = \boldsymbol{P}(k+1)\boldsymbol{\psi}(k+1)$$

$$= \frac{1}{(\boldsymbol{\psi}^T(k+1)\boldsymbol{P}(k)\boldsymbol{\psi}(k+1)+1)}\boldsymbol{P}(k)\boldsymbol{\psi}(k+1) \tag{4.30}$$

From (4.27), it follows that (4.31) can be obtained.

$$\boldsymbol{P}(k+1) = \left(\boldsymbol{I} - \boldsymbol{\gamma}(k)\boldsymbol{\psi}^T(k+1)\right)\boldsymbol{P}(k) \tag{4.31}$$

The recursive method of least squares is, therefore, given by the three equations above, which need to be performed in the sequence of (4.30), (4.29) and (4.31). It should be noted that only the network's model parameters, not the whole model of the network, is updated recursively. If the model of the entire network is updated using a recursive approach, then the computation burden is significantly experienced in the proposed method. To avoid the computation burden, only the parameters of the hypothesis model that show a significant effect in the estimation process are updated recursively. The order dimension of the identified hypothesis model is kept constant throughout the simulation time.

4.3.3 Model reduction

Big dataset-driven system identification methods are associated with huge and complex models. Besides, the obtained models have very high degrees of freedom that represent the network. The high order models obtained, which are also complex to analyse, result in high computational burden algorithms. Due to these reasons, the resulted high order models need to be reduced. However, the application of reduction methods should be done in such a way it maintains the essential dynamics of the system. To achieve low order models from high order models, the singular value decomposition (SVD) technique can be applied. To obtain the decomposed model, the SVD technique is applied to the oblique projection vector of the model $\boldsymbol{\mathcal{O}_i}$, which is defined in (4.32) [183].

$$\boldsymbol{\mathcal{O}_i} = \triangleq \boldsymbol{Y_N} \,/\, \boldsymbol{W_p} \tag{4.32}$$

where $\boldsymbol{W_p} = \begin{bmatrix} X_N \\ Y_N \end{bmatrix}$

As a result, SVD is given as (4.33).

$$\boldsymbol{W_1 \mathcal{O}_i W_2 = U \Sigma V^T} \tag{4.33}$$

where $\boldsymbol{W_1}$ and $\boldsymbol{W_2}$ are the identity weighting matrices, $\boldsymbol{U}$ and $\boldsymbol{V}$ are orthogonal matrices, while matrix $\boldsymbol{\Sigma}$ is the diagonal matrix with real entries. Likewise, SVD can be presented as a matrix multiplication by (4.34). The decomposed order of the system is chosen as σ_1 provided σ_1 major singular values are identified in matrix $\boldsymbol{\Sigma}$ [183].

$$\boldsymbol{U \Sigma V^T} = [U_1 \;\; U_2]. \begin{bmatrix} \sigma_1 & 0 \\ 0 & \sigma_2 \end{bmatrix} . \begin{bmatrix} V_1^T \\ V_2^T \end{bmatrix} \tag{4.34}$$

where U_1 and U_2 are the components of $\boldsymbol{U}$, while V_1 and V_2 are the components of $\boldsymbol{V}$. Then, the TF model of the network at each sample time step is transformed into a state-space representation. From the state-space model, the dynamic matrix $\boldsymbol{A}$ of the system that contains the dynamic behaviour of the system can be extracted.

4.3.4 Inertia extraction

The dynamic matrix $\boldsymbol{A}$ can be represented by an estimated general form of a dynamic system as in (4.4). Then, the aggregated system dynamic behaviour is estimated by the swing equation (4.35).

$$2H\dot{\omega} + D\omega = \; P_m - \; P_e \tag{4.35}$$

Since the mechanical power is constant during the transient state, the linearized form of the swing equation can be represented as (4.36).

$$2H\Delta\dot{\omega} + D\Delta\omega = \; - P_e \tag{4.36}$$

The related TF of the swing equation is given in (4.37).

$$G(s) = \frac{\Delta\omega}{\Delta P_e} \approx - \frac{1}{2Hs + D} \tag{4.37}$$

For any output signal $y(t)$, the system model comprises a sequence of the dynamic behaviour of d modes. This sequence can be approximated in a linear model around a stable operating point where TF is written as (4.38).

$$G_j(s) = \frac{\Delta y_j(s)}{\Delta u(s)} = \sum_{i=1}^{d} \frac{R_i}{s - \lambda_i} \tag{4.38}$$

where $j = 1,2, \dots, m; \; i = 1,2, \dots, d$; with m being the number of outputs and d is the number of modes. R_i is the residual, which is directly coupled with the amplitude of each mode to generate the output signal. When the output signal of the system is sampled at a constant sampling rate Δt, the sampled signal is represented as (4.39).

$$y_j(k) = \sum_{i=1}^{d} R_i z_i^k \tag{4.39}$$

where k denotes the samples, and $z_i = e^{\lambda_i \Delta t}$ is the discretization of model variable $z(t)$, with $\lambda = \sigma + j\omega$ (eigenvalue). The set of snapshot matrix of $\boldsymbol{A}$ representing the dynamic modes of the system is given by (4.40).

$$X = [\Delta f \ \ \Delta P_e]^T \in \mathbb{R}^{2\times N} \tag{4.40}$$

Since the states of the system in the time domain can be estimated as a linear combination of the terms $\alpha_i e^{\lambda_i t}$, it can be seen that eigenvalues λ_i can be linked to the physical parameters of the system by a linear combination factor (LCF) α_i [231]. Considering that dynamic modes are observed during the dynamic response of the system and each observed variable is recorded by N samples with interval Δt, the dynamic modes and eigenvalues can be used to approximate the dynamic characteristics of the system.

To estimate the inertia, the frequency and power deviations are recorded as input and output of the reduced power system model in samples to construct the snapshot matrix. Considering that the LCFs for the frequency deviation and active power variation for i^{th} dynamic modes are $\alpha_{i,\Delta f}$ and $\alpha_{i,\Delta P_e}$, respectively, and λ_i is the i^{th} eigenvalue, the time progressions of the dynamic mode reconstructions for the frequency and power deviations can be given as (4.41) [233].

$$\begin{bmatrix} \Delta f \\ \Delta P_e \end{bmatrix} = \sum_{i=1}^{d} e^{\lambda_i t} \mathscr{b}_i \begin{bmatrix} \alpha_{i,\Delta f} \\ \alpha_{i,\Delta P_e} \end{bmatrix} \tag{4.41}$$

where $\mathscr{b}_i$ represents initial value coefficient corresponding to the i^{th} eigenvalue. Inserting (4.41) in the linearized swing equation (4.36) and neglecting the damping, the linearized dynamic equation is reconstructed by the dynamic mode as presented in (4.42).

$$\frac{2H}{\omega_0} \sum_{i=1}^{d} \lambda_i \, e^{\lambda_i t} \mathscr{b}_i \alpha_{i,\Delta f} = -\sum_{i=1}^{d} \lambda_i \, e^{\lambda_i t} \mathscr{b}_i \alpha_{i,\Delta P_e} \tag{4.42}$$

Rewriting (4.42) for arbitrary t, $e^{\lambda t}$ can be eliminated from (4.42) to obtain (4.43).

$$2H \alpha_{i,\Delta f} \lambda \mathscr{b} = -\alpha_{i,\Delta P_e} \mathscr{b} \omega_0 \tag{4.43}$$

The effective inertia of the system H_e can therefore be obtained by solving (4.43). Since the equation is linear and does not contain the derivative of the rotor speed, the proposed methodology can accommodate large-scale power systems with high dimension.

Also, to avoid some eigenvalue computation problems such as singularity in state matrices and difficulty in finding a complete set of unstable poles of the state matrices in analysing big power systems, the proposed algorithm is incorporated with the following additional attributes:

- The algorithm extracts only significant eigenvalues.
- The algorithm incorporates subspace accelerated Rayleigh quotient iteration to speed up eigenvalue computation, improve convergence, and compute poorly damped eigenvalues.
- The algorithm is designed to avoid any singularity in state matrices.

Fig. 4.2 presents the generalized flow diagram of the proposed method. Likewise, additional clarity of the proposed technique is provided on algorithms 4.1 and 4.2.

Algorithm 4.1: Online inertia estimation – part I

Part I: System identification and recursive parameters estimation
Collect a sequence of input-output data vectors, $u(k)$, $y(k)$ measured at time step k. Estimate the hypothesis of the system TF model using (4.10) to (4.17) applying the non-recursive least-squares approach. Start a recursive least squares method to estimate the parameters of the model by running (4.31), (4.30) and (4.32) sequentially. Perform the SVD of the weighted oblique projection to determine the order by inspecting the singular values in S using: $$W_1 \mathcal{O}_i W_2 = USV^T$$ Transform TF to state-space model and extract system dynamic matrix $\boldsymbol{A}$.

Algorithm 4.2: Online inertia estimation – part II

Part II: Eigenvalue and inertia extraction
Determine the eigenvectors and eigenvalues from the obtained dynamic matrix $\boldsymbol{A}$ of the system. $$\dot{x} = \boldsymbol{A}x$$ $$\boldsymbol{A}\vec{V} = \lambda\vec{V}$$ Determine the quantitative relationship between the eigenvalue of the dynamic matrix $\boldsymbol{A}$ of the model and the linear estimated swing equation. $$\frac{2H}{\omega_0}\sum_{i=1}^{d}\lambda_i\, e^{\lambda_i t}\mathscr{b}_i\alpha_{i,\Delta f} = -\sum_{i=1}^{d}\lambda_i\, e^{\lambda_i t}\mathscr{b}_i\alpha_{i,\Delta P_e}$$ Extract the estimated inertia of the system by defining the dynamic mode corresponding to the eigenvalue that corresponds to the inertia of the system. $$2H\alpha_{i,\Delta f}\lambda\mathscr{b} = -\alpha_{i,\Delta P_e}\mathscr{b}\omega_0$$

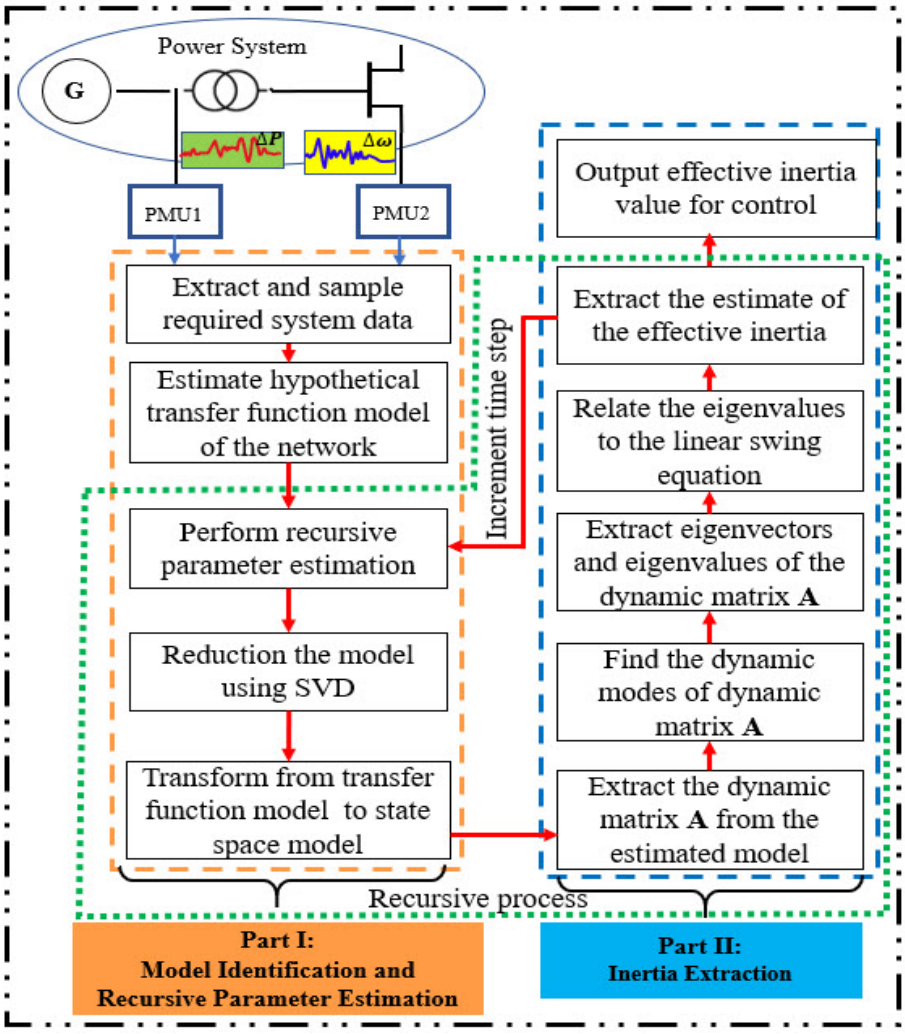

Fig. 4.2 Flow diagram of the proposed recursive algorithm for online inertia estimation

4.4 Simulation case study: IEEE 39 bus network

In this section, a modified IEEE 39-bus system is considered to demonstrate the applicability and accuracy of the proposed method. The system is a typical interconnected power system, which can be used to validate a proposed technique in power system studies. The network has 10 generators, 12 transformers and 19 loads. Besides, the network is interconnected by 34 lines as depicted in Fig. 4.3, which includes RESs. DIgSILENT™ PowerFactory® 2019 is used to model, test and simulate the dynamic behaviour of the system.

4.4.1 Data pre-processing and model preparation

The case study network is used to obtain data sets to be used for the proposed online inertia constant estimation method. The real theoretical inertia constant value (H) is entered for each synchronous generator in the case study network. Then, the technique is used to estimate individual inertia value of each generator in the network by investigating the electromechanical

responses of the generators. Subsequently, the related modes are extracted. To perform these steps, the algorithms to estimate the total inertia constant for the aggregated network are presented on algorithms 4.1 and 4.2 and summarized in Fig. 4.2. For the aggregated network, permanent magnet synchronous generator (PMSG) wind power plants with synthetic inertia controls are also integrated into the model to replace some of the synchronous generators. The PMSG wind power plants with synthetic inertia controls are integrated step by step to emulate different levels of penetration of RESs into the grid as presented in the modified IEEE 39-bus network in Fig. 4.3. For each level of RESs penetration, the algorithm is used to estimate the available inertia in the system.

To capture the network transients, root mean square/electro-magnetic transient is used as the simulation type in PowerFactory®. For the modes and eigenstructure analysis, Model/Eigenvalue analysis is used as the simulation type in PowerFactory®. The case study network is aggregated to perform as a single generator network. Furthermore, all the PMUs measurements from all generator buses are aggregated to perform as a single machine infinity bus network.

Before performing the algorithm for online effective inertia estimation of the network, it is essential to construct the operational structure of the system and to determine the required measurements and the COI where the effective inertia can be estimated. Equation (4.3) is used to locate the relatively acceptable COI, and frequency is measured from this COI. By definition, the COI frequency is the frequency of the bus at or around the centre of the network relative to other buses of the network [158]. For the aggregated IEEE 39-bus network, Fig. 4.4 presents the frequency of bus 14 as the selected best bus to represent the COI frequency using (4.3), where all frequency measurements for effective inertia estimation are taken.

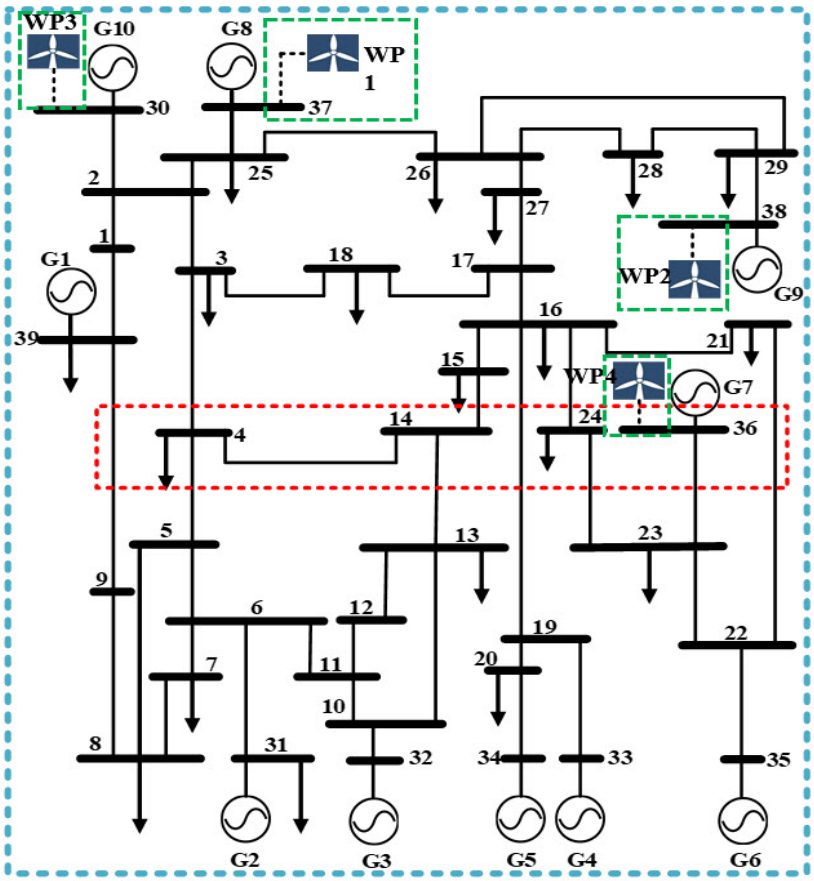

Fig. 4.3 A modified single line diagram representing the IEEE 39-bus network

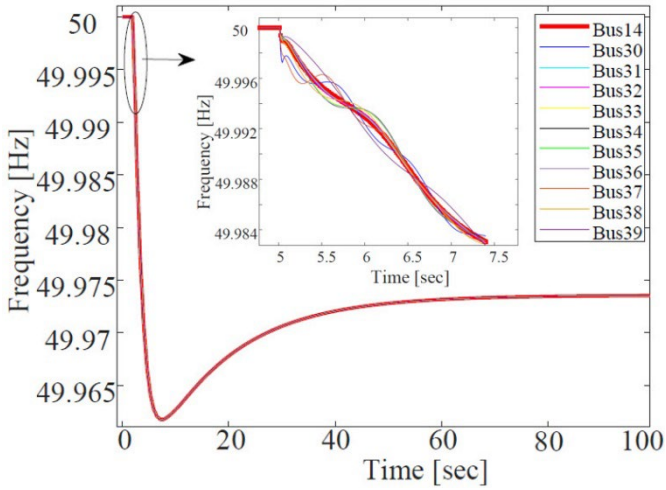

Fig. 4.4 Step response of the IEEE 39-bus network model showing frequencies at different generator buses and COI frequency

Based on power variations at different buses, which further cause frequency responses of the network, the data are collected as presented in Fig. 4.5. Before the model identification step, the data is pre-processed to improve the identification process and the estimation performance. In this case, the algorithm part I procedure of the proposed method, as presented in algorithm 4.1, is

performed to estimate the hypothesis model and recursive parameters of the system model. The model is cross-validated using data collected in a different time span. The cross-validation is intended to authenticate the relevance of the model in representing the dynamics of the system. The cross-validation for the model is presented in Fig. 4.6, which gives a fitting ratio (FR) of 96%.

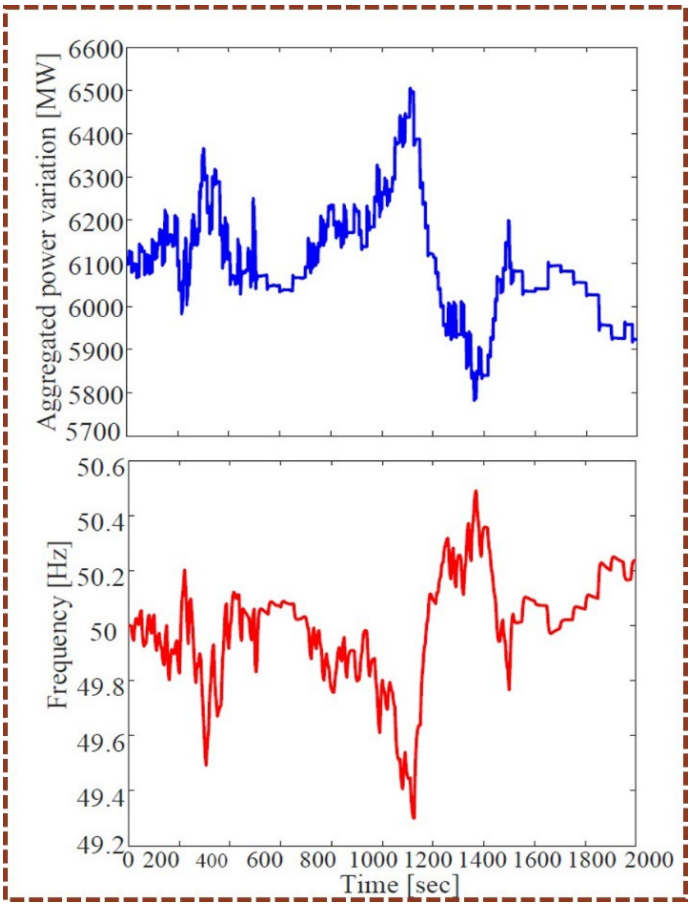

Fig. 4.5 Simulation results of case study network indicating trajectories of active power and COI frequency

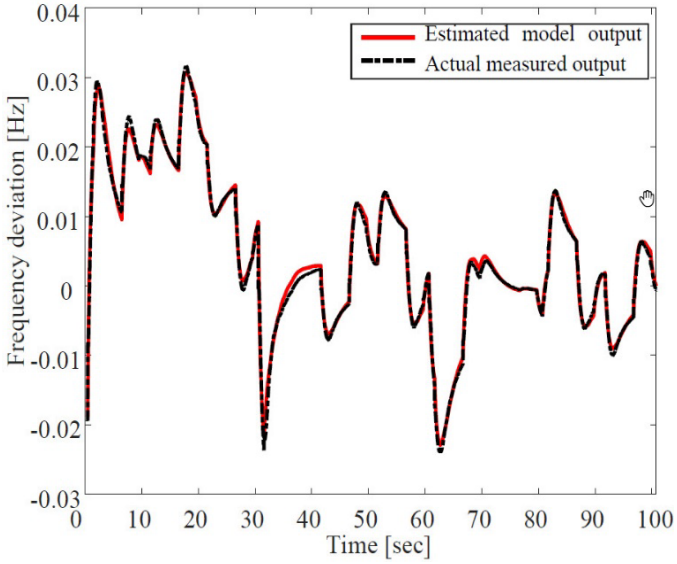

Fig. 4.6 Representation of 96% FR to justify the estimated model

4.4.2 Online inertia constant estimation for each generator

Based on the recorded rotor speed response at each generator as shown in Fig. 4.7, the input snapshot matrix for the dynamic modes of generator G01 and the dynamic matrix $\boldsymbol{A}$ extraction as presented in (4.4) is constructed. The examples of extracted dynamic modes of G01 are presented in Fig. 4.8. The eigenvalues are extracted from the dynamic matrix $\boldsymbol{A}$ as presented in Fig. 4.9. According to the suggested approach in [39], estimating inertia for each generator requires at least a fourth-order estimated state-space model. This means that at least four distinctive eigenvalues must be attained. Fig. 4.9 shows a reasonable number of obtained stable pair of conjugate and real eigenvalues. By using the FR comparison, the results show that the extracted eigenvalues and eigenvectors are acceptable by achieving the FR of more than 95% [162]. In this simulation, the inertia values are provided by each synchronous generator.

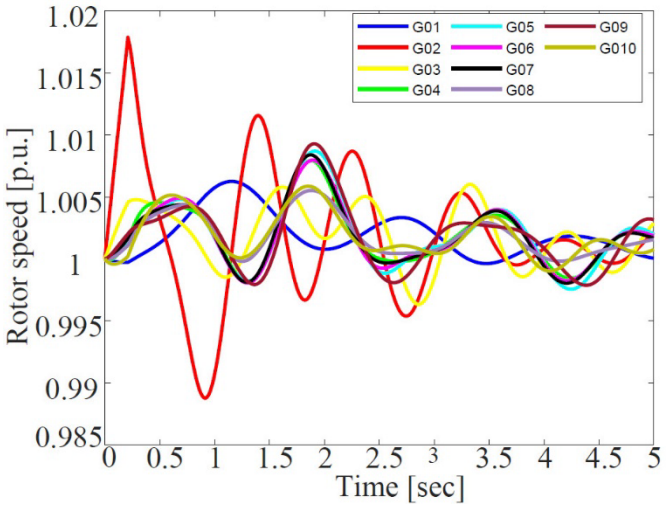

Fig. 4.7 The time-domain trajectory of rotor speed for generators

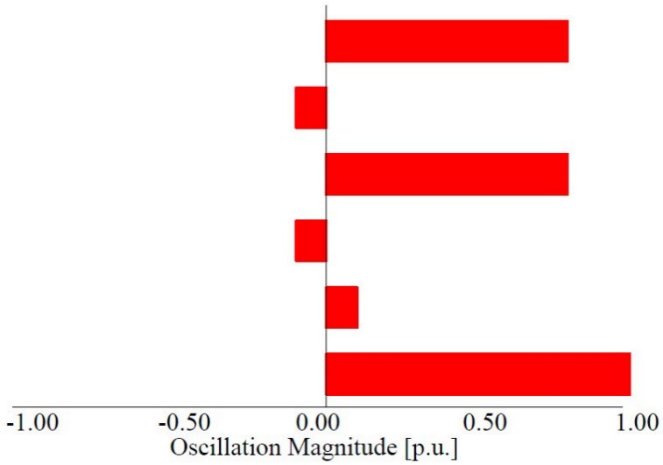

Fig. 4.8 Oscillation modes extracted from generator G01

The proposed algorithm is intended to estimate the inertias from different generators. The comparison between the actual inertia and the average estimated inertia results in an estimation error. Table 4.3 presents the average estimated inertia for each generator in the network with the associated percentage error for each estimation. Fig. 4.10 presents pictorial comparisons of the actual and the average estimated inertia for each generator in the network. The corresponding error graph for each generator is depicted in Fig. 4.11. The worst-case is observed at bus 38, where G09 is located. At this generator, the algorithm returns the inertia estimation with a percentage error of 3.57, which is the worst-case compared to the rest of the generators' estimations.

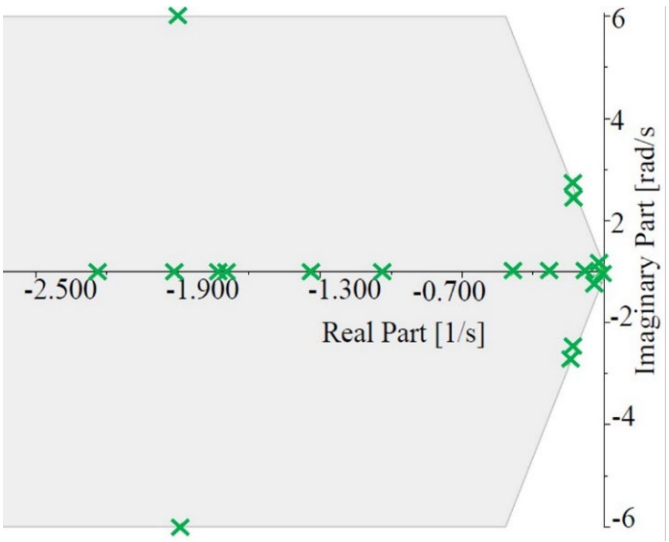

Fig. 4.9 Stable eigenvalues of generator G01

Table 4.1

Inertia estimation for different generators

G/No	Bus No	Actual inertia[s]	Estimated inertia[s]	%Error
G01	39	5.00	4.861	2.78
G02	31	4.329	4.508	1.94
G03	32	4.475	3.459	0.74
G04	33	3.575	3.459	3.24
G05	34	4.333	4.402	1.59
G06	35	4.35	4.451	2.32
G07	36	3.771	3.671	2.65
G08	37	3.471	3.497	0.75
G09	38	3.45	3.573	3.57
G10	30	4.2	4.110	2.14

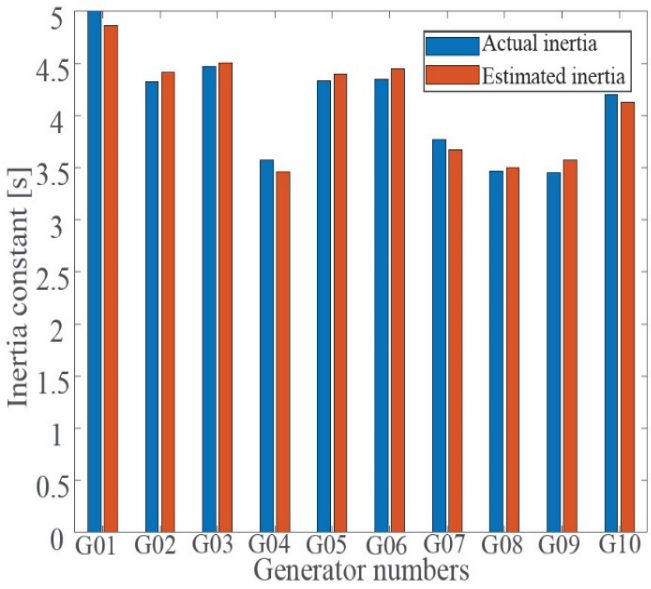

Fig. 4.10 Comparison of actual inertia and average estimated inertia for different generators

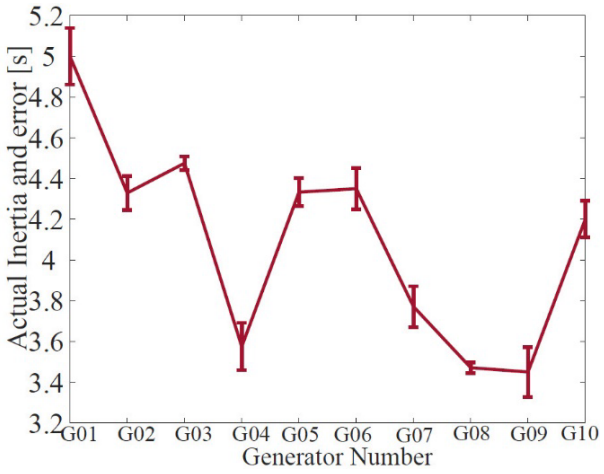

Fig. 4.11 Actual inertia and corresponding estimation error for different generators in the case study network

4.4.3 Online inertia constant estimation for aggregated network

The proposed inertia estimation technique is tested on the aggregated IEEE 39-bus network to further verify its applicability and accuracy. Initially, the equivalent inertia (H_{eq}) is calculated using (4.3) for all generators in the network as presented in Table 4.4.

Table 4.2

Generators' actual inertias and the total inertia constant for the case study network

Bus No	Generator	*SB [MVA]*	*H [s]*	*SB*x*H*
Bus39	G_1	10,000	5	50,000
Bus31	G_2	700	4.329	3,030.3
Bus32	G_3	800	4.475	3,580
Bus33	G_4	800	3.575	2,860
Bus34	G_5	300	4.333	1,299.9
Bus35	G_6	800	4.35	3,480
Bus36	G_7	700	3.771	2,639.7
Bus37	G_8	700	3.471	2,429.7
Bus38	G_9	1,000	3.45	3,450
Bus30	G_10	1,000	4.2	4,200
			Total	76,969.6
			SB	10,000
			Heq	7.6969

To incorporate RESs in the network, PMSG wind power plants are used to replace the conventional synchronous generators in the network. Based on the topology of the IEEE 39-bus network, a modified system is generated in steps by increasing the percentage of RESs in the network from 0% to 65%. The first scenario considers a purely conventional network driven by traditional synchronous generators only. Then, wind generators replace synchronous generators G08 and G09 at buses 37 and 38, respectively, to incorporate the second scenario of 10% RESs penetration in the network. The third scenario is the replacement of generators G07, G08, G09 and G10 for penetration of 20% RESs in the network. The fourth scenario is the replacement of generators G02, G03, G04, G05, G06, G07, G08, G09 and G10 to obtain a penetration of 40% in the network. Furthermore, the fifth scenario of 60% penetration is obtained by replacing G01 in the network. The last scenario is obtained by replacing G01, G02 and G05 to achieve a 65% penetration of RESs in the network.

For each penetration of RESs in the network, the average RoCoF is obtained. Table 4.5 presents different average RoCoF values as recorded for different levels of RESs penetration in the case study network used for simulations.

Table 4.3

Average RoCoF values for various percentages of RESs penetration

RESs Penetration in [%]	RoCoF value recorded *[Hz/s]*
0	0.01
10	0.25
20	0.5
40	1.1
60	2.0
65	2.2

The electromechanical response of each of the modified network scenario is stimulated by power variations to record the frequency response. The measured data of power variations and frequency response of each scenario as presented in Fig. 4.5 are employed in the proposed algorithm to estimate the total inertia of the study case network with the corresponding percentage of RESs penetration. The effective inertia value corresponding to every level of RESs penetration in the network is presented in Table 4.6. Fig. 4.12 compares the actual inertia in the case study network to the average inertia estimated by the proposed method. The corresponding errors are presented in Fig. 4.13.

Table 4.4

Actual inertia compared to average estimated inertia for various percentages of RES in the case study network

RESs penetration [%]	Actual Inertia value, H [s]	Average Estimated Inertia [s]	Percentage error [%]
0	7.69	7.48	2.73
10	7.11	6.94	2.39
20	6.69	6.50	2.80
40	5.01	4.85	3.10
60	3.73	3.60	3.50
65	3.08	2.96	3.80

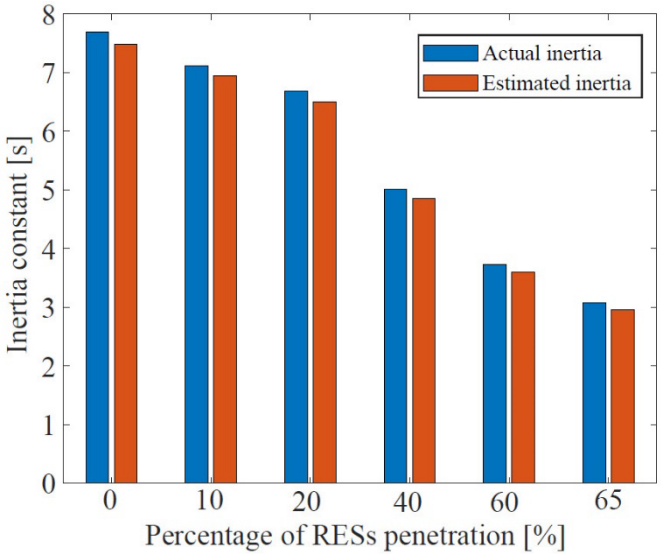

Fig. 4.12 Actual inertia compared to average estimated inertia for various percentages of RES in the aggregated case study network

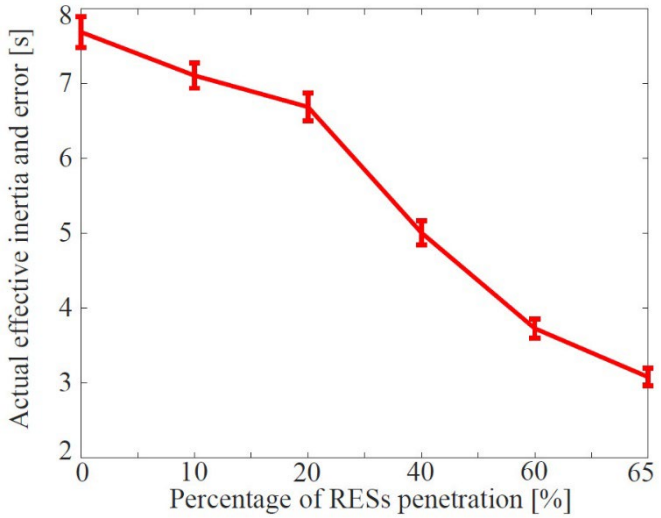

Fig. 4.13 Actual inertia and corresponding estimation error for the aggregated IEEE 39-bus network with different RESs penetrations

4.4.4 Online inertia constant tracking for aggregated network

In support of the applicability of the proposed method, Fig. 4.14 presents the simulation results of time-varying inertia together with a tracking estimation trajectory. The tracking trajectory is obtained using the proposed method explained in Section 3. Using the recursive model parameters estimation to track the inertia of the aggregated network, it takes a total of 8 s to run a 200 s simulation with a sampling time of 0.01 s. On the other hand, a 1 s simulation of the entire hypothesis model with a sampling time of 0.01 s updated using the recursive method takes a total time of 5.6 hours to complete. For these simulations, an office computer (Intel(R)

Core (TM) i7-9700 CPU @ 3GHz, 32GB RAM) is used to simulate both models. A massive difference in computation time can be noted between the two approaches. Hence, the significant reduction in computation burden using the proposed method is verified.

It can also be noted from the simulation result on Fig. 4.14 that the tracked inertia, which is obtained by using (1) for each step of inertia reduction, exhibits a step change for each variation. It should be noted that even after the penetration of RESs, the network frequency response is still dictated by the synchronous generator inertia though at a reduced level. With these fast-changing actual inertia values, the proposed method can still track the changes. It can further be noted from Fig. 4.14 that the tracking trajectory has an average speed of 1.5 s in tracking the actual inertia changes. This means, after each step change in the actual inertia, the proposed method takes an average of 1.5 s to estimate the new value of inertia change in the network. This is a good speed of estimation given the fact that weather changes might not result in a step change of the actual inertia in the network. The step changes of inertia provided in the simulation are faster than weather dependent inertia changes. For this reason, the proposed method can easily track the weather-dependent time-changing inertia in power systems.

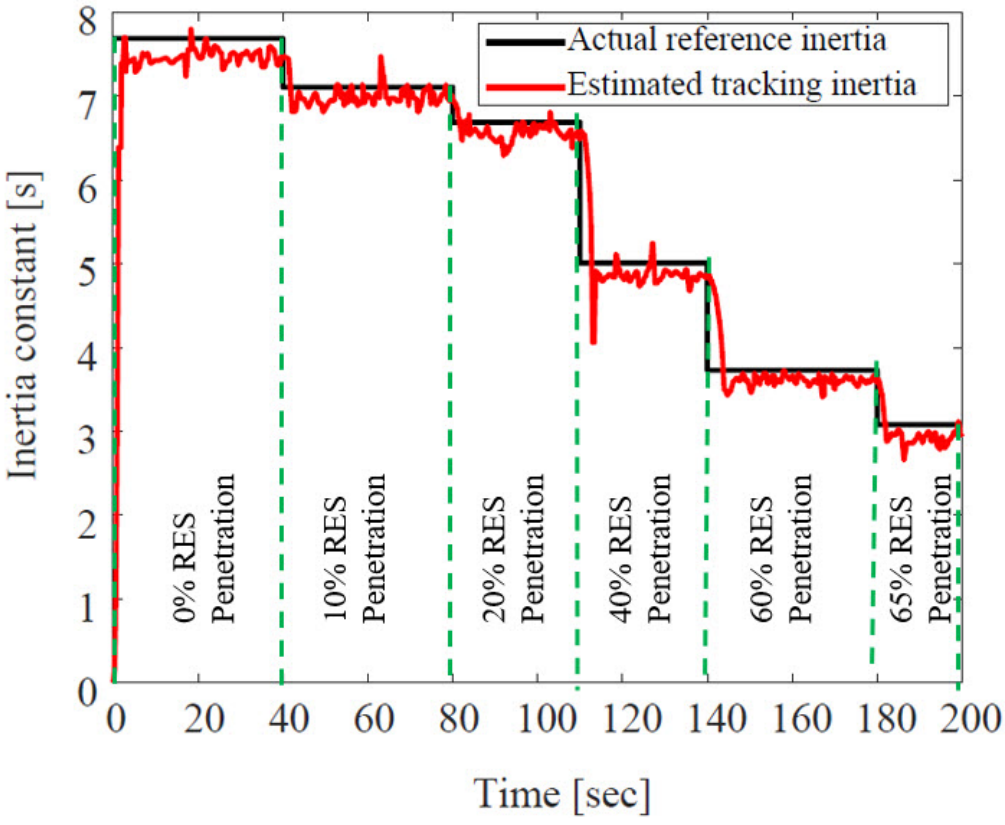

Fig. 4.14 Online inertia constant tracking for the aggregated IEEE 39-bus network with different RESs penetrations

4.5 Validation using real measurements data

The effectiveness of the proposed technique is tested using data from the New Zealand network. The New Zealand network is one of the smallest networks worldwide [93]. It includes North and South islands, which are interlinked with an HVDC line. The network consists of hydro generators, Combined Cycle Gas Turbines and geothermal stations. The respective ranges of inertias for the generators are 2 s to 4 s, 5 s to 6 s and 3 s to 6 s. In addition, the network comprises wind generation units that do not supply any inertia to the network. Therefore, more integration of wind power units into power systems, which may replace some synchronous generators, reduces the total inertia of the network.

The wind power contribution in the current status of the New Zealand network is small as it contributes less than 5% of the entire installed capacity. The total inertia value of the network is calculated by using (4.3) as presented in Table 4.7. Fig. 4.15 shows the normal record of the network frequency on December 15, 2019, from 09:10:00 to 09:35:00 as recorded from the COI. The information of the generators including the inertia values for the network is obtained from Ref. [219].

Using (4.3), the total inertia value of the network was calculated to be 8.02 s. This value was obtained with a wind power contribution of 0.9% in the network. This contribution is too low to make a sound effect of the total inertia variation in the network. The system bases power and frequency used for the calculation of the total inertia constant value in the network are 3000 MVA and 50 Hz, respectively. Table 4.6 also presents different information for different types of generators at the time of data recording. The field measured data is pre-processed to enhance identification by improving efficiency and accuracy. The obtained signals are detrended by eliminating mean values. To remove noise from the data, the signals are passed through an order of ten non-causal, zero-phase low-pass filter set at 3 Hz and then down-sampled to four samples per second [234]. The data is down-sampled to increase the estimation accuracy of modes of the generators.

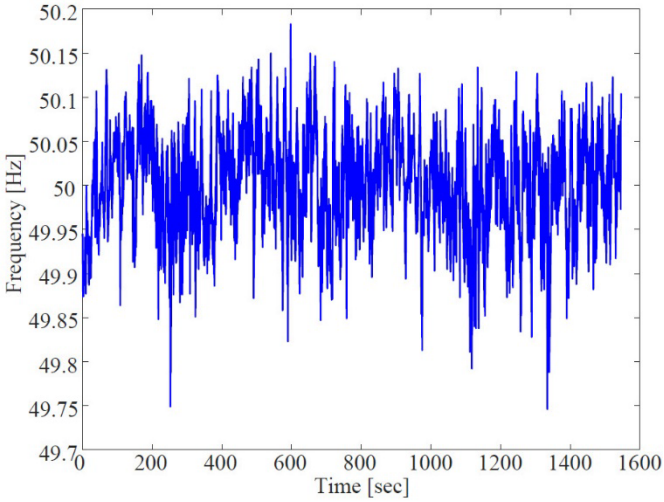

Fig. 4.15 Logged frequency fluctuations at the COI of the New Zealand network

The recorded active power variation and the frequency responses are sampled to represent input data $u(t)$ and output data $y(t)$, respectively. Then, the non-recursive least-squares approach steps 1 and 2 from the algorithm 4.1 are used to estimate the model of the network. Then, the comparison between the estimated and the actual models is done by calculating their FR. For this test network, the resulted FR is 85%. This FR is good, satisfactory and acceptable for the network data used [179]. Fig. 4.16 represents the graphs of the actual and estimated models of the network with the FR of 85%.

The proposed recursive least squares method is used for parameters estimation of the estimated model and recursively estimating and extracting the inertia value of the network. Using the proposed method, the estimation of the average inertia constant ($\bar{H}$) of the network is found to be 7.5 s. Comparing the actual total inertia constant H with estimated inertia as presented in Table 4.6, the percentage error is computed to be 8.54%. As the percentage error is less than 10%, this confirms and validates the applicability of the proposed method.

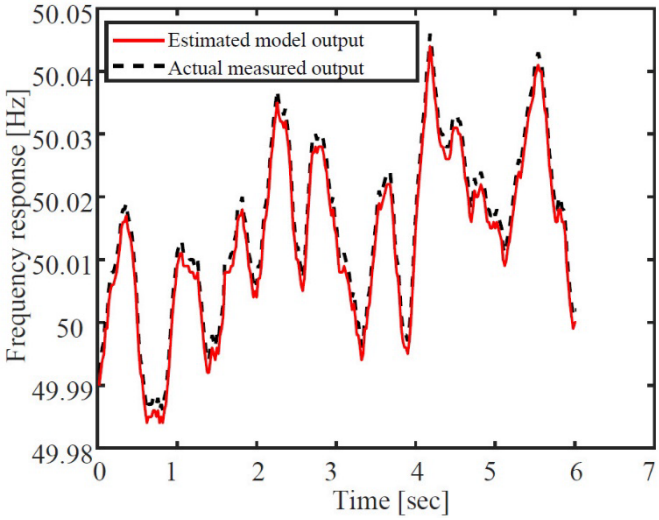

Fig. 4.16 A FR of 85% to justify the estimated model when compared to the actual New Zealand network model

Table 4.5

New Zealand network power generating units with related power capacities and inertia constants

Generating units	Average active power (MW)	Average capacity (MVA)	Average Inertia H (s)
	North Island (NI)		
Wind	240	564	0
Hydro	720	1838	3.4
Geothermal	882	1064	3.1
Coal	184	500	1.5
Gas	797	1150	3.8
Co-Generation	160	277	1.2
NI Total	2799		
	South Island (SI)		
Wind	45	94	0
Hydro	2410	3670	3.5
SI Total	2455		
NZ Total	5254		8.02

4.6 Conclusion and future work

An online inertia estimation technique is presented in this paper. First, the inertia estimation is carried out for each generator in the network. Second, inertia estimation is also carried out for different levels of inertia constant in the aggregated case study network. The

different levels of inertia constant presented are a result of different percentage of RESs in the network. Further, consistent estimates using the proposed online inertia estimation technique are obtained, which are in the range of 0.74% to 3.57% for individual generators in the network. Besides, the error range of 2.39% to 3.80% is observed for the equivalent inertia of the aggregated network. Finally, an error of 8.54% is obtained for the actual data from the real network. Besides, the proposed method proves to be effective in online estimating the power system inertia. On top of that, since the method does not need to store previous data after each sample step, the computation burden is significantly reduced in the proposed technique. More importantly, the technique incorporates the use of available electromechanical oscillation modes in the system, which can be linked to parameters of the power system for online estimation of the network inertia.

Future work of this research is to extend the online inertia estimation method while incorporating coordinated synthetic inertia in the network as a support for reduced inertia in future power systems. Likewise, due to the high penetration of weather-dependent generation units, the study of weather forecast effects in the equivalent inertia of the network is important to be incorporated. In the same way, how fast the estimated inertia can be communicated to PSOs for fast stability control of the network will be looked at.

Chapter 5 Manuscript 4: Inertia Forecasting

Preamble

The need for prior knowledge of network inertia is another area requiring attention in modern power networks with uncertainty behaviour and quick inertial responses. Prior information of network inertia is crucial for planning, controlling and protecting the network with reduced inertia. Knowing the inertia values in a network in advance will identify when the network is likely to be potentially at risk in a reasonable time ahead. Therefore, Chapter 5 provides a long-range inertia forecasting method in modern networks. The proposed method uses an improved ARIMA model ($\boldsymbol{i}$-ARIMA) approach. Furthermore, the method introduces a moving observant predictor used in the strong periodicity and seasonality patterns of the historical data and a smoothing factor to improve the accuracy of the forecasted values. Compared to other forecasting methods in the literature, the presented method can forecast inertia values in the network for a longer time ahead.

Long-range forecasting and tracking of inertia values in modern power systems

Peter Makolo[1,2,*], Ramon Zamora[1] and Tek-Tjing Lie[1]

[1]Department of Electrical and Electronic Engineering, Auckland University of Technology, Auckland 1010, New Zealand
[2]Department of Electrical Engineering, University of Dar es Salaam – Dar es Salaam, Tanzania

Abstract: Reduced network inertia due to high levels of penetration of non-synchronous generators in modern power systems is becoming a pressing issue. As a result, very quick inertial responses are observed when power imbalances happen in networks. Due to quick inertial responses, there is practically a very short time for control actions in real-time. Therefore, system operators need to priorly understand the inertia values in order to plan, control and operate the network securely. Unlike short-range forecasting methods, long-range forecasting of inertia values in the network will identify when the network is likely to be potentially at risk in a reasonable time ahead. Thus, this paper proposes an improved ARIMA model (***𝒊***-ARIMA) approach to long-range forecast inertia values in a modern network. The ***𝒊***-ARIMA uses strong periodic and seasonality patterns of historical time series data to long-range forecast future inertia values. The ***𝒊***-ARIMA method is tuned for optimal values of a moving observant predictor $\mathfrak{P}$, periodicity and seasonality factor $\mathcal{s}$ and smoothing factor $\mathcal{n}$ that give the best forecasts with competitive accuracy. Rigorous evaluation and tests of the method, which are done on the New Zealand network data, show the ***𝒊***-ARIMA to be fast, robust, accurate and superior to other forecasting methods.

5.1 Introduction

5.1.1 Background and motivation

Synchronous generators have been an integral part of power systems for several decades. They have been used conventionally to generate active power, regulate frequency and voltage, and provide inertia in power systems [42]. The power system's inertia potentially determines the ability of the network to maintain stability when subjected to power imbalances. More specifically, power system inertia is vital in compensating for variations and disturbances up to 5 seconds after the contingency [42, 162]. Although inertia is important only in the first instants after the occurrence of power imbalance, its impact is very crucial in the network as it determines the stability of the network.

Conventional synchronous generators that are synchronised to the power system are the fundamental source of inertia in the grid. Synchronous generator inertia provides a natural response during power contingencies by limiting the rate of change of frequency (RoCoF) when power imbalances occur in the grid [18]. The process of limiting the RoCoF in the network allows other protective and control actions such as primary frequency control to be taken before power failures happen in the network [235]. It should be noted that networks with more conventional synchronous generators (SGs) than non-synchronous generators (NSGs) are rich in inertia values. These networks are said to have high operational stability as they can withstand several contingencies before failures. Contrary, networks with less conventional synchronous generators have less inertia property and therefore are weak networks as they are prone to contingencies. Power imbalances in low inertia networks can lead to serious problems such as load-shedding, generator damages and possibly power blackouts [71]. Therefore, inertia is such an important property in power systems, which can decide the operational stability of the network.

On the other side, increasing integration of renewable energy sources (RESs) such as wind, solar power and a large fleet of electric vehicles, which are linked to the network using converter-based technologies, is rapidly replacing SGs in the modern network [67]. Most of these RESs are non-synchronous generators with zero or very small inertia contribution to the grid. It should be noted that one of the fundamental impacts of increasing penetration of RESs to the network is the decrease of the conventional inertia from the grid. Although these RESs can be controlled to provide the so-called synthetic inertia and frequency support to boost the low inertia grid, the time variability of the total inertia is another concern to be addressed for the stability analysis of the power system [8].

Therefore, it is worth highlighting the time variability of inertia in the power system as the penetration level of converter based RESs increases to the grid. As most of RESs depend on

weather conditions to harness their energy, their power contribution to the grid will vary from time to time [236]. In this way, the number of connected synchronous generators may as well change from time to time. Thus, the values of inertia in the network will be fluctuating from time to time depending on the number of SGs connected or replaced by NSGs [19]. If weather conditions such as wind and solar allow more power to be fed to the network from RESs, then more conventional synchronous generators will be replaced for economic reasons [7]. The intensive replacement of conventional synchronous generators causes traditional inertia to be dramatically reduced from the grid. Hence, the system inertia varies with time depending on the weather conditions and the status of the synchronous generators over time [7].

The fact that network inertia can be a variable quantity in the network triggered transmission system operators' (TSOs) interest to prior understand the system inertia behaviour in power systems [7]. Prior understanding of system inertia will enable power system operators (PSOs) to take the right control actions related to the system stability and operate the network securely [19]. Regarding understanding the behaviour of network inertia, several offline and online inertia estimation techniques have been established in the body of literature. The techniques are intended to understand the values of inertia in the power system. For instance, offline techniques such as in [14-16] are established to understand the historical inertia values when events happened in power systems for analysis purposes. This is to say, information obtained from offline inertia estimation techniques cannot be used for protection and remedial measures in real-time. For this reason, online inertia estimation techniques such as in [6, 17, 18] are then established to monitor the inertia values in the power system and, therefore, can be used for analysis in real-time.

Nevertheless, as inertia is becoming a time-dependent parameter in the power system, offline and online inertia estimation techniques cannot serve grid protection purposes. Also, it should be noted that due to fast transient response, the online inertia techniques may be prone to instabilities in power systems in case of contingencies happening at low inertia, which is not predicted in the time ahead [19]. Therefore, prior understanding of network inertia well in the time ahead is important to long-range forecast the behaviour of the power system. The reduction of total rotating inertias, which results in fast transients, needs to be forecasted in networks.

Again, synthetic inertias (a term consistently used in this paper) that may be also known as virtual or digital inertias are becoming tradable quantities to support frequency in power systems [20]. Synthetic inertias are gaining popularity as they supplement conventional inertia in supporting frequency stability networks. Thus, purchasing a fixed quantity of synthetic inertia and applying it into the network is not effective and economical as the system inertia can vary over a wide range in a year. Undetermined low inertia conditions and inadequate auxiliary frequency support services could pose a serious risk to the reliability and security of the network. For this reason, real-time and prior knowledge of the system inertia is crucial so that a minimum

level of inertia can be planned, determined and purchased well in the time ahead to maintain stability, security, and reliability of the network when contingencies happen. A minimum level of inertia should be always maintained in the network to assure secure operation of the network [20]. Therefore, understanding the network inertia values in the time ahead gives the assurance to avoid possible risks of instability in the power system. In addition to maintaining the minimum level of inertia in the network, PSOs can schedule fast frequency response services and appropriate reserves to provide appropriate responses to the network under contingencies [8].

Consequently, appropriate methods to precisely forecast inertia values in the power systems are crucial to avoid risks associated with extended low inertia operating times. To achieve this goal, this research work proposes a method for short- and long-range forecast of network inertia. The proposed method introduces an improved ARIMA (i-ARIMA) algorithm. The i-ARIMA uses strong periodic patterns and seasonality of historical time series data to short- and long-range forecast future values. The i-ARIMA method is tuned for optimal values of moving observant predictor $\mathfrak{P}$, periodicity and seasonality factor s and smoothing factor n, which collectively give best forecasts with competitive accuracy. Rigorous evaluation and tests of the method, which are done on the New Zealand data, reveal the i-ARIMA to be fast, robust, accurate and superior to other forecasting methods.

5.1.2 Overview of the New Zealand network

The applicability of the proposed method is evaluated and tested on the data obtained from the New Zealand network. The available data used are for the years from 2012 to 2016. Therefore, to get a clue of the network, this subsection gives an overview of the New Zealand network.

New Zealand grid is owned and operated by Transpower New Zealand, a state-owned enterprise, which transports bulky electricity from generation centres to load centres as depicted in Fig. 5.1(a). As part of the network, there is a high voltage direct current (HVDC), which part of it is a submarine cable that inter-links North and South islands as shown in Fig. 5.1(a). New Zealand is among the few countries with a high percentage of RESs in its energy mix. New Zealand's electricity generation is around 80% renewable with hydropower contributing just over half of that energy [237]. With rising power demand on electric vehicles, New Zealand through the Net Zero Grid Pathways (NZGP) project intends to boost the RESs to 96% by 2025 and full 100% by 2035 [237]. Next to hydropower, wind power contributes significantly to New Zealand's energy mix. New Zealand wind energy association (NZWEA) has the vision to increase wind power contribution to 20% by 2035. As it stands, the current wind contribution is around 8% in New Zealand [238]. Fig. 5.1(b) shows the geographical locations of the wind power plants in New Zealand.

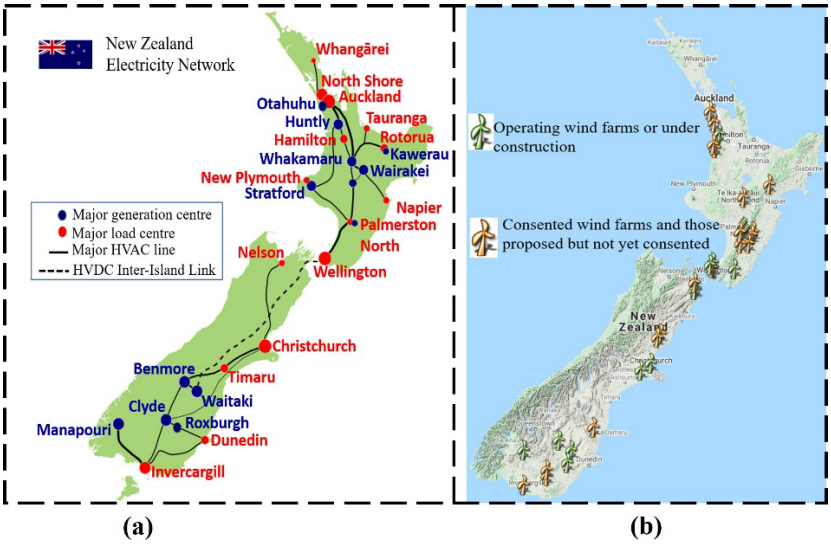

Fig. 5.1 (a) New Zealand grid showing the interconnection of major power generation centres to major load centres, (b) Geographical locations of wind power plants in New Zealand

In the process to achieve 100% renewable power generation, the country would need to retire its old and less efficient fossil fuel plants and build more wind farms as well as erect more solar panels. For this reason, as noted in subsection (1.1), inertia will be significantly affected in the future of the New Zealand network [15]. Therefore, while embarking on more renewable energy sources, inertia tracking and forecasting are crucial for ensuring that the stability of the future network is maintained. To achieve this, this paper proposes the inertia tracking and forecasting method in which New Zealand data are used to validate the method [219, 239].

5.1.3 Literature review

Inertia estimation techniques have become more popular as more integration of RESs takes place in the power system. Offline and online inertia estimations approaches have been intensively explored in the body of literature. However, inertia forecasting has not been intensively discussed in this research direction. Therefore, it is important to understand why inertia estimation is crucial in power systems. In this context, it should be known that the replacement of traditional synchronous power plants by stochastic non-synchronous generation units leads to lowered power system inertia. This trend weakens frequency stability in the power system. To avoid the risk of weakened frequency stability, inertia estimation techniques are necessary to understand the level of inertia in the network. Understanding the level of inertia in the network is key for scheduling power reserves and for the deployment of fast frequency support devices to maintain frequency stability in the grid [20].

There are plenty of techniques proposed in the literature for power system's inertia estimations. Established on the time horizon of interest, the inertia estimation techniques can be classified as offline, online and forecast techniques. All these estimation methods can further be

grouped into two main groups, namely disturbance data-based and non-disturbance data-based approaches. Within the disturbance data-based group, some methods are based on swing equations and others are based on electromechanical wave theory. Most of the disturbance-based techniques are offline as they are post-mortem approaches. For non-disturbance methods, some methods use probing signal technique and other use ambient signal approach. Most of the later techniques are used in the online (real-time) and forecast (time-ahead) inertia estimation approaches. Most of the proposed techniques employing the swing equation approach estimate the inertia by monitoring the dynamics of active power and the resulting frequency responses. Other approaches link between inertia and the rotor angle of the generator together with the power mismatch in the network.

The following offline inertia estimation techniques, which are mainly used for analytical and post-event assessment of the inertia level in the systems, are analysed. A switching Markov Gaussian model, which is a statistical-based approach is developed in [214]. In this approach, historical data are used to estimate the inertia of the network. The methods developed in [158, 235], which are based on the regression approach, use real-time data of online load and generation mix to estimate the inertia of the network. In [14] a method to estimate the inertia of Great Britain by considering the magnitude of the disturbance and frequency response in the network is proposed. On the other hand, the proposed method in [84] uses transients of frequency measured during an event in connection with the use of swing equation to estimate the inertia of the power system. However, the method is affected by the presence of noise content in the measured transients of the frequency. The methods proposed in [13] and in [11] use autoregressive moving average exogenous models to estimate the system inertia.

The goal of online or real-time inertia estimation techniques is to get an immediate estimate of the inertia based on instantly accessible measurements of the system variables. Several methods with different approaches are proposed in the body of literature. For instance, an online inertia estimation method using data of the active power balance from a wide-area measurement of a power system for the period of large disturbances is presented in [169]. Another online inertia estimation technique using an injection of an additional probing signal is proposed in [162]. In Ref. [186], a recursive adaptive subspace identification algorithm to track oscillation modes in real-time is proposed. The algorithm uses ambient data obtained from phasor measurements units to estimate the inertia of different areas of an interconnected power system. Another ambient-data-based online inertia estimation technique is proposed in Ref. [11].

Generally, the post-mortem offline inertia estimation approaches have three pitfalls as specified in [20], which are:

The techniques depend on networks events to estimate the system inertia. This dependency needs to accurately understand the sizes of the events, which is something difficult.

On top of this, not all events in the power system are suitable for inertia estimation and analytical purposes in the network [167].

The techniques also suffer the problem of time determination for the onset of the events. This is an important feature as stated in [240].

RoCoF is another challenge facing the accuracy of post-mortem inertia estimation techniques. The frequency oscillations and noise content after an event make it difficult to obtain error-free RoCoF [241].

All the offline and online inertia estimation techniques cannot adequately protect the low inertia network from instabilities when contingencies happen in the network. For instance, offline techniques provide a posteriori information, which can only be useful in scheduling stages but not be useful for control actions in real-time [242]. On the other hand, online inertia estimation techniques give the real-time estimation of inertia in the network. However, they are not practical for power system protection as the estimation are provided in real-time. Given the speed of faults in the network, there is not enough time to communicate the estimation to the PSOs and immediately take actions to control the network in case of low inertia values in the network [6, 20, 42]. This is because there is not enough time to plan for fast frequency support facilities as the responses are so quick. The only solution is to accurately forecast the inertia values in the network. Prior knowledge of system inertia and behaviour will allow PSOs to get reasonable time to plan for control, support and protect the network [19].

Given the risks of unanticipated low network inertia conditions and limited time for taking actions after power imbalances in the network, there is an increasing need to forecast and anticipate the values of inertia constant in the modern network [7, 14, 30, 34, 35]. Forecasting of network inertia will anticipate when the grid is likely to be at risk of low inertia. In this way, appropriate measures can be taken well in advance to protect the network stability [8, 9, 20]. Unlike offline and online inertia estimations, this area of inertia forecasting has not been intensively researched. There are only a few proposed methods to forecast the inertia constants in power systems. Some of the methods are discussed in the subsequent paragraph.

Ref. [19] proposes a new tool to forecast the system inertia and evaluates the adequacy of frequency response reserves. In this literature, the need for forecasting network inertia as an important characteristic to evaluate the operational impact of non-synchronous machines on a power grid is justified. Besides, a short-term kinetic energy forecast using a decomposable time series model approach is proposed in [164]. Also in [165], a two-stage stochastic generation and primary frequency response scheduling model to predict the network inertia for primary frequency response adequacy under uncertain wind generation is proposed. On the other hand, an artificial intelligence-based technique is proposed in [177]. In this technique, inertia in a power system with high penetration of wind power plants is forecasted.

Yet, the proposed inertia forecasting methods discussed in the previous paragraphs have some limitations as presented in the following bullets:

- The method proposed in [242] focuses more on online inertia estimation, enhanced by a prediction method for a very short time ahead. System monitoring data can be used to improve the method for long-range forecasting of inertia values in the network.
- The method proposed in [165] fails to justify the accuracy of claimed one-day prediction on system inertia.
- The one hour and three hour time ahead prediction of inertia in [164] and [19], respectively, are relatively short times for reliable planning especially for stability control in large power systems comprising large power plants. It should be noted that large power plants may take a reasonably long time to start and synchronise in the network. It is possible to extend the forecasting time to two days ahead.
- The method proposed in [177] is based on simulation data only. Its application accuracy on real network data is not justified. There is a need to justify the proposed method on the real network data.

5.1.4 Novelties and organization of the paper

The contributions of the method proposed in this paper are of three folds as presented below:

- introduces i-ARIMA algorithm that uses strong periodic patterns and seasonality of historical time series data to long-range forecast inertia values,
- uses moving observant predictor $\mathfrak{P}$ to improve the accuracy of the short-range forecasts, and
- uses a combination of optimal values of moving observant predictor $\mathfrak{P}$, periodicity and seasonality factor s and smoothing factor n at different lags k that give best long-range inertia forecasts with competitive accuracy.

The rest of this paper is organized as follows: Section 2 presents the theoretical background of this research work. The role of inertia in modern network stability, the impact of RESs and the role of synthetic inertia are discussed in this section. Besides, an overview and application of the ARIMA model in forecasting are presented. Section 3 explains the steps of the proposed method. The steps include model identification, inertia extraction, inertia tracking and inertia forecasting. Moreover, the application of the proposed method on the New Zealand network data is presented in section 4. The performance analysis of the proposed method is examined in section 5. Eventually, section 6 presents the conclusion of the discussion.

5.2 Theoretical background

5.2.1 The role of inertia in power systems

Inertia is an important property in maintaining the stability of the power system. Conventionally, inertia represents the turbine-synchronous generator rotating mass, which is well defined by the swing equation as given in (5.1) [8].

$$J\frac{d}{dt}\omega_m(t) = T_m(t) - T_e(t) \tag{5.1}$$

where J represents the total moment of inertia of the rotating masses, ω_m represents the mechanical rotational speed, while T_m and T_e represent the mechanical and electromagnetic torques, respectively. By converting the torques into power, the swing equation can be written in terms of power and frequency as in (5.2) [20]:

$$\frac{J\omega_e(t)}{\mathcal{p}^2}\frac{d}{dt}\omega_e(t) = P_m(t) - P_e(t) \tag{5.2}$$

where $\omega_e(t)$ is the instantaneous electrical rotor speed, i.e., $\omega_e(t) = 2\pi f(t)$, while $f(t)$ is the instantaneous frequency of the generator terminal voltage, and $\mathcal{p}$ is the pole pair number of the generator. The kinetic energy (KE) of the generator rotating masses is given by (5.3).

$$KE = \frac{J\omega_{e,0}^2}{2\mathcal{p}^2} \tag{5.3}$$

where $\omega_{e,0} = 2\pi f_0$ is the rated electrical rotor speed of the generator at the rated frequency f_0 of the power system. The stored kinetic energy is an important property in the power system.

During the power imbalances in the network, the stored KE is either released or absorbed by the generator to counteract the power imbalance. By so doing, the speed and hence the frequency are instantly contained within allowable limits depending on the magnitude of the power imbalance. This process is referred to inertial response of the generator, which plays an important role in reducing the RoCoF of the system. Low values of RoCoF give the generator's governor the necessary time needed to regulate the turbine power to restore the power balance. When the KE is divided by the nominal power of the generator (S_n), the inertia constant H can be obtained as in (5.4).

$$H = \frac{KE}{S_n} = \frac{J\omega_{e,0}^2}{2p^2S_n} \tag{5.4}$$

when the rotor speed $\omega_e(t) = 2\pi f(t)$ is different from the rated rotor speed $\omega_{e,0} = 2\pi f_0$, the swing equation can be written as in (5.5).

$$2H\frac{d}{dt}\frac{f(t)}{f_0} = \frac{P_m(t) - P_e(t)}{S_n} \tag{5.5}$$

For the system with multi-generators, the swing equation of the system can be written in terms of total system inertia H_{sys} and centre of inertia frequency, f_{COI} as in (5.6) [177].

$$2H_{sys}\frac{d}{dt}\frac{f_{COI}\,(t)}{f_0} = \frac{P_m(t) - P_e(t)}{S_n} \tag{5.6}$$

where the total system inertia H_{sys} is given as in (5.7).

$$H_{sys} = \frac{\sum_{i=1}^{N} H_i \times S_{n,i}}{\sum_{i=1}^{N} S_{n,i}} \tag{5.7}$$

And the centre of inertia frequency f_{COI} is given by (5.8).

$$f_{COI} = \frac{\sum_{i=1}^{N} H_i \times f_i}{\sum_{i=1}^{N} H_i} \tag{5.8}$$

5.2.2 The impact of renewables and the role of synthetic inertia in modern power systems

In the case of power systems with high penetration of renewable energy sources, the conventional synchronous generators are replaced and hence inertia is reduced in power systems [67]. To obtain the dynamic values of inertia, the supervisory control and data acquisition (SCADA) system needs to provide the timely status of the synchronous generators in the system. By so doing, equation (5.7) can be modified to update the amount of inertia in the network. Equation (5.7) needs to be appropriately modified to account for the non-synchronous generators that do not add up to the KE of the system [243]. To modify (5.7), Ref. [243] introduces a factor S_R that accounts for the total amount of active power injected by each RE plant in the network that doesn't contribute to the total inertia of the network. Employing S_R for N number of RE plants in the network, equation (5.7) can be re-written in the form as presented in (5.9).

$$H_{sys}^{RE} = \frac{\sum_{i=1}^{N} H_i \times S_{n,i}}{\sum_{i=1}^{N} S_{n,i} + \sum_{i=1}^{N} S_{R,i}} \tag{5.9}$$

As a result of reduced conventional inertia H_{sys} of the network due to penetration of RESs, different controls of different energy storage systems and other RESs for frequency support have been gaining popularity in power systems. Supercapacitors and battery storage, for instance, have been used for fast frequency response, frequency support and inertia response. On the other hand, WTs have been applied for frequency support in terms of synthetic inertia and fast frequency support [244]. It should be noted that fast frequency response differs from synthetic inertia in the concept that, fast frequency response is applied during frequency deviation; while for the synthetic inertia, the controller response is linked to the RoCoF to support network with low inertia values [37].

5.2.3 Overview of ARIMA model in forecasting

Autoregressive integrated moving average (ARIMA) is a useful time series-based forecasting algorithm that takes into account previous values of the time series dataset to predict future values. The previous and historical values can be indicative of future values [245, 246]. For the ARIMA (p, d, q) model, p stands for the order of the Autoregressive (AR) term, d is the number of differences required to make the time series stationary and q is the order of the moving average (MA) term. A stationary ARIMA model uses its lags as predictors. Besides, ARIMA model can capture probability distribution and time-correlation of different time-series data sets in power systems [247]. Consequently, when an appropriate time series model is determined to fit a certain data set, the model may be used to forecast future values of the observed time series [248]. In this way, the ARIMA model can be used to analyse, track and forecast time series data in power systems [248, 249].

For the forecasting process, it should be known that the time base is partitioned into two disjoint intervals. First is the forecast period (forecast horizon), which is the length partition at the end of the time base during which the forecast algorithm generates the forecast observations from the fitted model. The second is the pre-forecast period, which is the partition occurring before the time base. The forecast algorithm requires previously observed responses and conditional variances in the pre-sample period to initialize the dynamic forecasting model. A common practice is to fit a dynamic forecasting model to a portion of the data set to learn the data pattern and be able to predict future values [245].

5.2.4 Application of ARIMA model in forecasting

If current time in the time-series data set is signified by T, then time ahead prediction for $y_{T+\tau}$ is referred to the τ-period-ahead forecast and is represented by $\hat{y}_{T+\tau}(T)$. For the analysis of the forecasted observation, minimisation of mean squared error (MSE) can be employed as shown in (5.10).

$$E\left[\left(y_{T+\tau} - \hat{y}_{T+\tau}(T)\right)^2\right] = E[e_T(T)^2] \tag{5.10}$$

where $\hat{y}_{T+\tau}(T) = E[y_{T+\tau}|y_T, y_{T-1}]$ for current and previous observations, i.e., $y_T, y_{T-1}, \ldots$ Therefore, using the ARIMA model approach, the forecast error can be calculated as given in (5.11) [38].

$$e_T(T) = y_{T+\tau} - \hat{y}_{T+\tau}(T) = \sum_{i=0}^{\tau-1} \psi_i \varepsilon_{T+\tau-i} \tag{5.11}$$

where ψ is the time-invariant weight of the input data and ε is a white noise time-series. And the variance of the forecasted error can be given as in (5.12).

$$Var[e_T(T)] = Var\left[\sum_{i=0}^{\tau-1}\psi_i\varepsilon_{T+\tau-i}\right] = \sum_{i=0}^{\tau-1}{\psi_i}^2 Var(\varepsilon_{T+\tau-i})$$

$$= \sigma^2\sum_{i=0}^{\tau-1}{\psi_i}^2 \tag{5.12}$$

$$= \sigma^2(\tau), \tau = 1, 2, \ldots$$

From (5.12), it is obvious that the variance of the forecasted error gets bigger with increasing forecast lead times τ. This increase in the forecasted error is expected as uncertainty increases as time increases in the future [248].

5.3 The proposed method to forecast inertia in power systems

The proposed inertia forecasting method is subdivided into three main algorithms, namely power system model identification, inertia extraction and finally inertia tracking and forecasting. The algorithms are interconnected from power model identification to inertia forecasting. Fig. 5.2(a) and (b) show in detail the generalized flow block diagrams of model identification and inertia extraction, respectively, while Fig. 5.3 shows inertia forecasting algorithm.

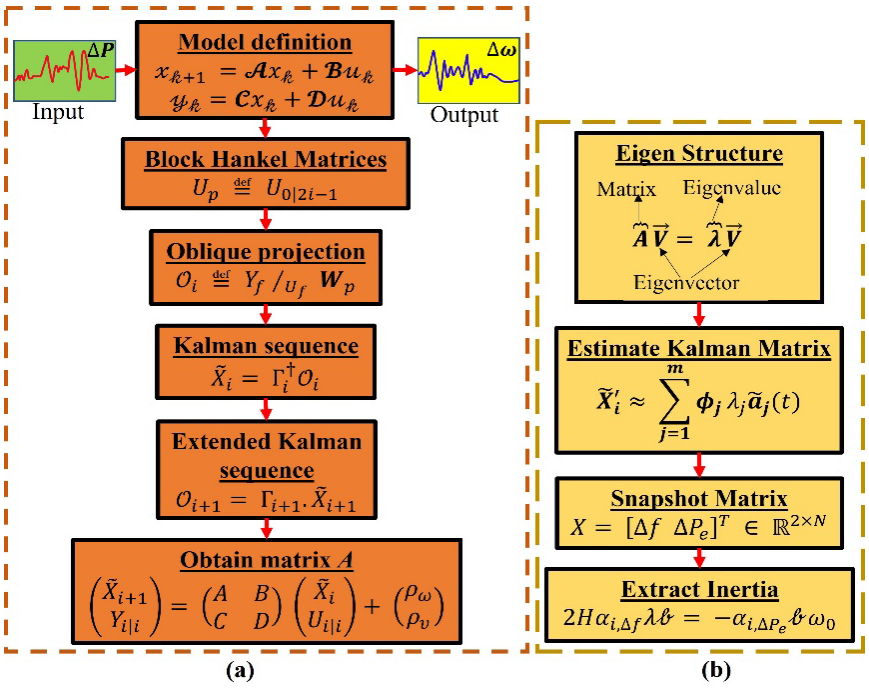

Fig. 5.2 Algorithm flow diagrams of: (a) network model identification and (b) inertia extraction

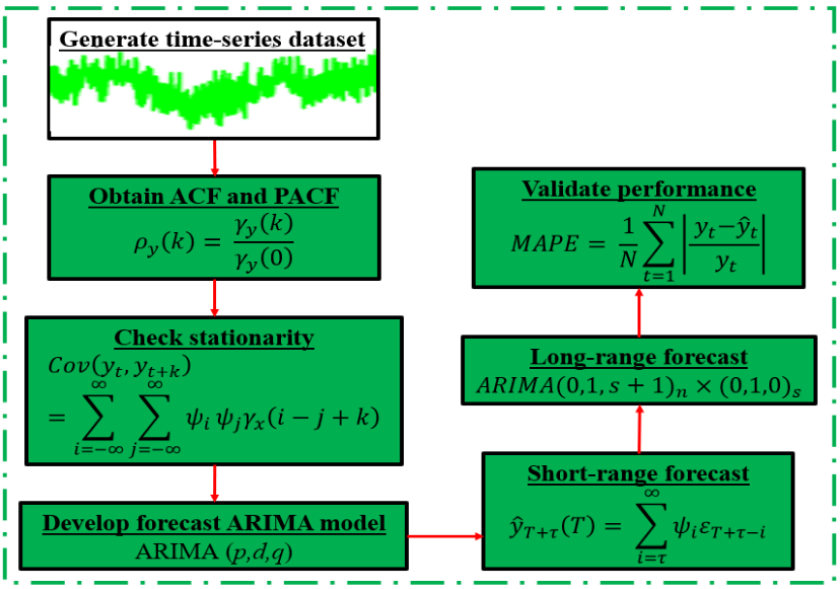

Fig. 5.3 Flow diagram of inertia forecasting algorithm

5.3.1 Model identification

Given the network measurements for the input parameter $u_k \in \mathbb{R}^m$ and the output $y_k \in \mathbb{R}^l$ generated by the unknown combined system of order n, the system can be represented by the state-space equation (5.13).

$$\begin{aligned} x_{k+1} &= Ax_k + Bu_k + w_k \\ y_k &= Cx_k + Du_k + v_k \end{aligned} \tag{5.13}$$

where u_k and y_k represent the inputs and outputs of the system, respectively, x_k represent the states, while w_k and v_k are the process and measurement noises. The coefficient A, B, C, D denote the matrices of the system. Considering the noise of the system, the combined (deterministic-stochastic) subspace identification algorithm is employed to compute the state-space model from the given input-output data of the network. A system can be represented by a linear time-invariant combined deterministic-stochastic system. Matrix A in a combined deterministic-stochastic system specifically denotes a dynamic system matrix as completely characterized by its eigenvalues [232].

When a system has available (measured) signals u_k and y_k and $v_k$and w_k unknown disturbances, the system can be split into a deterministic and stochastic subsystem by splitting the state (x_k) and output (y_k) in a deterministic $(\bullet^d)$ and stochastic $(\bullet^s)$ components as in (5.14).

$$\begin{aligned} x_k &= x_k^d + x_k^s \\ y_k &= y_k^d + y_k^s \end{aligned} \tag{5.14}$$

The deterministic state (x_k^d) and output (y_k^d) follow from the deterministic subsystem, which describes the influence of the deterministic input (u_k) on the deterministic output as shown in (5.15).

$$x_{k+1}^d = Ax_k^d + Bu_k$$
$$y_k^d = Cx_k^d + Du_k \tag{5.15}$$

The stochastic state (x_k^s) and the output (y_k^s) follow from the stochastic subsystem, which describes the influence of the noise sequences (w_k) and (v_k) on the stochastic output as depicted in (5.16).

$$x_{k+1}^s = Ax_k^s + w_k$$
$$y_k^s = Cx_k^s + v_k \tag{5.16}$$

The deterministic and stochastic subsystems may have completely decoupled input-output dynamics. For this reason, the block Hankel matrices, which relate the measured input-output dynamic data are defined as in (5.17) [183].

$$U_{\mathcal{P}} \overset{\text{def}}{=} U_{0|2i-1} \overset{\text{def}}{=} \begin{pmatrix} u_0 & u_1 & u_2 & \cdots & u_{j-1} \\ u_1 & u_2 & u_3 & \cdots & u_j \\ \cdots & \cdots & \cdots & \cdots & \cdots \\ u_{i-1} & u_i & u_{i+1} & \cdots & u_{i+j-2} \end{pmatrix} \in \mathbb{R}^{li \times j}$$

$$U_{\mathcal{f}} \overset{\text{def}}{=} U_{i|2i-1} \overset{\text{def}}{=} \begin{pmatrix} u_i & u_{i+1} & u_{i+2} & \cdots & u_{i+j-1} \\ u_{i+1} & u_{i+2} & u_{i+3} & \cdots & u_{i+j} \\ \cdots & \cdots & \cdots & \cdots & \cdots \\ u_{2i-1} & u_{2i} & u_{2i+1} & \cdots & u_{2i+j-2} \end{pmatrix} \in \mathbb{R}^{li \times j}$$

$$U_{\mathcal{P}}^{+} \overset{\text{def}}{=} U_{0|i} \overset{\text{def}}{=} \begin{pmatrix} u_0 & u_1 & u_2 & \cdots & u_{j-1} \\ u_1 & u_2 & u_3 & \cdots & u_j \\ \cdots & \cdots & \cdots & \cdots & \cdots \\ u_{i-1} & u_i & u_{i+1} & \cdots & u_{i+j-2} \\ u_i & u_{i+1} & u_{i+2} & \cdots & u_{i+j-1} \end{pmatrix} \in \mathbb{R}^{l(i+1) \times j}$$

$$U_{\mathcal{f}}^{-} \overset{\text{def}}{=} U_{i+1|2i-1} \overset{\text{def}}{=} \begin{pmatrix} u_{i+1} & u_{i+2} & u_{i+3} & \cdots & u_{i+j} \\ \cdots & \cdots & \cdots & \cdots & \cdots \\ u_{2i-1} & u_{2i} & u_{2i+1} & \cdots & u_{2i+j-2} \end{pmatrix}$$
$$\in \mathbb{R}^{l(i-1) \times j} \tag{5.17}$$

where the subscripts in $U_{0|2i-1}, U_{0|i}, U_{i+1|2i-1}$ denote the first and last element of the first column in the input block Hankel matrix. The subscripts "$\mathcal{P}$" and "$\mathcal{f}$" stand for "past" and "future" respectively. On the other hand, $U_{\mathcal{P}}^{+}$ and $U_{\mathcal{f}}^{-}$ are defined by shifting the border between past and

future one block row down. The superscripts "+" and "-" stand for "add one block row" and "delete one block row", respectively. The output block Hankel matrices $Y_{\mathcal{P}}$, $Y_{\mathcal{f}}$, $Y_{\mathcal{P}}^{+}$and $Y_{\mathcal{f}}^{-}$ are defined in the same way as the input block Hankel matrices. Likewise, the block Hankel matrices $Y_{0|2i-1}^{d}$ and $Y_{0|2i-1}^{s}$ are also defined in a similar way using the deterministic and stochastic output matrices, respectively. The block Hankel matrices consisting of inputs and outputs as $W_{0|i-1}$ is defined in (5.18).

$$\begin{aligned} W_{0|i-1} &\overset{\text{def}}{=} \begin{pmatrix} U_{0|i-1} \\ Y_{0|i-1} \end{pmatrix} \\ &= \begin{pmatrix} U_{\mathcal{P}} \\ Y_{\mathcal{P}} \end{pmatrix} \\ &= W_{\mathcal{P}} \end{aligned} \tag{5.18}$$

Similarly, $W_p^{+} = \begin{pmatrix} U_{\mathcal{P}}^{+} \\ Y_{\mathcal{P}}^{+} \end{pmatrix}$.

The state sequence related to the Hankel matrices of the system is defined as (5.19).

$$X_i \overset{\text{def}}{=} \begin{pmatrix} x_i & x_{i+1} & \dots & x_{i+j-2} & x_{i+j-1} \end{pmatrix} \in \mathbb{R}^{n \times j} \tag{5.19}$$

Likewise, the deterministic state sequence X_i^d and stochastic state sequence X_i^s are defined as (5.20).

$$\begin{aligned} X_i^d &\overset{\text{def}}{=} \begin{pmatrix} x_i^d & x_{i+1}^d & \dots & x_{i+j-2}^d & x_{i+j-1}^d \end{pmatrix} \in \mathbb{R}^{n \times j} \\ X_i^s &\overset{\text{def}}{=} \begin{pmatrix} x_i^s & x_{i+1}^s & \dots & x_{i+j-2}^s & x_{i+j-1}^s \end{pmatrix} \in \mathbb{R}^{n \times j} \end{aligned} \tag{5.20}$$

Hankel block matrices allow calculation of the row space of a Kalman filter state sequence and of the column space of the extended observability matrix Γ_i directly from the input-output data [183]. The oblique projection $\mathcal{O}_i$ is, therefore, defined as in (5.21).

$$\mathcal{O}_i \overset{\text{def}}{=} Y_{\mathcal{f}} / U_{\mathcal{f}} \, \boldsymbol{W}_{\mathcal{P}} \tag{5.21}$$

However, the matrix $\mathcal{O}_i$ is equal to the product of the extended observability matrix Γ_i and the Kalman filter state sequence $\tilde{X}_i$ as depicted in (5.22) [6, 232].

$$\mathcal{O}_i = \Gamma_i . \tilde{X}_i \tag{5.22}$$

Besides, the Kalman filter state sequence $\tilde{X}_i$ is given as in (5.23).

$$\tilde{X}_i \overset{\text{def}}{=} \hat{X}_{i[\hat{X}_0]} \tag{5.23}$$

where $\hat{X}_0 = X_{\mathcal{P}}^{d} /_{U_{\mathcal{f}}} \boldsymbol{U}_{\mathcal{P}}$. Also, the observability matrix Γ_i is given by $\Gamma_i = W_1^{-1} U_1 S_1^{\frac{1}{2}} . T$.

The part of the state sequence $\tilde{X}_i$ that lies in the column space of W_2 can be recovered from (5.24).

$$\tilde{X}_i \, W_2 = \, T^{-1} S_1^{\frac{1}{2}} V_1^T \tag{5.24}$$

It should be noted that the Kalman state sequence can also be defined by (5.25), which can simplify the model identification procedure.

$$\tilde{X}_i = \, \Gamma_i^{\dagger} \mathcal{O}_i \tag{5.25}$$

The goal of model identification procedure is to find an optimal model of which the input-output data approximates the process under consideration. To do this, the prediction of the future outputs ($Y_{f\!f}$) can be achieved using the information obtained from the past ($\boldsymbol{W}_{\mathcal{P}}$) and the knowledge of the inputs that will be presented to the system in the future ($U_{f\!f}$). The prediction of future outputs ($Y_{f\!f}$) helps to forecast other network parameters. Inspired by the linearity approximation of the system, the past ($\boldsymbol{W}_{\mathcal{P}}$) and the future inputs ($U_{f\!f}$) can be combined linearly to predict the future outputs ($Y_{f\!f}$). If the linear combination is denoted as $L_{\mathcal{P}}$, the optimal combination of the past to predict the future is $L_{\mathcal{P}}.W_{\mathcal{P}}$, which is exactly equal to the oblique projection $\mathcal{O}_i = \, L_{\mathcal{P}}.W_{\mathcal{P}}$ [232].

To determine states $\tilde{X}_i$ from the system data collected, the oblique projection in (5.26) can be used [183].

$$\mathcal{O}_{i+1} = \, Y_{f\!f}^{-} \, /_{\mathrm{U}_{f\!f}^{-}} \, W_{\mathcal{P}}^{+}$$

$$\mathcal{O}_{i+1} = \, \Gamma_{i+1}.\tilde{X}_{i+1} \tag{5.26}$$

In this way, $\tilde{X}_i$ and $\tilde{X}_{i+1}$ can be obtained. However, this new Kalman filter sequence $\tilde{X}_{i+1}$ has a different initial state as the sequence $\tilde{X}_i$. In this way, matrices A, B, C and D can be finally obtained from the set of linear equations of (5.27).

$$\begin{pmatrix} \tilde{X}_{i+1} \\ Y_{i|i} \end{pmatrix} = \begin{pmatrix} A & B \\ C & D \end{pmatrix} \begin{pmatrix} \tilde{X}_i \\ U_{i|i} \end{pmatrix} + \begin{pmatrix} \rho_\omega \\ \rho_\upsilon \end{pmatrix} \tag{5.27}$$

where ρ_ω and ρ_υ are Kalman filter residuals related to process and measurement noises of the system. The discussion is mainly based on the system matrix A as it describes the dynamics of the system as characterized by its eigenvalues. Therefore, the modes of the system have to be obtained by calculating the eigenvalues of the matrix A, which are the poles of the system.

5.3.2 Online inertia extraction and tracking

An interesting interpretation of system dynamic behaviour can be obtained by analysing the eigenvalues of a dynamic matrix A of the identified model of the power system. The system matrix A is of interest as it describes the dynamics of the system as characterized by its eigenvalue structure. To analyse the dynamics of the system, the dynamic modes of the system must be found [6]. The next step is to obtain the eigenvalues of matrix A, which are the poles of the system.

Considering that the input u_k is always the same during the experiment, the Kalman residual process noise ρ_ω in (5.27) can be estimated to a zero mean, and the block Hankel matrix $U_{i|i}$ can asymptotically resolve to zero. In this way, the dynamic matrix A in (5.27) can be represented by an estimated general form of a dynamic system as (5.28).

$$\tilde{X}'_{i+1} = A'\tilde{X}'_i \tag{5.28}$$

where $\tilde{X}'_{i+1}$ and $\tilde{X}'_i$ represent estimated Kalman filter state sequences, and A' represents the estimated dynamic state matrix. If it is assumed that matrix A' is diagonalizable with eigenvalue decomposition, Kalman filter sequences can be estimated as in (5.29).

$$\tilde{\boldsymbol{X}}'_{\boldsymbol{i}} = \boldsymbol{\Phi\Lambda\tilde{\Gamma}_m} \tag{5.29}$$

where $\boldsymbol{\Phi}$ is a set of functions obtained from the system data, which physically represent standing oscillations of the system, $\tilde{\boldsymbol{\Gamma}}_{\boldsymbol{m}}$ represents row vectors containing the temporary coefficient evaluated at each observation and $\boldsymbol{\Lambda} = diag[\lambda_1 \ \ \lambda_2 \ \ \ldots \ \ \lambda_m] \in \mathbb{R}^{m\times m}$ is a diagonal matrix consisting of empirical Ritz eigenvalues λ_j of dynamic matrix $\boldsymbol{A'}$ [230]. Therefore, the estimated Kalman sequence matrix $\tilde{\boldsymbol{X}}'_{\boldsymbol{i}}$ can then be expanded in a linear combination of modal components as in (5.30).

$$\tilde{\boldsymbol{X}}'_{\boldsymbol{i}} \approx \sum_{\boldsymbol{j=1}}^{\boldsymbol{m}} \boldsymbol{\phi_j}\,\lambda_j\tilde{\boldsymbol{a}}_{\boldsymbol{j}}(t) \tag{5.30}$$

where $\tilde{\boldsymbol{a}}_{\boldsymbol{j}}$ contains the temporal amplitudes, $\boldsymbol{\phi_j}$ contains the dynamic modes while λ_j contains the associated eigenvalues of dynamic matrix $\boldsymbol{A'}$ of the system model. In this way, eigenvalues and vectors of the state matrices can then be found.

Since system dynamics depend on eigenvalue and eigenvector, any change in dynamic parameters can indirectly change the eigenvalue and eigenvector through the Kalman state sequence matrix. By determining the modes of the system by calculating the eigenvalues of the dynamic matrix $\boldsymbol{A'}$, parameters of the system such as inertia can be determined by relating the eigenvalue of the dynamic matrix $\boldsymbol{A'}$ to a linearized form of the swing equation (5.31).

$$2H\Delta\dot{\omega} + D\Delta\omega = -P_e \tag{5.31}$$

The related transfer function of the swing equation is given in (5.32).

$$G(s) = \frac{\Delta\omega}{\Delta P_e} \approx -\frac{1}{2Hs + D} \tag{5.32}$$

When the output of the system is sampled at a constant sampling rate Δt, the sampled signal is represented as per (5.33).

$$y_j(k) = \sum_{i=1}^{n} R_i z_i^k \tag{5.33}$$

where k indicates the samples, and $z_i = \exp(\lambda_i \Delta t)$ is the discretization of model variable $z(t)$ and $\lambda = \sigma + j\omega$. These are the modes that represent the system. The set of snapshot matrix of $\boldsymbol{A}'$ representing the dynamic modes of the system is given by (5.34) [230].

$$X = [\Delta f \ \ \Delta P_e]^T \in \mathbb{R}^{2\times N} \tag{5.34}$$

The snapshot matrix (5.34) can further be evaluated as presented in [6] using a linear combination factor (LCF) α_i to obtain (5.35) [6].

$$2H\alpha_{i,\Delta f}\lambda\mathscr{b} = -\alpha_{i,\Delta P_e}\mathscr{b}_i\omega_0 \tag{5.35}$$

where $\mathscr{b}_i$ represents the initial value coefficient corresponding to the i^{th} eigenvalue. To estimate the inertia, the power deviations and frequency responses deviations are recorded as input (u_k) and output (y_k) of the network in terms of sampled data. Then, dynamic modes relating to eigenvalues and eigenvectors are extracted to construct the snapshot matrix. Therefore, the effective inertia H_e can be obtained by solving (5.35). Since the equation is linear and does not contain the derivative of the rotor speed, the proposed methodology can accommodate large-scale power systems with high dimensionality.

5.3.3 Inertia tracking and forecasting

From the previous subsection (3.2), the effective inertia H_e of the network is extracted and stored in a dataset with a time interval of 10 s. The stored inertia data create a historical time-series data set. The historical data is potentially used to form recognizable patterns, such as trends and seasonal events that are important inputs for long-range forecasting. An appropriate time-series dynamic model is fitted in the historical inertia data set stored. The obtained fitted dynamic model is then used to generate forecasts of future observations. Fig. 5.4 shows the concept of moving observant predictor $\mathfrak{P}$ for a dynamic forecasting model to forecast the future inertia values. The moving observant predictor moves around the historical time-series data to establish the data patterns and trends. The observed patterns and trends are used to increase the accuracy of time ahead prediction.

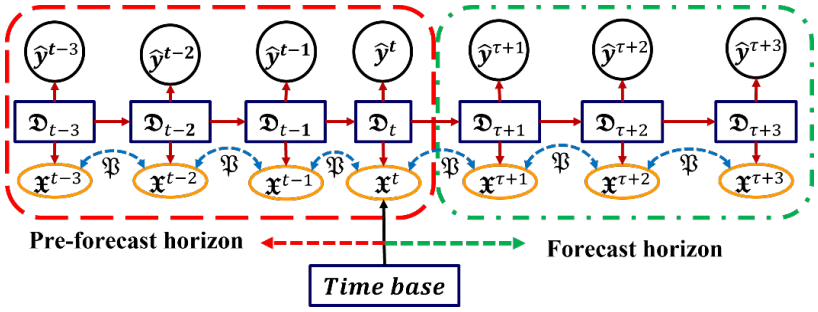

Fig. 5.4 Diagram showing moving observant predictor $\mathfrak{P}$ in the dynamic forecasting model

Inertia tracking

A time-series data based ARIMA (p,d,q) process at time $T+\tau$ is expressed as (5.36) [248].

$$y_{T+\tau} = \delta + \sum_{i=1}^{p+d} \phi_i y_{T+\tau-i} + \varepsilon_{T+\tau} - \sum_{i=1}^{q} \theta_i \varepsilon_{T+\tau-i} \tag{5.36}$$

where δ is a data initialization constant, ϕ_i is a correlation constant between adjacent datasets, $\varepsilon_{T+\tau}$ is the forecast error at lead time τ and θ_i is error correction factor at lead time τ. Considering a partitioned MA representation of (5.36), equation (5.37) is obtained.

$$y_{T+\tau} = \mu + \sum_{i=0}^{\tau-1} \psi_i \, \varepsilon_{T+\tau-i} + \sum_{i=\tau}^{\infty} \psi_i \varepsilon_{T+\tau-i} \tag{5.37}$$

The component $\sum_{i=0}^{\tau-1} \psi_i \, \varepsilon_{T+\tau-i}$ represents the future errors, while $\sum_{i=\tau}^{\infty} \psi_i \varepsilon_{T+\tau-i}$ represents the present and past errors. As the extraction of the inertia is done in the network, the moving average $MA(q+1)$ property of the ARIMA model presented in (5.36) is a powerful property that can be used to track the extracted inertia values. As the inertia series extracted is non-invertible, the maximum likelihood estimates move with q^{th}-order of the MA component enhancing tracking the time changing inertia in the network. The extracted inertia values are compared with the available actual inertia values of the network.

Short-range forecasting

On the other side, when the disturbances are assumed to have mean zero and independent on different lags, the forecast estimation for the time ahead τ taking into account the moving observant predictor $\mathfrak{P}$ is given by (5.38) [232].

$$\left(\hat{y}_{T+\tau}(T)\right)^{\mathfrak{P}} = \left(\sum_{i=\tau}^{\infty} \psi_i \varepsilon_{T+\tau-i}\right)^{\mathfrak{P}} \tag{5.38}$$

where $E[y_{T+\tau}|y_T, y_{T-1}, \ldots] = \begin{cases} 0 & if\ i < \tau \\ \varepsilon_{T+\tau-i} & if\ i \geq \tau \end{cases}$

Then, the improved forecast error when $\mathfrak{P}$ is taken into consideration around the historical data is calculated as in (5.39).

$$\left(e_T(\tau)\right)^{\mathfrak{P}} = \left(\sum_{i=0}^{\tau-1} \psi_i \, \varepsilon_{T+\tau-i}\right)^{\mathfrak{P}} \tag{5.39}$$

For a linear combination of random disturbances, $E[e_T(\tau)] = 0$. Therefore, equation (5.40) is obtained.

$$= (\sigma^2)^{\mathfrak{P}} \sum_{i=0}^{\tau-1} \left(\psi_i{}^2\right)^{\mathfrak{P}} = (\sigma^2)^{\mathfrak{P}}(\tau), \quad \tau = 1, 2, \ldots \tag{5.40}$$

The variance of the forecast error gets bigger with increasing the forecast lead times τ. This increase is expected and makes sense as uncertainty increases for the forecasts further into the future.

Long-range forecasting

The property that time-series data have strong periodic patterns and seasonality can be used as a crucial input to improve the ARIMA model for long-range forecasting. The improvement is done by including additive model and exponential smoothing, which are linked by a moving observant predictor $\mathfrak{P}$ at different lags $\mathscr{k}$ for n samples of the dataset before and after the time base. For this case, data y_t can be represented using the additive model as in (5.41).

$$y_t = S_t + N_t \tag{5.41}$$

where S_t is a deterministic component with periodicity and seasonality factor $\mathscr{s}$ in the time-series dataset, while N_t is a component that may be modelled as the ARIMA process. Equation (5.41) can further be modified into (5.42).

$$w_t = (1 - B^{\mathscr{s}})N_t \tag{5.42}$$

where w_t is a process with predictable periodic behaviour and $1 - B^{\mathscr{s}}$ is an operator. On the other hand, using the Holt-Winters method [250], a seasonal with time trend effects exponential smoothing approach for parameters before base time is optimal for an $ARIMA(0,1,\mathscr{s}+1) \times (0,1,0)_{\mathscr{s}}$. The exponential smoothing can be improved using the moving observant predictor in line with the additive model for n sampled parameters to extend the forecasting for long ranges with improved accuracy. Therefore, the improved ARIMA for $\mathscr{n}$ correlated smoothing factor is given by $ARIMA(0,1,\mathscr{s}+1)_n \times (0,1,0)_{\mathscr{s}}^{\mathfrak{P}}$. This improved ARIMA model for long range forecasting is referred to as $\mathscr{i}$-ARIMA.

Algorithm 5.1: Inertia monitoring

Part I: Network Model Identification

Input: *Aggregated active power disturbance of the network* $(\boldsymbol{u_k = \Delta P})$

Output: *Frequency response deviations at the centre of inertia,* $(\boldsymbol{y_k = \Delta\omega})$

State-space model:

$$x_{k+1} = Ax_k + Bu_k + w_k$$
$$y_k = Cx_k + Du_k + v_k$$

Block Hankel: *Generate input and output block Hankel, extended block Hankel matrices as well as past and future matrices using input-output data vectors,* $\boldsymbol{u_k}$, $\boldsymbol{y_k}$

Oblique projection: *Calculate the oblique and orthogonal projections using block Hankel matrices*

$$\mathcal{O}_i \overset{\text{def}}{=} Y_f /_{U_f} \boldsymbol{W_p}$$
$$\mathcal{O}_{i+1} = Y_f^- /_{U_f^-} W_p^+$$

SVD: *Calculate the* ***SVD*** *of the weighted oblique projection using*

$$W_1 \mathcal{O}_i W_2 = USV^T$$

Kalman sequence: *Determine the Kalman state sequences*

$$\tilde{X}_i = \Gamma_i^{\dagger} \mathcal{O}_i$$
$$\tilde{X}_{i+1} = \Gamma_{i-1}^{\dagger} \mathcal{O}_{i+1}$$

Dynamic matrix $\boldsymbol{A}$**:** *Solve the set of linear equations for* A, B, C *and* D

$$\begin{pmatrix} \tilde{X}_{i+1} \\ Y_{i|i} \end{pmatrix} = \begin{pmatrix} A & B \\ C & D \end{pmatrix} \begin{pmatrix} \tilde{X}_i \\ U_{i|i} \end{pmatrix} + \begin{pmatrix} \rho_\omega \\ \rho_v \end{pmatrix}$$

Pass *on the dynamic matrix* $\boldsymbol{A}$ *to the next algorithm*

Algorithm 5.2: Inertia extraction

Part II: Inertia extraction from dynamic matrix $\boldsymbol{A}$

Eigen structure: *Determine the eigenvectors and eigenvalues from the obtained dynamic matrix* $\boldsymbol{A}$ *of the system.*

$$\tilde{X}'_{i+1} = A' \tilde{X}'_i$$
$$A\vec{V} = \lambda \vec{V}$$

Kalman matrix: *Obtain the Kalman sequence matrix* $\boldsymbol{\tilde{X}'_i}$ *as*

$$\tilde{X}'_i \approx \sum_{j=1}^{m} \phi_j \lambda_j \tilde{a}_j(t)$$

Snapshot matrix: *Determine the snapshot matrix of the estimated dynamic matrix* $\boldsymbol{A'}$ *representing the dynamic modes of the system.*

$$X = [\Delta f \ \ \Delta P_e]^T \in \mathbb{R}^{2\times N}$$

Inertia extraction: *Extract the estimated inertia of the system by defining the dynamic mode corresponding to the eigenvalue that corresponds to the inertia of the system.*

$$2H\alpha_{i,\Delta f} \lambda \not{b} = -\alpha_{i,\Delta P_e} \not{b} \omega_0$$

Pass *on the extracted inertia to the next algorithm*

Algorithm 5.3: Inertia forecasting

Part III: Inertia tracking and forecasting

Time-series: *Generate historical time series data set of the extracted inertia values from the network model.*

ACF & PACF: *Obtain the autocorrelation function (ACF) and partial autocorrelation function (PACF).*

$$\rho_y(k) = \frac{\gamma_y(k)}{\gamma_y(0)}$$

Check stationarity: *Based on ACF and PACF the stationarity of the time series data set is checked.*

$$Cov(y_t, y_{t+k}) = \sum_{i=-\infty}^{\infty} \sum_{j=-\infty}^{\infty} \psi_i \psi_j \gamma_x(i-j+k)$$

Fit ARIMA model: *An ARIMA (p,d,q) is fitted on the checked data set and based on the moving average component of ARIMA, the inertia data are tracked.*

Forecast: *Develop forecast models for short- and long-range forecasting of inertia values.*

$$\left(\hat{y}_{T+\tau}(T)\right)^{\mathfrak{P}} = \left(\sum_{i=\tau}^{\infty} \psi_i \varepsilon_{T+\tau-i}\right)^{\mathfrak{P}}$$

$$ARIMA(0,1,\mathfrak{s}+1)_n \times (0,1,0)_{\mathfrak{s}}^{\mathfrak{P}}$$

Validate: *The performances of the forecasting model's accuracy are tested and validated using the appropriate validating metrics.*

$$MAPE = \frac{1}{N}\sum_{t=1}^{N}\left|\frac{y_t - \hat{y}_t}{y_t}\right|$$

5.4 Application of the proposed method on the New Zealand network data

5.4.1 Data preparation and processing

The time series representing the power profiles for the years 2012 to 2016 is presented in Fig. 5.5. In this power profile, the time resolution is 30 minutes as obtained from New Zealand's Electricity Authority webpage [239]. Fig. 5.5(a) shows the total power profile in the network, Fig. 5.5(b) show the power profile for total renewable power contribution in the network, and Fig. 5.5(c) represents the contribution of wind power in the network. It can further be noted that the presented power profiles follow strong periodic and seasonality patterns.

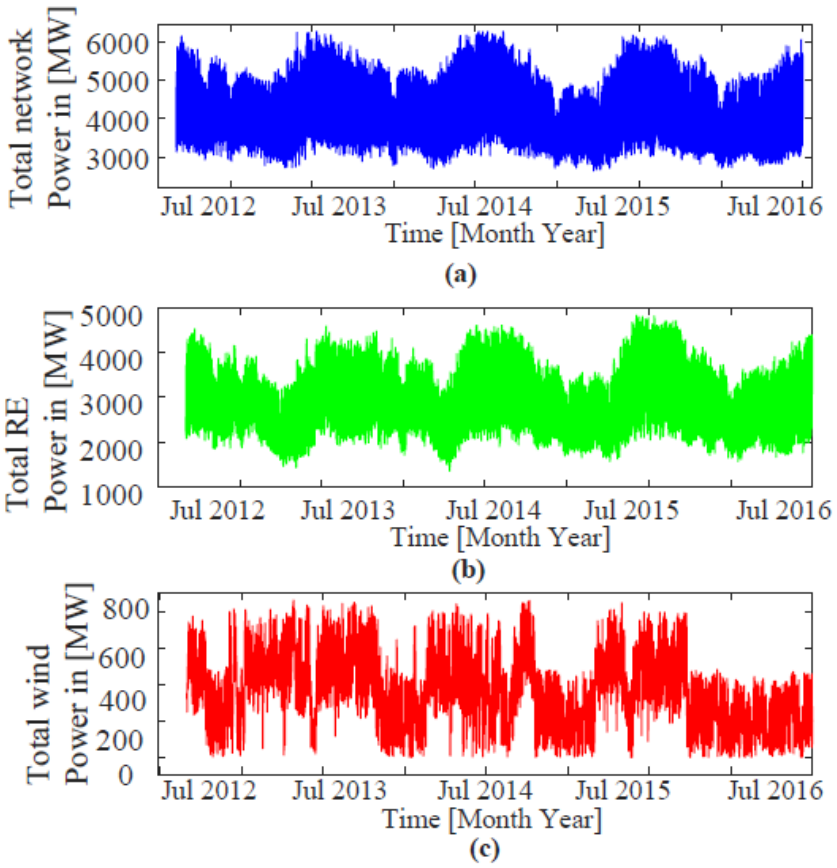

Fig. 5.5 New Zealand power profiles for the years 2012 to 2016

For inertia is the centre of the discussion in this paper, the available inertia and related power data are digested and analysed to verify the proposed method. The time series for the total inertia values of the network are derived using the supervisory control and data acquisition (SCADA) data obtained from Transpower, which determines when an SG is online. The inertia values for each generator are obtained from a report by Transpower [251]. Equation (7) is used to derive the time series inertia of the network and is presented with a time resolution of 10 seconds. Fig. 5.6(a) presents the time-series inertia of the network in (s), while Fig. 5.6(b) represents the time-series of the aggregated kinetic energy of the connected synchronous generators in (MWs).

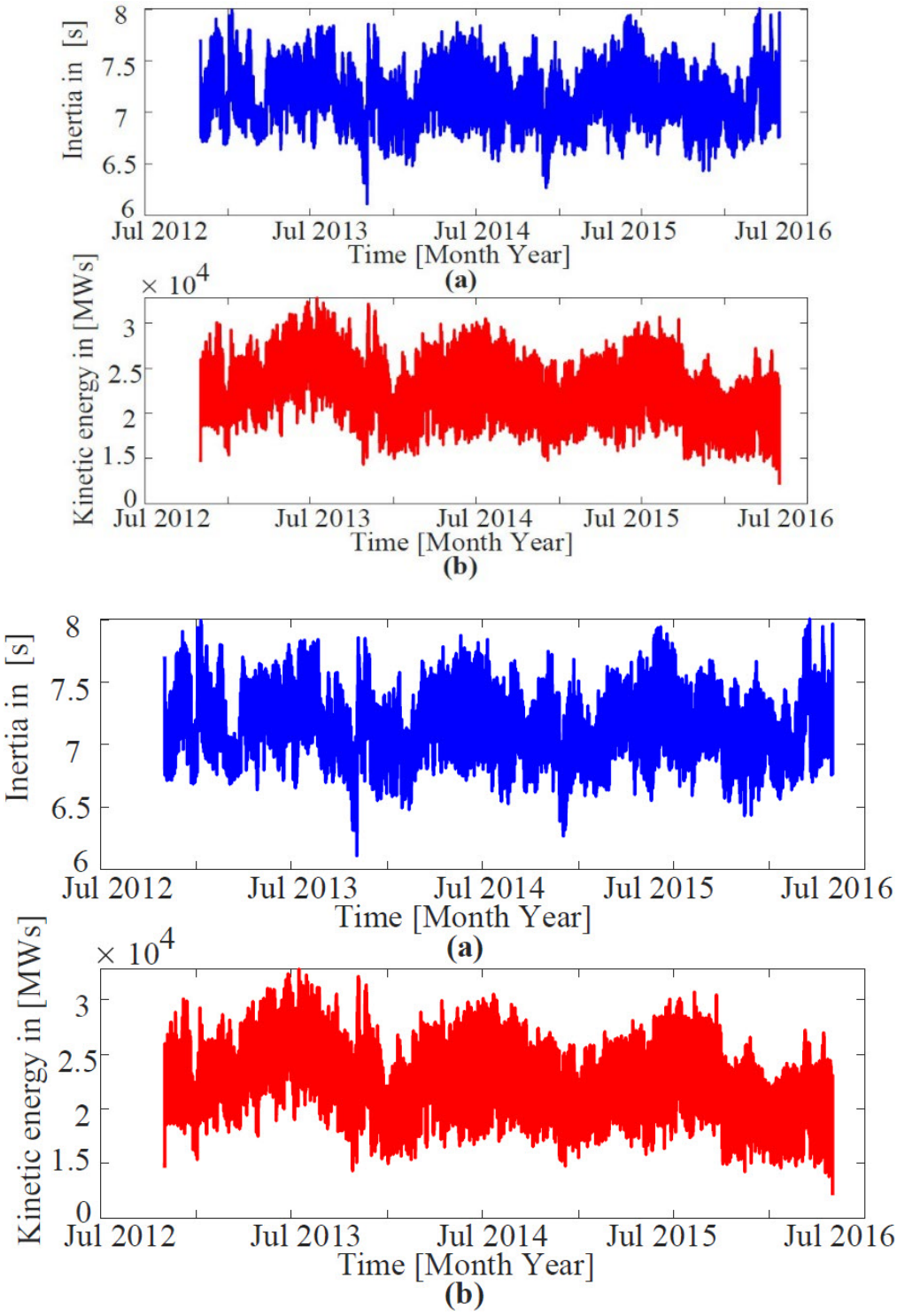

Fig. 5.6 (a) Time-series of inertia in (s) and (b) Aggregated kinetic energy in (MWs) of the New Zealand network

5.4.2 Checking stationarity of the data

After obtaining the time-series data profiles of power generation and the inertia of the network for the years under consideration, stationarity check is carried out to identify the stationarity status of the time series data profile of inertia. Autocorrelation function (ACF) and

partial autocorrelation function (PACF) at different lags plots are obtained to check the stationarity of the time-series data.

For stationary time series data, the ARIMA (p, d, q) with appropriate values of p, d and q is selected that can be used to estimate, analyse, and forecast observations based on the presented time series data. From ACF and PACF, stationary time-series data is identified. As the presented time series data satisfy the stationarity conditions, suitable selected ARIMA (p, d, q) is fitted on the inertia time-series data from October – December 2012 to represent the rest of the data. As a representative of the selected ARIMA (p, d, q) models, Fig. 5.7 shows how the ARIMA (1,1,1) model fits the data for 98% in (a), which is further proven with the residual index plot in (b).

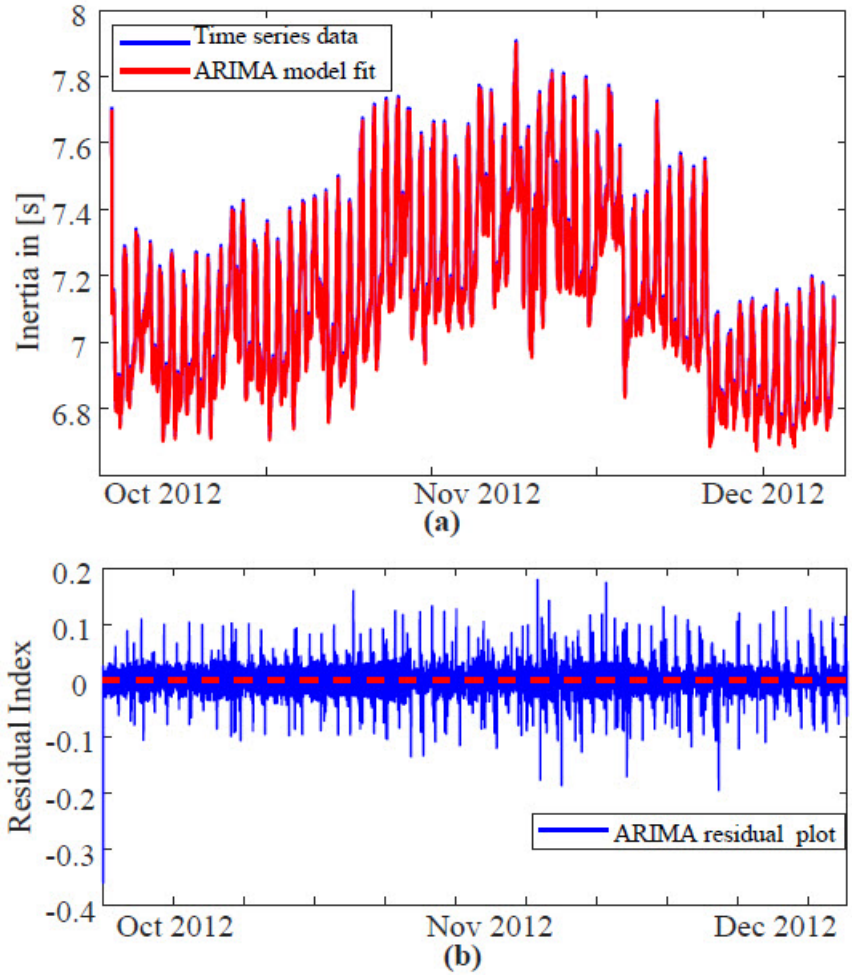

Fig. 5.7 (a) ARIMA (1,1,1) model Fitting historical data set by 98%, (b) Residual index plot

5.4.3 Inertia tracking

The proposed method uses the generated time-series data to track the dynamics of inertia values in the network. The tracking speed of the method is very quick in such a way that when inertia changes, the estimation from the improved moving average (MA) of the ARIMA model

takes only $25\mu s$ to track the actual inertia signal. Evidence is shown in Fig. 5.8(a) when tracking is done for the data set of one month. In the figure, the inertia dynamics of the network in (s) are shown for one month period. To closely observe the effectiveness of the proposed method, few data sets are used. In Fig. 5.8(b), the method is tested with data set of one week (seven days.) It can be seen how the improved MA of the ARIMA model tracks the actual original inertia signal effectively. Furthermore, Fig. 5.8(c) zooms the tracking for two days for a close and clear view.

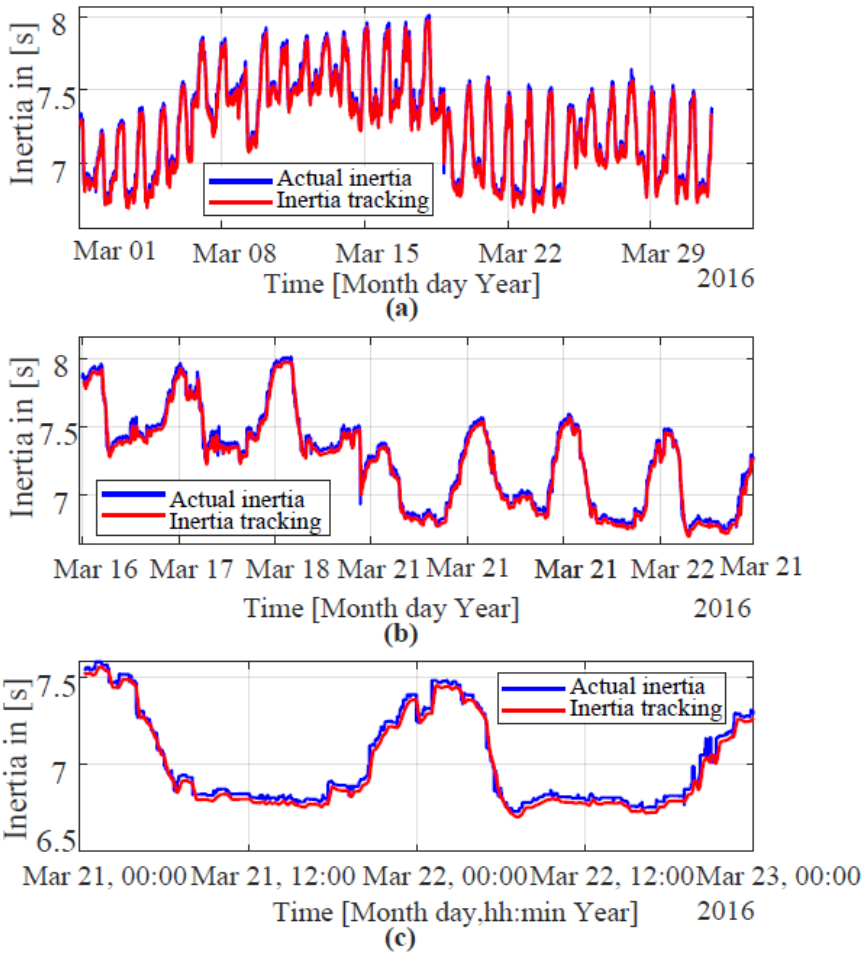

Fig. 5.8 (a), (b) and (c) Tracking of inertia for one month, one week and two days, respectively

Next, the method is tested on the stored kinetic energy in [MWs] data of the network. To represent the data, a one-month data set is presented in Fig. 5.9(a). Like in inertia in (s), the dataset range is decreased to increase the visibility of the efficiency of the proposed method. Therefore, Fig. 5.9(b) presents the tracking of the stored kinetic inertia of the network for ten days data set.

Fig. 5.10(a) and Fig. 5.10(b) show the tracking of the stored kinetic energy of the network for seven days and two days data sets, respectively. The view is clear that the proposed tracking method monitors the stored kinetic energy effectively.

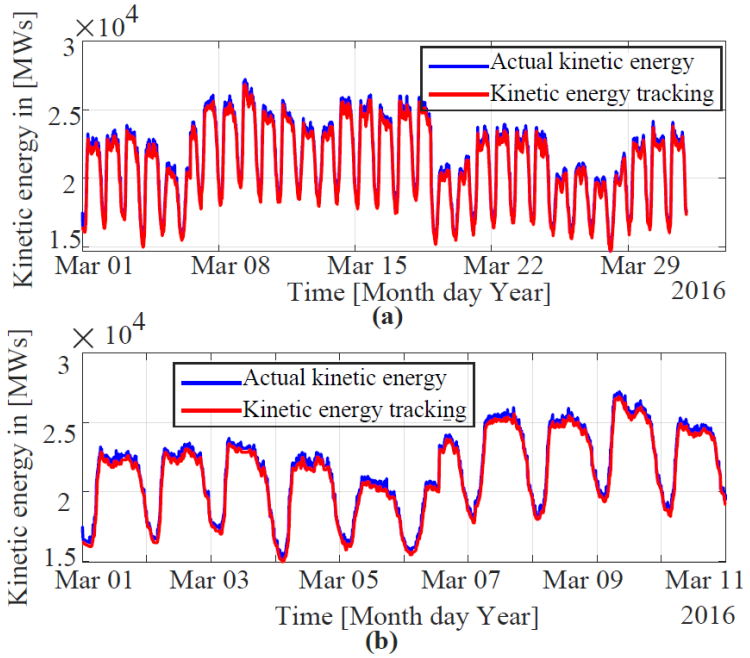

Fig. 5.9 (a) Tracking of inertia data for one month. (b) Tracking of inertia data for one week

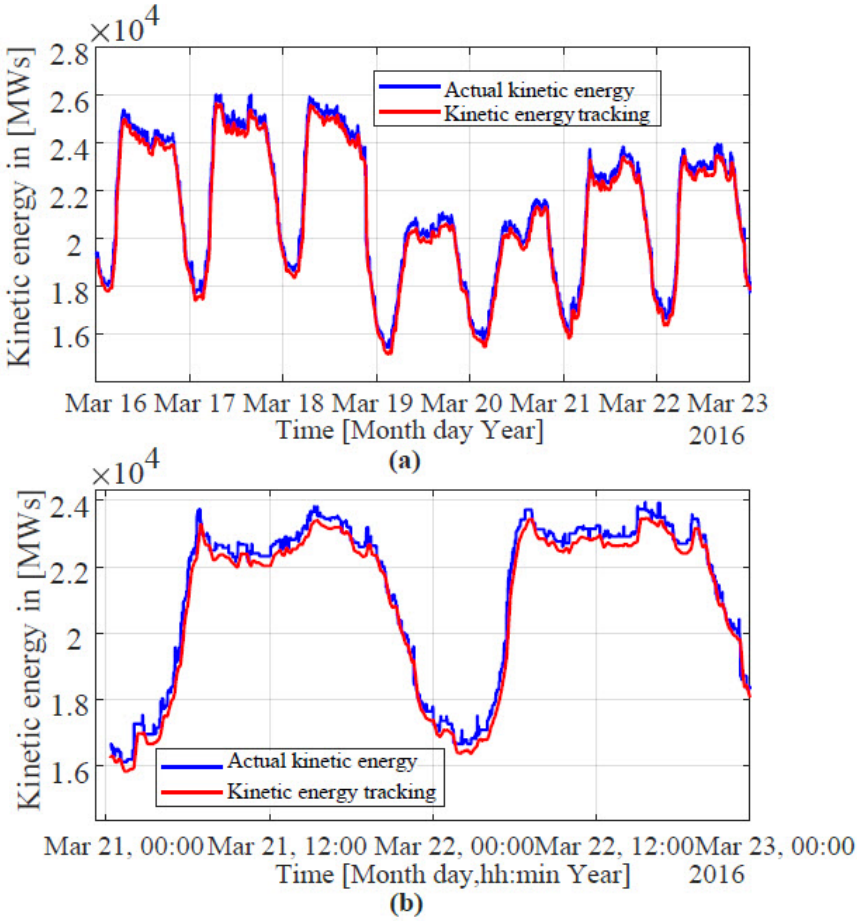

Fig. 5.10 (a) and (b) Tracking of kinetic energy for one week and two days, respectively

5.4.4 Inertia forecasting

The proposed method is tested for the time ahead prediction of the equivalent system inertia in (s) and the kinetic inertia of the network in (MWs). The historical measurement data presented in the previous section are used to validate the proposed method. The proposed method is tested for different time horizons, which are classified as short-range and long-range forecasting. The results are compared with other forecasting methods from [242] and [177]. The performances of the comparing forecasting methods are tested on the same presented actual New Zealand network data. The different time horizon forecasts are tested for different times ahead of the given current time.

The method is tested for the time ahead forecasting for seven days as observed in Fig. 5.11(a). The results are not good as the variance of the forecasting error is analysed to be around 24% which is outside the acceptable range of 4% to 15% according to [252]. Therefore, further investigations are done to identify the longest time ahead the proposed method can give results with acceptable forecasting error. Finally, the optimal time ahead is identified to be a maximum of two days that results in variance of forecasting error to be within acceptable range. An example of the two days forecasting is presented in Fig. 5.11(b).

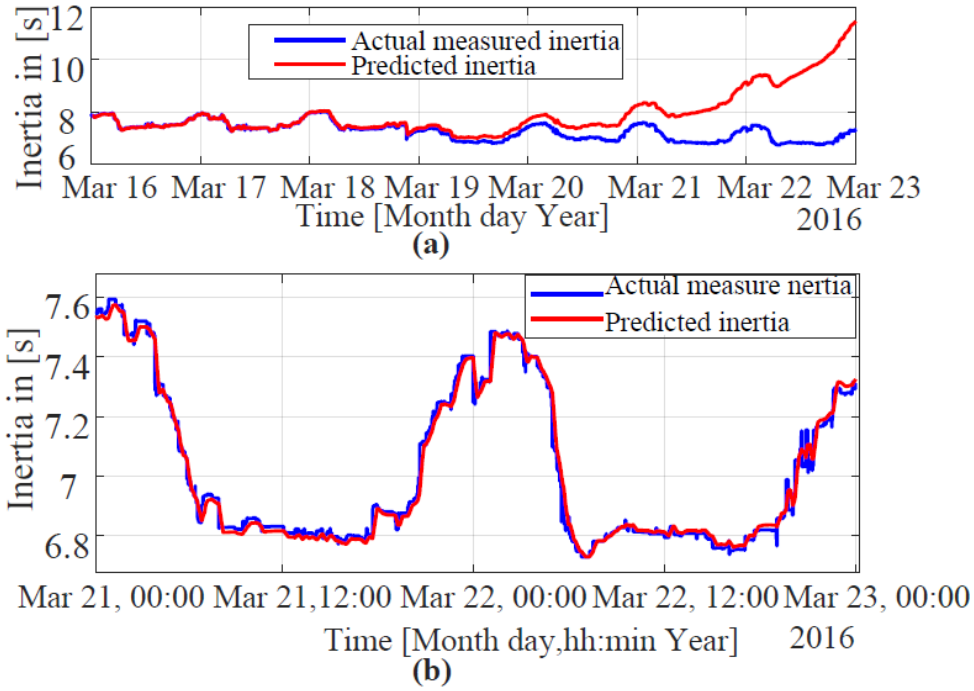

Fig. 5.11 (a) and (b) Inertia forecasting for seven days and two days, respectively

As it is done for inertia, the method is also tested for the stored kinetic energy in the network the method is tested for seven days as shown in Fig. 5.12(a). Finally, again the optimal maximum forecasting time that gives reasonable variance is limited to two days as depicted in Fig. 5.12(b).

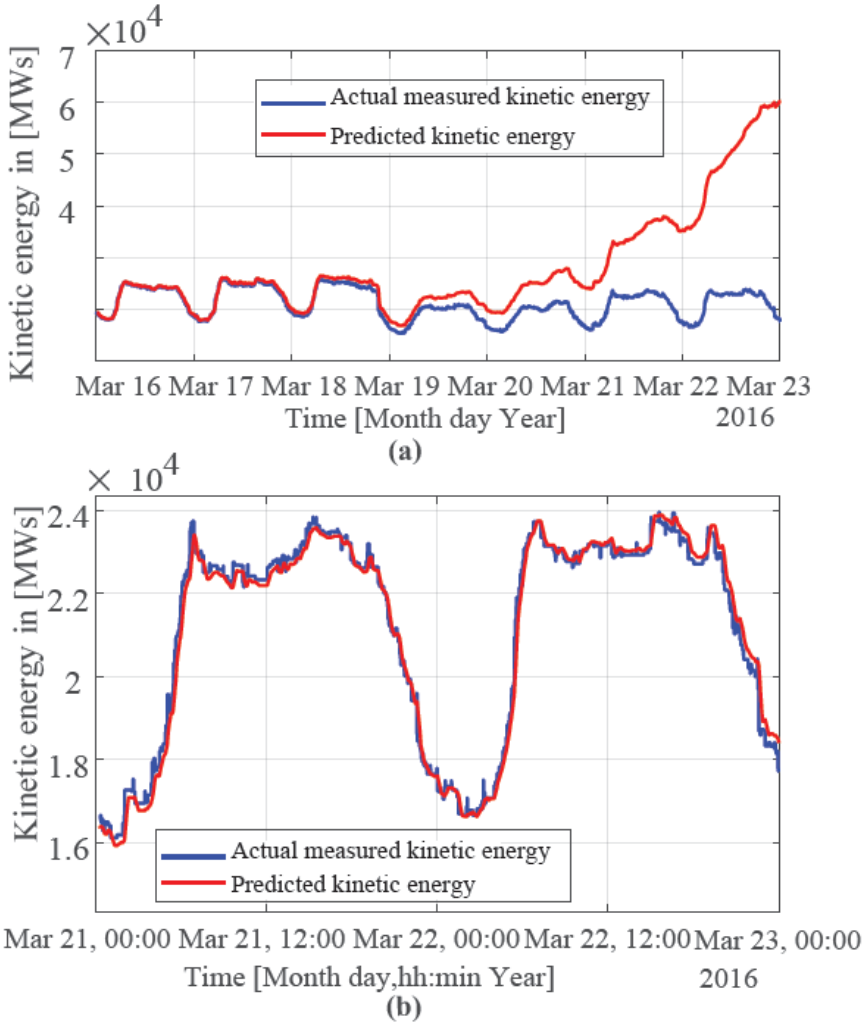

Fig. 5.12 (a) and (b) Kinetic energy forecasting for seven days and two days, respectively

5.5 Performance analysis of the proposed method

The widely used metrics to evaluate forecasting methods are mean square error (MSE), root mean square error, mean absolute percentage error (MAPE) and mean absolute error (MAE). However, due to some denunciations that these metrics are undefined in some cases [252, 253], the performance accuracy and quality for short-range are evaluated using symmetric mean absolute error (SMAE). This metric is defined as in (5.46).

$$SMAE = \frac{1}{N}\sum_{t=1}^{N}\left\{\frac{|y_t - \hat{y}_t|}{|y_t| + |\hat{y}_t|}\right\} \tag{5.46}$$

where N denotes the number of observation sample data, y_t and $\hat{y}_t$ are the actual and forecast inertia at t^{th} time, respectively.

On the other hand, due to no fact that SMAE can be used for long-range forecast, the long-range forecast performance accuracy and quality are still checked by MAPE. The MAPE metric is defined as in (5.47).

$$MAPE = \frac{1}{N}\sum_{t=1}^{N}\left|\frac{y_t - \hat{y}_t}{y_t}\right| \tag{5.47}$$

The performance superiority of the method presented in this paper is tested in reference to the other two different forecasting methods presented in [242] and in [177]. Testing of the proposed and the comparing methods is conducted using the historical inertia data for the New Zealand network to validate the method. The testing is conducted to examine the important aspects for modern power systems application, which are accuracy, robustness, time horizon and speed of communication to the PSOs. While examining these aspects, other features such as stochasticity and latent temporal patterns in the data are considered.

As noted from the presented power and inertia data in Fig. 5.5 and Fig. 5.6, respectively, the characteristics of datasets can be autoregressive, moving average and seasonal [248]. The repeating patterns observed in historical datasets covering a long time such as for few years help the moving observant predictor to forecast the trends of the data for long ranges. The use of the stationarity assured approach in data allows the proposed method to cope with stochasticity in datasets with well-standardized uncertainty estimates [248].

5.5.1 Online tracking

The proposed method is tested to monitor/track the inertia values in the network for all the days with the availability of historical data. To evaluate the accuracy of the tracking capability, the improved moving average window in the ARIMA model is used to track inertia measurements from the network. As presented in the given inertia data with a time resolution of 10 sec, the algorithm gets enough time to prepare and track the next observation measurement with a speed of $25\mu s$ and a refresh rate of 2 s. For each set of estimation data obtained at different levels of RESs penetration, a statistical analysis is carried out. As shown from Fig. 5.8-Fig. 5.10, the tracking signal tracks/monitors effectively the actual system inertia signal throughout the data presented.

5.5.2 Short-range forecasting

The proposed method is tested for a short time ahead forecasting of the network inertia. In this case, the time ahead is limited to only four hours. The comparing methods are also subjected to four-hour time ahead forecasting tested on New Zealand data. Table 5.4 reports the performance comparison of the proposed method with the other two methods as measured by SMAE on various datasets. The proposed method gives superior results over the other competing methods as shown in Table 5.4.

Table 5.1

SMAE comparison for the proposed method with the other two forecasting methods

Method	SMAE
Proposed i-ARIMA method	**0.051**
Artificial Neural Network method	0.101
MVHFIR method	0.130

Table 5.5 also gives a further SMAE comparison of the proposed method with the other forecasting methods for the specific different time ahead forecasts. For a maximum of four hours forecast, the proposed method proves to have better accuracy for each step of time ahead forecast.

Table 5.2

SMAE comparison of the proposed method with the other two forecasting methods for the different time ahead forecasts

Forecast time ahead (hour)	SMAE		
	Proposed method	Method 1 in [30]	Method 2 in [35]
0.0	0.001	0.015	0.005
0.5	0.003	0.021	0.009
1.0	0.005	0.028	0.014
1.5	0.008	0.034	0.022
2.0	0.010	0.039	0.031
2.5	0.017	0.051	0.045
3.0	0.022	0.067	0.052
3.5	0.028	0.083	0.064
4.0	0.035	0.110	0.078

The trend of the proposed method on the test data demonstrates the forecasting power of the proposed method in capturing essential dynamic features of the effective inertia in the considered network. For the considered short time, the comparing forecast methods hardly performed better. The influence of the moving observant predictor gives the proposed method an advanced performance as it improves the forecast time horizon, accuracy, and robustness to variations in inertia and prevalent patterns. The predictor further reduces variances in the predictions and gives better probabilistic outputs with reduced residual errors.

5.5.3 Long-range forecasting

The i-ARIMA is further tuned for different values of moving observant predictor $\mathfrak{P}$, periodicity and seasonality factor of the time-series data set s and the smoothing factor n. After several tunings, the five combinations of the parameters that give good forecasts and accuracy for

one-hour forecasts in terms of MAPE [%] are presented in Table 5.6. The optimal combination values that give the best forecasts and accuracy are 0.235, 10 and 17 for $\mathfrak{P}$, $\mathcal{s}$ and $\mathcal{n}$, respectively, as shown in Table 5.6. Using this combination, the method is tested for one day ahead forecast and then for two days ahead forecast. The proposed method does very well for one day ahead forecast of the network inertia giving MAPE of 3.06%. It also gives good forecasts for 48 hours with the maximum MAPE of 8.89% before the accuracy reduces significantly for further predictions of the inertia values beyond 48 hours. This result makes the proposed method the best method to long-range forecast inertia values in modern power systems.

Table 5.3

Tuned moving observant predictor $\mathfrak{P}$, periodicity and seasonality factor $\mathcal{s}$ and the smoothing factor $\mathcal{n}$ for best forecasts

Tuning score	$\mathfrak{P}$	$\mathcal{s}$	$\mathcal{n}$	MAPE
1	**0.235**	**10**	**17**	**1.23**
2	**0.341**	**12**	**16**	**3.41**
3	0.862	11	15	6.82
4	0.541	14	16	8.11
5	0.439	9	14	12.97

5.6 Conclusion

This paper presents an effective and improved ARIMA framework termed i-ARIMA that forecasts inertia values in a network for both short-and long-range. The approach uses the power of strong periodic and seasonality patterns of the time series data to introduce a moving observant predictor at different lags to give it a superior capability for long-range inertia forecast in power systems. The best accuracy of the i-ARIMA is achieved by fine-tuning and selecting the optimal combination of the moving observant predictor, periodicity and seasonality factor and smoothing factor at different lags. Based on previous historical inertia data set observations in the New Zealand network, the i-ARIMA is evaluated and tested. The results show that -ARIMA is fast, robust accurate and superior to other forecasting methods.

Chapter 6 Manuscript 5: Inertia Optimisation

Preamble

The recent advancements in converter applications in modern power system have opened a way to control RES to provide synthetic inertia (SyI). The participation of SyI in the market of RES-rich networks to provide instant frequency support when required proposes an increase in the overall operation cost of contemporary networks. Subsequently, reducing operation costs by optimizing the required SyI in the network is unavoidable. Therefore, Chapter 6 studies and presents the flexible optimisation method for modern networks with various constraints at different levels of contingency events and inertia values in the network. The proposed method reduces the operation cost of networks based on optimising synthetic inertia to be procured during contingencies. The technique uses the co-existence of synchronous generator inertia and synthetic inertia in modern networks to provide insights on how they affect the operating costs of the network and how optimisation can help reduce the operation costs.

Flexible synthetic inertia optimisation in modern power systems

Peter Makolo[1,2,*], Ramon Zamora[1] and Tek-Tjing Lie[1]

[1]Department of Electrical and Electronic Engineering, Auckland University of Technology, Auckland 1010, New Zealand
[2]Department of Electrical Engineering, University of Dar es Salaam – Dar es Salaam, Tanzania

Abstract: Increasing the replacement of conventional synchronous machines by non-synchronous renewable machines reduces the conventional synchronous generator (SG) inertia in the modern network. Synthetic inertia (SyI) control topologies to provide frequency support are becoming a new frequency control tactic in the new network. However, the participation of SyI in the market of RES-rich networks to provide instant frequency support when required proposes an increase in the overall marginal operation cost of contemporary networks. Consequently, depreciation of operation costs by optimizing the required SyI in the network is inevitable. The provided optimal values of SyI should also ensure stability resilience of the network is retained. Therefore, this paper proposes a flexible SyI optimisation method to address these issues. The algorithm developed in the proposed method minimizes the operation cost of the network by giving flexible SyI at a given SG inertia and different sizes of contingency events. The proposed method uses Box's evolutionary optimiser with a self-tuning capability of the SyI control parameters. The proposed method is validated using the modified New England 39-bus network. The results show that provided SyIs support the available SG inertia to reduce the RoCoF values and contain them within acceptable limits to increase the network's resilience.

6.1 Introduction

The electric power system industry is witnessing a structural reformation for the generation portfolios dominated by renewable energy sources (RES). Motivated by the global target to reduce carbon emission, the reformation is shifting towards 100% clean energy and phasing-out traditional synchronous generators (SGs) from the conventional network [50, 55, 85, 88, 91]. The replaced SGs have significant inertia and damping constants crucial for frequency stability. However, most integrated RES, such as solar photovoltaic (PV), do not have inertia. On the other hand, inertia from WT is decoupled from the rest of the network by the converters connecting them to the grid. Therefore, this reformation technically reduces the conventional inertia in the modern grid. An example of countries embarking on RES is Great Britain. The total SG in the Great Britain network is anticipated to be at most 30% by 2033/34 due to the penetration of RES [254].

Nevertheless, this phase-out of traditional SGs leads to problems related to reduced rotational inertia in the modern network [4, 7]. It should be noted that the reduced rotational inertia and damping, which are the essential properties of the replaced traditional SGs, are involved in stability control in traditional networks [8]. System inertia is a crucial property that responds immediately after power contingencies to slow down the rate of change of frequency (RoCoF) in the network. Therefore, networks with reduced SG inertia experience significant operational and stability challenges [5].

To address the underlying operational and stability challenges, hence, achieving secure network operations, different control strategies of non-synchronous renewable energy sources have been introduced to the modern network [8, 9]. The control strategies primarily provide the so-called synthetic inertia (SyI) to improve the stability of the network in case of low SG inertia. On one hand, SyI involves control topologies to emulate the behaviour of synchronous generators in supporting frequency control in low conventional inertia networks [4]. On the other hand, SyI is commonly explained as the controlled input of electrical torque from a unit to give additional power comparable to the RoCoF. This control is implemented to reduce the impact caused by low inertia in the network after a contingency event [244]. In short, SyI is an extra power component injected to or absorbed from the network to support frequency stability when the network is subjected to contingencies [255].

Generally, inertia is crucial in overcoming the immediate frequency deviation due to power imbalances. It is believed that SyI can play a massive role in the stability resilience of modern power systems [256]. SyI can be temporarily obtained from the control of RES, such as battery storage systems (BESS), variable speed wind turbines (VSWT), and supercapacitors [256]. SyI can play an essential role during frequency deviation to safeguard frequency stability before primary frequency control comes into play [257].

Several control topologies in the literature are proposed to provide SyI inertia for frequency control in the modern network. For instance, in [258], a control topology for SyI is included in managing frequency dynamics in networks. Likewise, in [21], a complex control topology of WT gives SyI at different times during contingency events. All SyI topologies require a primary energy source behind a converter that connects the energy source to the network [26]. This energy source is from the RES that replaces the kinetic energy from the retired conventional SGs. As SyI depends on the capacity of the primary energy sources such as BESS, supercapacitors, and flywheels, it is becoming an important participant in the inertia market framework in modern networks as proposed in [21-23]. As SyI is a short term-quantity that functions in line with the available conventional synchronous generator inertia, it needs to be operated depending on the size of the contingency event and the pre-known values of available traditional SG inertia in the network [24]. The amount of SyI to be procured depends mainly on how much conventional system inertia is available online. The lower the traditional inertia of the system, the higher the SyI to be procured [24, 25].

Apart from SyI becoming a critical quantity for providing frequency stability and raising its value in the modern network, it also plays a major role for ancillary service [26]. For these reasons, SyI is an inevitable quantity for current network operation. However, considering the operation cost of the modern network, which is appreciated because of the procurement of SyI, there is a need of methods to give optimal values of SyI for frequency control at different conditions. The provision of SyI to control frequency during contingency events in low inertia networks needs to be at values that can achieve as minimum operating cost as possible [27, 28].

However, there is a challenge in providing an optimum value of SyI, especially during contingency events in modern networks. The current research works such as [258-260] suggest various approaches to address the problem of low inertia in modern networks. Yet, most methods focus only on the provision of SyI but not on optimised values. For instance, in a study [257], the approach focuses on optimised power point tracking (OPPT) for VSWT to provide virtual inertia (VI) for frequency control. Nevertheless, it does not offer optimal SyI at the minimal operating cost of the network. The research in [261] assesses the potential tuning of WT parameters to provide SyI for the timely and effective rescue of frequency in various network circumstances. The research neither considers the dynamics of the WTs in the network nor focuses on providing optimal SyI for effective cost saving in the network operation.

Furthermore, the study in [28] describes the need to dynamically optimise the values of SyI for frequency control in low inertia networks. The research in [262] develops an optimisation method based on conventional economic dispatch. In the method, distributed

energy resources (DERs) participate in inertial and primary frequency response by sharing power injections relative to their power ratings. Furthermore, [4, 35, 109] employ the $\mathcal{H}_2$ performance metric to address the optimal inertia placement problem concerning network coherency. Specifically, research works in Refs. [4, 35] focus on enhancing frequency response for networks with high penetration of RES by finding the optimal inertia placements that reduce the performance metric $\mathcal{H}_2$. Not only do these methods face a limitation of not giving the optimal values of SyI but also their models are inadequate to illustrate the dynamics of the real low inertia network. As a result, the applicability of the system performance metric $\mathcal{H}_2$ raises a concern.

Considering the limitations from other research works, a novel model to dynamically optimise values of SyI according to the size of contingency and a minimum value of SG inertia in a network is proposed. The proposed optimisation algorithm provides a new degree of SyI freedom at minimum SG inertia values in networks. Depending on the value of minimum SG inertia in the network and the size of the contingency, the algorithm proposed can flexibly adjust the amount of optimal value of SyI required by the system to keep the frequency stable. This approach assumes enough energy storage from the controlled RES to provide this optimal value until the network frequency reaches a safe value.

The novelties of the proposed method are summarized as follows:

- RoCoFs and frequency nadir are improved due to optimal SyI activation following a contingency event in the network.
- The best values of SyI are provided at the given minimum value of SG inertia at the optimal cost.
- SyI flexibility is assured depending on the values of minimum SG inertia and the size of the contingency event.

The rest of this paper is organized as follows: In Section 2, the problem formulation for SyI provision in the modern network is described. In Section 3, the proposed SyI optimisation method is described. The network description and simulation results to validate the effectiveness of the proposed method are presented in Section 4. Besides, discussions of the results are given alongside each result. Ultimately, the conclusion is drawn in Section 5.

6.2 Problem formulation for optimal synthetic inertia provision in power systems

Synthetic inertia can be implemented in different ways in modern power systems, as explained in [8, 69, 263]. In order to achieve the objective of this research, this paper uses the control of solar PV and BESS in provision of SyI. Even though BESS is a non-rotational generation unit, it can quickly regulate its power outputs to make it suitable for SyI provision in the power system [264]. The conceptual diagram showing how a non-dispatchable generating unit can be configured to provide SyI in a network with SG inertia is presented in Fig. 6.1.

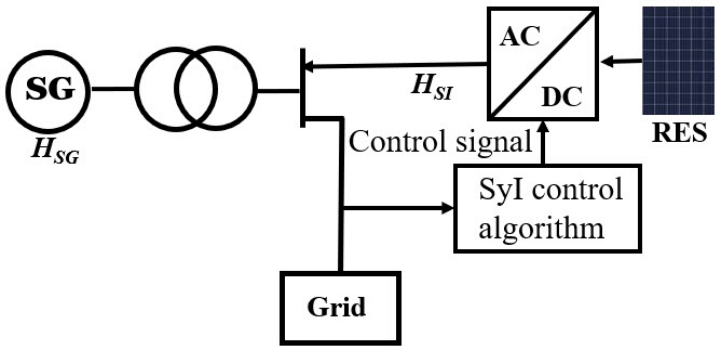

Fig. 6.1 Schematic diagram showing SyI provision from RES in a network with SG inertia

Various research works such as [244, 265, 266] explain that the available synchronous generator inertia responds instantly after detecting a contingency event in the network. Then, the controlled SyI takes over after a specific time, subject to the control topology as shown in Fig. 6.2. Depending on the topology that provides SyI in the network, the problem in this research is formulated in three stages:

- After a contingency event is detected in the network, the initial RoCoF is obtained.
- The algorithm reads the resulting RoCoF and compares it with the set threshold and critical values of RoCoF.
- Based on the recorded value of the initial RoCoF and the minimum value of SG inertia, the question is to work out the amount of SyI needed to contain the RoCoF in case the initial RoCoF is beyond the threshold value is evaluated.

Therefore, this research work determines how much SyI is needed to be activated for different sizes of contingency events in the network. Depending on a size of a contingency event, a suitable amount of SyI in terms of the output power P_i is activated as described in Fig. 6.2. In this figure, the contingency event occurs at the time t_0 and injection of SyI is done at the time t_i to deliver extra power P_i depending on the size of the event and the initial RoCoF detected. For a small size of a contingency event, P_1 can be activated while P_{Max} is for the maximum contingency event. P_{Max} depends on the capacity of the energy source of SyI. P_2 and P_3 stand for any other values of SyI to be activated depending on the level of contingency event and initial RoCoF detected. The delay between t_0 and t_i is due to the time taken for the communication from activation of the fault, performing control algorithm, and provision of SyI activation signal. After the activation of SyI, the initial RoCoF and frequency deviation are reduced to save the network from frequency instabilities. The activation process comes in only if the available minimum value of SG inertia cannot keep the frequency within safe values. Therefore, in this research, it is critical to pre-quantify the minimum value of SG inertia in the network to plan for sufficient resources that can provide adequate SyI to retain the frequency within acceptable limits.

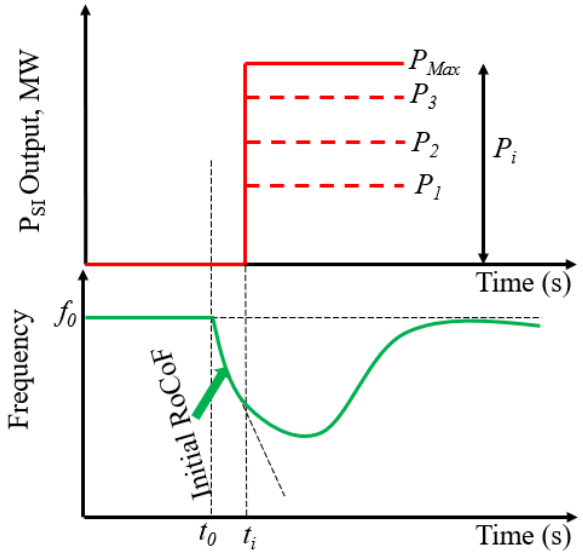

Fig. 6.2 Synthetic inertia provision to support frequency stability in low synchronous inertia networks

An optimisation problem is formulated to answer how much SyI is needed to support frequency in low synchronous inertia networks and attain the performance targets. The problem is developed based on the minimum level of SG inertia present in the network, the initial value of RoCoF, set threshold and critical values of RoCoF and finally, the operating cost of the network. Based on the minimum SG inertia, the developed algorithm should decide the minimum possible value of SyI to be provided to support frequency stability at different levels of contingency events. This problem is formulated using the network model given in Fig. 6.3. Based on the figure, various design variables are considered in the formulation of the problem. The design parameters considered in the problem formulation include the minimum level of SG inertia and damping constant and the contingency event.

The solution of the formulated optimisation problem can be obtained by considering various constraints. In approaching this problem, the RoCoF of the network is the main deciding parameter. Suppose the RoCoF is below the set threshold value. In that case, the resulted frequency following a contingency event is within the range, and the minimum SG inertia can contain the frequency without any need for additional SyI. However, when the RoCoF is beyond the threshold, and below the critical value set, the minimum SG inertia is insufficient to contain the frequency within allowable ranges. Therefore, an additional optimal value of SyI has to supplement SG inertia to manage the frequency response in safe limits. On the other hand, when the RoCoF is beyond the critical value, this condition is beyond the combined inertia response. Therefore, the generator protection schemes have to be activated for further protection.

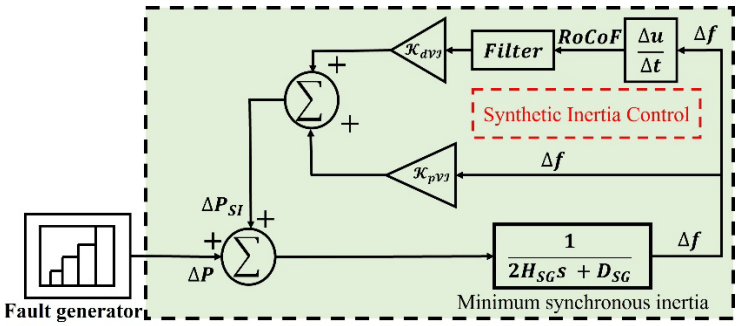

Fig. 6.3 A model to provide optimal values of SyI in a low synchronous inertia network

To achieve the goal of optimal SyI provision in the network, the parameters required to be tuned to supplement SG inertia in containing frequency are the proportional and derivative gains $\mathcal{K}_{pVJ}$ and $\mathcal{K}_{dVJ}$ of the SyI controller. These parameters mainly depend on SG inertia, contingency event level, and the initial RoCoF in the network. The objective function of the optimisation problem is formulated depending on contingency events taking into account limitations of SG inertia in the network. The goal is to tune the SyI control gains parameters to obtain the optimal value of SyI required to contain frequency within allowable ranges.

6.3 The proposed flexible inertia optimisation method

6.3.1 Model description and inertial response

As the load profile dictates how much the generation should be in the network, for light loads fewer synchronous generators are required online to power the load. The conventional SGs can further be reduced from the grid when weather conditions and pricing allow more RESs to be operational. However, the operational risk is high. When any contingency event happens during this light load with reduced conventional SG inertia, RoCoFs and frequency deviations are enormous. In such circumstances, threshold values may be exceeded and lead to cascading tripping of online synchronous generators, resulting in blackouts [24].

As load profiles forecasts are well established in the literature, they can be used to schedule the minimum level of SGs online as presented in [24]. This research work develops a graphical relation to match contingency size and minimum required SG in a network, as shown in Fig. 6.4. The level of SG inertia online and the size of the contingency event determine the size of the RoCoF. For constant SG inertia, the contingency event is directly proportional to the RoCoF. This information concludes that system inertia and the size of the contingency event mainly dictate the initial frequency response in the network. Likewise, the RoCoF, which is the time derivative of the system frequency response, primarily depends on both size of contingency

event ΔP and the system inertia H_{sys} as seen in (6.1) [60, 244] where f_0 represents the nominal network frequency.

$$RoCoF = \frac{\Delta P f_0}{2H_{sys}} \tag{6.1}$$

Now, to formulate the dynamic model for flexible SyI inertia provision in the low SG inertia network, the size of contingency event and the minimum value of SG inertia are crucial inputs. When a contingency event ΔP happens in a network, there will be a reaction from the rotating masses of the SGs in the network by changing their rotor speed $\Delta\omega$. The approximated swing equation (6.2) gives the relation of speed deviation to the power imbalance.

$$\frac{2H_{sys}}{\omega_0}\frac{d\Delta\omega}{dt} = -\Delta P \tag{6.2}$$

For a constant value of system inertia, the size of the contingency event determines the RoCoF. If maximum power imbalance ΔP_{max} is assumed, the maximum RoCoF is given by (6.3) [244].

$$RoCoF_{max} = \frac{f_0}{2H_{sys}}\Delta P_{max} \tag{6.3}$$

And if a threshold power imbalance is considered, the RoCoF will be equal to a threshold value. The relationship is presented in (6.4).

$$RoCoF_{thres} = \frac{f_0}{2H_{sys}}\Delta P_{thres} \tag{6.4}$$

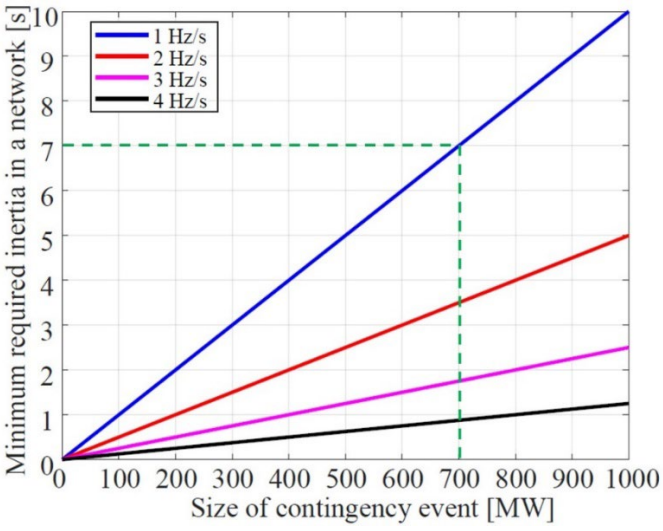

Fig. 6.4 A diagram to show minimum required inertia for different sizes of contingency events at different RoCoFs

To limit the RoCoF to a threshold value means extra power must be supplied to or absorbed from an external entity. Equation (6.5), which is the difference between maximum

RoCoF and threshold RoCoF, is presented to obtain the minimum required additional power to maintain the RoCoF below the threshold value as explained in [60, 244].

$$\Delta RoCoF = RoCoF_{max} - RoCoF_{thres} = \frac{f_0}{2H_{sys}}\Delta P_{req} \tag{6.5}$$

As successful frequency control requires specific RoCoF threshold values for different networks, in this research, a generalized RoCoF value of 1 Hz/s is the threshold value set in place to evaluate the provision of optimal values of SyI in the network after a contingency.

Any network can use the developed concept for frequency control. In this approach, the network model is approximated using the system identification approach as explained in [6, 16]. From the estimated model, the dynamics of the system frequency are captured. The network dynamics are defined by the traditional swing equation (6.6) where ΔP_m and ΔP_e represent mechanical power and active power deviations, respectively while D_{sys} is the total damping constant of the network. The values of available SG inertia can be obtained and used in the optimisation algorithm from the identified dynamics.

$$\Delta\omega = \frac{1}{2H_{sys}s + D_{sys}}(\Delta P_m - \Delta P_e) \tag{6.6}$$

If the network comprises both SG inertia and SyI inertia, equation (6) can be split into two, as shown in [262]. The swing equations for the network with conventional SG inertia and SyI are (6.7) and (6.8), respectively.

$$\Delta\omega = \frac{1}{2H_{SG}s + D_{SG}}(\Delta P_m - \Delta P_e) \tag{6.7}$$

$$\Delta\omega = \frac{1}{2H_{SI}s + D_{SI}}(\Delta P_m - \Delta P_e) \tag{6.8}$$

where H_{SG} and D_{SG} are the effective inertia constant and damping constant for the SGs in the network while H_{SI} and D_{SI} are the effective inertia constant and damping constant for the SyI resources in the network. The total system inertia constant H_{sys} and damping constant D_{sys} are defined by (6.9) and (6.10), respectively.

$$H_{sys} = H_{SG} + H_{SI} \tag{6.9}$$

$$D_{sys} = D_{SG} + D_{SI} \tag{6.10}$$

From the model identification, the network dynamics are identified using the s-domain transfer function from the contingency event ΔP to frequency deviation as given in (6.11).

$$\frac{\Delta\omega(s)}{\Delta P} = \frac{\hbar(s+\zeta)}{s^2 + 2\xi\omega_n s + \omega_n^2} \tag{6.11}$$

The Laplace transform of (6.11) gives (6.12) for underdamped systems.

$$\Delta\omega(t) = \Delta\omega_{ss}\left(1 - \frac{e^{-\xi\omega_n t}}{\sqrt{1-\xi^2}}(\sin(\omega_d t + \varphi) - \frac{\omega_n}{\zeta}\sin(\omega_d t))\right) \quad (6.12)$$

where $\omega_d = \omega_n\sqrt{1-\zeta^2}$, $\varphi = \tan^{-1}\left(\zeta^{-1}\sqrt{1-\zeta^2}\right)$, $\Delta\omega_{ss} = \frac{\Delta P}{D_{eq}}$, $\hbar = 2H_{sys}$, $\zeta = \tau^{-1}$,

$\omega_n = \sqrt{\frac{D_{eq}}{2\tau H_{sys}}}$, $\xi = \frac{1}{2}\frac{2H_{sys}+\tau D_{eq}}{\sqrt{2\tau H_{sys} D_{eq}}}$, τ is the system turbine time constant

Solving for the total required network inertia H_{sys} at a given contingency event ΔP as described in [262] and knowing the minimum value of SG inertia in the network, the required SyI can be calculated using the optimisation approach described in the following subsection.

6.3.2 Synthetic inertia optimisation

This subsection introduces the optimisation approach to work out the required optimal amount of SyI to be provided at different levels of contingency events. This paper's optimisation problem is based on the cost function of the overall economic dispatch of SGs and the cost of RES resources to provide SyI. In presenting the optimisation approach, the cost function is an essential condition to be considered, given the additional operational cost of RES to provide an inertial response during contingencies in the network. In this approach, the traditional linear Box's evolutionary optimisation (BEO) algorithm is used [267]. The Box's evolutionary optimiser has a self-tuning capability of the parameters in the environment where it is used [267]. As the optimisation problem is based on the cost of minimum SG inertia in the network, the BEO algorithm is a perfect choice in this approach. During the contingency event cycle, the parameters of the SyI controller are tuned by Box's evolutionary optimiser to provide the minimum required SyI from the RES. In this way, the SyI from RES is optimised to minimize the overall cost of the network operation.

The overall cost function of the network considering only inertia can be formulated by (6.13) [24]. In this formulation, the cost function involves only the sum of all the components required for inertial response in the network. Therefore, the cost function is approximated by considering only the cost of SG inertia and the cost of SyI in the network at a particular time t.

$$C(t) \approx \sum_{i-1}^{N_{SG}} C_i(H_{SG}(t)) + \sum_{i=1}^{N} C_i(H_{SI}(t)) \quad (6.13)$$

where $C(t)$ is the approximate of the overall cost function as a function of the cost of all SG inertia in $C_i(H_{SG})$ and SyI inertia resources $C_i(H_{SI})$ in the network. If the cost function $C(t)$ is assumed to be strictly convex, then the Karush-Kuhn Tucker (KKT) terms [35] suggest that the derivative of the cost function (6.14) has a distinctive set of optimisers, $\mathfrak{F}$.

$$C'(t) \approx \frac{\partial f C_i\left(H_{SG}(t)\right)}{\partial t} + \frac{\partial f C_i\left(H_{SI}(t)\right)}{\partial t}\bigg|_{\Delta P} = \mathfrak{F} \tag{6.14}$$

The optimisers, $\mathfrak{F}$ hold as long as all variables considered in the optimisation problem do not cross their limits [268].

To ensure RESs respond optimally during contingencies, their injected power would have to solve the optimisation problem (6.14) [262]. The minimum amount of total SG inertia and the additional SyI should help the RoCoF and frequency deviation within their constraints for the acceptable level of contingency event. The constraints required to formulate the optimisation problem are presented in (6.15).

$$\begin{cases} RoCoF_{thres} \leq RoCoF \leq RoCoF_{crit} \\ -f_{crit} \leq f \leq f_{crit} \\ \Delta E_{req} \geq \Delta E_{crit} \\ t \leq t_{crit} \end{cases} \tag{6.15}$$

For the optimisation algorithm to obtain a distinctive set of optimisers for the cost function (6.14), first, the RoCoF should be between threshold and critical values $RoCoF_{thres} \leq RoCoF \leq RoCoF_{crit}$. Second, the frequency should be within the critical values $-f_{crit} \leq f \leq f_{crit}$. Third, the energy level from the frequency support resources should be higher than the critical value $\Delta E_{req} \geq \Delta E_{crit}$. Fourth, the response time of the frequency support resources should be less than a critical set value $t \leq t_{crit}$. Using these constraints, the optimisation algorithm should carefully tune the SyI parameters to limit the RoCoF and frequency nadir within acceptable limits. In this way, frequency profile can be maintained and avoid compromising its security and making it vulnerable to instability.

Therefore, minimizing the SyI in terms of additional power at a given SG's value inertia in the network is the optimisation objective of this problem. To minimize the cost function provided in (6.13) as a function of levels of contingency events ΔP follows as given in (6.16).

$$\underset{\Delta P,\, t}{min} C(t) = \frac{\partial f\left(\sum_{i-1}^{N_{SG}} C_i(H_{SG}(t))\right)}{\partial t} + \frac{\partial f\left(\sum_{i=1}^{N} C_i(H_{SI}(t))\right)}{\partial t}\bigg|_{\Delta P} \tag{6.16}$$

As H_{SG} is considered to be a constant quantity throughout the contingency event time t, then the optimisation problem is a function of SyI H_{SI} in the network. Since SyI controller is the function of $\mathcal{K}_{p\mathcal{VI}}, \mathcal{K}_{d\mathcal{VI}}$ [256], then the optimisation function solely depends on the tuning of these parameters. Tuning these parameters and minimizing SyI at constant minimum SG inertia should dictate the marginal cost of the network operation under contingency events.

To minimise the cost function, the primary input in the developed algorithm is the forecasted minimum synchronous generation units in the network as determined by the forecasted net load. Based on the forecasted SGs in the network, the minimum total SG inertia can be defined by (6.17).

$$H_{Total} \times S_{Total} = \sum_{i=1}^{N_{SG}} H_i \times S_i \tag{6.17}$$

where H_{Total} and S_{Total} are the total inertia constant and the capacity of the entire system, respectively; H_i and S_i are the inertia constant and the capacity of the i[th] SG, respectively; N_{SG} is the number of SGs in the network.

The following are the steps of the BEO algorithm:

- Step 1: Choose initial points $\boldsymbol{x^{(0)}}$ for $\boldsymbol{\mathcal{K}_{PVJ}}$ and $\boldsymbol{\mathcal{K}_{JVJ}}$ of SyI, $\boldsymbol{H_{SI}}$ based on the available SG inertia $\boldsymbol{H_{SG}}$ in the network. Choose also the size reduction parameter $\boldsymbol{\Delta_i}$ for each variable and a termination parameter $\in$. Set $\boldsymbol{\overline{x} = x^{(0)}}$,
- Step 2: If $\|\Delta\| < \in$, Terminate the optimisation process; else create $\boldsymbol{2^N}$ by adding and subtracting $\boldsymbol{\Delta_i}/2$ from each variable at the point $\boldsymbol{\overline{x}}$,
- Step 3: Compute function values at all ($\boldsymbol{2^N}$ +1) points. Find the point having the minimum function value. Designate the minimum point to be $\boldsymbol{\overline{x}}$,
- Step 4: If $\boldsymbol{\overline{x} = x^{(0)}}$, reduce size parameters $\boldsymbol{\Delta_i} = \boldsymbol{\Delta_i}/2$ and go to Step 2; else set $\boldsymbol{x^{(0)} = \overline{x}}$ and go to Step 2.

The overall algorithm of the proposed method is summarized in this paragraph. When a contingency event happens in the network, the algorithm is started by checking the size of the contingency in relation to the minimum SG inertia in the network. For the first case, if the initial RoCoF is less than the threshold value, the minimum SG inertia in the network can contain the event to maintain frequency stability. For the second case, if the response results in a RoCoF higher than the threshold value but less than the critical value, the minimum SG inertia is not enough and hence incapable of containing the event alone to support frequency stability. Therefore, the optimal value of SyI must be activated to support the available SG inertia to contain the contingency event and thus save the network from frequency instabilities. Meeting these constraints is adequate for keeping modern networks reliable and in safe operation. For the third case, if the frequency response results in a RoCoF higher than a set critical value, the inertial response cannot contain the frequency. In this scenario, therefore, generation protection controls are activated to protect damages in the network. The concept of the proposed algorithm is summarized in the flow diagram in Fig. 6.5. The process is performed once for every contingency event happening in the network. When there is no any contingency event, the algorithm is not started.

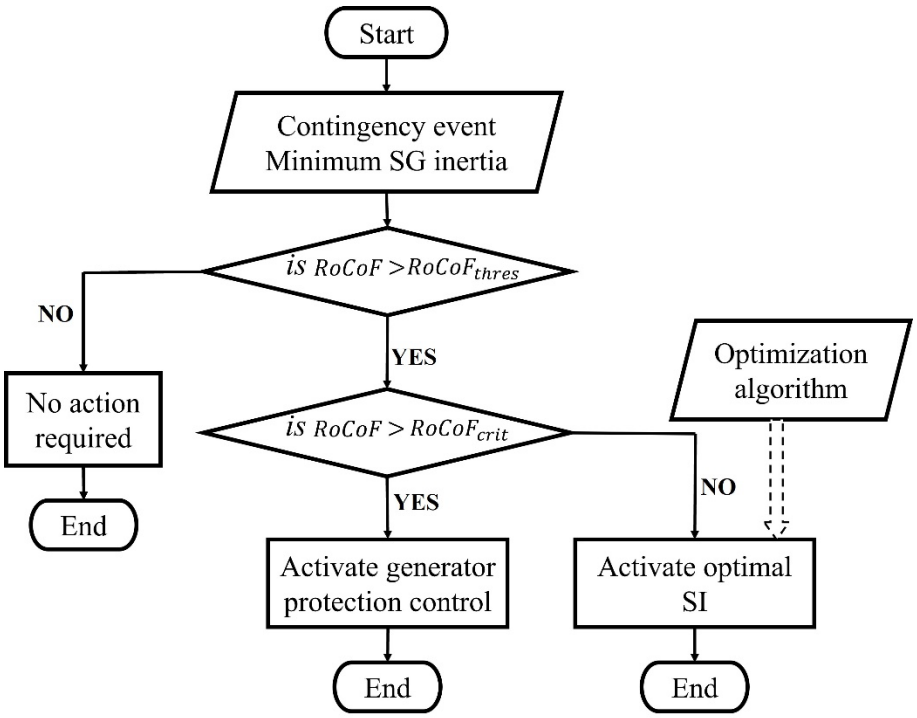

Fig. 6.5 Flow diagram of the proposed decision algorithm to activate the required SyI in the network

6.4 System description and results

This research uses a modified New England 39-bus with ten SGs for numerical simulation to validate the proposed method. The network is modelled in DIgSILENT, and Fig. 6.6 presents its schematic. The obtained data is exported to Matlab, where the optimisation algorithm is implemented. To emulate the low inertia conditions, some of the traditional SGs in the network are sequentially replaced by solar PV power plants to adjust the minimum value of SG inertia in the network. Alongside the solar PV plants, BESS provides the SyI in the network under contingency events. The controller at the converter controls BESS to give optimal SyI subject to the size of the event, as shown in Fig. 6.3. The threshold, critical RoCoFs and maximum frequency deviation are set to 1 Hz/s, 2 Hz/s and 0.7 Hz, respectively.

Using the optimisation algorithm presented in section 3, several contingency events ΔP are applied, as illustrated in Fig. 6.3. Then, depending on the size of the event, the activation of the SyI control algorithm is done when the initial RoCoF crosses the threshold value. When SyI is activated, tuning of SyI controller parameters is performed to give optimal values of SyI. The contingency events in this simulation are generated by tripping different loads in the network model. The resulted RoCoF is recorded and compared with RoCoF threshold and critical values for each contingency event. One generation unit G1 at bus 39 is tripped to obtain the largest contingency event. Table 6.1 shows the data used in the proposed approach. The table gives the

inertia values and time constants of different SGs used in the network. All the frequency readings are taken from the centre of inertia bus number 14.

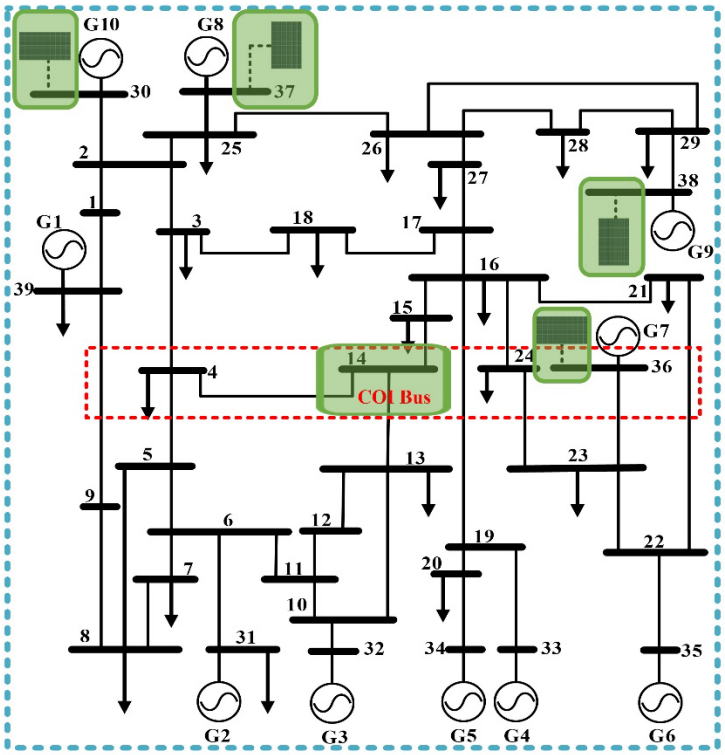

Fig. 6.6 A modified New England 39-bus with ten SGs and four solar PV plants to replace some SGs

Table 6.1

Parameters of the network used for the numerical simulation of the network

Parameter	Value [s]	Parameter	Value [s]
H_{SG1}	4.0	τ_{SG1}	3.5
H_{SG2}	3.6	τ_{SG2}	4.5
H_{SG3}	3.8	τ_{SG3}	5.0
H_{SG4}	3.2	τ_{SG4}	4.0
H_{SG5}	3.6	τ_{SG5}	4.6
H_{SG6}	3.7	τ_{SG6}	4.5
H_{SG7}	3.3	τ_{SG7}	5.0
H_{SG8}	3.2	τ_{SG8}	4.0
H_{SG9}	3.1	τ_{SG9}	4.5
H_{SG10}	3.5	τ_{SG10}	5.5

Various simulations are done to validate the applicability of the proposed method. For a constant total SG inertia in the network, different sizes of contingency events are applied, and the

BEO tunes the appropriate values of parameters $\mathcal{K}_{PVJ}, \mathcal{K}_{JVJ}$, and the corresponding SyI is given in the network. Then, the value of total SG inertia is changed by replacing some of the SG with solar PV plants. The simulation is done for four different values of SG inertia in the network, which are 6 s, 5 s, 4 s, and 3 s. Table 6.2 and Table 6.3 present the results for different sizes of contingency events for two separate cases of SG inertia to represent the rest of the cases in the network. The corresponding tuned parameters $\mathcal{K}_{PVJ}, \mathcal{K}_{JVJ}$, and the optimal SyI for each case is provided. Furthermore, the percentage contribution of SyI in the inertial response for each contingency event is provided.

Table 6.2

Tuned parameters for different sizes of contingency events at SG inertia = 6 s

Contingency events ΔP [MW]	$\mathcal{K}_{pVJ}$	$\mathcal{K}_{dVJ}$	SyI [s]	% of SyI in inertial response
0	0	0	0	0
100	0	0	0	0
200	0	0	0	0
300	12	6.2	0.61	5
400	11	6.0	0.82	8
500	9.8	6.1	1.01	11
600	9.5	5.8	1.25	13
700	8.1	4.7	1.43	15
1200	0	0	0	0

The minimum value of synchronous generator inertia = 6 s

It is noted from Table 6.2 that with minimum SG inertia of 6 s, contingency events with values 100 MW and 200 MW do not lead to activation of SyI. The resulted RoCoF is lower than the threshold value. This scenario of low RoCoF means the available SG inertia is enough to respond to the event without resulting instability. The developed algorithm for this condition does not activate the SyI controller. On the other hand, the contingency events with 300 MW to 700 MW result in RoCoF beyond the threshold value. Therefore, the SyI controller is activated, and the BEO tunes its parameters to provide SyI to supplement the available SG inertia in the network. For this scenario, if the SyI controller is not activated, the SG inertia cannot ensure frequency stability after the events. On the other scenario, the contingency event with a value of 1200 MW results in a very high RoCoF beyond the critical value set. In this scenario, the algorithm does not activate the SyI controller; instead, it sends information to the generator protection relays for further protection actions.

Table 6.3 presents the optimisation results for a network with a low total SG inertia of 3 s related to a maximum penetration of RES in the network. For this case of highly reduced SG inertia, contingency events from100 MW to 500 MW need activation of SyI controller. Contingency events from 600 MW to 1200 MW result in RoCoF beyond the set critical value.

Therefore, the SyI controller is not activated; instead, protection relays are activated. For each event, the percentage contribution of SyI in the inertia response is given. It is noted that the SyI contribution percentage increases with the increase of contingency events size.

Table 6.3

Tuned parameters for different sizes of contingency events at SG inertia = 3 s

Contingency events ΔP [MW]	$\mathcal{K}_{pVJ}$	$\mathcal{K}_{dVJ}$	SyI [s]	% of SyI in inertial response
0	0	0	0	0
100	4.5	2.2	1.44	15
200	4.2	1.8	1.86	20
300	3.6	1.5	2.17	23
400	3.5	1.2	2.50	27
500	3.1	0.8	2.88	31
600	0	0	0	0
700	0	0	0	0
1200	0	0	0	0

The minimum value of synchronous generator inertia = 3 s

It can be observed that as the minimum value of SG inertia is reduced in the network, large amounts of optimal SyI need to be applied in the network during contingency events. The large amounts of optimal SyI increase the operation cost of the network. Therefore, it is recommended to have the SG inertia in the network as much as possible to avoid the increased operating cost of the modern networks.

The numerical simulations in Fig. 6.7-Fig. 6.10 showcase the four cases of frequency responses with different amounts of SG inertia at various contingency events. The frequency responses presented are obtained from the centre of inertia bus 14, as shown in the study case network in Fig. 6.6. However, the SyI controls are done at the local buses where the BESS are located. Fig. 6.7 presents the first case where a low power contingency event is activated by increasing the load at bus 20 by 30%. The resulted frequency response has the RoCoF lower than the threshold RoCoF value. Therefore, the available minimum available SG inertia in the network can contain the frequency response within safe limits. For this case, consequently, the SyI control is not activated.

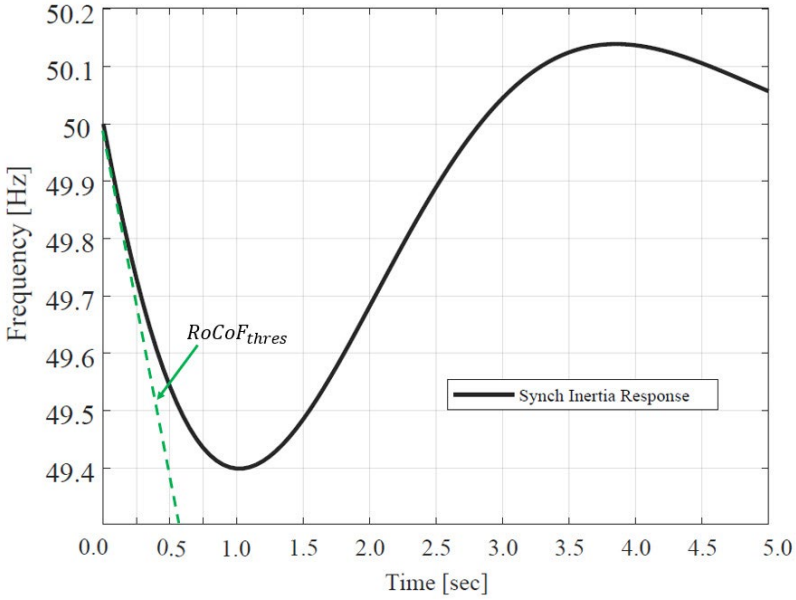

Fig. 6.7 Frequency response with a low contingency event that results in RoCoF lower than the threshold value

The second case involves a higher contingency event than the first case at the same minimum SG inertia as in case one. In this case, two loads from bus 20 and 28 are simultaneously increased by 30% each. Therefore, the resulted initial RoCoF is higher than the threshold RoCoF set value, as observed in Fig. 6.8. The algorithm activates the SyI inertia control as the initial RoCoF is higher than the threshold RoCoF value. The optimisation algorithm provides the required value of SyI for the size of the contingency event. The added SyI increases the value of total inertia in the network, and therefore, modifies the frequency response from the black line with higher RoCoF to the red line with reduced RoCoF. In this phenomenon, the added SyI saves the frequency response from instabilities.

On the other hand, to observe the effect of the increased size of contingency event on the amount of SyI to be added, case three is given as presented in Fig. 6.9. The loads at buses 20, 28 and 39 are simultaneously increased by 50%, 30% and 25%, respectively. The minimum SG inertia in the network is the same as cases one and two. The resulted contingency event is higher than that in case two. Consequently, the resulted initial RoCoF is much higher than that in case two, and therefore, crosses the threshold value as well. Likewise, the algorithm checks if the initial RoCoF value does not cross the critical value.

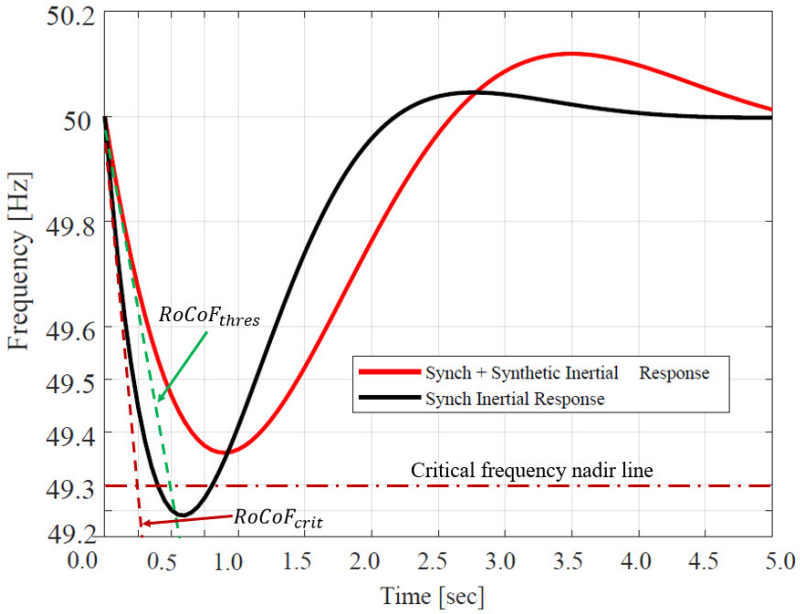

Fig. 6.8 Frequency response at a contingency event that results in RoCoF beyond the threshold value

The resulting RoCoF does not cross the critical value set for this case. For that reason, the algorithm again activates the SyI inertia control. In this case, the optimisation algorithm provides the optimal SyI value with a higher value than that in case two. According to (3), a bigger size of contingency events results in a higher RoCoF and frequency deviation. According to Fig. 6.5, more significant events require a higher inertia value to contain them.

Therefore, for the same minimum SG inertia in case three as in cases one and two, a higher value of SyI in case three than in cases one and two must be applied to contain the higher contingency event. As expected, the higher added value of SyI in case three modifies the frequency response from the black line with higher RoCoF to the red line with a reduced RoCoF as noted in Fig 6.9. In this phenomenon again, the added SyI saves the frequency response from instabilities.

The last case involves the disconnection of generator G1 at bus 39. In this case, the registered initial RoCoF is higher than both the threshold and the critical RoCoF values set. The network's generator disconnection is a colossal contingency event given the same minimum amount of SG inertia as in the previous cases. This event results in the network experiencing huge frequency oscillations, as presented in Fig. 6.10. For this condition, the algorithm is designed not to activate the SyI control, but to send information to generator protection relays to further protect the network for safety purposes, instead.

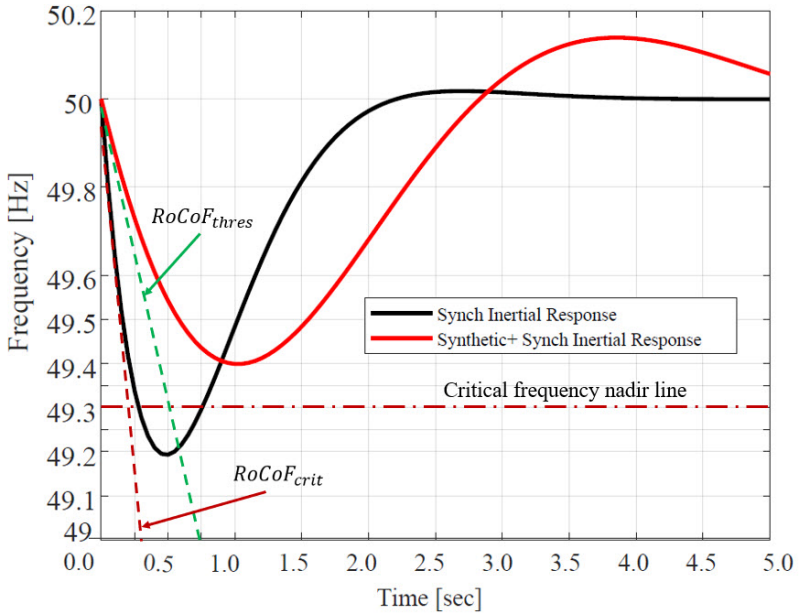

Fig. 6.9 Frequency response at a more significant contingency event that results in RoCoF beyond the threshold value

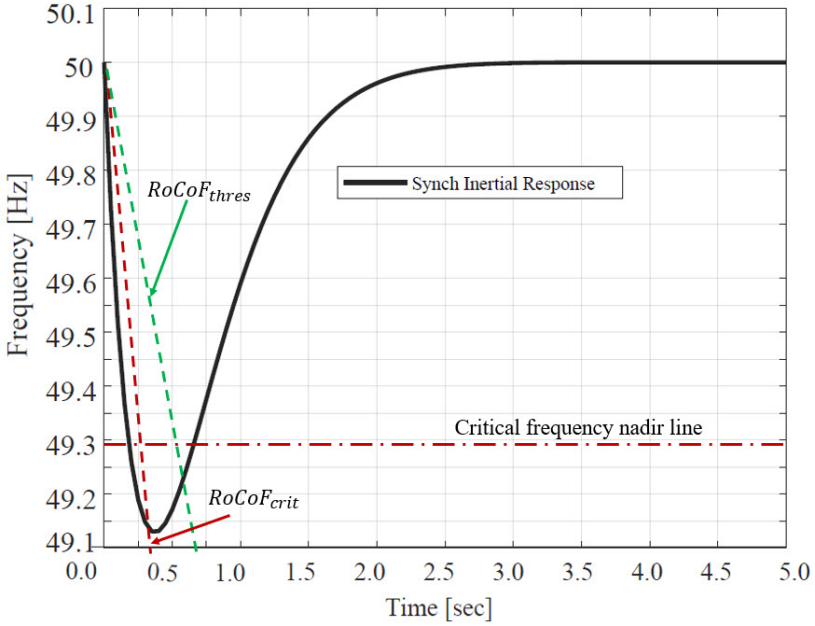

Fig. 6.2 Frequency response at an extreme significant contingency event that results in RoCoF beyond the threshold and critical values

As seen from cases one to three, the amount of SyI added to the network to increase the amount of total inertia in the network to save the frequency response from instabilities depends on the value of SG inertia and the size of contingency event in the network. As contingency events increase at the same SG inertia in the network, the amount of SyI required increases proportionally. Therefore, Fig. 6.11 presents the approximate values of SyI required at different

SG inertia values and different contingency events. The higher the value of SG inertia in the network, the lower the value of needed SyI to be added during events is. For instance, the blue line representing the network with a SG inertia value of 6 s, the SyI is not activated for a contingency event lower than 200 MW.

On the other hand, the black line representing the network with a SG inertia value of 3 s needs activation of SyI for any contingency event. Furthermore, the significant difference can be noted when comparing the values of SyI added in the network for blue and black lines. For example, when the contingency event is 300 MW, the required optimal SyIs are approximately 0.7 s and 2.5 s for SG inertia values of 6s and 3 s, respectively, as noted in Fig. 6.11. Moreover, the network with high SG inertia can withstand higher contingency events before the algorithm cannot provide SyI due to higher initial RoCoF beyond critical values, as explained in the preceding sections. This phenomenon can be observed from Fig. 6.11 as the blue and red lines with 6s and 5 s SG inertia, respectively, can withstand events with addition SyI until the event size is 700 MW. Beyond this size, the resulted initial RoCoFs are beyond the critical value set. Therefore, no further activation of SyI in the network. Other lines with SG inertia values of 4s and 3s can withstand events of maximum sizes 600 MW and 500 MW, respectively. The resulting initial RoCoFs are beyond the critical value set for circumstances beyond those values. Therefore, no further activation of SyI is processed in the network, as noted in Fig. 6.11.

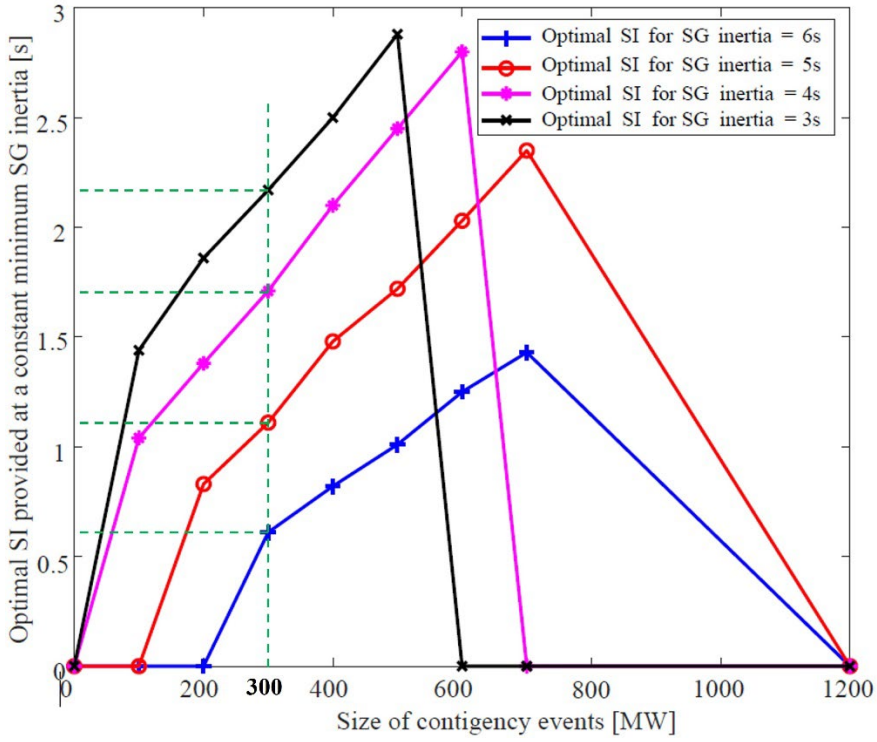

Fig. 6.3 Approximate values of SyI required at different SG inertia values and different contingency events

6.5 Conclusion

This paper proposes an algorithm that ensures RESs participate in inertial response by giving optimal SyI values depending on the SG inertia values and the size of contingency events in the network. Self-tuning the parameter of the SyI controller using the BEO approach improves frequency responses while optimizing the required SyI following contingency events in a network. The optimisation problem is based on the operational cost of the network. The operation cost is minimized by minimizing the cost function of inertia values in the network. The optimisation study is done using the modified New England 39-bus network. The optimisation algorithm proposed has the capability of self-tuning the proportional and derivative gains $\mathcal{K}_{pVJ}$ and $\mathcal{K}_{dVJ}$ parameters of the SyI controller. The results show that frequency support resources can provide different values of SyI at various contingency events to minimize the operation cost of the network. The provided SyI supports the available SG inertia in the network to reduce the RoCoF values and contain them within acceptable limits. Controlling the RoCoFs within acceptable values saves the network from frequency instabilities and increases stability resilience under various contingency events in the network. Therefore, the general merits of the proposed method are to provide flexible values of SyI under different contingency events, improve RoCoFs and reduce frequency nadir and finally, to provide the best values of SyI at various events to minimize the network's operation cost.

Chapter 7 Conclusion and Future Work

7.1 Conclusion

This Chapter summarizes the findings of this PhD thesis. It further draws conclusions based on the presented methods and results. It finally provides suggestions for future work.

This thesis investigates the modelling and dynamics of modern power networks with high shares of RES. It gives the potential of monitoring the dynamics as related to low conventional SG inertia and new topologies providing SyI. It also analyses the flexible optimisation of SyI regarding the dynamic behaviour of converter-dominated modern networks. The proposed method's primary purpose is to achieve modern networks' reliable and resilient operation. The results and validations on various data suggest that the proposed methods are helpful in the operation and cost reduction of current networks.

Chapter 2 reveals possible research areas to address the challenges in modern and future networks. Research areas with challenges suggested in future trends of this Chapter need to be researched more to get valuable solutions for implementation. In short, the discussion in this Chapter discloses that to fully enjoy the benefits and opportunities of the new power generation technologies, the conventional grid must transition to a dynamic interactive real-time infrastructure that can accommodate stochastic generation units more flexibly and efficiently. Synthetic inertia is a centre of discussion as traditional synchronous generators are getting replaced in the grid transformation. Therefore, proper estimation, monitoring, coordination, optimisation, and management of synthetic inertia related to conventional mechanical inertia may guarantee the achievement of a flexible modern renewable grid. These altogether can ensure the attainment of a complete renewable grid, which is environmentally friendly.

From a novel method of offline inertia estimation in networks with high penetration of RES developed in Chapter 3, the proposed approach introduces a decomposition technique to reduce unnecessary high orders of the model estimate and, therefore, reducing computation burden. It also reveals the ability to use the average operating dynamic data of the system for inertia estimation. Finally, the coordinated frequency gradient mapping on RoCoF is employed to make extracting inertia from the estimated network model easy. The proposed technique gives consistent estimates of the observed ranges of inertia with errors in the ranges of 4.14% to 8.79% for simulation network and 11.47% for actual network. Therefore, the technique presented in this Chapter proposes the use of operational data of the network to offline estimate the time-varying inertia of the network.

On the other hand, the proposed online inertia estimation method given in Chapter 4 gives consistent inertia estimates, which are in the range of 0.74% to 3.57% for individual generators in the network. Besides, the error range of 2.39% to 3.80% is observed for the equivalent inertia

of the aggregated network. Finally, an error of 8.54% is obtained for the actual data from the real network. Besides, the proposed method proves to be effective in online estimating the power system inertia. On top of that, since the method does not need to store previous data after each sample step, the computation burden is significantly reduced in the proposed technique. More importantly, the technique incorporates the use of available electromechanical oscillation modes in the system, which can be linked to parameters of the power system for online estimation of the network inertia.

Chapter 5 presents a compelling and improved ARIMA framework termed i-ARIMA that forecasts inertia values in a network with high shares of RES for both short-and long-range. The approach reveals the power of periodic solid and seasonality patterns of the time series data to introduce a moving observant predictor at different lags that gives the proposed method a superior capability for long-range inertia forecast in power systems. The best accuracy of the i-ARIMA is achieved by fine-tuning the optimal combination of the moving observant predictor, periodicity and seasonality factor and smoothing factor at different lags. Based on previous historical inertia data set observations in the New Zealand network, the i-ARIMA is evaluated and tested. The results show that the i-ARIMA is fast, robust, accurate and superior to other forecasting methods.

Finally, the inertia optimisation method proposed in Chapter 6 presents an algorithm that ensures RESs participate in inertial response by giving optimal SyI values depending on the SG inertia values and the size of contingency events in the network. Self-tuning the parameter of the SyI controller using the proposed optimisation approach improves frequency responses while optimizing the required SyI following contingency events in a network. The results show that frequency support resources can provide different values of SyI at various contingency events to minimize the operation cost of the network. The provided SyI supports the available SG inertia in the network to reduce the RoCoF values and contain them within acceptable limits to maintain stability resilience under various contingency events in the network.

The main concluding remarks and outcomes of this thesis are condensed as follows:

- The modern and future networks with high shares of RES necessitate comprehensive modelling to extract the fast dynamics related to low SG inertia.
- The low SG inertia networks are susceptible to frequency instabilities.
- Suitable reduced-order models of complex modern networks with converter-interfaced generation units are required to reduce the computation burdens during contingencies.
- Offline inertia estimation techniques can post-events analyse the dynamics of networks with high shares of RES.
- Real-time monitoring of modern networks' parameters can be easily achieved using online estimation methods.

- Time ahead estimation of inertia to predict the dynamics of the modern network is crucial for planning, operation and protection of the network.
- Optimizing the tradeable modern synthetic inertia in the frequency control during contingency events is inevitable to minimize the networks' operational costs.

7.2 Future work

Despite valuable findings from this study, there are opportunities for future work and prospects to broaden the subjects addressed in this study. Some of the issues that need further investigation are as follows:

- There are various proposed offline and online inertia estimation techniques in the literature. However, the techniques do not show how fast the estimated inertia can be communicated to PSO. Therefore, researchers should consider further investigations on the speed of communicating the inertia estimated to PSO. This can help reduce decision-making duration for stability control purposes in modern networks.
- There is a further need to develop coordinating algorithms between the traditional SG inertia and the synthetic inertia in the modern network. The different time scales in which these quantities give the inertial response is crucial for coordination.
- Likewise, due to the high penetration of weather-dependent generation units, the study of weather forecast effects in the equivalent inertia prediction of the network is essential to be researched. Further research can improve forecasting accuracy a long time ahead to reduce uncertainties in planning for secure network operation.

References

[1] W. Xiao, *Photovoltaic Power System: Modeling, Design, and Control*. John Wiley & Sons, 2017.

[2] M. Obi and R. Bass, "Trends and challenges of grid-connected photovoltaic systems – A review," *Renewable and Sustainable Energy Reviews,* vol. 58, pp. 1082-1094, 2016, doi: 10.1016/j.rser.2015.12.289.

[3] F. Blaabjerg, R. Teodorescu, M. Liserre, and A. V. Timbus, "Overview of control and grid synchronization for distributed power generation systems," *IEEE Transactions on industrial electronics,* vol. 53, no. 5, pp. 1398-1409, 2006.

[4] B. K. Poolla, D. Groß, and F. Dörfler, "Placement and implementation of grid-forming and grid-following virtual inertia and fast frequency response," *IEEE Transactions on Power Systems,* vol. 34, no. 4, pp. 3035-3046, 2019.

[5] P. Mancarella and F. Billimoria, "The Fragile Grid: The Physics and Economics of Security Services in Low-Carbon Power Systems," *IEEE Power and Energy Magazine,* vol. 19, no. 2, pp. 79-88, 2021.

[6] P. Makolo, R. Zamora, and T. Lie, "Online inertia estimation for power systems with high penetration of RES using recursive parameters estimation," *IET Renewable Power Generation,* 2021.

[7] P. Makolo, R. Zamora, and T.-T. Lie, "Heuristic Inertia Estimation Technique for Power Networks with High Penetration of RES," in *2020 2nd International Conference on Smart Power & Internet Energy Systems (SPIES)*, 2020: IEEE, pp. 356-361.

[8] P. Makolo, R. Zamora, and T.-T. Lie, "The role of inertia for grid flexibility under high penetration of variable renewables-A review of challenges and solutions," *Renewable and Sustainable Energy Reviews,* vol. 147, p. 111223, 2021.

[9] T. Ujjwol, S. Dipesh, M. Manisha, P. B. Bishnu, M. H. Timothy, and T. Reinaldo, "Virtual Inertia: Current Trends and Future Directions," *Applied Sciences, Vol 7, Iss 7, p 654 (2017),* article no. 7, p. 654, 2017, doi: 10.3390/app7070654.

[10] E. Ørum *et al.*, "Future system inertia," *ENTSOE, Brussels, Tech. Rep,* 2015.

[11] K. Tuttelberg, J. Kilter, D. H. Wilson, and K. Uhlen, "Estimation of Power System Inertia from Ambient Wide Area Measurements," *IEEE Transactions on Power Systems,* vol. 33, no. 6, pp. 7249 - 7257, 2018, doi: 10.1109/TPWRS.2018.2843381.

[12] D. Zografos, M. Ghandhari, and R. Eriksson, "Power system inertia estimation: Utilization of frequency and voltage response after a disturbance," *Electric Power Systems Research,* vol. 161, pp. 52-60, 2018.

[13] L. Lugnani, D. Dotta, C. Lackner, and J. Chow, "ARMAX-based method for inertial constant estimation of generation units using synchrophasors," *Electric Power Systems Research,* vol. 180, p. 106097, 2020.

[14] P. M. Ashton, C. S. Saunders, G. A. Taylor, A. M. Carter, and M. E. Bradley, "Inertia estimation of the GB power system using synchrophasor measurements," *IEEE Transactions on Power Systems,* vol. 30, no. 2, pp. 701-709, 2015.

[15] P. Wall and V. Terzija, "Simultaneous estimation of the time of disturbance and inertia in power systems," *IEEE Trans. Power Del.,* vol. 29, no. 4, pp. 2018-2031, 2014.

[16] P. Makolo, I. Oladeji, R. Zamora, and T.-T. Lie, "Data-driven inertia estimation based on frequency gradient for power systems with high penetration of renewable energy sources," *Electric Power Systems Research,* vol. 195, p. 107171, 2021.

[17] R. K. Panda, A. Mohapatra, S. Srivastava, and M. Kezunovic, "Energy Function based Approach for Online Inertia Estimation Utilizing Synchrophasor Measurements," in *2020 IEEE Texas Power and Energy Conference (TPEC)*, 2020: IEEE, pp. 1-6.

[18] M. Liu, J. Chen, and F. Milano, "On-line Inertia Estimation for Synchronous and Non-Synchronous Devices," *IEEE Transactions on Power Systems,* 2020.

[19] P. Du and J. Matevosyan, "Forecast system inertia condition and its impact to integrate more renewables," *IEEE Transactions on Smart Grid,* vol. 9, no. 2, pp. 1531-1533, 2017.

[20] E. Heylen, G. Strbac, and F. Teng, "Challenges and opportunities of inertia estimation and forecasting in low-inertia power systems," *arXiv preprint arXiv:2008.12692,* 2020.

[21] L. Badesa, F. Teng, and G. Strbac, "Pricing inertia and frequency response with diverse dynamics in a mixed-integer second-order cone programming formulation," *Applied Energy,* vol. 260, p. 114334, 2020.

[22] M. Paturet, U. Markovic, S. Delikaraoglou, E. Vrettos, P. Aristidou, and G. Hug, "Economic valuation and pricing of inertia in inverter-dominated power systems," *arXiv preprint arXiv:2005.11029,* 2020.

[23] B. K. Poolla, S. Bolognani, N. Li, and F. Dörfler, "A market mechanism for virtual inertia," *IEEE Transactions on Smart Grid,* vol. 11, no. 4, pp. 3570-3579, 2020.

[24] H. Gu, R. Yan, and T. K. Saha, "Minimum synchronous inertia requirement of renewable power systems," *IEEE Transactions on Power Systems,* vol. 33, no. 2, pp. 1533-1543, 2017.

[25] Z. Liang, R. Mieth, and Y. Dvorkin, "Inertia Pricing in Stochastic Electricity Markets," *arXiv preprint arXiv:2107.04101,* 2021.

[26] A. Venkatraman, U. Markovic, D. Shchetinin, E. Vrettos, P. Aristidou, and G. Hug, "Improving Dynamic Performance of Low-Inertia Systems through Eigensensitivity Optimization," *IEEE Transactions on Power Systems,* 2021.

[27] Z. Chu, U. Markovic, G. Hug, and F. Teng, "Towards optimal system scheduling with synthetic inertia provision from wind turbines," *IEEE Transactions on Power Systems,* vol. 35, no. 5, pp. 4056-4066, 2020.

[28] F. Teng and G. Strbac, "Assessment of the role and value of frequency response support from wind plants," *IEEE Transactions on Sustainable Energy,* vol. 7, no. 2, pp. 586-595, 2016.

[29] J. J. Justo, F. Mwasilu, J. Lee, and J.-W. Jung, "AC-microgrids versus DC-microgrids with distributed energy resources: A review," *Renewable and Sustainable Energy Reviews,* vol. 24, pp. 387-405, 2013.

[30] X. Liang, "Emerging Power Quality Challenges Due to Integration of Renewable Energy Sources," *IEEE Transactions on Industry Applications,* vol. 53, no. 2, p. 855, 03//Mar/Apr2017 2017..

[31] R. Zamora and A. K. Srivastava, "Controls for microgrids with storage: Review, challenges, and research needs," *Renewable and Sustainable Energy Reviews,* vol. 14, no. 7, pp. 2009-2018, 2010.

[32] P. Makolo, J. J. Justo, F. Mwasilu, and R. Zamora, "Fault Ride Through Technique for DFIG-based Wind Turbines Under Grid Three-phase Faults," in *2018 Australasian Universities Power Engineering Conference (AUPEC)*, 2018: IEEE, pp. 1-5.

[33] IEA, "Global Energy Review 2020," in "The impacts of the Covid-19 crisis on global energy demand and CO2 emissions," International Energy Agency, 2020.

[34] R. Secretariat, "Renewables 2019 Global Status Report," RES21 Secretariat, Paris, ISBN 978-3-9818911-7-1, 2019 2019.

[35] B. K. Poolla, S. Bolognani, and F. Dörfler, "Optimal placement of virtual inertia in power grids," (in English), *Institute of Electrical and Electronics Engineers. Transactions on Automatic Control,* vol. 62, no. 12, p. 6209, 01/01 2017.

[36] R. Zamora and A. K. Srivastava, "Energy management and control algorithms for integration of energy storage within microgrid," 2014 / 01 / 01 / 2014: Institute of Electrical and Electronics Engineers Inc., pp. 1805-1810, doi: 10.1109/ISIE.2014.6864889.

[37] S. Gabriel, B. M. Mwinyiwiwa, and M. J. Manyahi, "On the Viability Analysis of HVDC Light for Electrification of Mafia Island by National Grid," *International Refereed Journal of Engineerign and Science (IRJES),* vol. 4, no. 1, pp. 60-69, 2015.

[38] G. Yao, Z. Lu, Y. Wang, M. Benbouzid, and L. Moreau, "A Virtual Synchronous Generator Based Hierarchical Control Scheme of Distributed Generation Systems," *Energies,* vol. 10, no. 12, p. 2049, 2017.

[39] Y. Hirase, K. Abe, K. Sugimoto, K. Sakimoto, H. Bevrani, and T. Ise, "A novel control approach for virtual synchronous generators to suppress frequency and voltage fluctuations in microgrids," *Applied Energy,* vol. 210, pp. 699-710, 2018.

[40] A. Fathi, Q. Shafiee, and H. Bevrani, "Robust Frequency Control of Microgrids Using an Extended Virtual Synchronous Generator," *IEEE Transactions on Power Systems,* vol.

33, no. 6, pp. 6289-6297, 2018, doi: 10.1109/TPWRS.2018.2850880.
[41] H. Bevrani, T. Ise, and Y. Miura, "Virtual synchronous generators: A survey and new perspectives," *International Journal of Electrical Power & Energy Systems,* vol. 54, pp. 244-254, 2014.
[42] F. Milano, F. Dörfler, G. Hug, D. J. Hill, and G. Verbič, "Foundations and challenges of low-inertia systems," in *2018 Power Systems Computation Conference (PSCC)*, 2018: IEEE, pp. 1-25.
[43] A. Ortega and F. Milano, "Stochastic Transient Stability Analysis of Transmission Systems With Inclusion of Energy Storage Devices," *IEEE Transactions on Power Systems,* vol. 33, no. 1, pp. 1077-1079, 2018, doi: 10.1109/tpwrs.2017.2742400.
[44] P. Peltoniemi, "Compensating the rotating mass kinetic energy in grids including high shares of renewables," 2017 / 11 / 06 / 2017, vol. 2017-January: Institute of Electrical and Electronics Engineers Inc., doi: 10.23919/EPE17ECCEEurope.2017.8099346.
[45] A. U. Krismanto, N. Mithulananthan, and I. Kamwa, "Oscillatory stability assessment of microgrid in autonomous operation with uncertainties," *IET Renewable Power Generation,* vol. 12, no. 4, pp. 494-504, 2017.
[46] A. U. Krismanto, N. Mithulananthan, and O. Krause, "Stability of Renewable Energy based Microgrid in Autonomous Operation," *Sustainable Energy, Grids and Networks,* vol. 13, pp. 134-147, 2018.
[47] J. Hu, R. Harmsen, W. Crijns-Graus, E. Worrell, and M. van den Broek, "Identifying barriers to large-scale integration of variable renewable electricity into the electricity market: A literature review of market design," *Renewable and Sustainable Energy Reviews,* Review Article vol. 81, no. Part 2, pp. 2181-2195, 1/1/January 2018 2018, doi: 10.1016/j.rser.2017.06.028.
[48] S. R. Kumar, F. Gafaro, A. Daka, and A. Raturi, "Modelling and analysis of grid integration for high shares of solar PV in small isolated systems – A case of Kiribati," *Renewable Energy,* Article vol. 108, pp. 589-597, 8/1/August 2017 2017, doi: 10.1016/j.renene.2017.02.084.
[49] M. M. Haque and P. Wolfs, "A review of high PV penetrations in LV distribution networks: Present status, impacts and mitigation measures," *Renewable and Sustainable Energy Reviews,* Review Article vol. 62, pp. 1195-1208, 9/1/September 2016 2016, doi: 10.1016/j.rser.2016.04.025.
[50] B. Kroposki *et al.*, "Achieving a 100% Renewable Grid: Operating Electric Power Systems with Extremely High Levels of Variable Renewable Energy," *IEEE Power and Energy Magazine,* vol. 15, no. 2, pp. 61-73, 2017, doi: 10.1109/mpe.2016.2637122.
[51] I. PVPS, "Photovoltaic Power Systems: Annual Report 2019," International Energy Agency, Paris, France, Report 2020.
[52] F. Z. Joyce Lee, "Global Wind Report 2019," Brussels, Belgium, 2020.
[53] J. Matevosyan *et al.*, "Proposed future Ancillary Services in Electric Reliability Council of Texas," 2015 / 08 / 31 / 2015: Institute of Electrical and Electronics Engineers Inc., doi: 10.1109/PTC.2015.7232743.
[54] B. Meersman *et al.*, "Droop Control as an Alternative Inertial Response Strategy for the Synthetic Inertia on Wind Turbines," *IEEE TRANSACTIONS ON POWER SYSTEMS,* vol. 31, no. 2, pp. 1129-1138, 2016.
[55] H. Thiesen, C. Jauch, and A. Gloe, "Design of a system substituting today's inherent inertia in the European continental synchronous area," *Energies,* vol. 9, no. 8, p. 582, 2016.
[56] P. Kundur, N. J. Balu, and M. G. Lauby, *Power system stability and control*. McGraw-hill New York, 1994.
[57] M. F. M. Arani and E. F. El-Saadany, "Implementing virtual inertia in DFIG-based wind power generation," *IEEE Transactions on Power Systems,* vol. 28, no. 2, pp. 1373-1384, 2013.
[58] N. Kakimoto, S. Takayama, H. Satoh, and K. Nakamura, "Power modulation of photovoltaic generator for frequency control of power system," *IEEE Transactions on Energy Conversion,* vol. 24, no. 4, p. 943, 2009.
[59] J. Fang, H. Li, Y. Tang, and F. Blaabjerg, "Distributed power system virtual inertia

implemented by grid-connected power converters," *IEEE Transactions on Power Electronics,* vol. 33, no. 10, pp. 8488-8499, 2018.

[60] R. Eriksson, N. Modig, and K. Elkington, "Synthetic inertia versus fast frequency response: a definition," *IET Renewable Power Generation,* vol. 12, no. 5, pp. 507-514, 2017.

[61] H.-P. Beck and R. Hesse, "Virtual synchronous machine," in *Electrical Power Quality and Utilisation, 2007. EPQU 2007. 9th International Conference on*, 2007: IEEE, pp. 1-6.

[62] Y. Chen, R. Hesse, D. Turschner, and H.-P. Beck, "Dynamic properties of the virtual synchronous machine (VISMA)," *Proc. ICREPQ,* vol. 11, 2011.

[63] R. Hesse, D. Turschner, and H.-P. Beck, "Micro grid stabilization using the Virtual Synchronous Machine (VISMA)," in *Proceedings of the International Conference on Renewable Energies and Power Quality (ICREPQ'09), Valencia, Spain*, 2009, pp. 15-17.

[64] Q.-C. Zhong, "Virtual Synchronous Machines: A unified interface for grid integration," *IEEE Power Electronics Magazine,* vol. 3, no. 4, pp. 18-27, 2016..

[65] M. A. Awal and I. Husain, "Unified Virtual Oscillator Control for Grid-Forming and Grid-Following Converters," *IEEE Journal of Emerging and Selected Topics in Power Electronics,* 2020, doi: 10.1109.

[66] J. D. Glover, M. S. Sarma, and T. Overbye, *Power System Analysis & Design, SI Version*. Cengage Learning, 2012.

[67] K. S. Ratnam, K. Palanisamy, and G. Yang, "Future low-inertia power systems: Requirements, issues, and solutions-A review," *Renewable and Sustainable Energy Reviews,* vol. 124, p. 109773, 2020.

[68] C. L. DeMarco, C. A. Baone, Y. Han, and B. Lesieutre, "Primary and secondary control for high penetration renewables," *The Future Grid to Enable Sustainable Energy Systems,* 2012.

[69] M. Dreidy, H. Mokhlis, and S. Mekhilef, "Inertia response and frequency control techniques for renewable energy sources: A review," *Renewable and Sustainable Energy Reviews,* vol. 69, pp. 144-155, 2017.

[70] M. B. Rujiroj Leelaruji, "Synthetic inertia to improve frequency and how often it is needed," Energiforsk, STRI AB, Stockholm - Sweden, 2015:224, 25 February 2019 2015.

[71] A. Fernández-Guillamón, E. Gómez-Lázaro, E. Muljadi, and Á. Molina-García, "Power systems with high renewable energy sources: A review of inertia and frequency control strategies over time," *Renewable and Sustainable Energy Reviews,* vol. 115, p. 109369, 2019.

[72] M. Rezkalla, M. Pertl, and M. Marinelli, "Electric power system inertia: requirements, challenges and solutions," *Electrical Engineering,* vol. 100, no. 4, pp. 2677-2693, 2018.

[73] G. Delille, G. Malarange, and B. François, "Dynamic frequency control support by energy storage to reduce the impact of wind and solar generation on isolated power system's inertia," (in English), *IEEE Transactions on Sustainable Energy,* Article vol. 3, no. 4, pp. 931-939, 01 / 01 / 2012, doi: 10.1109/TSTE.2012.2205025.

[74] D. Shrestha, U. Tamrakar, Z. Ni, and R. Tonkoski, "Experimental verification of virtual inertia in diesel generator based microgrids," in *Industrial Technology (ICIT), 2017 IEEE International Conference on*, 2017: IEEE, pp. 95-100.

[75] T. S. Borsche, T. Liu, and D. J. Hill, "Effects of rotational inertia on power system damping and frequency transients," in *Decision and Control (CDC), 2015 IEEE 54th Annual Conference on*, 2015: IEEE, pp. 5940-5946.

[76] A. Ulbig, T. S. Borsche, and G. Andersson, "Impact of low rotational inertia on power system stability and operation," *IFAC Proceedings Volumes,* vol. 47, no. 3, pp. 7290-7297, 2014.

[77] H. Jiayi, J. Chuanwen, and X. Rong, "A review on distributed energy resources and MicroGrid," *Renewable and Sustainable Energy Reviews,* vol. 12, no. 9, pp. 2472-2483, 2008.

[78] A. S. Ahmadyar, S. Riaz, G. Verbic, A. Chapman, and D. J. Hill, "A Framework for Frequency Stability Assessment of Future Power Systems: An Australian Case Study,"

arXiv preprint arXiv:1708.00739, 2017.

[79] W. Uijlings, D. K. L. C. Street, and S. London, "An independent analysis on the ability of Generators to ride through Rate of Change of Frequency values up to 2Hz/s," Technical report, DNV KEMA2013, Available: www. eirgridgroup. com/sitefiles/library/EirGrid/DNV-KEMA_Report_RoCoF_20130208final_. pdf [Accessed: 20-Nov.-2016], 2013.

[80] E. Nycander and L. Söder, "Review of european grid codes for wind farms and their implications for wind power curtailments," in *17th International Wind Integration Workshop Stockholm, Sweden| 17–19 October 2018*, 2018.

[81] B. Nouri, A. Arasteh, Ö. Göksu, J. N. Sakamuri, and P. E. Sørensen, "Comparison of European Network Codes for AC and HVDC-connected Renewable Energy Sources," in *18th Wind Integration Workshop*, 2019, pp. 16-18.

[82] A. E. M. Operator, "Black system south australia 28 september 2016," *Report of the Australian Energy Market Operator Limited (AEMO),* 2017.

[83] N.-M. Vong, S. Pillay, and V. Lo, "Effect of solar PV on frequency management in New Zealand," in *2017 IEEE Innovative Smart Grid Technologies-Asia (ISGT-Asia)*, 2017: IEEE, pp. 1-6.

[84] T. Inoue, H. Taniguchi, Y. Ikeguchi, and K. Yoshida, "Estimation of power system inertia constant and capacity of spinning-reserve support generators using measured frequency transients," *IEEE Transactions on Power Systems,* vol. 12, no. 1, pp. 136-143, 1997.

[85] D. Connolly and B. V. Mathiesen, "A technical and economic analysis of one potential pathway to a 100% renewable energy system," *International Journal of Sustainable Energy Planning and Management,* vol. 1, pp. 7-28, 2014.

[86] D. Connolly, H. Lund, B. V. Mathiesen, and M. Leahy, "The first step towards a 100% renewable energy-system for Ireland," *Applied Energy,* vol. 88, no. 2, pp. 502-507, 2011.

[87] B. Elliston, M. Diesendorf, and I. MacGill, "Simulations of scenarios with 100% renewable electricity in the Australian National Electricity Market," *Energy Policy,* vol. 45, pp. 606-613, 2012.

[88] B. V. Mathiesen, H. Lund, and K. Karlsson, "100% Renewable energy systems, climate mitigation and economic growth," *Applied energy,* vol. 88, no. 2, pp. 488-501, 2011.

[89] H. Lund and B. V. Mathiesen, "Energy system analysis of 100% renewable energy systems—The case of Denmark in years 2030 and 2050," *Energy,* vol. 34, no. 5, pp. 524-531, 2009.

[90] G. Pleßmann, M. Erdmann, M. Hlusiak, and C. Breyer, "Global energy storage demand for a 100% renewable electricity supply," *Energy Procedia,* vol. 46, pp. 22-31, 2014.

[91] T. Brown, T. Bischof-Niemz, K. Blok, C. Breyer, H. Lund, and B. V. Mathiesen, "Response to 'Burden of proof: A comprehensive review of the feasibility of 100% renewable-electricity systems'," *Renewable and Sustainable Energy Reviews,* vol. 92, pp. 834-847, 2018.

[92] B. P. Heard, B. W. Brook, T. M. Wigley, and C. J. Bradshaw, "Burden of proof: A comprehensive review of the feasibility of 100% renewable-electricity systems," *Renewable and Sustainable Energy Reviews,* vol. 76, pp. 1122-1133, 2017.

[93] P. F. Gutman, P. Makolo, and R. Zamora, "Modelling and Analysis of Load Frequency Control in Small Power Systems: a Case Study of New Zealand Network," in *2020 Australasian Universities Power Engineering Conference (AUPEC)*, Hobart, Australia, 2020: IEEE, pp. 1-6.

[94] M. o. I. a. Innovation. "Energy." Government of Iceland. (accessed 18/02/2021, 2021).

[95] T. AAnensen. "Wind power generation continues to rise." Statistics Norway. (accessed 18/02/2021, 2021).

[96] P. Capros *et al.*, "EU Reference Scenario 2016-Energy, transport and GHG emissions Trends to 2050," 2016.

[97] H. Anand and R. Ramasubbu, "A real time pricing strategy for remote micro-grid with economic emission dispatch and stochastic renewable energy sources," *Renewable Energy,* vol. 127, pp. 779-789, 2018.

[98] M. Asensio, P. M. de Quevedo, G. Muñoz-Delgado, and J. Contreras, "Joint distribution network and renewable energy expansion planning considering demand response and

energy storage—Part I: Stochastic programming model," *IEEE Transactions on Smart Grid,* vol. 9, no. 2, pp. 655-666, 2018.

[99] R. Hemmati, H. Saboori, and M. A. Jirdehi, "Stochastic planning and scheduling of energy storage systems for congestion management in electric power systems including renewable energy resources," *Energy,* vol. 133, pp. 380-387, 2017.

[100] S. Tabatabaee, S. S. Mortazavi, and T. Niknam, "Stochastic scheduling of local distribution systems considering high penetration of plug-in electric vehicles and renewable energy sources," *Energy,* vol. 121, pp. 480-490, 2017.

[101] P. Makolo, "Wind Generator Co-Simulation with Fault Case Analysis," *Master of Science Thesis), Chalmers University of Technology, Department of Energy and Environment,* 2013.

[102] K. Shi and H. Ye, "Virtual Inertia Control Strategy in Microgrid Based on Virtual Synchronous Generator Technology," *IEEE Access,* 2018.

[103] Q.-C. Zhong and G. Weiss, "Synchronverters: Inverters that mimic synchronous generators," *IEEE Transactions on Industrial Electronics,* vol. 58, no. 4, pp. 1259-1267, 2011.

[104] W. Wu *et al.*, "A virtual inertia control strategy for dc microgrids analogized with virtual synchronous machines," *IEEE Transactions on Industrial Electronics,* vol. 64, no. 7, pp. 6005-6016, 2017.

[105] S. D'Arco and J. A. Suul, "Virtual synchronous machines—Classification of implementations and analysis of equivalence to droop controllers for microgrids," in *PowerTech (POWERTECH), 2013 IEEE Grenoble*, 2013: IEEE, pp. 1-7.

[106] T. Kerdphol, F. S. Rahman, Y. Mitani, M. Watanabe, and S. Küfeoğlu, "Robust virtual inertia control of an islanded microgrid considering high penetration of renewable energy," *IEEE Access,* vol. 6, pp. 625-636, 2018.

[107] M. Van Wesenbeeck, S. De Haan, P. Varela, and K. Visscher, "Grid tied converter with virtual kinetic storage," in *PowerTech, 2009 IEEE Bucharest*, 2009: IEEE, pp. 1-7.

[108] H. A. Alsiraji and J. M. Guerrero, "A new hybrid virtual synchronous machine control structure combined with voltage source converters in islanded ac microgrids," *Electric Power Systems Research,* p. 106976, 2021.

[109] A. Ademola-Idowu and B. Zhang, "Optimal Design of Virtual Inertia and Damping Coefficients for Virtual Synchronous Machines," *arXiv preprint arXiv:1806.08488,* 2018.

[110] J. Alipoor, Y. Miura, and T. Ise, "Power system stabilization using virtual synchronous generator with alternating moment of inertia," *IEEE Journal of Emerging and Selected Topics in Power Electronics,* vol. 3, no. 2, pp. 451-458, 2015.

[111] Y. Cao *et al.*, "A virtual synchronous generator control strategy for VSC-MTDC systems," *IEEE Transactions on Energy Conversion,* vol. 33, no. 2, pp. 750-761, 2017.

[112] D. Chen, Y. Xu, and A. Q. Huang, "Integration of dc microgrids as virtual synchronous machines into the ac grid," *IEEE Transactions on Industrial Electronics,* vol. 64, no. 9, pp. 7455-7466, 2017.

[113] S. D'Arco, J. A. Suul, and O. B. Fosso, "A Virtual Synchronous Machine implementation for distributed control of power converters in SmartGrids," *Electric Power Systems Research,* vol. 122, pp. 180-197, 2015.

[114] M. H. Fini and M. E. H. Golshan, "Determining optimal virtual inertia and frequency control parameters to preserve the frequency stability in islanded microgrids with high penetration of renewables," *Electric Power Systems Research,* vol. 154, pp. 13-22, 2018.

[115] N. S. Hasan, N. Rosmin, N. M. Nordin, and M. Y. Hassan, "Virtual inertial support extraction using a super-capacitor for a wind-PMSG application," *IET Renewable Power Generation,* vol. 13, no. 10, pp. 1802-1808, 2019.

[116] Y. Hirase *et al.*, "Decentralised and interlink-less power interchange among residences in microgrids using virtual synchronous generator control," *Applied energy,* vol. 228, pp. 2437-2447, 2018.

[117] D. J. Hogan, F. Gonzalez-Espin, J. G. Hayes, G. Lightbody, L. Albiol-Tendillo, and R. Foley, "Virtual synchronous-machine control of voltage-source converters in a low-voltage microgrid," in *Power Electronics and Applications (EPE'16 ECCE Europe), 2016*

18th European Conference on, 2016: IEEE, pp. 1-10.

[118] L. A. Lopes, "Self-tuning virtual synchronous machine: A control strategy for energy storage systems to support dynamic frequency control," *IEEE Transactions on Energy Conversion,* vol. 29, no. 4, pp. 833-840, 2014.

[119] M. Mehrasa, E. Pouresmaeil, H. Soltani, F. Blaabjerg, M. R. Calado, and J. P. Catalão, "Virtual inertia and mechanical power-based control strategy to provide stable grid operation under high renewables penetration," *Applied Sciences,* vol. 9, no. 6, p. 1043, 2019.

[120] R. Ofir, U. Markovic, P. Aristidou, and G. Hug, "Droop vs. virtual inertia: Comparison from the perspective of converter operation mode," in *2018 IEEE International Energy Conference (ENERGYCON)*, 2018: IEEE, pp. 1-6.

[121] F. Wang, L. Zhang, X. Feng, and H. Guo, "An adaptive control strategy for virtual synchronous generator," *IEEE Transactions on Industry Applications,* vol. 54, no. 5, pp. 5124-5133, 2018.

[122] B. Zhang, X. Yan, D. Li, X. Zhang, J. Han, and X. Xiao, "Stable Operation and Small-Signal Analysis of Multiple Parallel DG Inverters Based on a Virtual Synchronous Generator Scheme," *Energies,* vol. 11, no. 1, p. 203, 2018.

[123] G. Magdy, A. Bakeer, M. Nour, and E. Petlenkov, "A New Virtual Synchronous Generator Design Based on the SMES System for Frequency Stability of Low-Inertia Power Grids," *Energies,* vol. 13, no. 21, p. 5641, 2020.

[124] H. A. Alsiraji and R. El-Shatshat, "Comprehensive assessment of virtual synchronous machine based voltage source converter controllers," *IET Generation, Transmission & Distribution,* vol. 11, no. 7, pp. 1762-1769, 2017.

[125] J. Zhu *et al.*, "Synthetic inertia control strategy for doubly fed induction generator wind turbine generators using lithium-ion supercapacitors," *IEEE Transactions on Energy Conversion,* vol. 33, no. 2, pp. 773-783, 2017.

[126] J. Liu, D. Yang, W. Yao, R. Fang, H. Zhao, and B. Wang, "PV-based virtual synchronous generator with variable inertia to enhance power system transient stability utilizing the energy storage system," *Protection and Control of Modern Power Systems,* vol. 2, no. 1, pp. 1-8, 2017.

[127] K. Dhingra and M. Singh, "Frequency support in a micro-grid using virtual synchronous generator based charging station," *IET Renewable Power Generation,* vol. 12, no. 9, pp. 1034-1044, 2018.

[128] Y. Hirase, K. Abe, K. Sugimoto, and Y. Shindo, "A grid connected inverter with virtual synchronous generator model of algebraic type," *IJTPE,* vol. 132, no. 4, pp. 371-380, 2012.

[129] R. Aouini, B. Marinescu, K. B. Kilani, and M. Elleuch, "Synchronverter-based emulation and control of HVDC transmission," *IEEE Transactions on Power Systems,* vol. 31, no. 1, pp. 278-286, 2016.

[130] F. Gao and M. R. Iravani, "A control strategy for a distributed generation unit in grid-connected and autonomous modes of operation," *IEEE Transactions on power delivery,* vol. 23, no. 2, pp. 850-859, 2008.

[131] Y. Chen, R. Hesse, D. Turschner, and H.-P. Beck, "Improving the grid power quality using virtual synchronous machines," in *2011 International Conference on Power Engineering, Energy and Electrical Drives*, 2011: IEEE, pp. 1-6.

[132] L. Xiong *et al.*, "Static synchronous generator model: a new perspective to investigate dynamic characteristics and stability issues of grid-tied PWM inverter," *IEEE Transactions on Power Electronics,* vol. 31, no. 9, pp. 6264-6280, 2015.

[133] Y. Xiang-Zhen, S. Jian-hui, D. Ming, L. Jin-wei, and D. Yan, "Control strategy for virtual synchronous generator in microgrid," in *2011 4th International Conference on Electric Utility Deregulation and Restructuring and Power Technologies (DRPT)*, 2011: IEEE, pp. 1633-1637.

[134] Y. Hirase, O. Noro, E. Yoshimura, H. Nakagawa, K. Sakimoto, and Y. Shindo, "Virtual synchronous generator control with double decoupled synchronous reference frame for single-phase inverter," *IEEJ Journal of Industry Applications,* vol. 4, no. 3, pp. 143-151, 2015.

[135] Q.-C. Zhong, P.-L. Nguyen, Z. Ma, and W. Sheng, "Self-synchronized synchronverters: Inverters without a dedicated synchronization unit," *IEEE Transactions on Power Electronics,* vol. 29, no. 2, pp. 617-630, 2014.

[136] N. Soni, S. Doolla, and M. C. Chandorkar, "Improvement of transient response in microgrids using virtual inertia," *IEEE transactions on power delivery,* vol. 28, no. 3, pp. 1830-1838, 2013.

[137] A. D. Paquette, M. J. Reno, R. G. Harley, and D. M. Divan, "Sharing transient loads: Causes of unequal transient load sharing in islanded microgrid operation," *IEEE Industry Applications Magazine,* vol. 20, no. 2, pp. 23-34, 2013.

[138] J. Liu, Y. Miura, and T. Ise, "Comparison of dynamic characteristics between virtual synchronous generator and droop control in inverter-based distributed generators," *IEEE Trans. Power Electron,* vol. 31, no. 5, pp. 3600-3611, 2016.

[139] R. Zavadil, N. Miller, G. V. Knowe, J. Zack, R. Piwko, and G. Jordan, "Technical Requirements for Wind Generation Interconnection and Integration," GE Energy Applications and Systems Engineering EnerNex Corporation AWS Truewind England, 2009.

[140] A. Rasool, X. Yan, H. Rasool, H. Guo, and M. Asif, "VSG Stability and Coordination Enhancement under Emergency Condition," *electronics,* vol. 7, no. 9, p. 202, 2018.

[141] V. Natarajan and G. Weiss, "Synchronverters with better stability due to virtual inductors, virtual capacitors, and anti-windup," *IEEE Transactions on Industrial Electronics,* vol. 64, no. 7, pp. 5994-6004, 2017.

[142] P. Rodriguez, I. Candela, and A. Luna, "Control of PV generation systems using the synchronous power controller," in *Energy Conversion Congress and Exposition (ECCE), 2013 IEEE*, 2013: IEEE, pp. 993-998.

[143] Y. Du, J. M. Guerrero, L. Chang, J. Su, and M. Mao, "Modeling, analysis, and design of a frequency-droop-based virtual synchronous generator for microgrid applications," in *ECCE Asia Downunder (ECCE Asia), 2013 IEEE*, 2013: IEEE, pp. 643-649.

[144] J. C. Vasquez, J. M. Guerrero, A. Luna, P. Rodríguez, and R. Teodorescu, "Adaptive droop control applied to voltage-source inverters operating in grid-connected and islanded modes," *IEEE Transactions on Industrial Electronics,* vol. 56, no. 10, pp. 4088-4096, 2009.

[145] B. B. Johnson, S. V. Dhople, A. O. Hamadeh, and P. T. Krein, "Synchronization of parallel single-phase inverters with virtual oscillator control," *IEEE Transactions on Power Electronics,* vol. 29, no. 11, pp. 6124-6138, 2013.

[146] M. Ashabani, F. D. Freijedo, S. Golestan, and J. M. Guerrero, "Inducverters: PLL-less converters with auto-synchronization and emulated inertia capability," *IEEE Transactions on Smart Grid,* vol. 7, no. 3, pp. 1660-1674, 2015.

[147] M. Ashabani and Y. A. R. I. Mohamed, "Novel comprehensive control framework for incorporating VSCs to smart power grids using bidirectional synchronous-VSC," (in English), *IEEE Transactions on Power Systems,* Article vol. 29, no. 2, pp. 943-957, 03 / 01 / 2014, doi: 10.1109/TPWRS.2013.2287291.

[148] D. Li, Q. Zhu, S. Lin, and X. Bian, "A self-adaptive inertia and damping combination control of VSG to support frequency stability," *IEEE Transactions on Energy Conversion,* vol. 32, no. 1, pp. 397-398, 2017.

[149] L. F. Encarnação, D. Carletti, S. de Angeli Souza, O. de Barros Jr, D. C. Broedel, and P. T. Rodrigues, "Virtual Inertia for Power Converter Control," in *Advances in Renewable Energies and Power Technologies*, vol. 2: Elsevier, 2018, pp. 377-411.

[150] S. D'Arco, J. A. Suul, and O. B. Fosso, "Small-signal modeling and parametric sensitivity of a virtual synchronous machine in islanded operation," *International Journal of Electrical Power & Energy Systems,* vol. 72, pp. 3-15, 2015.

[151] X. Tian, W. Wang, Y. Chi, Y. Li, and C. Liu, "Adaptation virtual inertia control strategy of DFIG and assessment of equivalent virtual inertia time constant of connected power system," *The Journal of Engineering,* vol. 2017, no. 13, pp. 922-928, 2017.

[152] H. R. Chamorro, I. Riano, R. Gerndt, I. Zelinka, F. Gonzalez-Longatt, and V. K. Sood, "Synthetic inertia control based on fuzzy adaptive differential evolution," *International Journal of Electrical Power & Energy Systems,* vol. 105, pp. 803-813, 2019.

[153] A. Gloe, C. Jauch, B. Craciun, and J. Winkelmann, "Continuous provision of synthetic inertia with wind turbines: implications for the wind turbine and for the grid," *IET Renewable Power Generation,* vol. 13, no. 5, pp. 668-675, 2019.

[154] D. L. Nicholas Miller, Richard Piwko, "Technology Capabilities for Fast Frequency Response," General Electric International, Inc., New York, 2017. Accessed: 15 February 2019.

[155] S. C. Johnson, J. D. Rhodes, and M. E. Webber, "Understanding the impact of non-synchronous wind and solar generation on grid stability and identifying mitigation pathways," *Applied Energy,* vol. 262, p. 114492, 2020.

[156] M. Fischer, S. Engelken, N. Mihov, and A. Mendonca, "Operational experiences with inertial response provided by type 4 wind turbines," *IET Renewable Power Generation,* vol. 10, no. 1, pp. 17-24, 2016.

[157] J. Zhao, X. Lyu, Y. Fu, X. Hu, and F. Li, "Coordinated microgrid frequency regulation based on DFIG variable coefficient using virtual inertia and primary frequency control," *IEEE Transactions on Energy Conversion,* vol. 31, no. 3, pp. 833-845, 2016.

[158] D. P. Chassin, Z. Huang, M. K. Donnelly, C. Hassler, E. Ramirez, and C. Ray, "Estimation of WECC system inertia using observed frequency transients," *IEEE Transactions on Power Systems,* vol. 20, no. 2, pp. 1190-1192, 2005.

[159] P. Wall, F. Gonzalez-Longatt, and V. Terzija, "Estimation of generator inertia available during a disturbance," in *Power and Energy Society General Meeting, 2012 IEEE*, 2012: Citeseer, pp. 1-8.

[160] S. Sharma, S.-H. Huang, and N. Sarma, "System inertial frequency response estimation and impact of renewable resources in ERCOT interconnection," in *2011 IEEE power and energy society general meeting*, 2011: IEEE, pp. 1-6.

[161] M. Kuivaniemi *et al.*, "Estimation of System Inertia in the Nordic Power System Using Measured Frequency Disturbances," in *Cigre Conference*, 2015, pp. 27-28.

[162] J. Zhang and H. Xu, "Online Identification of Power System Equivalent Inertia Constant," *IEEE Transactions on Industrial Electronics,* vol. 64, no. 10, pp. 8098-8107, 2017.

[163] J. Chang, Y. Du, X. Chen, E. G. Lim, and K. Yan, "Forecasting Based Virtual Inertia Control of PV Systems for Islanded Micro-Grid," in *2019 29th Australasian Universities Power Engineering Conference (AUPEC)*, 2019: IEEE, pp. 1-6.

[164] F. Gonzalez-Longatt, M. Acosta, H. Chamorro, and D. Topic, "Short-term Kinetic Energy Forecast using a Structural Time Series Model: Study Case of Nordic Power System," in *2020 International Conference on Smart Systems and Technologies (SST)*, 2020: IEEE, pp. 173-178.

[165] V. Prakash, R. Bhakar, H. Tiwari, and K. C. Sharma, "System Inertia Prediction for Primary Frequency Response Adequacy Under Uncertain Wind Generation," in *2018 8th IEEE India International Conference on Power Electronics (IICPE)*, 2018: IEEE, pp. 1-6.

[166] D. del Giudice and S. Grillo, "Analysis of the sensitivity of extended Kalman filter-based inertia estimation method to the assumed time of disturbance," *Energies,* vol. 12, no. 3, p. 483, 2019.

[167] P. Ashton, G. Taylor, A. Carter, M. Bradley, and W. Hung, "Application of phasor measurement units to estimate power system inertial frequency response," in *2013 IEEE Power & Energy Society General Meeting*, 2013: IEEE, pp. 1-5.

[168] R. K. Panda, A. Mohapatra, and S. C. Srivastava, "Online Estimation of System Inertia in a Power Network utilizing Synchrophasor Measurements," *IEEE Transactions on Power Systems,* vol. 35, no. 4, pp. 3122 - 3132, 2019, doi: 10.1109/TPWRS.2019.2958603.

[169] M. Sun, Y. Feng, P. Wall, S. Azizi, J. Yu, and V. Terzija, "On-line power system inertia calculation using wide area measurements," *International Journal of Electrical Power & Energy Systems,* vol. 109, pp. 325-331, 2019.

[170] F. Zeng, J. Zhang, G. Chen, Z. Wu, S. Huang, and Y. Liang, "Online Estimation of Power System Inertia Constant Under Normal Operating Conditions," *IEEE Access,* vol. 8, pp. 101426 - 101436, 2020.

[171] J. Zhao, Y. Tang, and V. Terzija, "Robust online estimation of power system center of inertia frequency," *IEEE Transactions on Power Systems,* vol. 34, no. 1, pp. 821-825,

2018.
[172] J. Schiffer, P. Aristidou, and R. Ortega, "Online estimation of power system inertia using dynamic regressor extension and mixing," *IEEE Transactions on Power Systems,* vol. 34, no. 6, pp. 4993-5001, 2019.
[173] F. Allella, E. Chiodo, G. M. Giannuzzi, D. Lauria, and F. Mottola, "On-line estimation assessment of power systems inertia with high penetration of renewable generation," *IEEE Access,* vol. 8, pp. 62689-62697, 2020.
[174] F. Vanbecelaere *et al.*, "Online Tracking of Varying Inertia using a SDFT Approach," *Mechatronics,* vol. 68, p. 102361, 2020.
[175] B. Wang, D. Yang, G. Cai, J. Ma, Z. Chen, and L. Wang, "Online Inertia Estimation using Electromechanical Oscillation Modal Extracted from Synchronized Ambient Data," *Journal of Modern Power Systems and Clean Energy,* 2020.
[176] N. Petra, C. G. Petra, Z. Zhang, E. M. Constantinescu, and M. Anitescu, "A Bayesian approach for parameter estimation with uncertainty for dynamic power systems," *IEEE Transactions on Power Systems,* vol. 32, no. 4, pp. 2735-2743, 2016.
[177] E. R. Paidi, H. Marzooghi, J. Yu, and V. Terzija, "Development and Validation of Artificial Neural Network-Based Tools for Forecasting of Power System Inertia With Wind Farms Penetration," *IEEE Systems Journal,* vol. 14, no. 4, pp. 4978-4989, 2020.
[178] J. W. Pierre, D. Trudnowski, M. Donnelly, N. Zhou, F. K. Tuffner, and L. Dosiek, "Overview of system identification for power systems from measured responses," *IFAC Proceedings Volumes,* vol. 45, no. 16, pp. 989-1000, 2012.
[179] L. Ljung, *System Identification: Theory for the User*, 2nd ed. Upper Saddle River, NJ, USA: Prentice Hall, 1999.
[180] G. Rao and H. Garnier, "Numerical illustrations of the relevance of direct continuous-time model identification," *IFAC Proceedings Volumes,* vol. 35, no. 1, pp. 133-138, 2002.
[181] H. Garnier and P. Young, "Time-domain approaches to continuous-time model identification of dynamical systems from sampled data," in *Proceedings of the 2004 American Control Conference*, 2004, vol. 1: IEEE, pp. 667-672.
[182] M. Karrari and O. Malik, "Identification of physical parameters of a synchronous generator from online measurements," *IEEE transactions on energy conversion,* vol. 19, no. 2, pp. 407-415, 2004.
[183] N. Zhou, J. W. Pierre, and J. F. Hauer, "Initial results in power system identification from injected probing signals using a subspace method," *IEEE Transactions on power systems,* vol. 21, no. 3, pp. 1296-1302, 2006.
[184] H. Garnier and W. Liuping, *Identification of Continuous-time Models from Sampled Data*. Springer., 2008.
[185] D. N. Kosterev, C. W. Taylor, and W. A. Mittelstadt, "Model validation for the August 10, 1996 WSCC system outage," *IEEE transactions on power systems,* vol. 14, no. 3, pp. 967-979, 1999.
[186] D. Yang *et al.*, "Ambient-data-driven Modal-identification-based Approach to Estimate the Inertia of an Interconnected Power System," *IEEE Access,* vol. 8, pp. 118799 - 118807, 2020, doi: 10.1109/ACCESS.2020.3004335.
[187] J. W. Pierre, D. J. Trudnowski, and M. K. Donnelly, "Initial results in electromechanical mode identification from ambient data," *IEEE Transactions on Power Systems,* vol. 12, no. 3, pp. 1245-1251, 1997.
[188] N. Zhou, J. W. Pierre, D. J. Trudnowski, and R. T. Guttromson, "Robust RLS methods for online estimation of power system electromechanical modes," *IEEE Transactions on Power Systems,* vol. 22, no. 3, pp. 1240-1249, 2007.
[189] D. Chakravorty, B. Chaudhuri, and S. Y. R. Hui, "Rapid frequency response from smart loads in Great Britain power system," *IEEE Transactions on Smart Grid,* vol. 8, no. 5, pp. 2160-2169, 2016.
[190] D. Yang *et al.*, "Data-Driven Estimation of Inertia for Multi-area Interconnected Power Systems Using Dynamic Mode Decomposition," *IEEE Transactions on Industrial Informatics,* 2020.
[191] C. Phurailatpam, Z. H. Rather, B. Bahrani, and S. Doolla, "Measurement Based Estimation of Inertia in AC Microgrids," *IEEE Transactions on Sustainable Energy,* vol.

11, no. 3, pp. 1975 - 1984, 2019, doi: 0.1109/TSTE.2019.2948224.

[192] R. Azizipanah-Abarghooee, M. Malekpour, M. Paolone, and V. Terzija, "A new approach to the online estimation of the loss of generation size in power systems," *IEEE Transactions on Power Systems,* vol. 34, no. 3, pp. 2103-2113, 2018.

[193] F. Teng, V. Trovato, and G. Strbac, "Stochastic scheduling with inertia-dependent fast frequency response requirements," *IEEE Transactions on Power Systems,* vol. 31, no. 2, pp. 1557-1566, 2015.

[194] Watt-Logic. "Measuring grid inertia accurately will enable more efficient frequency management." Watt-Logic. http://watt-logic.com/2017/10/12/inertia/ (accessed 20 October 2018.

[195] R. A. van der Veen and R. A. Hakvoort, "The electricity balancing market: Exploring the design challenge," *Utilities Policy,* vol. 43, pp. 186-194, 2016.

[196] E. V. Hobman, E. R. Frederiks, K. Stenner, and S. Meikle, "Uptake and usage of cost-reflective electricity pricing: Insights from psychology and behavioural economics," *Renewable and Sustainable Energy Reviews,* vol. 57, pp. 455-467, 2016.

[197] P. Rodriguez, I. Candela, and A. Luna, "Control of PV generation systems using the synchronous power controller," in *2013 IEEE Energy Conversion Congress and Exposition*, 2013: IEEE, pp. 993-998.

[198] V. V. Terzija, "Adaptive underfrequency load shedding based on the magnitude of the disturbance estimation," *IEEE Transactions on Power Systems,* vol. 21, no. 3, pp. 1260-1266, 2006.

[199] S. R. Awasthi, S. Chalise, and R. Tonkoski, "Operation of datacenter as virtual power plant," in *2015 IEEE Energy Conversion Congress and Exposition (ECCE)*, 2015: IEEE, pp. 3422-3429.

[200] P. Tielens and D. Van Hertem, "Grid inertia and frequency control in power systems with high penetration of renewables," in *Young Researchers Symposium in Electrical Power Engineering, Date: 2012/04/16-2012/04/17, Location: Delft, The Netherlands*, 2012.

[201] O. Agranat, I. MacGill, and A. Bruce, "Fast frequency markets under high penetrations of renewable energy in the Australian National Electricity Market," in *Proceedings of the Asia-Pacific Solar Research Conference, Queensland, Australia*, 2015, pp. 8-10.

[202] A. K. Srivastava, R. Zamora, and D. Bowman, "Impact of distributed generation with storage on electric grid stability," in *2011 IEEE Power and Energy Society General Meeting*, 2011: IEEE, pp. 1-5.

[203] K. B. Samarakoon, "Use of smart meters for frequency and voltage control," Cardiff University, 2012.

[204] E. D. Sven Teske, Nicky Ison, Kristian Maras "100% Renewable Energy for Australia – Decarbonising
Australia's Energy Sector within one Generation.," Institute for Sustainable Futures, Sydney - Australia, 2016.

[205] G. Magdy, G. Shabib, A. A. Elbaset, and Y. Mitani, "Renewable power systems dynamic security using a new coordination of frequency control strategy based on virtual synchronous generator and digital frequency protection," *International Journal of Electrical Power & Energy Systems,* vol. 109, pp. 351-368, 2019.

[206] Watt-Logic. "What caused the UK's power blackout and will it happen again?" Watt-Logic. http://watt-logic.com/2019/08/12/august-2019-blackout/ (accessed 10th October, 2019).

[207] H. Tsai, A. Keyhani, J. Demcko, and R. Farmer, "On-line synchronous machine parameter estimation from small disturbance operating data," *IEEE Transactions on Energy Conversion,* vol. 10, no. 1, pp. 25-36, 1995.

[208] M. Ariff, B. Pal, and A. K. Singh, "Estimating dynamic model parameters for adaptive protection and control in power system," *IEEE Transactions on Power Systems,* vol. 30, no. 2, pp. 829-839, 2014.

[209] P. M. Ashton, C. S. Saunders, G. A. Taylor, A. M. Carter, and M. E. Bradley, "Inertia estimation of the GB power system using synchrophasor measurements," *IEEE Transactions on Power Systems,* vol. 30, no. 2, pp. 701-709, 2014.

[210] U. Tamrakar, N. Guruwacharya, N. Bhujel, F. Wilches-Bernal, T. M. Hansen, and R. Tonkoski, "Inertia Estimation in Power Systems using Energy Storage and System Identification Techniques," in *2020 International Symposium on Power Electronics, Electrical Drives, Automation and Motion (SPEEDAM)*, 2020: IEEE, pp. 577-582.

[211] G. Chavan, M. Weiss, A. Chakrabortty, S. Bhattacharya, A. Salazar, and F.-H. Ashrafi, "Identification and predictive analysis of a multi-area WECC power system model using synchrophasors," *IEEE Transactions on Smart Grid,* vol. 8, no. 4, pp. 1977-1986, 2016.

[212] A. J. Roscoe, A. Dyśko, B. Marshall, M. Lee, H. Kirkham, and G. Rietveld, "The case for redefinition of frequency and ROCOF to account for AC power system phase steps," in *2017 IEEE International Workshop on Applied Measurements for Power Systems (AMPS)*, 2017: IEEE, pp. 1-6.

[213] R. J. Best, P. V. Brogan, and D. J. Morrow, "Power System Inertia Estimation using HVDC Power Perturbations," *IEEE Transactions on Power Systems,* 2020.

[214] X. Cao, B. Stephen, I. F. Abdulhadi, C. D. Booth, and G. M. Burt, "Switching Markov Gaussian models for dynamic power system inertia estimation," *IEEE Transactions on Power Systems,* vol. 31, no. 5, pp. 3394-3403, 2016.

[215] J. Machowski, J. Bialek, J. R. Bumby, and J. Bumby, *Power system dynamics and stability*. John Wiley & Sons, 1997.

[216] C.-K. Nguyen, T.-T. Nguyen, H.-J. Yoo, and H.-M. Kim, "Improving Transient Response of Power Converter in a Stand-Alone Microgrid Using Virtual Synchronous Generator," *Energies,* vol. 11, no. 1, p. 27, 2017.

[217] F. Milano and A. O. Manjavacas, *Frequency Variations in Power Systems: Modeling, State Estimation, and Control*. John Wiley & Sons, 2020.

[218] R. Eriksson and L. Soder, "Wide-area measurement system-based subspace identification for obtaining linear models to centrally coordinate controllable devices," *IEEE Transactions on Power Delivery,* vol. 26, no. 2, pp. 988-997, 2011.

[219] J. Schipper, A. Wood, C. Edwards, and A. Miller, "Recommendations for Ancillary Service Markets under High Penetrations of Wind Generation in New Zealand," University of Canterbury, Christchurch, New Zealand, UC-GG-19-R-JNS-01, 2019. Accessed: 15th July 2020.

[220] L. Xiong, X. Liu, D. Zhang, and Y. Liu, "Rapid Power Compensation Based Frequency Response Strategy for Low Inertia Power Systems," *IEEE Journal of Emerging and Selected Topics in Power Electronics,* 2020.

[221] V. Gevorgian, Y. Zhang, and E. Ela, "Investigating the impacts of wind generation participation in interconnection frequency response," *IEEE transactions on Sustainable Energy,* vol. 6, no. 3, pp. 1004-1012, 2014.

[222] R. Yan, T. K. Saha, N. Modi, N.-A. Masood, and M. Mosadeghy, "The combined effects of high penetration of wind and PV on power system frequency response," *Applied Energy,* vol. 145, pp. 320-330, 2015.

[223] J. D. Lara-Jimenez, J. M. Ramırez, and F. Mancilla-David, "Allocation of PMUs for power system-wide inertial frequency response estimation," *IET Generation, Transmission & Distribution,* vol. 11, no. 11, pp. 2902-2911, 2017.

[224] Z. Huang, P. Du, D. Kosterev, and S. Yang, "Generator dynamic model validation and parameter calibration using phasor measurements at the point of connection," *IEEE transactions on power systems,* vol. 28, no. 2, pp. 1939-1949, 2013.

[225] Y. Zhang, J. Bank, E. Muljadi, Y.-H. Wan, and D. Corbus, "Angle instability detection in power systems with high-wind penetration using synchrophasor measurements," *IEEE Journal of Emerging and Selected Topics in Power Electronics,* vol. 1, no. 4, pp. 306-314, 2013.

[226] Y. Xu, L. Mili, X. Chen, M. Korkali, and L. Min, "A Bayesian Approach to Real-Time Dynamic Parameter Estimation Using Phasor Measurement Unit Measurement," *IEEE Transactions on Power Systems,* vol. 35, no. 2, pp. 1109-1119, 2019.

[227] F. Milano and Á. Ortega, "A Method for Evaluating Frequency Regulation in an Electrical Grid Part I: Theory," *IEEE Transactions on Power Systems,* 2020.

[228] A. Fernández-Guillamón, A. Vigueras-Rodríguez, and Á. Molina-García, "Analysis of power system inertia estimation in high wind power plant integration scenarios," *IET*

Renewable Power Generation, vol. 13, no. 15, pp. 2807-2816, 2019.
[229] C. A. Ordóñez and M. A. Ríos, "Electromechanical modes identification based on sliding-window data from a wide-area monitoring system," *Electric Power Components and Systems,* vol. 41, no. 13, pp. 1264-1279, 2013.
[230] E. Barocio, B. C. Pal, N. F. Thornhill, and A. R. Messina, "A dynamic mode decomposition framework for global power system oscillation analysis," *IEEE Transactions on Power Systems,* vol. 30, no. 6, pp. 2902-2912, 2015.
[231] J. Rommes, N. Martins, and F. D. Freitas, "Computing rightmost eigenvalues for small-signal stability assessment of large-scale power systems," *IEEE transactions on power systems,* vol. 25, no. 2, pp. 929-938, 2009.
[232] R. Isermann and M. Münchhof, *Identification of dynamic systems: an introduction with applications*. Springer Science & Business Media, 2010.
[233] P. J. Schmid, "Dynamic mode decomposition of numerical and experimental data," *Journal of fluid mechanics,* vol. 656, pp. 5-28, 2010.
[234] R. W. Wies, "Estimating low-frequency electromechanical modes of power systems using ambient data," Ph.D. Thesis, Department of Electrical Engineering, University of Wyoming, USA, AAI9933489, 2000.
[235] D. Zografos, M. Ghandhari, and R. Eriksson, "Real Time Frequency Response Assessment Using Regression," in *2020 IEEE PES Innovative Smart Grid Technologies Europe (ISGT-Europe)*, 2020: IEEE, pp. 399-403.
[236] B. Hartmann, I. Vokony, and I. Táczi, "Effects of decreasing synchronous inertia on power system dynamics—Overview of recent experiences and marketisation of services," *International Transactions on Electrical Energy Systems,* vol. 29, no. 12, p. e12128, 2019.
[237] Transpower. "Net Zero Grid Pathways: Phase One to 2035." Transpower. https://www.transpower.co.nz/NZGP (accessed 23/6/2021, 2021).
[238] N. Z. w. e. association. "New Zealand's wind farms." New Zealand wind energy association. https://www.windenergy.org.nz/wind-energy/nz-windfarms (accessed 06/23, 2021).
[239] E. A. T. M. Hiko. "Generation output by plant." Electricity Authority. https://www.emi.ea.govt.nz/Wholesale/Datasets/Generation/Generation_MD (accessed 15/05/2021, 2021).
[240] W. Wang, W. Yao, C. Chen, X. Deng, and Y. Liu, "Fast and accurate frequency response estimation for large power system disturbances using second derivative of frequency data," *IEEE Transactions on Power Systems,* vol. 35, no. 3, pp. 2483-2486, 2020.
[241] M. R. B. Tavakoli, M. Power, L. Ruttledge, and D. Flynn, "Load inertia estimation using white and grey-box estimators for power systems with high wind penetration," *IFAC Proceedings Volumes,* vol. 45, no. 21, pp. 399-404, 2012.
[242] E. Carlini, F. Del Pizzo, G. Giannuzzi, D. Lauria, F. Mottola, and C. Pisani, "Online analysis and prediction of the inertia in power systems with renewable power generation based on a minimum variance harmonic finite impulse response filter," *International Journal of Electrical Power & Energy Systems,* vol. 131, p. 107042, 2021.
[243] G. Donnini *et al.*, "On the Estimation of Power System Inertia accounting for Renewable Generation Penetration," in *2020 AEIT International Annual Conference (AEIT)*, 2020: IEEE, pp. 1-6.
[244] M. Kosmecki *et al.*, "A Methodology for Provision of Frequency Stability in Operation Planning of Low Inertia Power Systems," *Energies,* vol. 14, no. 3, p. 737, 2021.
[245] Y. Cui, J. Xie, and K. Zheng, "Historical Inertia: An Ignored but Powerful Baseline for Long Sequence Time-series Forecasting," *arXiv preprint arXiv:2103.16349,* 2021.
[246] A. Shrestha, B. Ghimire, and F. Gonzalez-Longatt, "A Bayesian Model to Forecast the Time Series Kinetic Energy Data for a Power System," *Energies,* vol. 14, no. 11, p. 3299, 2021.
[247] K. Yunus, T. Thiringer, and P. Chen, "ARIMA-based frequency-decomposed modeling of wind speed time series," *IEEE Transactions on Power Systems,* vol. 31, no. 4, pp. 2546-2556, 2015.
[248] D. C. Montgomery, C. L. Jennings, and M. Kulahci, *Introduction to time series analysis*

and forecasting. John Wiley & Sons, 2015.
[249] G. E. Box, G. M. Jenkins, G. C. Reinsel, and G. M. Ljung, *Time series analysis: forecasting and control*. John Wiley & Sons, 2015.
[250] C. Chatfield and M. Yar, "Prediction intervals for multiplicative Holt-Winters," *International Journal of Forecasting,* vol. 7, no. 1, pp. 31-37, 1991.
[251] Transpower, "System Operator TASC Report," in "TASC 033 report," Transpower, New Zealand, 2014. Accessed: 15/5/2021.
[252] S. Wambura, J. Huang, and H. Li, "Long-range forecasting in feature-evolving data streams," *Knowledge-Based Systems,* vol. 206, p. 106405, 2020.
[253] C. Chen, J. Twycross, and J. M. Garibaldi, "A new accuracy measure based on bounded relative error for time series forecasting," *PloS one,* vol. 12, no. 3, p. e0174202, 2017.
[254] E. Rakhshani, D. Gusain, V. Sewdien, J. L. R. Torres, and M. A. Van Der Meijden, "A key performance indicator to assess the frequency stability of wind generation dominated power system," *IEEE Access,* vol. 7, pp. 130957-130969, 2019.
[255] H. R. Chamorro, A. C. Sanchez, A. Øverjordet, F. Jimenez, F. Gonzalez-Longatt, and V. K. Sood, "Distributed synthetic inertia control in power systems," in *2017 international conference on energy and environment (CIEM)*, 2017: IEEE, pp. 74-78.
[256] M. Altin, J. C. Kuhlmann, K. Das, and A. D. Hansen, "Optimization of synthetic inertial response from wind power plants," *Energies,* vol. 11, no. 5, p. 1051, 2018.
[257] D. Ochoa and S. Martinez, "Fast-Frequency Response provided by DFIG-Wind Turbines and its impact on the grid," *IEEE Trans. Power Syst,* vol. 32, pp. 4002-4011, 2017.
[258] M. Paturet, U. Markovic, S. Delikaraoglou, E. Vrettos, P. Aristidou, and G. Hug, "Stochastic unit commitment in low-inertia grids," *IEEE Transactions on Power Systems,* vol. 35, no. 5, pp. 3448-3458, 2020.
[259] T. Kerdphol, F. S. Rahman, M. Watanabe, Y. Mitani, D. Turschner, and H.-P. Beck, "Enhanced virtual inertia control based on derivative technique to emulate simultaneous inertia and damping properties for microgrid frequency regulation," *IEEE Access,* vol. 7, pp. 14422-14433, 2019.
[260] J. Fang, R. Zhang, H. Li, and Y. Tang, "Frequency derivative-based inertia enhancement by grid-connected power converters with a frequency-locked-loop," *IEEE Transactions on Smart Grid,* vol. 10, no. 5, pp. 4918-4927, 2018.
[261] L. Ruttledge and D. Flynn, "Emulated inertial response from wind turbines: gain scheduling and resource coordination," *IEEE Transactions on Power Systems,* vol. 31, no. 5, pp. 3747-3755, 2015.
[262] S. S. Guggilam, C. Zhao, E. Dall'Anese, Y. C. Chen, and S. V. Dhople, "Optimizing DER participation in inertial and primary-frequency response," *IEEE Transactions on Power Systems,* vol. 33, no. 5, pp. 5194-5205, 2018.
[263] A. Fernández-Guillamón, E. Gómez-Lázaro, E. Muljadi, and Á. Molina-Garcia, "A review of virtual inertia techniques for renewable energy-based generators," *Renewable Energy-Technologies and Applications,* 2020.
[264] L. Yang and Z. Hu, "Implementation of Dynamic Virtual Inertia Control of Supercapacitors for Multi-Area PV-Based Microgrid Clusters," *Sustainability,* vol. 12, no. 8, p. 3299, 2020.
[265] L. Pagnier and P. Jacquod, "Optimal placement of inertia and primary control: a matrix perturbation theory approach," *Ieee Access,* vol. 7, pp. 145889-145900, 2019.
[266] H. Thiesen and C. Jauch, "Determining the load inertia contribution from different power consumer groups," *Energies,* vol. 13, no. 7, p. 1588, 2020.
[267] K. Deb, *Optimization for engineering design: Algorithms and examples*. PHI Learning Pvt. Ltd., 2012.
[268] D. Liberzon, *Calculus of variations and optimal control theory*. Princeton university press, 2011.